Medical Imaging Signals and Systems (2e): Solutions Manual

Version 1.4 (December 21, 2016)

Jerry L. Prince
Electrical and Computer Engineering
Whiting School of Engineering
Johns Hopkins University

Jonathan M. Links
Environmental Health Sciences
Bloomberg School of Public Health
Johns Hopkins University

PRENTICE HALL
Upper Saddle River, New Jersey 07458

Contents

Preface

These solutions have been prepared over the past 18 years or so during the process of teaching our course on Medical Imaging Systems at Johns Hopkins University. We would like to thank the following individuals for their help: William R. Brody, Elliot R. McVeigh, John I. Goutsias, Ergin Atalar, Scott Reeder, Bradley Wyman, Chris Constandinides, Rong Xue, Christopher Yeung, Maryam Rettmann, Duygu Tosun, M. Faisal Beg, Xiao Han, Li Pan, Pramodsingh H. Thakur, Vijay Parthasarathy, Tara Johnson, Abd El-Monem El-Sharkawy, Minnan Xu, Khaled Abd-Elmoniem, Lotta Ellingsen, Jing Wan, Snehashis Roy, Harsh Agarwal, Issel Lim, Xian Fan, Nan Li, Sahar Soleimanifard, Nathanael Kuo, Min Chen, Jeffrey Pompe, Daniel Tward, Sureerat Reaungamornrat, Shan Zhong, and Yansong Zhu. Special thanks to Xiaodong Tao, who created and solved a large number of problems specifically for the first edition and to Zhen Yang and Chuyang Ye for the problems they checked, corrected, and solved for this edition. As always, tremendous thanks to Aaron Carass, who patiently solved countless LaTeX and CVS problems that were encountered in the preparation of both the textbook and this solutions manual.

Jerry L. Prince
Jonathan M. Links
December 21, 2016

2

Signals and Systems

SIGNALS AND THEIR PROPERTIES

Solution 2.1

(a) $\delta_s(x,y) = \sum_{m=-\infty}^{\infty}\sum_{n=-\infty}^{\infty}\delta(x-m,y-n) = \sum_{m=-\infty}^{\infty}\delta(x-m)\cdot\sum_{n=-\infty}^{\infty}\delta(y-n)$, therefore it is a separable signal.

(b) $\delta_l(x,y)$ is separable if $\sin(2\theta)=0$. In this case, either $\sin\theta=0$ or $\cos\theta=0$, $\delta_l(x,y)$ is a product of a constant function in one axis and a 1-D *delta* function in another. But in general, $\delta_l(x,y)$ is not separable.

(c) $e(x,y) = \exp[j2\pi(u_0x+v_0y)] = \exp(j2\pi u_0x)\cdot\exp(j2\pi v_0y) = e_{1\mathrm{D}}(x;u_0)\cdot e_{1\mathrm{D}}(y;v_0)$, where $e_{1\mathrm{D}}(t;\omega) = \exp(j2\pi\omega t)$. Therefore, $e(x,y)$ is a separable signal.

(d) $s(x,y)$ is a separable signal when $u_0v_0=0$. For example, if $u_0=0$, $s(x,y)=\sin(2\pi v_0y)$ is the product of a constant signal in x and a 1-D sinusoidal signal in y. But in general, when both u_0 and v_0 are nonzero, $s(x,y)$ is not separable.

Solution 2.2

(a) Not periodic. $\delta(x,y)$ is non-zero only when $x=y=0$.

(b) Periodic. By definition

$$\mathrm{comb}(x,y) = \sum_{m=-\infty}^{\infty}\sum_{n=-\infty}^{\infty}\delta(x-m,y-n)\,.$$

For arbitrary integers M and N, we have

$$\begin{aligned}\mathrm{comb}(x+M,y+N) &= \sum_{m=-\infty}^{\infty}\sum_{n=-\infty}^{\infty}\delta(x-m+M,y-n+N)\\ &= \sum_{p=-\infty}^{\infty}\sum_{q=-\infty}^{\infty}\delta(x-p,y-q)\ [\text{let } p=m-M, q=n-N]\\ &= \mathrm{comb}(x,y)\,.\end{aligned}$$

So the smallest period is 1 in both x and y directions.

(c) Periodic. Let $f(x+T_x, y) = f(x,y)$, we have

$$\sin(2\pi x)\cos(4\pi y) = \sin(2\pi(x+T_x))\cos(4\pi y)\,.$$

Solving the above equation, we have $2\pi T_x = 2k\pi$ for arbitrary integer k. So the smallest period for x is $T_{x0} = 1$. Similarly, we find that the smallest period for y is $T_{y0} = 1/2$.

(d) Periodic. Let $f(x+T_x, y) = f(x,y)$, we have

$$\sin(2\pi(x+y)) = \sin(2\pi(x+T_x+y)).$$

So the smallest period for x is $T_{x0} = 1$ and the smallest period for y is $T_{y0} = 1$.

(e) Not periodic. We can see this by contradiction. Suppose $f(x,y) = \sin(2\pi(x^2+y^2))$ is periodic; then there exists some T_x such that $f(x+T_x, y) = f(x,y)$, and

$$\begin{aligned}\sin(2\pi(x^2+y^2)) &= \sin(2\pi((x+T_x)^2+y^2)) \\ &= \sin(2\pi(x^2+y^2+2xT_x+T_x^2))\,.\end{aligned}$$

In order for the above equation to hold, we must have that $2xT_x + T_x^2 = k$ for some integer k. The solution for T_x depends on x. So $f(x,y) = \sin(2\pi(x^2+y^2))$ is not periodic.

(f) Periodic. Let $f_d(m+M, n) = f_d(m,n)$. Then

$$\sin\left(\frac{\pi}{5}m\right)\cos\left(\frac{\pi}{5}n\right) = \sin\left(\frac{\pi}{5}(m+M)\right)\cos\left(\frac{\pi}{5}n\right)\,.$$

Solving for M, we find that $M = 10k$ for any integer k. The smallest period for both m and n is therefore 10.

(g) Not periodic. Following the same strategy as in (f), we let $f_d(m+M, n) = f_d(m,n)$, and then

$$\sin\left(\frac{1}{5}m\right)\cos\left(\frac{1}{5}n\right) = \sin\left(\frac{1}{5}(m+M)\right)\cos\left(\frac{1}{5}n\right)\,.$$

The solution for M is $M = 10k\pi$. Since $f_d(m,n)$ is a discrete signal, its period must be an integer if it is to be periodic. There is no integer k that solves the equality for $M = 10k\pi$ for some M. So, $f_d(m,n) = \sin\left(\frac{1}{5}m\right)\cos\left(\frac{1}{5}n\right)$ is not periodic.

Solution 2.3

(a) We have

$$\begin{aligned}E_\infty(\delta_s) &= \int_{-\infty}^{\infty}\int_{-\infty}^{\infty}\delta_s^2(x,y)\,dx\,dy \\ &= \lim_{X\to\infty}\lim_{Y\to\infty}\int_{-X}^{X}\int_{-Y}^{Y}\sum_{m=-\infty}^{\infty}\sum_{n=-\infty}^{\infty}\delta(x-m,y-n)\,dx\,dy \\ &= \lim_{X\to\infty}\lim_{Y\to\infty}(2\lfloor X\rfloor+1)(2\lfloor Y\rfloor+1) \\ &= \infty\,,\end{aligned}$$

where $\lfloor X \rfloor$ is the greatest integer that is smaller than or equal to X. We also have

$$\begin{aligned}
P_\infty(\delta_s) &= \lim_{X\to\infty}\lim_{Y\to\infty}\frac{1}{4XY}\int_{-X}^{X}\int_{-Y}^{Y}\delta_s^2(x,y)\,dx\,dy \\
&= \lim_{X\to\infty}\lim_{Y\to\infty}\frac{1}{4XY}\int_{-X}^{X}\int_{-Y}^{Y}\sum_{m=-\infty}^{\infty}\sum_{n=-\infty}^{\infty}\delta(x-m,y-n)\,dx\,dy \\
&= \lim_{X\to\infty}\lim_{Y\to\infty}\frac{(2\lfloor X\rfloor+1)(2\lfloor Y\rfloor+1)}{4XY} \\
&= \lim_{X\to\infty}\lim_{Y\to\infty}\left\{\frac{4\lfloor X\rfloor\lfloor Y\rfloor}{4XY}+\frac{2\lfloor X\rfloor+2\lfloor Y\rfloor}{4XY}+\frac{1}{4XY}\right\} \\
&= 1\,.
\end{aligned}$$

(b) We have

$$\begin{aligned}
E_\infty(\delta_l) &= \int_{-\infty}^{\infty}\int_{-\infty}^{\infty}|\delta(x\cos\theta+y\sin\theta-l)|^2\,dx\,dy \\
&= \int_{-\infty}^{\infty}\int_{-\infty}^{\infty}\delta(x\cos\theta+y\sin\theta-l)\,dx\,dy \\
&\overset{①}{=} \begin{cases} \displaystyle\int_{-\infty}^{\infty}\tfrac{1}{|\sin\theta|}\,dx, & \sin\theta\neq 0 \\ \displaystyle\int_{-\infty}^{\infty}\tfrac{1}{|\cos\theta|}\,dy, & \cos\theta\neq 0 \end{cases} \\
E_\infty(\delta_l) &= \infty\,.
\end{aligned}$$

Equality ① comes from the scaling property of the point impulse. The 1-D version of Eq. (2.8) in the text is $\delta(ax)=\frac{1}{|a|}\delta(x)$. Suppose $\cos\theta\neq 0$. Then

$$\delta(x\cos\theta+y\sin\theta-l)=\frac{1}{|\cos\theta|}\,\delta\left(x+y\frac{\sin\theta}{\cos\theta}-\frac{l}{\cos\theta}\right).$$

Therefore,

$$\int_{-\infty}^{\infty}\delta(x\cos\theta+y\sin\theta-l)dx=\frac{1}{|\cos\theta|}\,.$$

We also have

$$\begin{aligned}
P_\infty(\delta_l) &= \lim_{X\to\infty}\lim_{Y\to\infty}\frac{1}{4XY}\int_{-X}^{X}\int_{-Y}^{Y}|\delta(x\cos\theta+y\sin\theta-l)|^2dx\,dy \\
&= \lim_{X\to\infty}\lim_{Y\to\infty}\frac{1}{4XY}\int_{-X}^{X}\int_{-Y}^{Y}\delta(x\cos\theta+y\sin\theta-l)dx\,dy\,.
\end{aligned}$$

Without loss of generality, assume $\theta=0$ and $l=0$, so that we have $\sin\theta=0$ and $\cos\theta=1$. Then it follows

that

$$\begin{aligned} P_\infty(\delta_l) &= \lim_{X\to\infty}\lim_{Y\to\infty}\frac{1}{4XY}\int_{-X}^{X}\int_{-Y}^{Y}\delta(x)\,dx\,dy \\ &= \lim_{X\to\infty}\lim_{Y\to\infty}\frac{1}{4XY}\int_{-Y}^{Y}\left\{\int_{-X}^{X}\delta(x)dx\right\}dy \\ &= \lim_{X\to\infty}\lim_{Y\to\infty}\frac{1}{4XY}\int_{-Y}^{Y}1dx \\ &= \lim_{X\to\infty}\lim_{Y\to\infty}\frac{2Y}{4XY} \\ &= \lim_{X\to\infty}\frac{1}{2X} \\ &= 0\,. \end{aligned}$$

(c) We have

$$\begin{aligned} E_\infty(e) &= \int_{-\infty}^{\infty}\int_{-\infty}^{\infty}\left|\exp\left[j2\pi(u_0x+v_0y)\right]\right|^2\,dx\,dy \\ &= \int_{-\infty}^{\infty}\int_{-\infty}^{\infty}1\,dx\,dy \\ &= \infty\,. \end{aligned}$$

And also

$$\begin{aligned} P_\infty(e) &= \lim_{X\to\infty}\lim_{Y\to\infty}\frac{1}{4XY}\int_{-X}^{X}\int_{-Y}^{Y}\left|\exp[j2\pi(u_0x+v_0y)]\right|^2\,dx\,dy \\ &= \lim_{X\to\infty}\lim_{Y\to\infty}\frac{1}{4XY}\int_{-X}^{X}\int_{-Y}^{Y}1\,dx\,dy \\ &= 1\,. \end{aligned}$$

(d) We have

$$\begin{aligned} E_\infty(s) &= \int_{-\infty}^{\infty}\int_{-\infty}^{\infty}\sin^2[2\pi(u_0x+v_0y)]\,dx\,dy \\ &\overset{②}{=} \int_{-\infty}^{\infty}\int_{-\infty}^{\infty}\frac{1-\cos[4\pi(u_0x+v_0y)]}{2}\,dx\,dy \\ &= \int_{-\infty}^{\infty}\int_{-\infty}^{\infty}\frac{1}{2}\,dx\,dy - \int_{-\infty}^{\infty}\int_{-\infty}^{\infty}\frac{\cos[4\pi(u_0x+v_0y)]}{2}\,dx\,dy \\ &\overset{③}{=} \infty\,. \end{aligned}$$

Equality ② comes from the trigonometric identity $\cos(2\theta) = 1 - 2\sin^2(\theta)$. Equality ③ holds because the first integral goes to infinity. The absolute value of the second integral is bounded, although it does not

converge as X and Y go to infinity. We also have

$$\begin{aligned}
P_\infty(s) &= \lim_{X\to\infty}\lim_{Y\to\infty}\frac{1}{4XY}\int_{-X}^{X}\int_{-Y}^{Y}\sin^2[2\pi(u_0x+v_0y)]\,dx\,dy \\
&= \lim_{X\to\infty}\lim_{Y\to\infty}\frac{1}{4XY}\int_{-Y}^{Y}\left\{\int_{-X}^{X}\frac{1-\cos[4\pi(u_0x+v_0y)]}{2}\,dx\right\}dy \\
&= \lim_{X\to\infty}\lim_{Y\to\infty}\frac{1}{4XY}\int_{-Y}^{Y}\left[X+\frac{\sin[4\pi(u_0X+v_0y)]-\sin[4\pi(-u_0X+v_0y)]}{8\pi u_0}\right]dy \\
&\overset{④}{=} \lim_{X\to\infty}\lim_{Y\to\infty}\frac{1}{4XY}\int_{-Y}^{Y}\left[X-\frac{\sin(4\pi u_0X)\cos(4\pi v_0y)}{4\pi u_0}\right]dy \\
&= \lim_{X\to\infty}\lim_{Y\to\infty}\frac{1}{4XY}\left(2XY-\frac{2\sin(4\pi u_0X)\sin(4\pi v_0Y)}{(4\pi)^2u_0v_0}\right) \\
&= \frac{1}{2}\,.
\end{aligned}$$

In order to get ④, we have used the trigonometric identity $\sin(\alpha+\beta)=\sin\alpha\cos\beta+\cos\alpha\sin\beta$. The rest of the steps are straightforward.

Since $s(x,y)$ is a periodic signal with periods $X_0=1/u_0$ and $Y_0=1/v_0$, we have an alternative way to compute P_∞ by considering only one period in each dimension. Accordingly,

$$\begin{aligned}
P_\infty(s) &= \frac{1}{4X_0Y_0}\int_{-X_0}^{X_0}\int_{-Y_0}^{Y_0}\sin^2[2\pi(u_0x+v_0y)]\,dx\,dy \\
&= \frac{1}{4X_0Y_0}\left(2X_0Y_0-\frac{2\sin(4\pi u_0X_0)\sin(4\pi v_0Y_0)}{(4\pi)^2u_0v_0}\right) \\
&= \frac{1}{4X_0Y_0}\left(2X_0Y_0-\frac{2\sin(4\pi)\sin(4\pi)}{(4\pi)^2u_0v_0}\right) \\
&= \frac{1}{2}\,.
\end{aligned}$$

SYSTEMS AND THEIR PROPERTIES

Solution 2.4

Suppose two LSI systems $\mathcal{S}_1$ and $\mathcal{S}_2$ are connected in cascade. For any two input signals $f_1(x,y)$, $f_2(x,y)$, and two constants a_1 and a_2, we have the following:

$$\begin{aligned}
\mathcal{S}_2[\mathcal{S}_1[a_1f_1(x,y)+a_2f_2(x,y)]] &= \mathcal{S}_2[a_1\mathcal{S}_1[f_1(x,y)]+a_2\mathcal{S}_1[f_2(x,y)]] \\
&= a_1\mathcal{S}_2[\mathcal{S}_1[f_1(x,y)]]+a_2\mathcal{S}_2[\mathcal{S}_1[f_2(x,y)]]\,.
\end{aligned}$$

So the cascade of two LSI systems is also linear. Now suppose for a given signal $f(x,y)$ we have $\mathcal{S}_1[f(x,y)]=g(x,y)$, and $\mathcal{S}_2[g(x,y)]=h(x,y)$. By using the shift-invariance of the systems, we can prove that the cascade of two LSI systems is also shift invariant:

$$\mathcal{S}_2[\mathcal{S}_1[f(x-\xi,y-\eta)]]=\mathcal{S}_2[g(x-\xi,y-\eta)]=h(x-\xi,y-\eta)\,.$$

This proves that two LSI systems in cascade is an LSI system

To prove Eq. (2.46) we carry out the following:

$$\begin{aligned}
g(x,y) &= h_2(x,y) * [h_1(x,y) * f(x,y)] \\
&= h_2(x,y) * \int_{-\infty}^{\infty}\int_{-\infty}^{\infty} h_1(\xi,\eta) f(x-\xi, y-\eta)\, d\xi\, d\eta \\
&= \int_{-\infty}^{\infty}\int_{-\infty}^{\infty} h_2(u,v) \left[\int_{-\infty}^{\infty}\int_{-\infty}^{\infty} h_1(\xi,\eta) f(x-u-\xi, y-v-\eta)\, d\xi\, d\eta\right] du\, dv \\
&= \int_{-\infty}^{\infty}\int_{-\infty}^{\infty}\int_{-\infty}^{\infty}\int_{-\infty}^{\infty} h_2(u,v) h_1(\xi,\eta) f(x-u-\xi, y-v-\eta)\, d\xi\, d\eta du\, dv \\
&= \int_{-\infty}^{\infty}\int_{-\infty}^{\infty} h_1(\xi,\eta) \left[\int_{-\infty}^{\infty}\int_{-\infty}^{\infty} h_2(u,v) f(x-\xi-u, y-\eta-v)\, du\, dv\right] d\xi\, d\eta \\
&= h_1(x,y) * [h_2(x,y) * f(x,y)]\,.
\end{aligned}$$

This proves the second equality in (2.46). By letting $\alpha = u + \xi$, and $\beta = v + \eta$, we have

$$\begin{aligned}
g(x,y) &= \int_{-\infty}^{\infty}\int_{-\infty}^{\infty}\int_{-\infty}^{\infty}\int_{-\infty}^{\infty} h_2(u,v) h_1(\xi,\eta) f(x-u-\xi, y-v-\eta)\, d\xi\, d\eta du\, dv \\
&= \int_{-\infty}^{\infty}\int_{-\infty}^{\infty} \left[\int_{-\infty}^{\infty}\int_{-\infty}^{\infty} h_2(\alpha-\xi, \beta-\eta) h_1(\xi,\eta)\, d\xi\, d\eta\right] f(x-\alpha, y-\beta)\, d\alpha\, d\beta \\
&= [h_1(x,y) * h_2(x,y)] * f(x,y)\,,
\end{aligned}$$

which proves the second equality in (2.46).

To prove (2.47) we start with the definition of convolution

$$\begin{aligned}
g(x,y) &= \int_{-\infty}^{\infty}\int_{-\infty}^{\infty} h_2(\xi,\eta) h_1(x-\xi, y-\eta) d\xi\, d\eta \\
&= h_1(x,y) * h_2(x,y)\,.
\end{aligned}$$

We then make the substitution $\alpha = x - \xi$ and $\beta = y - \eta$ and manipulate the result

$$\begin{aligned}
g(x,y) &= \int_{+\infty}^{-\infty}\int_{+\infty}^{-\infty} h_2(x-\alpha, y-\beta) h_1(\alpha,\beta)(-d\alpha)\,(-d\beta) \\
&= \int_{-\infty}^{+\infty}\int_{-\infty}^{+\infty} h_1(\alpha,\beta) h_2(x-\alpha, y-\beta) d\alpha\, d\beta \\
&= \int_{-\infty}^{+\infty}\int_{-\infty}^{+\infty} h_1(\xi,\eta) h_2(x-\xi, y-\eta) d\xi\, d\eta \\
&= h_2(x,y) * h_1(x,y)\,,
\end{aligned}$$

where the next to last equality follows since α and β are just dummy variables in the integral.

Solution 2.5

1. Suppose the PSF of an LSI system is absolutely integrable.

$$\int_{-\infty}^{\infty}\int_{-\infty}^{\infty}|h(x,y)|\,dx\,dy \le C < \infty \tag{S2.1}$$

where C is a finite constant. For a bounded input signal $f(x,y)$

$$|f(x,y)| \le B < \infty\,, \quad \text{for every } (x,y)\,, \tag{S2.2}$$

for some finite B, we have

$$\begin{aligned} |g(x,y)| &= |h(x,y) * f(x,y)| \\ &= \left|\int_{-\infty}^{\infty}\int_{-\infty}^{\infty} h(x-\xi,y-\eta)f(\xi,\eta)d\xi d\eta\right| \\ &\le \int_{-\infty}^{\infty}\int_{-\infty}^{\infty}|h(x-\xi,y-\eta)|\cdot|f(\xi,\eta)|\,d\xi d\eta \\ &\le B\int_{-\infty}^{\infty}\int_{-\infty}^{\infty}|h(x,y)|\,dx\,dy \\ &\le BC < \infty\,, \quad \text{for every } (x,y) \end{aligned} \tag{S2.3}$$

So $g(x,y)$ is also bounded. The system is BIBO stable.

2. We use contradiction to show that if the LSI system is BIBO stable, its PSF must be absolutely integrable. Suppose the PSF of a BIBO stable LSI system is $h(x,y)$, which is not absolutely integrable, that is,

$$\int_{-\infty}^{\infty}\int_{-\infty}^{\infty}|h(x,y)|\,dx\,dy$$

is not bounded. Then for a bounded input signal $f(x,y)=1$, the output is

$$|g(x,y)| = |h(x,y) * f(x,y)| = \int_{-\infty}^{\infty}\int_{-\infty}^{\infty}|h(x,y)|\,dx\,dy,$$

which is also not bounded. So the system can not be BIBO stable. This shows that if the LSI system is BIBO stable, its PSF must be absolutely integrable.

Solution 2.6

(a) If $g'(x,y)$ is the response of the system to input $\sum_{k=1}^{K} w_k f_k(x,y)$, then

$$\begin{aligned} g'(x,y) &= \sum_{k=1}^{K} w_k f_k(x,-1) + \sum_{k=1}^{K} w_k f_k(0,y) \\ &= \sum_{k=1}^{K} w_k [f_k(x,-1) + f_k(0,y)] \\ &= \sum_{k=1}^{K} w_k g_k(x,y) \end{aligned}$$

where $g_k(x, y)$ is the response of the system to input $f_k(x, y)$. Therefore, the system is linear.

(b) If $g'(x, y)$ is the response of the system to input $f(x - x_0, y - y_0)$, then

$$g'(x, y) = f(x - x_0, -1 - y_0) + f(-x_0, y - y_0);$$

while

$$g(x - x_0, y - y_0) = f(x - x_0, -1) + f(0, y - y_0).$$

Since $g'(x, y) \neq g(x - x_0, y - y_0)$, the system is not shift-invariant.

Solution 2.7

(a) If $g'(x, y)$ is the response of the system to input $\sum_{k=1}^{K} w_k f_k(x, y)$, then

$$\begin{aligned} g'(x, y) &= \left(\sum_{k=1}^{K} w_k f_k(x, y) \right) \left(\sum_{k=1}^{K} w_k f_k(x - x_0, y - y_0) \right) \\ &= \sum_{i=1}^{K} \sum_{j=1}^{K} w_i w_j f_i(x, y) f_j(x - x_0, y - y_0), \end{aligned}$$

while

$$\sum_{k=1}^{K} w_k g_k(x, y) = \sum_{k=1}^{K} w_k f_k(x, y) f_k(x - x_0, y - y_0).$$

Since $g'(x, y) \neq \sum_{k=1}^{K} g_k(x, y)$, the system is nonlinear.

On the other hand, if $g'(x, y)$ is the response of the system to input $f(x - a, y - b)$, then

$$\begin{aligned} g'(x, y) &= f(x - a, y - b) f(x - a - x_0, y - b - y_0) \\ &= g(x - a, y - b) \end{aligned}$$

and the system is thus shift-invariant.

(b) If $g'(x, y)$ is the response of the system to input $\sum_{k=1}^{K} w_k f_k(x, y)$, then

$$\begin{aligned} g'(x, y) &= \int_{-\infty}^{\infty} \sum_{k=1}^{K} w_k f_k(x, \eta)\, d\eta \\ &= \sum_{k=1}^{K} w_k \left(\int_{-\infty}^{\infty} f_k(x, \eta)\, d\eta \right) \\ &= \sum_{k=1}^{K} w_k g_k(x, y), \end{aligned}$$

where $g_k(x, y)$ is the response of the system to input $f_k(x, y)$. Therefore, the system is linear.

On the other hand, if $g'(x,y)$ is the response of the system to input $f(x-x_0, y-y_0)$, then

$$\begin{aligned} g'(x,y) &= \int_{-\infty}^{\infty} f(x-x_0, \eta-y_0)\, d\eta \\ &= \int_{-\infty}^{\infty} f(x-x_0, \eta-y_0)\, d(\eta-y_0) \\ &= \int_{-\infty}^{\infty} f(x-x_0, \eta)\, d\eta. \end{aligned}$$

Since $g(x-x_0, y-y_0) = \int_{-\infty}^{\infty} f(x-x_0, \eta)\, d\eta$, the system is shift-invariant.

Solution 2.8

From the results in Problem 2.5, we know that an LSI system is BIBO stable if and only if its PSF is absolutely integrable.

(a) Not stable. The PSF $h(x,y)$ goes to infinite when x and/or y go to infinity. $\int_{-\infty}^{\infty}\int_{-\infty}^{\infty} |h(x,y)|\, dx\, dy = \int_{-\infty}^{\infty}\int_{-\infty}^{\infty}(x^2+y^2)dx\, dy = \int_{-\infty}^{\infty}\left[\int_{-\infty}^{\infty} x^2 dx\right] dy + \int_{-\infty}^{\infty}\left[\int_{-\infty}^{\infty} y^2 dy\right] dx$. Since $\int_{-\infty}^{\infty} x^2 dx = \int_{-\infty}^{\infty} y^2 dy$ is not bounded, then $\int_{-\infty}^{\infty}\int_{-\infty}^{\infty}(x^2+y^2)dx\, dy$ is not bounded.

(b) Stable. $\int_{-\infty}^{\infty}\int_{-\infty}^{\infty} |h(x,y)|\, dx\, dy = \int_{-\infty}^{\infty}\int_{-\infty}^{\infty}(\exp\{-(x^2+y^2)\})dx\, dy = \left[\int_{-\infty}^{\infty} e^{-x^2} dx\right]^2 = \pi$, which is bounded. So the system is stable.

(c) Not stable. The absolute integral $\int_{-\infty}^{\infty}\int_{-\infty}^{\infty} x^2 e^{-y^2} dx\, dy = \int_{-\infty}^{\infty} x^2 \left[\int_{-\infty}^{\infty} e^{-y^2} dy\right] dx = \int_{-\infty}^{\infty} \sqrt{\pi} x^2 dx$ is unbounded. So the system is not stable.

Solution 2.9

(a) $g(x) = \int_{-\infty}^{\infty} f(x-t)f(t)dt$.

(b) Given an input as $af_1(x) + bf_2(x)$, where a, b are some constant, the output is

$$\begin{aligned} g'(x) &= [af_1(x) + bf_2(x)] * [af_1(x) + bf_2(x)] \\ &= a^2 f_1(x) * f_1(x) + 2ab f_1(x) * f_2(x) + b^2 f_2(x) * f_2(x) \\ &\neq ag_1(x) + bg_2(x), \end{aligned}$$

where $g_1(x)$ and $g_2(x)$ are the output corresponding to an input of $f_1(x)$ and $f_2(x)$ respectively. Hence, the system is nonlinear.

(c) Given a shifted input $f_1(x) = f(x-x_0)$, the corresponding output is

$$\begin{aligned} g_1(x) &= f_1(x) * f_1(x) \\ &= \int_{-\infty}^{\infty} f_1(x-t) f_1(t) dt \\ &= \int_{-\infty}^{\infty} f(x-t-x_0) f_1(t-x_0) dt. \end{aligned}$$

Changing variable $t' = t - x_0$ in the above integration, we get

$$\begin{aligned} g_1(x) &= \int_{-\infty}^{\infty} f(x - 2x_0 - t') f_1(t') dt' \\ &= g(x - 2x_0). \end{aligned}$$

Thus, if the input is shifted by x_0, the output is shifted by $2x_0$. Hence, the system is not shift-invariant.

CONVOLUTION OF SIGNALS

Solution 2.10

(a)

$$\begin{aligned} f(x,y)\delta(x-1,y-2) &= f(1,2)\delta(x-1,y-2) \\ &= (1+2^2)\delta(x-1,y-2) \\ &= 5\delta(x-1,y-2) \end{aligned}$$

(b)

$$\begin{aligned} f(x,y) * \delta(x-1,y-2) &= \int_{-\infty}^{\infty}\int_{-\infty}^{\infty} f(\xi,\eta)\delta(x-\xi-1,y-\eta-2)\, d\xi\, d\eta \\ &= \int_{-\infty}^{\infty}\int_{-\infty}^{\infty} f(x-1,y-2)\delta(x-\xi-1,y-\eta-2)\, d\xi\, d\eta \\ &= f(x-1,y-2)\int_{-\infty}^{\infty}\int_{-\infty}^{\infty} \delta(x-\xi-1,y-\eta-2)\, d\xi\, d\eta \\ &= f(x-1,y-2) \\ &= (x-1)+(y-2)^2 \end{aligned}$$

(c)

$$\begin{aligned} \int_{-\infty}^{\infty}\int_{-\infty}^{\infty} \delta(x-1,y-2)f(x,3)dx\,dy &\overset{①}{=} \int_{-\infty}^{\infty}\int_{-\infty}^{\infty} \delta(x-1,y-2)f(1,3)dx\,dy \\ &= \int_{-\infty}^{\infty}\int_{-\infty}^{\infty} \delta(x-1,y-2)(1+3^2)dx\,dy \\ &= 10\int_{-\infty}^{\infty}\int_{-\infty}^{\infty} \delta(x-1,y-2)dx\,dy \\ &\overset{②}{=} 10 \end{aligned}$$

Equality ① comes from the Eq. (2.7) in the text. Equality ② comes from the fact:

$$\int_{-\infty}^{\infty}\int_{-\infty}^{\infty} \delta(x-1,y-2)dx\,dy = \int_{-\infty}^{\infty}\int_{-\infty}^{\infty} \delta(x,y)dx\,dy = 1.$$

(d)

$$\begin{aligned}
\delta(x-1,y-2)*f(x+1,y+2) &\overset{③}{=} \int_{-\infty}^{\infty}\int_{-\infty}^{\infty}\delta(x-\xi-1,y-\eta-2)f(\xi+1,\eta+2)d\xi\,d\eta \\
&\overset{④}{=} \int_{-\infty}^{\infty}\int_{-\infty}^{\infty}\delta(x-\xi-1,y-\eta-2)f((x-1)+1,(y-2)+2)d\xi\,d\eta \\
&= \int_{-\infty}^{\infty}\int_{-\infty}^{\infty}\delta(x-\xi-1,y-\eta-2)f(x,y)d\xi\,d\eta \\
&\overset{⑤}{=} f(x,y)=x+y^2
\end{aligned}$$

③ comes from the definition of convolution; ④ comes from the Eq. (2.7) in text; ⑤ is the same as ② in part (c). Alternatively, by using the sifting property of $\delta(x,y)$ and defining $g(x,y)=f(x+1,y+2)$, we have

$$\begin{aligned}
\delta(x-1,y-2)*g(x,y) &= g(x-1,y-2) \\
&= f(x-1+1,y-2+2) \\
&= f(x,y) \\
&= x+y^2\,.
\end{aligned}$$

Solution 2.11

(a)

$$\begin{aligned}
f(x,y)*g(x,y) &= \int_{-\infty}^{\infty}\int_{-\infty}^{\infty} f(\xi,\eta)g(x-\xi,y-\eta)\,d\xi\,d\eta \\
&= \int_{-\infty}^{\infty}\int_{-\infty}^{\infty} f_1(\xi)f_2(\eta)g_1(x-\xi)g_2(y-\eta)\,d\xi\,d\eta \\
f(x,y)*g(x,y) &= \left(\int_{-\infty}^{\infty} f_1(\xi)g_1(x-\xi)\,d\xi\right)\left(\int_{-\infty}^{\infty} f_2(\eta)g_2(y-\eta)\,d\eta\right).
\end{aligned}$$

Hence, their convolution is also separable.

(b)

$$f(x,y)*g(x,y)=\left(f_1(x)*g_1(x)\right)\left(f_2(y)*g_2(y)\right).$$

Solution 2.12

$$\begin{aligned} g(x,y) &= f(x,y) * h(x,y) \\ &= \int_{-\infty}^{\infty}\int_{-\infty}^{\infty} f(x-\xi, y-\eta)h(\xi,\eta)d\xi d\eta \\ &= \int_{-\infty}^{\infty}\int_{-\infty}^{\infty} (x-\xi+y-\eta)\exp\{-(\xi^2+\eta^2)\}d\xi d\eta \\ &= (x+y)\int_{-\infty}^{\infty}\int_{-\infty}^{\infty} e^{-\xi^2-\eta^2}d\xi d\eta - \int_{-\infty}^{\infty}\int_{-\infty}^{\infty}\xi e^{-\xi^2-\eta^2}d\xi d\eta - \int_{-\infty}^{\infty}\int_{-\infty}^{\infty}\eta e^{-\xi^2-\eta^2}d\xi d\eta \\ &= (x+y)\left[\int_{-\infty}^{\infty} e^{-\xi^2}d\xi\right]^2 - \int_{-\infty}^{\infty} e^{-\eta^2}\left[\int_{-\infty}^{\infty}\xi e^{-\xi^2}d\xi\right]d\eta - \int_{-\infty}^{\infty} e^{-\xi^2}\left[\int_{-\infty}^{\infty}\eta e^{-\eta^2}d\eta\right]d\xi \\ &= \pi(x+y) \qquad \text{(S2.4)} \end{aligned}$$

We get (S2.4) by noticing that since ξ is an odd function and $e^{-\xi^2}$ is an even function, we must have

$$\int_{-\infty}^{\infty}\xi e^{-\xi^2}d\xi = 0\,.$$

Also,

$$\int_{-\infty}^{\infty} e^{-\xi^2}d\xi = \sqrt{\pi}\,.$$

FOURIER TRANSFORMS AND THEIR PROPERTIES

Solution 2.13

(a) See the solution to part **(b)** below. The Fourier transform is

$$\mathcal{F}_2\{\delta_s(x,y)\} = \delta_s(u,v)$$

(b)

$$\mathcal{F}_2\{\delta_s(x,y;\Delta x,\Delta y)\} = \int_{-\infty}^{\infty}\int_{-\infty}^{\infty}\delta_s(x,y;\Delta x,\Delta y)e^{-j2\pi(ux+vy)}\,dx\,dy$$

$\delta_s(x,y;\Delta x,\Delta y)$ is a periodic signal with periods Δx and Δy in x and y axes. Therefore it can be written as a Fourier series expansion. (Please review Oppenheim, Willsky, and Nawad, *Signals and Systems* for the definition of *Fourier series expansion* of periodic signals.)

$$\delta_s(x,y;\Delta x,\Delta y) = \sum_{m=-\infty}^{\infty}\sum_{n=-\infty}^{\infty} C_{mn}e^{j2\pi\left(\frac{mx}{\Delta x}+\frac{ny}{\Delta y}\right)}\,,$$

where

$$\begin{aligned} C_{mn} &= \frac{1}{\Delta x \Delta y} \int_{-\frac{\Delta x}{2}}^{\frac{\Delta x}{2}} \int_{-\frac{\Delta y}{2}}^{\frac{\Delta y}{2}} \delta_s(x, y; \Delta x, \Delta y) e^{-j2\pi\left(\frac{mx}{\Delta x} + \frac{ny}{\Delta y}\right)} \, dx \, dy \\ &= \frac{1}{\Delta x \Delta y} \int_{-\frac{\Delta x}{2}}^{\frac{\Delta x}{2}} \int_{-\frac{\Delta y}{2}}^{\frac{\Delta y}{2}} \sum_{m=-\infty}^{\infty} \sum_{n=-\infty}^{\infty} \delta(x - m\Delta x, y - n\Delta y) e^{-j2\pi\left(\frac{mx}{\Delta x} + \frac{ny}{\Delta y}\right)} \, dx \, dy. \end{aligned}$$

In the integration region $-\frac{\Delta x}{2} < x < \frac{\Delta x}{2}$ and $-\frac{\Delta y}{2} < y < \frac{\Delta y}{2}$ there is only one impulse corresponding to $m = 0$, $n = 0$. Therefore, we have

$$\begin{aligned} C_{mn} &= \frac{1}{\Delta x \Delta y} \int_{-\frac{\Delta x}{2}}^{\frac{\Delta x}{2}} \int_{-\frac{\Delta y}{2}}^{\frac{\Delta y}{2}} \delta(x, y) e^{-j2\pi\left(\frac{0 \cdot x}{\Delta x} + \frac{0 \cdot y}{\Delta y}\right)} \, dx \, dy \\ &= \frac{1}{\Delta x \Delta y}. \end{aligned}$$

We have:

$$\delta_s(x, y; \Delta x, \Delta y) = \frac{1}{\Delta x \Delta y} \sum_{m=-\infty}^{\infty} \sum_{n=-\infty}^{\infty} e^{j2\pi\left(\frac{mx}{\Delta x} + \frac{ny}{\Delta y}\right)}.$$

Therefore,

$$\begin{aligned} \mathcal{F}_2\{\delta_s\} &= \int_{-\infty}^{\infty} \int_{-\infty}^{\infty} \delta_s(x, y; \Delta x, \Delta y) e^{-j2\pi(ux+vy)} dx \, dy \\ &= \int_{-\infty}^{\infty} \int_{-\infty}^{\infty} \frac{1}{\Delta x \Delta y} \sum_{m=-\infty}^{\infty} \sum_{n=-\infty}^{\infty} e^{j2\pi\left(\frac{mx}{\Delta x} + \frac{ny}{\Delta y}\right)} e^{-j2\pi(ux+vy)} \, dx \, dy \\ &= \sum_{m=-\infty}^{\infty} \sum_{n=-\infty}^{\infty} \frac{1}{\Delta x \Delta y} \int_{-\infty}^{\infty} \int_{-\infty}^{\infty} e^{j2\pi\left(\frac{mx}{\Delta x} + \frac{ny}{\Delta y}\right)} e^{-j2\pi(ux+vy)} \, dx \, dy \\ &= \sum_{m=-\infty}^{\infty} \sum_{n=-\infty}^{\infty} \frac{1}{\Delta x \Delta y} \mathcal{F}_2 \left\{ e^{j2\pi\left(\frac{mx}{\Delta x} + \frac{ny}{\Delta y}\right)} \right\} \\ &= \sum_{m=-\infty}^{\infty} \sum_{n=-\infty}^{\infty} \frac{1}{\Delta x \Delta y} \delta\left(u - \frac{m}{\Delta x}, v - \frac{n}{\Delta y}\right) \\ &\overset{⑤}{=} \sum_{m=-\infty}^{\infty} \sum_{n=-\infty}^{\infty} \frac{1}{\Delta x \Delta y} \cdot \Delta x \Delta y \delta(u\Delta x - m, v\Delta y - n) \\ \mathcal{F}_2\{\delta_s\} &= \delta_s(u\Delta x, v\Delta y) \end{aligned}$$

Equality ⑤ comes from the property $\delta(ax) = \frac{1}{|a|}\delta(x)$.

(c)

$$\begin{aligned}
\mathcal{F}_2\{s(x,y)\} &= \int_{-\infty}^{\infty}\int_{-\infty}^{\infty} s(x,y)e^{-j2\pi(ux+vy)}\,dx\,dy \\
&= \int_{-\infty}^{\infty}\int_{-\infty}^{\infty} \sin[2\pi(u_0x+v_0y)]e^{-j2\pi(ux+vy)}\,dx\,dy \\
&= \int_{-\infty}^{\infty}\int_{-\infty}^{\infty} \frac{1}{2j}\left[e^{j2\pi(u_0x+v_0y)} - e^{-j2\pi(u_0x+v_0y)}\right]e^{-j2\pi(ux+vy)}\,dx\,dy \\
&= \frac{1}{2j}\left[\int_{-\infty}^{\infty}\int_{-\infty}^{\infty} e^{j2\pi(u_0x+v_0y)}e^{-j2\pi(ux+vy)}\,dx\,dy\right. \\
&\qquad \left. -\int_{-\infty}^{\infty}\int_{-\infty}^{\infty} e^{-j2\pi(u_0x+v_0y)}e^{-j2\pi(ux+vy)}\,dx\,dy\right] \\
&= \frac{1}{2j}\left[\int_{-\infty}^{\infty}\int_{-\infty}^{\infty} e^{-j2\pi[(u-u_0)x+(v-v_0)y]}\,dx\,dy\right. \\
&\qquad \left. -\int_{-\infty}^{\infty}\int_{-\infty}^{\infty} e^{-j2\pi[(u+u_0)x+(v+v_0)y]}\,dx\,dy\right] \\
\mathcal{F}_2\{s(x,y)\} &= \frac{1}{2j}\left[\delta(u-u_0,v-v_0) - \delta(u+u_0,v+v_0)\right].
\end{aligned}$$

We used Eq. (2.69) twice to get the last equality.

(d)

$$\begin{aligned}
\mathcal{F}_2(c)(u,v) &= \int_{-\infty}^{\infty}\int_{-\infty}^{\infty} c(x,y)e^{-j2\pi(ux+vy)}\,dx\,dy \\
&= \int_{-\infty}^{\infty}\int_{-\infty}^{\infty} \cos[2\pi(u_0x+v_0y)]e^{-j2\pi(ux+vy)}\,dx\,dy \\
&= \int_{-\infty}^{\infty}\int_{-\infty}^{\infty} \frac{1}{2}[e^{j2\pi(u_0x+v_0y)} + e^{-j2\pi(u_0x+v_0y)}]e^{-j2\pi(ux+vy)}\,dx\,dy \\
&= \frac{1}{2}\left[\int_{-\infty}^{\infty}\int_{-\infty}^{\infty} e^{j2\pi(u_0x+v_0y)}e^{-j2\pi(ux+vy)}\,dx\,dy\right. \\
&\qquad \left. +\int_{-\infty}^{\infty}\int_{-\infty}^{\infty} e^{-j2\pi(u_0x+v_0y)}e^{-j2\pi(ux+vy)}\,dx\,dy\right] \\
&= \frac{1}{2}\left[\int_{-\infty}^{\infty}\int_{-\infty}^{\infty} e^{-j2\pi[(u-u_0)x+(v-v_0)y]}\,dx\,dy\right. \\
&\qquad \left. +\int_{-\infty}^{\infty}\int_{-\infty}^{\infty} e^{-j2\pi[(u+u_0)x+(v+v_0)y]}\,dx\,dy\right] \\
\mathcal{F}_2(c)(u,v) &= \frac{1}{2}[\delta(u-u_0,v-v_0) + \delta(u+u_0,v+v_0)].
\end{aligned}$$

We used Eq. (2.69) twice to get the last equality.

(e)

$$\begin{aligned}
\mathcal{F}_2(f)(u,v) &= \int_{-\infty}^{\infty}\int_{-\infty}^{\infty} f(x,y)e^{-j2\pi(ux+vy)}\,dx\,dy \\
&= \int_{-\infty}^{\infty}\int_{-\infty}^{\infty} \frac{1}{2\pi\sigma^2}e^{-(x^2+y^2)/2\sigma^2}e^{-j2\pi(ux+vy)}\,dx\,dy \\
&= \int_{-\infty}^{\infty}\int_{-\infty}^{\infty} \frac{1}{2\pi\sigma^2}e^{-(x^2+j4\pi\sigma^2ux)/2\sigma^2}e^{-(y^2+j4\pi\sigma^2vy)/2\sigma^2}\,dx\,dy \\
&= \left[\int_{-\infty}^{\infty} \frac{1}{\sqrt{2\pi\sigma^2}}e^{-(x^2+j4\pi\sigma^2ux)/2\sigma^2}\,dx\right]\left[\int_{-\infty}^{\infty} \frac{1}{\sqrt{2\pi\sigma^2}}e^{-(y^2+j4\pi\sigma^2vy)/2\sigma^2}\,dy\right] \\
&= \left[\int_{-\infty}^{\infty} \frac{1}{\sqrt{2\pi\sigma^2}}e^{-(x+j2\pi\sigma^2u)^2/2\sigma^2}e^{(j2\pi\sigma^2u)^2/2\sigma^2}\,dx\right]\cdot \\
&\quad \left[\int_{-\infty}^{\infty} \frac{1}{\sqrt{2\pi\sigma^2}}e^{-(y+j2\pi\sigma^2v)^2/2\sigma^2}e^{(j2\pi\sigma^2v)^2/2\sigma^2}\,dy\right] \\
&= \left[e^{-2\pi^2\sigma^2u^2}\int_{-\infty}^{\infty} \frac{1}{\sqrt{2\pi\sigma^2}}e^{-(x+j2\pi\sigma^2u)^2/2\sigma^2}\,dx\right]\cdot \\
&\quad \left[e^{-2\pi^2\sigma^2v^2}\int_{-\infty}^{\infty} \frac{1}{\sqrt{2\pi\sigma^2}}e^{-(y+j2\pi\sigma^2v)^2/2\sigma^2}\,dy\right] \\
&= e^{-2\pi^2\sigma^2u^2}\cdot e^{-2\pi^2\sigma^2v^2} \\
\mathcal{F}_2(f)(u,v) &= e^{-2\pi^2\sigma^2(u^2+v^2)}.
\end{aligned}$$

Solution 2.14

The Fourier transform of $f(x)$ is

$$F(u) = \int_{-\infty}^{\infty} f(x)e^{-j2\pi ux}dx.$$

(a) Assuming $f(x)$ is real and $f(x) = f(-x)$,

$$\begin{aligned}
F^*(u) &= \int_{-\infty}^{\infty} \left[f(x)e^{-j2\pi ux}\right]^* dx \\
&= \int_{-\infty}^{\infty} f^*(x)e^{j2\pi ux}dx \\
&= \int_{-\infty}^{\infty} f^*(-\xi)e^{-j2\pi u\xi}d\xi, \text{ let } \xi = -x \\
&= \int_{-\infty}^{\infty} f(\xi)e^{-j2\pi u\xi}d\xi, \text{ since } f(-x) = f(x) \text{ and } f(x) \text{ is real} \\
&= F(u)\,.
\end{aligned}$$

(b) Similarly, assuming $f(x)$ is real and $f(x) = -f(-x)$,

$$\begin{aligned} F^*(u) &= \int_{-\infty}^{\infty} f^*(-\xi) e^{-j2\pi u\xi} d\xi \\ &= \int_{-\infty}^{\infty} -f(\xi) e^{-j2\pi u\xi} d\xi, \text{ since } f(-x) = -f(x) \\ &= -F(u)\,. \end{aligned}$$

Solution 2.15

In deriving the symmetric property $F^*(u) = F(u)$, we used the fact that $f(x)$ is real. If $f(x)$ is a complex signal, we have $f^*(-\xi) = f^*(\xi)$ instead of $f^*(-\xi) = f(\xi)$. Therefore,

$$\begin{aligned} F^*(u) &= \int_{-\infty}^{\infty} \left[f(x) e^{-j2\pi ux}\right]^* dx \\ &= \int_{-\infty}^{\infty} f^*(-\xi) e^{-j2\pi u\xi} d\xi, \text{ let } \xi = -x \\ &= \int_{-\infty}^{\infty} f^*(\xi) e^{-j2\pi u\xi} d\xi, \\ &= \mathcal{F}\left\{f^*(x)\right\} \end{aligned}$$

Solution 2.16

(a) Conjugate property: $\mathcal{F}_2(f^*)(u,v) = F^*(-u,-v)$.

$$\begin{aligned} \mathcal{F}_2(f^*)(u,v) &= \int_{-\infty}^{\infty}\int_{-\infty}^{\infty} f^*(x,y) e^{-j2\pi(ux+vy)}\, dx\, dy \\ &= \left[\int_{-\infty}^{\infty}\int_{-\infty}^{\infty} f(x,y) e^{j2\pi(ux+vy)}\, dx\, dy\right]^* \\ &= \left[\int_{-\infty}^{\infty}\int_{-\infty}^{\infty} f(x,y) e^{-j2\pi[(-u)x+(-v)y]}\, dx\, dy\right]^* \\ &= \left[F(-u,-v)\right]^* \\ &= F^*(-u,-v)\,. \end{aligned}$$

Conjugate symmetry property: If $f(x,y)$ is real, $F(u,v) = F^*(-u,-v)$. Since $f(x,y)$ is real, $f^*(x,y) = f(x,y)$. Therefore,

$$F^*(-u,-v) = \mathcal{F}_2\{f^*(x,y)\} = \mathcal{F}_2\{f(x,y)\} = F(u,v)\,.$$

(b) Scaling property: $\mathcal{F}_2(f^{ab})(u,v) = \frac{1}{|ab|}\mathcal{F}_2(f)\left(\frac{u}{a}, \frac{v}{b}\right)$.

$$\begin{aligned}
\mathcal{F}_2(f^{ab})(u,v) &= \int_{-\infty}^{\infty}\int_{-\infty}^{\infty} f(ax,by)e^{-j2\pi(ux+vy)}\,dx\,dy \\
&= \int_{-\infty}^{\infty}\int_{-\infty}^{\infty} f(ax,by)e^{-j2\pi[u(ax)/a+v(by)/b]}\frac{1}{ab}\,d(ax)\,d(by) \\
&= \frac{1}{|ab|}\int_{-\infty}^{\infty}\int_{-\infty}^{\infty} f(p,q)e^{-j2\pi[(u/a)p+(v/b)q]}\,dp\,dq \\
&= \frac{1}{|ab|}\mathcal{F}_2(f)\left(\frac{u}{a}, \frac{v}{b}\right).
\end{aligned}$$

(c) Convolution property: $\mathcal{F}_2(f*g)(u,v) = \mathcal{F}_2(g)(u,v)\cdot\mathcal{F}_2(f)(u,v)$.

$$\mathcal{F}_2(f*g)(u,v) = \int_{-\infty}^{\infty}\int_{-\infty}^{\infty}\left[\int_{-\infty}^{\infty}\int_{-\infty}^{\infty} f(\xi,\eta)g(x-\xi,y-\eta)d\xi\,d\eta\right]e^{-j2\pi(ux+vy)}dx\,dy.$$

Interchange the order of integration to yield

$$\begin{aligned}
\mathcal{F}_2(f*g)(u,v) &= \int_{-\infty}^{\infty}\int_{-\infty}^{\infty} f(\xi,\eta)\left[\int_{-\infty}^{\infty}\int_{-\infty}^{\infty} g(x-\xi,y-\eta)e^{-j2\pi(ux+vy)}dx\,dy\right]d\xi\,d\eta \\
&= \int_{-\infty}^{\infty}\int_{-\infty}^{\infty} f(\xi,\eta)\left[\int_{-\infty}^{\infty}\int_{-\infty}^{\infty} g(x-\xi,y-\eta)\right. \\
&\qquad \left. e^{-j2\pi[u(x-\xi)+v(y-\eta)]}e^{-j2\pi(u\xi+v\eta)}dx\,dy\right]d\xi\,d\eta \\
&= \int_{-\infty}^{\infty}\int_{-\infty}^{\infty} f(\xi,\eta)e^{-j2\pi(u\xi+v\eta)}\left[\int_{-\infty}^{\infty}\int_{-\infty}^{\infty} g(x-\xi,y-\eta)\right. \\
&\qquad \left. e^{-j2\pi[u(x-\xi)+v(y-\eta)]}dx\,dy\right]d\xi\,d\eta \\
&= \int_{-\infty}^{\infty}\int_{-\infty}^{\infty} f(\xi,\eta)e^{-j2\pi(u\xi+v\eta)}\left[\int_{-\infty}^{\infty}\int_{-\infty}^{\infty} g(p,q)e^{-j2\pi[up+vq]}dp\,dq\right]d\xi\,d\eta \\
&= \int_{-\infty}^{\infty}\int_{-\infty}^{\infty} f(\xi,\eta)e^{-j2\pi(u\xi+v\eta)}\mathcal{F}_2(g)(u,v)\,d\xi\,d\eta \\
&= \mathcal{F}_2(g)(u,v)\cdot\int_{-\infty}^{\infty}\int_{-\infty}^{\infty} f(\xi,\eta)e^{-j2\pi(u\xi+v\eta)}\,d\xi\,d\eta \\
\mathcal{F}_2(f*g)(u,v) &= \mathcal{F}_2(g)(u,v)\cdot\mathcal{F}_2(f)(u,v).
\end{aligned}$$

(d) Product property: $\mathcal{F}_2(fg)(u,v) = F(u,v) * G(u,v)$.

$$\begin{aligned}
\mathcal{F}_2(fg)(u,v) &= \int_{-\infty}^{\infty}\int_{-\infty}^{\infty} f(x,y)g(x,y)e^{-j2\pi(ux+vy)}\,dx\,dy \\
&= \int_{-\infty}^{\infty}\int_{-\infty}^{\infty}\left[\int_{-\infty}^{\infty}\int_{-\infty}^{\infty} G(\xi,\eta)e^{j2\pi(x\xi+y\eta)}\,d\xi\,d\eta\right] f(x,y)e^{-j2\pi(ux+vy)}\,dx\,dy \\
&= \int_{-\infty}^{\infty}\int_{-\infty}^{\infty} G(\xi,\eta)\left[\int_{-\infty}^{\infty}\int_{-\infty}^{\infty} f(x,y)e^{j2\pi(x\xi+y\eta)}e^{-j2\pi(ux+vy)}\,dxdy\right] d\xi\,d\eta \\
&= \int_{-\infty}^{\infty}\int_{-\infty}^{\infty} G(\xi,\eta)\left[\int_{-\infty}^{\infty}\int_{-\infty}^{\infty} f(x,y)e^{-j2\pi[(u-\xi)x+(v-\eta)y]}\,dx\,dy\right] d\xi\,d\eta \\
&= \int_{-\infty}^{\infty}\int_{-\infty}^{\infty} G(\xi,\eta)F(u-\xi,v-\eta)\,d\xi\,d\eta \\
&= F(u,v) * G(u,v).
\end{aligned}$$

Solution 2.17

Since both the rect and sinc functions are separable, it is sufficient to show the result for 1-D rect and sinc functions. A 1-D rect function is

$$\mathrm{rect}(x) = \begin{cases} 1, & \text{for } |x| < \dfrac{1}{2} \\ \\ 0, & \text{for } |x| > \dfrac{1}{2} \end{cases}$$

$$\begin{aligned}
\mathcal{F}\{\mathrm{rect}(x)\} &= \int_{-\infty}^{\infty} \mathrm{rect}(x)e^{-j2\pi ux}dx \\
&= \int_{-1/2}^{1/2} e^{-j2\pi ux}dx \\
&= \int_{-1/2}^{1/2} \cos(2\pi ux)dx - j\int_{-1/2}^{1/2} \sin(2\pi ux)dx, \quad e^{j\theta} = \cos\theta + j\sin\theta \\
&= \int_{-1/2}^{1/2} \cos(2\pi ux)dx \\
&= \frac{\sin(\pi u)}{\pi u} \\
&= \mathrm{sinc}(u)\,.
\end{aligned}$$

Therefore, we have $\mathcal{F}\{\mathrm{sinc}(x)\} = \mathrm{rect}(u)$. Using Parseval's Theorem, we have

$$\begin{aligned}
E_\infty &= \int_{-\infty}^{\infty}\int_{-\infty}^{\infty} \|\,\mathrm{rect}(x,y)\|^2 dx\,dy \\
&= \int_{-1/2}^{1/2}\int_{-1/2}^{1/2} dx\,dy \\
&= 1
\end{aligned}$$

For the sinc function, $P_\infty = 0$, because E_∞ is finite.

Solution 2.18

Since the signal is separable, we have

$$\begin{aligned}\mathcal{F}[f(x,y)] &= \mathcal{F}_{1\mathrm{D}}[\sin(2\pi ax)]\mathcal{F}_{1\mathrm{D}}[\cos(2\pi by)]\,,\\ \mathcal{F}_{1\mathrm{D}}[\sin(2\pi ax)] &= \frac{1}{2j}\left[\delta\left(u-a\right)-\delta\left(u+a\right)\right]\,,\\ \mathcal{F}_{1\mathrm{D}}[\cos(2\pi by)] &= \frac{1}{2}\left[\delta\left(v-b\right)+\delta\left(v+b\right)\right]\,.\end{aligned}$$

So,

$$\mathcal{F}[f(x,y)] = \frac{1}{4j}\left[\delta(u-a)\delta(v-b)-\delta(u+a)\delta(v-b)+\delta(u-a)\delta(v+b)-\delta(u+a)\delta(v+b)\right]\,.$$

Now we need to show that $\delta(u)\delta(v) = \delta(u,v)$ (in a generalized way):

$$\delta(u)\delta(v) = 0, \quad \text{for } u \neq 0, \text{ or } v \neq 0$$

Therefore,

$$\int_{-\infty}^{\infty}\int_{-\infty}^{\infty} f(u,v)\delta(u)\delta(v)du\,dv = \int_{-\infty}^{\infty}\left[\int_{-\infty}^{\infty} f(u,v)\delta(u)du\right]\delta(v)dv = \int_{-\infty}^{\infty} f(0,v)\delta(v)dv = f(0,0)\,.$$

Based on the argument above $\delta(u)\delta(v) = \delta(u,v)$, and

$$\mathcal{F}[f(x,y)] = \frac{1}{4j}\left[\delta(u-a,v-b)-\delta(u+a,v-b)+\delta(u-a,v+b)-\delta(u+a,v+b)\right]\,.$$

The above solution can also be obtained by using the relationship:

$$\sin(2\pi ax)\cos(2\pi by) = \frac{1}{2}\left[\sin(2\pi(ax-by))+\sin(2\pi(ax+by))\right]\,.$$

Solution 2.19

A function $f(x,y)$ can be expressed in polar coordinates as:

$$f(x,y) = f(r\cos\theta, r\sin\theta) = f_p(r,\theta)\,.$$

If it is circularly symmetric, we have $f_p(r,\theta)$ is constant for fixed r. The Fourier transform of $f(x,y)$ is defined as:

$$\begin{aligned}F(u,v) &= \int_{-\infty}^{\infty}\int_{-\infty}^{\infty} f(x,y)e^{-j2\pi(ux+vy)}dx\,dy\\ &= \int_0^{\infty}\int_0^{2\pi} f_p(r,\theta)e^{-j2\pi(ur\cos\theta+vr\sin\theta)}r\,dr\,d\theta\\ &= \int_0^{\infty} f_p(r,\theta)\left[\int_0^{2\pi} e^{-j2\pi(ur\cos\theta+vr\sin\theta)}d\theta\right]r\,dr\,.\end{aligned}$$

Letting $u = q\cos\phi$ and $v = q\sin\phi$, the above equation becomes:

$$F(u,v) = \int_0^\infty f_p(r,\theta)\left[\int_0^{2\pi} e^{-j2\pi qr\cos(\phi-\theta)}d\theta\right] r\,dr\,.$$

Since $F(u,v)$ is also circularly symmetric, it can be written as $F_q(q,\phi)$ and is constant for fixed q. In particular, $F_q(q,\phi) = F_q(q,\pi/2)$, and therefore

$$F_q(q,\phi) = F_q(q,\pi/2) = \int_0^\infty f_p(r,\theta)\left[\int_0^{2\pi} e^{-j2\pi qr\sin\theta}d\theta\right] r\,dr\,.$$

Now we will show that (2.108) holds.

$$\begin{aligned}\int_0^{2\pi} e^{-j2\pi qr\sin\theta}d\theta &= \int_0^{2\pi}\cos(2\pi qr\sin\theta)d\theta - j\int_0^{2\pi}\sin(2\pi qr\sin\theta)\\ &\overset{①}{=} 2\int_0^{\pi}\cos(2\pi qr\sin\theta)d\theta\\ &= 2\pi J_0(2\pi qr)\,.\end{aligned}$$

Equality ① holds because $\cos(-\theta) = \cos(\theta)$, and $\sin(\theta) = -\sin(\theta)$.

Based on the above derivation, we have proven (2.108).

Solution 2.20

The unit disk is expressed as $f(r) = \mathrm{rect}(r)$ and its Hankel transform is

$$\begin{aligned}F(q) &= 2\pi\int_0^\infty f(r)J_0(2\pi qr)r\,dr\\ &= 2\pi\int_0^\infty \mathrm{rect}(r)J_0(2\pi qr)r\,dr\\ &= 2\pi\int_0^{1/2} J_0(2\pi qr)r\,dr\,.\end{aligned}$$

Now apply the following change of variables

$$\begin{aligned}s &= 2\pi qr\,,\\ r &= \frac{s}{2\pi q}\,,\\ dr &= \frac{ds}{2\pi q}\,,\end{aligned}$$

to yield

$$F(q) = \frac{1}{2\pi q^2}\int_0^{\pi q} J_0(s)s\,ds\,.$$

From mathematical tables, we note that

$$\int_0^x J_0(\epsilon)\epsilon d\epsilon \quad = \quad xJ_1(x)\,.$$

Therefore,

$$\begin{aligned} F(q) &= \frac{J_1(\pi q)}{2q} \\ &= \text{jinc}(q)\,. \end{aligned}$$

TRANSFER FUNCTION

Solution 2.21

(a) The impulse response function is shown in Figure S2.1.

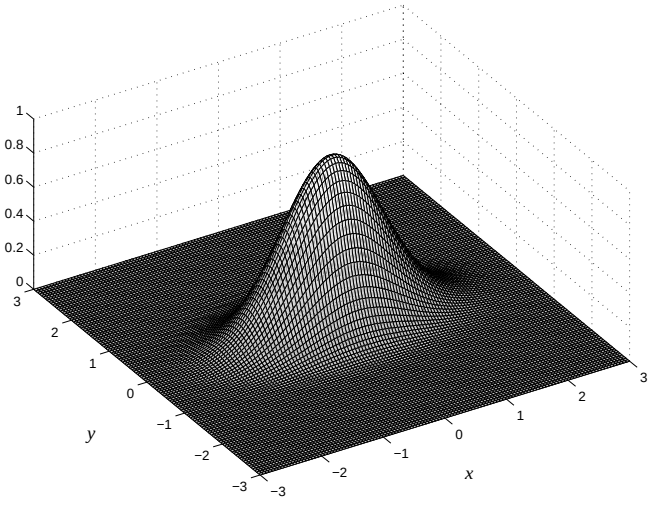

Figure S2.1 Impulse response function of the system. See Problem 2.21(a).

(b) The transfer function of the function is the Fourier transform of the impulse response function:

$$\begin{aligned} H(u,v) &= \mathcal{F}\{h(x,y)\} \\ &= \mathcal{F}\{e^{-\pi x^2}\}\mathcal{F}\{e^{-\pi y^2/4}\}\,, \text{ since } h(x,y) \text{ is separable} \\ &= 2e^{-\pi(u^2+4v^2)}\,. \end{aligned}$$

Solution 2.22

(a) The 1D profile of the bar phantom is:

$$f(x) = \begin{cases} 1, & \frac{k-1}{2}w \le x \le \frac{k+1}{2}w \\ 0, & \frac{k+1}{2}w \le x \le \frac{k+3}{2}w \end{cases},$$

where k is an integer. The response of the system to the bar phantom is:

$$g(x) = f(x) * l(x) = \int_{-\infty}^{\infty} f(x-\xi)l(\xi)d\xi\,.$$

At the center of the bar, we have

$$\begin{aligned} g(0) &= \int_{-\infty}^{\infty} f(0-\xi)l(\xi)d\xi \\ &= \int_{-w/2}^{w/2} \cos(\alpha\xi)d\xi \\ &= \frac{2}{\alpha}\sin\left(\frac{\alpha w}{2}\right). \end{aligned}$$

At the point halfway between two adjacent bars, we have

$$\begin{aligned} g(w) &= \int_{-\infty}^{\infty} f(w-\xi)l(\xi)d\xi \\ &= \int_{w-\pi/2\alpha}^{w/2} \cos(\alpha\xi)d\xi + \int_{3w/2}^{w+\pi/2\alpha} \cos(\alpha\xi)d\xi \\ &= 2\int_{w-\pi/2\alpha}^{w/2} \cos(\alpha\xi)d\xi \\ &= \frac{2}{\alpha}\left[\sin\left(\frac{\alpha w}{2}\right) - \sin\left(\alpha w - \frac{\pi}{2}\right)\right]. \end{aligned}$$

(b) From the line spread function alone, we cannot tell whether the system is isotropic. The line spread function is a "projection" of the PSF. During the projection, the information along the y direction is lost.

(c) Since the system is separable with $h(x,y) = h_{1\mathrm{D}}(x)h_{1\mathrm{D}}(y)$, we know that

$$\begin{aligned} l(x) &= \int_{-\infty}^{\infty} h(x,y)dy \\ &= h_{1\mathrm{D}}(x)\int_{-\infty}^{\infty} h_{1\mathrm{D}}(y)dy\,. \end{aligned}$$

Therefore $h_{1\mathrm{D}}(x) = cl(x)$ where $1/c = \int_{-\infty}^{\infty} h_{1\mathrm{D}}(y)dy$. Hence,

$$\begin{aligned} 1/c &= \int_{-\infty}^{\infty} cl(y)dy\,, \\ 1/c^2 &= \int_{-\pi/2\alpha}^{\pi/2\alpha} \cos(\alpha y)dy\,, \\ 1/c^2 &= 2/\alpha\,. \end{aligned}$$

Therefore,

$$h(x,y) = \begin{cases} \dfrac{\alpha}{2}\cos(\alpha x)\cos(\alpha y) & |\alpha x| \le \pi/2 \text{ and } |\alpha y| \le \pi/2 \\ 0 & \text{otherwise} \end{cases}.$$

The transfer function is

$$\begin{aligned} H(u,v) &= \mathcal{F}_{2\mathrm{D}}\{h(x,y)\} \\ &= \int_{-\infty}^{\infty}\left[\int_{-\infty}^{\infty} h(x,y)e^{j2\pi ux}dx\right]e^{j2\pi uy}dy \\ &= \int_{-\infty}^{\infty}\left[\int_{-\infty}^{\infty} h_{1\mathrm{D}}(x)h_{1\mathrm{D}}(y)e^{j2\pi ux}dx\right]e^{j2\pi uy}dy \\ &= \int_{-\infty}^{\infty}\left[\int_{-\infty}^{\infty} h_{1\mathrm{D}}(x)e^{j2\pi ux}dx\right]h_{1\mathrm{D}}(y)e^{j2\pi uy}dy \\ &= \int_{-\infty}^{\infty} h_{1\mathrm{D}}(x)e^{j2\pi ux}dx\int_{-\infty}^{\infty} h_{1\mathrm{D}}(y)e^{j2\pi uy}dy \\ &= H_{1\mathrm{D}}(u)H_{1\mathrm{D}}(v)\,, \end{aligned}$$

which is also separable with $H(u,v) = H_{1\mathrm{D}}(u)H_{1\mathrm{D}}(v)$. We have

$$\begin{aligned} H_{1\mathrm{D}} &= \sqrt{\frac{\alpha}{2}}\mathcal{F}_{1\mathrm{D}}\{l(x)\} \\ &= \sqrt{\frac{\alpha}{2}}\mathcal{F}_{1\mathrm{D}}\{\cos(\alpha x)\} * \mathcal{F}_{1\mathrm{D}}\left\{\mathrm{rect}\left(\frac{\alpha x}{\pi}\right)\right\} \\ &= \sqrt{\frac{\pi}{2}}\left[\mathrm{sinc}\left(\frac{\pi}{\alpha}(u-\alpha/2\pi)\right) + \mathrm{sinc}\left(\frac{\pi}{\alpha}(u+\alpha/2\pi)\right)\right]. \end{aligned}$$

Therefore, the transfer function is

$$\begin{aligned} H(u,v) = \frac{\pi}{2}&\left[\mathrm{sinc}\left(\frac{\pi}{\alpha}(u-\alpha/2\pi)\right) + \mathrm{sinc}\left(\frac{\pi}{\alpha}(u+\alpha/2\pi)\right)\right] \\ &\left[\mathrm{sinc}\left(\frac{\pi}{\alpha}(v-\alpha/2\pi)\right) + \mathrm{sinc}\left(\frac{\pi}{\alpha}(v+\alpha/2\pi)\right)\right]. \end{aligned}$$

APPLICATIONS, EXTENSIONS AND ADVANCED TOPICS

Solution 2.23

(a) The system is separable because $h(x,y) = e^{-(|x|+|y|)} = e^{-|x|}e^{-|y|}$.

(b) The system is not isotropic since $h(x,y)$ is not a function of $r = \sqrt{x^2+y^2}$.

Additional comments: An easy check is to plug in $x = 1$, $y = 1$ and $x = 0$, $y = \sqrt{2}$ into $h(x,y)$. By noticing that $h(1,1) \neq h(0,\sqrt{2})$, we can conclude that $h(x,y)$ is not rotationally invariant, and hence not isotropic.

Isotropy is rotational symmetry around the origin, not just symmetry about a few axes, e.g., the x- and y-axes. $h(x,y) = e^{-(|x|+|y|)}$ is symmetric about a few lines, but it is not rotationally invariant.

When we studied the properties of Fourier transform, we learned that if a signal is isotropic then its Fourier transform has a certain symmetry. Note that the symmetry of the Fourier transform is only a necessary, but not sufficient, condition for the signal to be isotropic.

(c) The response is

$$\begin{aligned}
g(x,y) &= h(x,y) * f(x,y) \\
&= \int_{-\infty}^{\infty}\int_{-\infty}^{\infty} h(\xi,\eta) f(x-\xi, y-\eta) d\xi\, d\eta \\
&= \int_{-\infty}^{\infty}\int_{-\infty}^{\infty} e^{-(|\xi|+|\eta|)} \delta(x-\xi) d\xi\, d\eta \\
&= \int_{-\infty}^{\infty} e^{-(|x|+|\eta|)} d\eta \\
&= e^{-|x|}\int_{-\infty}^{\infty} e^{-|\eta|} d\eta \\
&= e^{-|x|}\left[\int_{-\infty}^{0} e^{\eta} d\eta + \int_{0}^{\infty} e^{-\eta} d\eta\right] \\
&= 2e^{-|x|}\,.
\end{aligned}$$

(d) The response is

$$\begin{aligned}
g(x,y) &= h(x,y) * f(x,y) \\
&= \int_{-\infty}^{\infty}\int_{-\infty}^{\infty} h(\xi,\eta) f(x-\xi, y-\eta) d\xi\, d\eta \\
&= \int_{-\infty}^{\infty}\int_{-\infty}^{\infty} e^{-(|\xi|+|\eta|)} \delta(x-\xi-y+\eta) d\xi\, d\eta \\
&= \int_{-\infty}^{\infty} e^{-|\eta|}\left[\int_{-\infty}^{\infty} e^{-|\xi|}\delta(x-\xi-y+\eta) d\xi\right] d\eta \\
&= \int_{-\infty}^{\infty} e^{-|\eta|} e^{-|x-y+\eta|} d\eta\,.
\end{aligned}$$

1. Now assume $x - y < 0$, then $x - y + \eta < \eta$. The range of integration in the above can be divided into three parts (see Fig. S2.2):

I. $\eta \in (-\infty, 0)$. In this interval, $x - y + \eta < \eta < 0$. $|\eta| = -\eta$, $|x - y + \eta| = -(x - y + \eta)$;

II. $\eta \in [0, -(x-y))$. In this interval, $x - y + \eta < 0 \leq \eta$. $|\eta| = \eta$, $|x - y + \eta| = -(x - y + \eta)$;

III. $\eta \in [-(x-y), \infty)$. In this interval, $0 \leq x - y + \eta < \eta$. $|\eta| = \eta$, $|x - y + \eta| = x - y + \eta$.

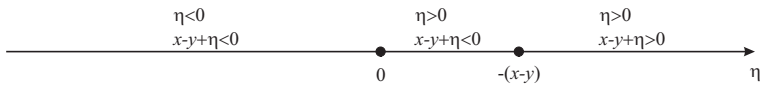

Figure S2.2 For $x - y < 0$ the integration interval $(-\infty, \infty)$ can be partitioned into three segments. See Problem 2.23(d).

Based on the above analysis, we have:

$$\begin{aligned} g(x,y) &= \int_{-\infty}^{\infty} e^{-|\eta|} e^{-|x-y+\eta|} d\eta \\ &= \int_{-\infty}^{0} e^{-(|\eta|+|x-y+\eta|)} d\eta + \int_{0}^{-(x-y)} e^{-(|\eta|+|x-y+\eta|)} + \int_{-(x-y)}^{\infty} e^{-(|\eta|+|x-y+\eta|)} \\ &= \int_{-\infty}^{0} e^{x-y+2\eta} d\eta + \int_{0}^{-(x-y)} e^{x-y} d\eta + \int_{-(x-y)}^{\infty} e^{-(x-y+2\eta)} d\eta \\ &= \frac{1}{2} e^{x-y} - (x-y) e^{x-y} + \frac{1}{2} e^{x-y} \\ &= [1-(x-y)] e^{x-y} . \end{aligned}$$

2. For $x - y \geq 0$, $\eta < x - y + \eta$. The range of integration in the above can be divided into three parts (see Fig. S2.3):

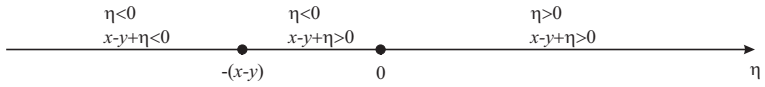

Figure S2.3 For $x - y > 0$ the integration interval $(-\infty, \infty)$ can be partitioned into three segments. See Problem 2.23(d).

I. $\eta \in (-\infty, -(x-y))$. In this interval, $\eta < x - y + \eta < 0$. $|\eta| = -\eta$, $|x - y + \eta| = -(x - y + \eta)$;
II. $\eta \in [-(x-y), 0)$. In this interval, $\eta < 0 \leq x - y + \eta$. $|\eta| = -\eta$, $|x - y + \eta| = x - y + \eta$;
III. $\eta \in [0, \infty)$. In this interval, $0 \leq \eta < x - y + \eta$. $|\eta| = \eta$, $|x - y + \eta| = x - y + \eta$.
Based on the above analysis, we have:

$$\begin{aligned} g(x,y) &= \int_{-\infty}^{\infty} e^{-|\eta|} e^{-|x-y+\eta|} d\eta \\ &= \int_{-\infty}^{-(x-y)} e^{-(|\eta|+|x-y+\eta|)} d\eta + \int_{-(x-y)}^{0} e^{-(|\eta|+|x-y+\eta|)} + \int_{0}^{\infty} e^{-(|\eta|+|x-y+\eta|)} \\ &= \int_{-\infty}^{-(x-y)} e^{x-y+2\eta} d\eta + \int_{-(x-y)}^{0} e^{-(x-y)} d\eta + \int_{0}^{\infty} e^{-(x-y+2\eta)} d\eta \\ &= \frac{1}{2} e^{-(x-y)} + (x-y) e^{-(x-y)} + \frac{1}{2} e^{-(x-y)} \\ &= [1+(x-y)] e^{-(x-y)} . \end{aligned}$$

Based on the above two steps, we have:

$$g(x,y) = (1 + |x-y|)e^{-|x-y|}\,.$$

Solution 2.24

(a) Yes, it is shift invariant because its impulse response depends on $x - \xi$.

(b) By linearity, the output is

$$g(x) = e^{\frac{-(x+1)^2}{2}} + e^{\frac{-(x)^2}{2}} + e^{\frac{-(x-1)^2}{2}}\,.$$

Solution 2.25

(a) The impulse response of the filter is the inverse Fourier transform of $H(u)$, which can be written as

$$H(u) = 1 - \text{rect}\left(\frac{u}{2U_0}\right)\,.$$

Using the linearity of the Fourier transform and the Fourier transform pairs

$$\begin{aligned}\mathcal{F}\{\delta(t)\} &= 1\,,\\ \mathcal{F}\{\text{sinc}(t)\} &= \text{rect}(u)\,,\end{aligned}$$

we have

$$\begin{aligned}h(t) &= \mathcal{F}^{-1}\{H(u)\}\\ &= \delta(t) - 2U_0\,\text{sinc}(2U_0 t)\,.\end{aligned}$$

(b) The system response to $f(t) = c$ is 0, since $f(t)$ contains only a zero frequency component while $h(t)$ passes only high frequency components. Formal proof:

$$\begin{aligned}f(t) * h(t) &= f(t) * [\delta(t) - 2U_0\,\text{sinc}(2U_0 t)]\\ &= f(t) - 2U_0 f(t) * \text{sinc}(2U_0 t)\\ &= c - c\int_{-\infty}^{\infty} 2U_0\,\text{sinc}(2U_0 t)dt\\ &= c - c\int_{-\infty}^{\infty} \text{sinc}(\tau)d\tau\\ &= 0\,.\end{aligned}$$

The system response to $f(t) = \begin{cases} 1, & t \geq 0 \\ 0, & t < 0 \end{cases}$ is

$$\begin{aligned}
f(t) * h(t) &= f(t) * [\delta(t) - 2U_0 \operatorname{sinc}(2U_0 t)] \\
&= f(t) - 2U_0 f(t) * \operatorname{sinc}(2U_0 t) \\
&= f(t) - \int_{-\infty}^{\infty} f(x) 2U_0 \operatorname{sinc}(2U_0(t-x))dx \\
&= f(t) - \int_{0}^{\infty} 2U_0 \operatorname{sinc}(2U_0(t-x))dx \\
&= f(t) + \int_{t}^{-\infty} 2U_0 \operatorname{sinc}(2U_0(y))dy \\
&= f(t) - \int_{-\infty}^{t} 2U_0 \operatorname{sinc}(2U_0(y))dy \\
&= \begin{cases} 1 - \displaystyle\int_{-\infty}^{0} 2U_0 \operatorname{sinc}(2U_0(y))dy + \int_{t}^{0} 2U_0 \operatorname{sinc}(2U_0(y))dy & t < 0 \\ 1 - \displaystyle\int_{-\infty}^{0} 2U_0 \operatorname{sinc}(2U_0(y))dy - \int_{0}^{t} 2U_0 \operatorname{sinc}(2U_0(y))dy & t > 0 \end{cases} \\
&= \begin{cases} -\dfrac{1}{2} + \displaystyle\int_{t}^{0} 2U_0 \operatorname{sinc}(2U_0(y))dy & t < 0 \\ 1 - \dfrac{1}{2} - \displaystyle\int_{0}^{t} 2U_0 \operatorname{sinc}(2U_0(y))dy & t > 0 \end{cases} \\
&= \begin{cases} -\dfrac{1}{2} + \displaystyle\int_{t}^{0} 2U_0 \operatorname{sinc}(2U_0(y))dy & t < 0 \\ \dfrac{1}{2} - \displaystyle\int_{0}^{t} 2U_0 \operatorname{sinc}(2U_0(y))dy & t > 0 \end{cases}.
\end{aligned}$$

Solution 2.26

(a) The rect function is defined as

$$\text{rect}(t) = \begin{cases} 1, & |t| \le 1/2 \\ 0, & \text{otherwise} \end{cases} .$$

So we have

$$\text{rect}\left(\frac{t}{T}\right) = \begin{cases} 1, & |t| \le T/2 \\ 0, & \text{otherwise} \end{cases}$$

and

$$\text{rect}\left(\frac{t+0.75T}{0.5T}\right) = \begin{cases} 1, & |t+0.75T| \le T/4 \\ 0, & \text{otherwise} \end{cases} .$$

Therefore,

$$h(t) = \begin{cases} -1/T, & -T < t < -T/2 \\ 1/T, & -T/2 < t < T/2 \\ -1/T, & T/2 < t < T \\ 0, & \text{otherwise} \end{cases} .$$

The impulse response is plotted in Fig. S2.4.

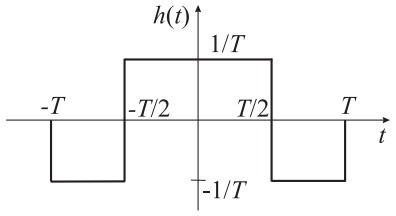

Figure S2.4 The impulse response $h(t)$. See Problem 2.26(a).

The absolute integral of $h(t)$ is $\int_{-\infty}^{\infty} |h(t)|^2 dt = 2/T$. So The system is stable when $T > 0$. The system is not causal, since $h(t) \neq 0$ for $-T < t < 0$.

(b) The response of the system to a constant signal $f(t) = c$ is

$$g(t) = f(t) * h(t) = \int_{-\infty}^{\infty} f(t-\tau)h(\tau)d\tau = c\int_{-\infty}^{\infty} h(\tau)d\tau = 0 .$$

(c) The response of the system to the unit step function is

$$g(t) = f(t) * h(t) = \int_{-\infty}^{\infty} f(t-\tau)h(\tau)d\tau = \int_{-\infty}^{t} h(\tau)d\tau$$

$$g(t) = \begin{cases} 0, & t < -T \\ -t/T - 1, & -T < t < -T/2 \\ t/T, & -T/2 < t < T/2 \\ -t/T + 1, & T/2 < t < T \\ 0, & t > T \end{cases}$$

The response of the system to the unit step signal is plotted in Figure S2.5.

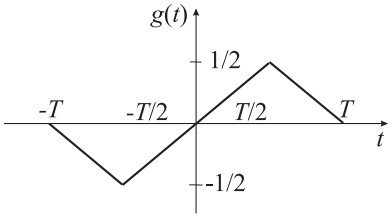

Figure S2.5 The response of the system to the unit step signal. See Problem 2.26(c).

(d) The Fourier transform of a rect function is a sinc function (see Problem 2.17). By using the properties of the Fourier transform (scaling, shifting, and linearity), we have

$$\begin{aligned} H(u) &= \mathcal{F}\{h(t)\} \\ &= -0.5e^{-j2\pi u(-0.75T)}\,\mathrm{sinc}(0.5uT) + \mathrm{sinc}(uT) - 0.5e^{-j2\pi u(0.75T)}\,\mathrm{sinc}(0.5uT) \\ &= \mathrm{sinc}(uT) - \cos(1.5\pi uT)\,\mathrm{sinc}(0.5uT)\,. \end{aligned}$$

(e) The magnitude spectrum of $h(t)$ is plotted in Figure S2.6.

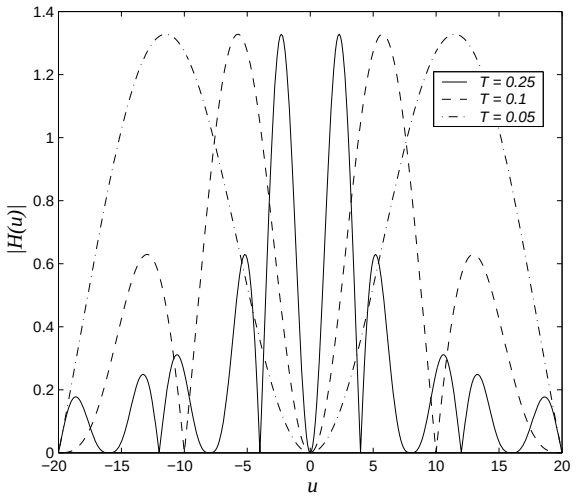

Figure S2.6 The magnitude spectrum of $h(t)$. See Problem 2.26(e).

(f) From the calculation in part **(d)** and the plot in part **(c)**, it can be seen that $|H(0)| = 0$. So the output of the system does not have a DC component. The system is not a low pass filter. The system is not a high-pass filter since it also filters out high frequency components. As $T \to 0$, the pass band of the system moves to higher frequencies, and the system tends toward a high-pass filter.

Solution 2.27

(a) The inverse Fourier transform of $\hat{H}(\varrho)$ is

$$\begin{aligned}
\hat{h}(r) &= \mathcal{F}^{-1}\{\hat{H}(\varrho)\} \\
&= \int_{-\infty}^{\infty} \hat{H}(\varrho) e^{j2\pi r\varrho} d\varrho \\
&= \int_{-\varrho_0}^{\varrho_0} |\varrho| e^{j2\pi r\varrho} d\varrho \\
&= \int_{0}^{\varrho_0} \varrho e^{j2\pi r\varrho} d\varrho - \int_{-\varrho_0}^{0} \varrho e^{j2\pi r\varrho} d\varrho \\
&= \int_{0}^{\varrho_0} \varrho e^{j2\pi r\varrho} d\varrho + \int_{0}^{-\varrho_0} \varrho e^{j2\pi r\varrho} d\varrho \\
&= \int_{0}^{\varrho_0} \varrho e^{j2\pi r\varrho} d\varrho + \int_{0}^{\varrho_0} \varrho e^{-j2\pi r\varrho} d\varrho \\
&= \int_{0}^{\varrho_0} \varrho \left[e^{j2\pi r\varrho} + e^{-j2\pi r\varrho}\right] d\varrho \\
&= 2\int_{0}^{\varrho_0} \varrho \cos(2\pi r\varrho) d\varrho \\
&= 2\left[\frac{\varrho \sin(2\pi r\varrho)}{2\pi r}\bigg|_{\varrho=0}^{\varrho_0} - \int_{0}^{\varrho_0} \frac{\sin(2\pi r\varrho)}{2\pi r} d\varrho\right] \\
&= 2\left[\frac{\varrho \sin(2\pi r\varrho_0)}{2\pi r} + \frac{\cos(2\pi r\varrho)}{4\pi^2 r^2}\bigg|_{\varrho=0}^{\varrho_0}\right] \\
&= \frac{1}{2\pi^2 r^2}\left[\cos(2\pi r\varrho_0) + 2\pi r\varrho_0 \sin(2\pi r\varrho_0) - 1\right] .
\end{aligned}$$

(b) The response of the filter is $g(r) = f(r) * \hat{h}(r)$, hence $G(\varrho) = F(\varrho)\hat{H}(\varrho)$. i) A constant function $f(r) = c$ has the Fourier transform

$$F(\varrho) = c\delta(\varrho) .$$

The transfer function of a ramp filter has a value zero at $\varrho = 0$. So the system response has the Fourier transform

$$G(\varrho) = 0 .$$

Therefore, the responses of a ramp filter to a constant function is $g(r) = 0$. ii) The Fourier transform of a sinusoid function $f(r) = \sin(\omega r)$ is

$$F(\varrho) = \frac{1}{2j}\left[\delta(\varrho - \frac{\omega}{2\pi}) - \delta(\varrho + \frac{\omega}{2\pi})\right] .$$

Hence,

$$G(\varrho) = \begin{cases} \frac{\omega}{4\pi j}\left[\delta\left(\varrho - \frac{\omega}{2\pi}\right) - \delta\left(\varrho + \frac{\omega}{2\pi}\right)\right] & \varrho_0 = \omega \\ 0 & \text{otherwise} \end{cases} .$$

Therefore, the response of a ramp filter to a sinusoid function is

$$g(r) = \begin{cases} \dfrac{\omega}{2\pi}\sin(\omega r) & \varrho_0 = \omega \\ 0 & \text{otherwise} \end{cases} .$$

Solution 2.28

Suppose the Fourier transform of $f(x,y)$ is $F(u,v)$. Using the scaling properties, we have that the Fourier transform of $f(ax,by)$ is $\frac{1}{|ab|}F\left(\frac{u}{a},\frac{v}{b}\right)$. The output of the system is

$$\begin{aligned} g(x,y) &= \mathcal{F}\left\{\frac{1}{|ab|}F\left(\frac{u}{a},\frac{v}{b}\right)\right\} \\ &= \int_{-\infty}^{\infty}\int_{-\infty}^{\infty}\frac{1}{|ab|}F\left(\frac{u}{a},\frac{v}{b}\right)e^{-j2\pi(ux+vy)}du\,dv \\ &= \frac{1}{|ab|}\int_{-\infty}^{\infty}\int_{-\infty}^{\infty}F(\xi,\eta)e^{j2\pi(a\xi(-x)+b\eta(-y))}|ab|d\xi\,d\eta\,. \end{aligned}$$

Given the inverse Fourier transform

$$f(x,y) = \int_{-\infty}^{\infty}\int_{-\infty}^{\infty}F(u,v)e^{j2\pi(ux+vy)}du\,dv$$

we have

$$\int_{-\infty}^{\infty}\int_{-\infty}^{\infty}F(\xi,\eta)e^{j2\pi(a\xi(-x)+b\eta(-y))}|ab|d\xi d\eta = |ab|f(-ax,-by)\,.$$

Therefore, $g(x,y) = f(-ax,-by)$ is a scaled and inverted replica of the input.

Solution 2.29

The Fourier transform of the signal $f(x,y)$ and the noise $\eta(x,y)$ are:

$$\begin{aligned} F(u,v) &= \mathcal{F}\{f(x,y)\} \\ &= |ab|\mathcal{F}\{\text{sinc}(ax,by)\} \\ &= |ab|\left\{\frac{1}{|ab|}\,\text{rect}\left(\frac{u}{a},\frac{v}{b}\right)\right\} \\ &= \text{rect}\left(\frac{u}{a},\frac{v}{b}\right) \\ &= \begin{cases} 1, & |x| < |a|/2 \text{ and } |y| < |b|/2 \\ 0, & \text{otherwise} \end{cases}, \\ E(u,v) &= \mathcal{F}\{\eta(x,y)\} \\ &= \frac{1}{2}\left[\delta(u-A,v-B)+\delta(u+A,v+B)\right]. \end{aligned}$$

Using the linearity of Fourier transform, the Fourier transform of the measurements $g(x,y)$ is

$$G(u,v) = \text{rect}\left(\frac{u}{a},\frac{v}{b}\right) + \frac{1}{2}\left[\delta(u-A,v-B)+\delta(u+A,v+B)\right],$$

which is plotted in Figure S2.7. In order for an ideal low pass filter to recover $f(x, y)$, the cutoff frequencies of the

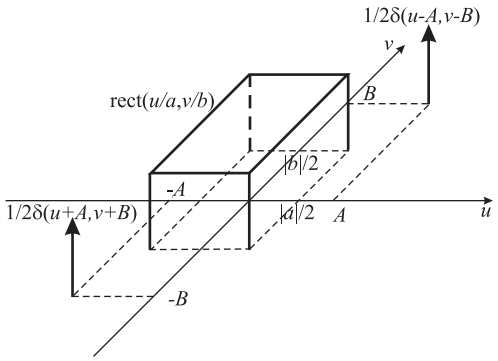

Figure S2.7 The Fourier transform of $g(x, y)$. See Problem 2.29.

filter must satisfy

$$|a|/2 < U < A \text{ and } |b|/2 < V < B\,.$$

The Fourier transform of $h(x, y)$ is $\text{rect}\left(\frac{u}{2U}, \frac{v}{2V}\right)$; therefore, the impulse response is

$$h(x, y) = \mathcal{F}^{-1}\left\{\text{rect}\left(\frac{u}{2U}, \frac{v}{2V}\right)\right\} = 4UV\,\text{sinc}(2Ux)\,\text{sinc}(2Vy)\,.$$

For given a and b, we need $A > |a|/2$ and $B > |b|/2$. Otherwise we cannot find an ideal low pass filter to exactly recover $f(x, y)$.

Solution 2.30

(a) The continuous Fourier transform of a rect function is a sinc function. Using the scaling property of the Fourier transform, we have:

$$G(u) = \mathcal{F}_{1\text{D}}\{g(x)\} = 2\,\text{sinc}(2u).$$

A sinc function, $\text{sinc}(x)$, is shown in Figure 2.4(b).

(b) If the sampling period is $\Delta x_1 = 1/2$, we have

$$g_1(m) = g(m/2) = \begin{cases} 1, & -2 \le m \le 2 \\ 0, & \text{otherwise} \end{cases}\,.$$

Its DTFT is

$$\begin{aligned} G_1(\omega) &= \mathcal{F}_{\text{DTFT}}\{g_1(m)\} \\ &= e^{j2\omega} + e^{j\omega} + 1e^{j0\omega} + e^{-j\omega} + 2e^{-j2\omega} \\ &= 1 + 2\cos(\omega) + 2\cos(2\omega)\,. \end{aligned}$$

The DTFT of $g_1(m)$ is shown in Figure S2.8.

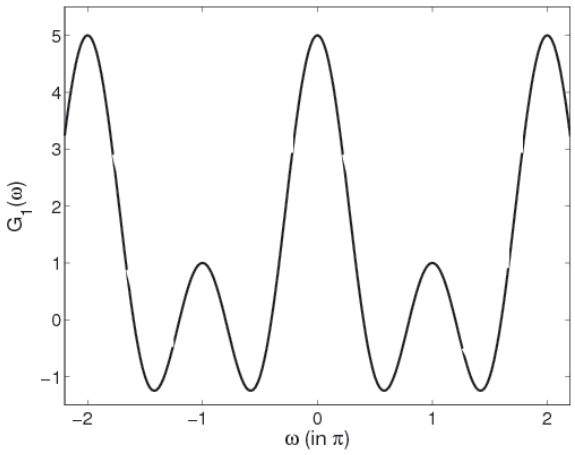

Figure S2.8 The DTFT $g_1(m)$. See Problem 2.30(b).

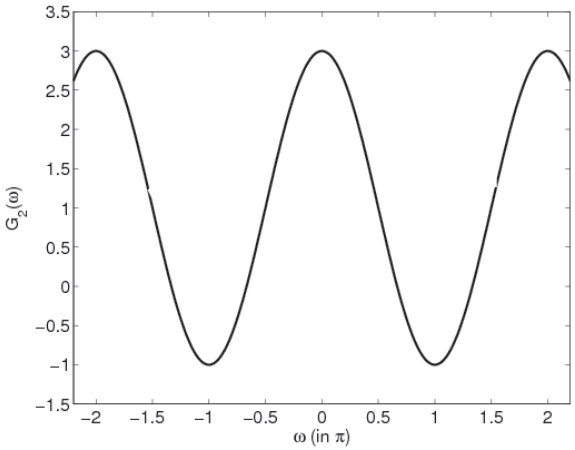

Figure S2.9 The DTFT $g_2(m)$. See Problem 2.30(c).

(c) If the sampling period is $\Delta x_2 = 1$, we have

$$g_2(m) = g(m) = \begin{cases} 1, & -1 \leq m \leq 1 \\ 0, & \text{otherwise} \end{cases} .$$

Its DTFT is

$$\begin{aligned} G_2(\omega) &= \mathcal{F}_{\text{DTFT}}\{g_2(m)\} \\ &= e^{j\omega} + 1e^{j0\omega} + e^{-j\omega} \\ &= 1 + 2\cos(\omega)\,. \end{aligned}$$

The DTFT of $g_2(m)$ is shown in Figure S2.9.

(d) The discrete version of signal $g(x)$ can be written as

$$g_1(m) = g(x - m\Delta x_1), \quad m = -\infty, \cdots, -1, 0, 1, \cdots, +\infty\,.$$

The DTFT of $g_1(m)$ is

$$\begin{aligned} G_1(\omega) &= \mathcal{F}_{\text{DTFT}}\{g_1(m)\} \\ &= \sum_{m=-\infty}^{+\infty} g_1(m)e^{-j\omega m} \\ &= \sum_{m=-\infty}^{+\infty} g(m\Delta x_1)e^{-j\omega m} \\ &= \int_{-\infty}^{\infty} g(x)\delta_s(x;\Delta x_1)e^{-j\omega\frac{x}{\Delta x_1}}dx\,. \end{aligned}$$

In the above, $\delta_s(x;\Delta x_1)$ is the sampling function with the space between impulses equal to Δx_1. Because of the sampling function, we are able to convert the summation into integration. The last equation in the above is the continuous Fourier transform of the product of $g(x)$ and $\delta_s(x;\Delta x_1)$ evaluated as $u = \omega/(2\pi\Delta x_1)$. Using the product property of the continuous Fourier transform, we have:

$$\begin{aligned} G_1(\omega) &= \mathcal{F}\{g(x)\} * \mathcal{F}\{\delta_s(x;\Delta x_1)\}|_{u=\omega/(2\pi\Delta x_1)} \\ &= G(u) * \text{comb}(u\Delta x_1)|_{u=\omega/(2\pi\Delta x_1)}\,. \end{aligned}$$

The convolution of $G(u)$ and $\text{comb}(u\Delta x_1)$ is to replicate $G(u)$ to $u = k/\Delta x_1$. Since $u = \omega/(2\pi\Delta x_1)$, $G_1(\omega)$ is periodic with period $\Omega = 2\pi$.

(e) The proof is similar to that for the continuous Fourier transform:

$$\begin{aligned} \mathcal{F}_{\text{DTFT}}\{x(m) * y(m)\} &= \mathcal{F}_{\text{DTFT}}\left\{x(m) * y(m)\right\} \\ &= \mathcal{F}_{\text{DTFT}}\left\{\sum_{n=-\infty}^{\infty} x(m-n)y(n)\right\} \\ &= \sum_{m=-\infty}^{\infty} e^{-j\omega m}\sum_{n=-\infty}^{\infty} x(m-n)y(n) \\ &= \sum_{n=-\infty}^{\infty}\left[\sum_{m=-\infty}^{\infty} e^{-j\omega m}x(m-n)\right]y(n) \\ &= \sum_{n=-\infty}^{\infty} e^{-j\omega n}\left[\sum_{k=-\infty}^{\infty} e^{-j\omega k}x(k)\right]y(n) \\ &\qquad (\text{let } k = m-n) \\ &= \sum_{n=-\infty}^{\infty} e^{-j\omega n}\mathcal{F}_{\text{DTFT}}\{x(m)\}y(n) \\ &= \mathcal{F}_{\text{DTFT}}\{x(m)\}\mathcal{F}_{\text{DTFT}}\{y(m)\}\,. \end{aligned}$$

(f) First we evaluate the convolution of $g_1(m)$ with $g_2(m)$:

$$g_1(m) * g_2(m) = \begin{cases} 3, & -1 \le m \le 1 \\ 2, & m = \pm 2 \\ 1, & m = \pm 3 \\ 0, & \text{otherwise} \end{cases} .$$

Then by direct computation, we have

$$\begin{aligned} \mathcal{F}_{\mathrm{DTFT}}\{g_1(m) * g_2(m)\} &= 3 + 3 \times 2\cos(\omega) + 2 \times 2\cos(2\omega) + 2\cos(3\omega) \\ &= 3 + 6\cos(\omega) + 4\cos(2\omega) + 2\cos(3\omega) . \end{aligned}$$

On the other hand, we have

$$\mathcal{F}_{\mathrm{DTFT}}\{g_1(m)\} = 1 + 2\cos(\omega) + 2\cos(2\omega)$$

and

$$\mathcal{F}_{\mathrm{DTFT}}\{g_2(m)\} = 1 + 2\cos(\omega) .$$

So, the product of the DTFT's of $g_1(m)$ and $g_2(m)$ is

$$\begin{aligned} \mathcal{F}_{\mathrm{DTFT}}\{g_1(m)\}\mathcal{F}_{\mathrm{DTFT}}\{g_2(m)\} &= [1 + 2\cos(\omega)][1 + 2\cos(\omega) + 2\cos(2\omega)] \\ &= 1 + 4\cos(\omega) + 2\cos(2\omega) \\ &\quad +4\cos^2(\omega) + 4\cos(\omega)\cos(2\omega) \\ &= 1 + 4\cos(\omega) + 2\cos(2\omega) \\ &\quad +4\frac{1 + \cos(2\omega)}{2} + 4\frac{\cos(\omega) + \cos(3\omega)}{2} \\ &= 3 + 6\cos(\omega) + 4\cos(2\omega) + 2\cos(3\omega) . \end{aligned}$$

Therefore,

$$\mathcal{F}_{\mathrm{DTFT}}\{g_1(m) * g_2(m)\} = \mathcal{F}_{\mathrm{DTFT}}\{g_1(m)\}\mathcal{F}_{\mathrm{DTFT}}\{g_2(m)\} .$$

3
Image Quality

CONTRAST

Solution 3.1

$$\begin{aligned}
g(x,y) &= \int_{-\infty}^{\infty}\int_{-\infty}^{\infty} h(\xi,\eta) f(x-\xi, y-\eta)\, d\xi d\eta \\
&= AH(0,0) + \frac{B}{2j}\int_{-\infty}^{\infty}\int_{-\infty}^{\infty} h(\xi,\eta) e^{j2\pi u_0(x-\xi)}\, d\xi d\eta \\
&\quad - \frac{B}{2j}\int_{-\infty}^{\infty}\int_{-\infty}^{\infty} h(\xi,\eta) e^{-j2\pi u_0(x-\xi)}\, d\xi d\eta \\
&= AH(0,0) + \frac{B}{2j} e^{j2\pi u_0 x}\int_{-\infty}^{\infty}\int_{-\infty}^{\infty} h(\xi,\eta) e^{-j2\pi u_0 \xi}\, d\xi d\eta \\
&\quad - \frac{B}{2j} e^{-j2\pi u_0 x}\int_{-\infty}^{\infty}\int_{-\infty}^{\infty} h(\xi,\eta) e^{j2\pi u_0 \xi}\, d\xi d\eta \\
&= AH(0,0) + \frac{B}{2j}\left[e^{j2\pi u_0 x} H(u_0,0) - e^{-j2\pi u_0 x} H(-u_0,0)\right] \\
&= AH(0,0) + B|H(u_0,0)|\sin(2\pi u_0 x)\,.
\end{aligned}$$

Solution 3.2

(a) The PSF of the medical imaging system is isotropic, so we have:

$$\begin{aligned}
\text{MTF}(u) &= |H(u,0)| \\
&= |\mathcal{F}\{h\}(u,0)|\,.
\end{aligned}$$

From Table 2.1, we have $\mathcal{F}\{h\}(u,v) = \int_{-\infty}^{\infty}\int_{-\infty}^{\infty} \frac{1}{2\pi} e^{-(x^2+y^2)/2} e^{-j2\pi(ux+vy)}\, dx\, dy = e^{-2\pi^2(u^2+v^2)}$. The

MTF associated with the system is:

$$\text{MTF}(u) = e^{-2\pi^2 u^2}.$$

(b) See Figure S3.1.

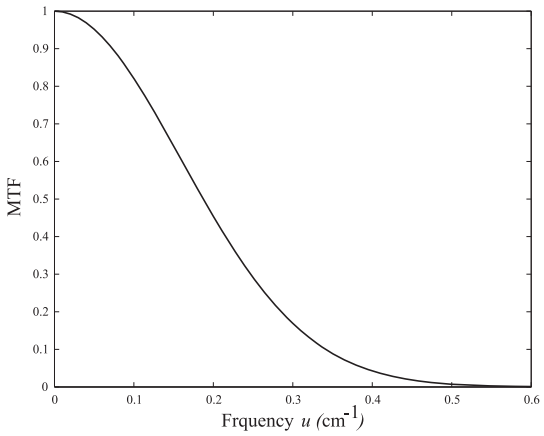

Figure S3.1 The modulation transfer function of the system. See Problem 3.2(b).

(c) The spatial frequency of the input signal $f(x, y) = 2 + \sin(\pi x)$ is $u = 1/2$. At this frequency, the MTF has a value $\text{MTF}(0.5) = e^{-2\pi^2 0.5^2} = 0.0072$. So the percentage change in modulation caused by this system is $100 \times (1 - 0.0072)\% = 99.28\%$.

Solution 3.3

(a) Given $h_1(x)$ we first find the Fourier Transform $H_1(u)$ as follows:

$$\begin{aligned}
H_1(u) &= \int_{-\infty}^{\infty} e^{-x^2/5} e^{-j2\pi ux} dx \\
&= \int_{-\infty}^{\infty} e^{-(x^2 + j10\pi ux)/5} dx \\
&= \int_{-\infty}^{\infty} e^{-(x^2 + j10\pi ux - 25\pi^2 u^2)/5} e^{-5\pi^2 u^2} dx \\
&= e^{-5\pi^2 u^2} \int_{-\infty}^{\infty} e^{-(x + j5\pi u)^2/5} dx \\
&= \sqrt{5\pi} e^{-5\pi^2 u^2}.
\end{aligned}$$

Hence, the MTF is given as:

$$\begin{aligned}
\text{MTF}_1(u) &= \frac{|H_1(u)|}{H_1(0)} \\
&= e^{-5\pi^2 u^2}.
\end{aligned}$$

(b) The Fourier transform of the second system $h_2(x)$ can be computed by analogous methods, and is found to be

$$H_2(u) = \sqrt{10\pi}e^{-10\pi^2u^2}\,.$$

Since the two systems are in serial cascade, the overall system transfer function is

$$\begin{aligned} H(u) &= H_1(u)H_2(u) \\ &= \sqrt{5\pi}\sqrt{10\pi}e^{-5\pi^2u^2}e^{-10\pi^2u^2} \\ &= \sqrt{50}\pi e^{-15\pi^2u^2}\,. \end{aligned}$$

Hence, the MTF is MTF$(u) = e^{-15\pi^2u^2}$.

Solution 3.4

Let $h(x,y)$ denote the PSF of the nonisotropic medical imaging system, and we assume $h(x,y)$ is normalized to 1; i.e.,

$$\int_{-\infty}^{\infty}\int_{-\infty}^{\infty} h(\xi,\eta)\,d\xi d\eta = 1\,.$$

Given the input

$$\begin{aligned} f(x,y) &= A + B\sin(2\pi(ux+vy)) \\ &= A + \frac{B}{2}\left[e^{j2\pi(ux+vy)} - e^{-j2\pi(ux+vy)}\right], \end{aligned}$$

the output $g(x,y)$ of the system is given by

$$\begin{aligned} g(x,y) &= \int_{-\infty}^{\infty}\int_{-\infty}^{\infty} h(\xi,\eta)f(x-\xi,y-\eta)\,d\xi d\eta \\ &= A + \frac{B}{2j}\int_{-\infty}^{\infty}\int_{-\infty}^{\infty} h(\xi,\eta)e^{j2\pi[u(x-\xi)+v(y-\eta)]}\,d\xi d\eta \\ &\quad -\frac{B}{2j}\int_{-\infty}^{\infty}\int_{-\infty}^{\infty} h(\xi,\eta)e^{-j2\pi[u(x-\xi)+v(y-\eta)]}\,d\xi d\eta \\ &= A + \frac{B}{2j}e^{j2\pi(ux+vy)}\int_{-\infty}^{\infty}\int_{-\infty}^{\infty} h(\xi,\eta)e^{-j2\pi(u\xi+v\eta)}\,d\xi d\eta \\ &\quad -\frac{B}{2j}e^{-j2\pi(ux+vy)}\int_{-\infty}^{\infty}\int_{-\infty}^{\infty} h(\xi,\eta)e^{j2\pi(u\xi+v\eta)}\,d\xi d\eta \\ g(x,y) &= A + \frac{B}{2j}\left[e^{j2\pi(ux+vy)}H(u,v) - e^{-j2\pi(ux+vy)}H(-u,-v)\right]. \end{aligned}$$

Assuming that $h(x,y)$ is a real function, we have $H(u,v) = H^*(-u,-v) = |H(u,v)|\exp(j\phi)$, where ϕ denotes the phase angle of $H(u,v)$. Hence,

$$\begin{aligned} g(x,y) &= A + \frac{B}{2j}|H(u,v)|\left[e^{j[2\pi(ux+vy)+\phi]} - e^{-j[2\pi(ux+vy)+\phi]}\right] \\ &= A + B|H(u,v)|\sin(2\pi(ux+vy)+\phi)\,. \end{aligned}$$

The output $g(x, y)$ is again sinusoidal with $g_{\max} = A + B|H(u, v)|$, and $g_{\min} = A - B|H(u, v)|$. Therefore, the modulation of $g(x, y)$ is

$$m_g = \frac{B}{A}|H(u, v)| = m_f|H(u, v)|\,.$$

Thus, the MTF of the system is given by

$$\text{MTF}(u, v) = \frac{m_g}{m_f} = |H(u, v)|\,.$$

Solution 3.5

(a) By multiplying the image with a constant α, the intensities of the background and the target become $f_b = \alpha I_o$, and $f_t = \alpha I_t$. The local contrast of the processed image is:

$$C' = \frac{f_t - f_b}{f_b} = \frac{\alpha I_t - \alpha I_o}{\alpha I_o} = \frac{I_t - I_o}{I_o} = C\,,$$

where C is the local contrast of the original image.

(b) By subtracting a constant I_s from the image, the intensities of the background and the target become $f_b = I_o - I_s$, and $f_t = I_t - I_s$. The local contrast of the processed image is:

$$C'' = \frac{(I_t - I_s) - (I_o - I_s)}{I_o - I_s} = \frac{I_t - I_o}{I_o - I_s} = C\frac{I_o}{I_o - I_s} > C\,.$$

So, by subtracting a constant $0 < I_s < I_o$ from the image will improve the local contrast, while scaling the intensity will not change the local contrast.

RESOLUTION

Solution 3.6

The profile of the impulse response as a function of the polar angle θ can be expressed as:

$$h(r, \theta) = e^{-\pi(r^2\cos^2\theta + (r^2\sin^2\theta)/4)}\,. \tag{S3.1}$$

For a fixed θ, the maximal value occurs at $r = 0$ with $h(0, \theta) = 1$. Solving for r in

$$h(r, \theta) = e^{-\pi(r^2\cos^2\theta + (r^2\sin^2\theta)/4)} = 1/2$$

yields

$$r_{1/2} = \sqrt{\frac{\ln 2}{\pi\left(\cos^2\theta + \sin^2\theta/4\right)}}\,.$$

The FWHM is therefore

$$\text{FWHM} = 2 * r_{1/2} = 2\sqrt{\frac{\ln 2}{\pi\left(\cos^2\theta + \sin^2\theta/4\right)}}\,.$$

which is plotted as a function of θ in Figure S3.2.

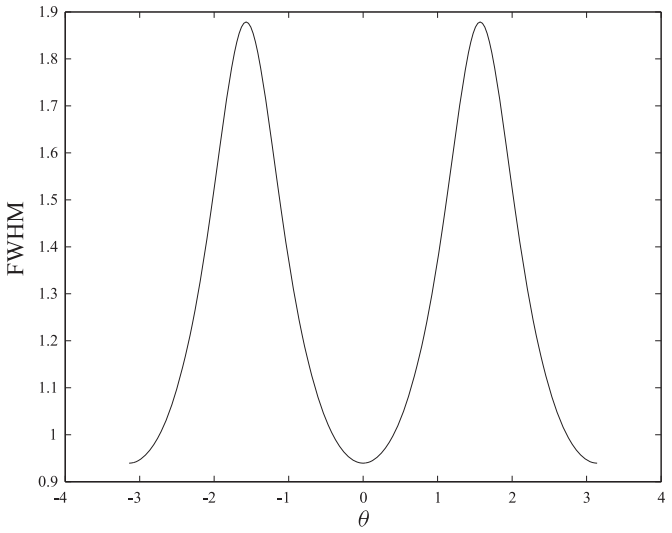

Figure S3.2 FWHM as a function of θ for an anisotropic system. See Problem 3.6.

Solution 3.7

(a) We have

$$\frac{l(x_{1/2})}{l(0)} = \frac{1}{2} = \cos(\alpha x_{1/2}) \quad \Rightarrow \quad \alpha x_{1/2} = \frac{\pi}{3} \quad \Rightarrow \quad x_{1/2} = \frac{\pi/3}{\alpha} = \frac{\pi}{6}\,\text{cm}\,.$$

FWHM is twice $x_{1/2}$, so

$$\text{FWHM} = 2x_{1/2} = \frac{\pi}{3}\,\text{cm}\,.$$

(b) The resolution of the system is the inverse of the FWHM:

$$\frac{1}{\text{FWHM}} = \frac{3}{\pi}\,\text{cm}^{-1}\,.$$

Solution 3.8

(a) We have $h_0(x) = e^{-x^2/2}$ and $h_a(x) = e^{-ax^2/2}$. We need to find a so that x_a at half maximum of $h_a(x)$ is half of x_0 at half maximum of $h_0(x)$, i.e. $x_a = x_0/2$.

$$\left.\begin{aligned} e^{-x_0^2/2} &= 1/2 \\ e^{-ax_a^2/2} &= 1/2 \end{aligned}\right\} \quad \Rightarrow \quad e^{-a(x_0/2)^2/2} = e^{-ax_0^2/8} = 1/2 \quad \Rightarrow \quad ax_0^2/8 = x_0^2/2 \quad \Rightarrow \quad a = 4\,.$$

The impulse response for the new system is:

$$h_{\text{new}}(x) = e^{-2x^2}\,.$$

(b) Yes. The resolution improves. The system with smaller FWHM can distinguish objects that are closer together.

(c) The system should pass higher frequency signals. In other words, the MTF of the system should have a broader pass band.

Solution 3.9

(a) The *line spread function* (LSF) $l(x)$ is defined as the output of the system to a line impulse function $f(x,y) = \delta(x)$:

$$\begin{aligned} l(x) &= \int_{-\infty}^{\infty} h(x,\eta)\, d\eta \\ &= \int_{-\infty}^{\infty} \frac{1}{2\pi} e^{-(x^2+\eta^2)/2}\, d\eta \\ &= \frac{1}{\sqrt{2\pi}} e^{-x^2/2} \int_{-\infty}^{\infty} \frac{1}{\sqrt{2\pi}} e^{-\eta^2/2}\, d\eta \\ &= \frac{1}{\sqrt{2\pi}} e^{-x^2/2}\,. \end{aligned}$$

(b) FWHM is the *full width at half maximum*. The maximum value of LSF occurs at $x = 0$, i.e., $l(0) = \frac{1}{\sqrt{2\pi}}$. Solve $l(x_h) = l(0)/2$ (we can ignore the constant $\frac{1}{\sqrt{2\pi}}$ and solve $e^{-x_h^2/2} = 1/2$) for x_h to get $x_h = 1.1774$ mm. So FWHM $= 2x_h = 2.3548$ mm.

Solution 3.10

(a) We have

$$\max_x h_1(x) = h_1(0) = 1\,.$$

Solving

$$h_1(x_{0_1}) = e^{-x_{0_1}^2/2} = \frac{1}{2}$$

yields

$$x_{0_1} = \sqrt{2\ln 2}\,.$$

Thus, the FWHM of subsystem $h_1(x)$ is

$$\text{FWHM}_1 = 2x_{0_1} = 2\sqrt{2\ln 2} \approx 2.35\,.$$

Similarly,

$$\max_x h_2(x) = h_2(0) = 1\,.$$

Solving

$$h_2(x_{0_2}) = e^{-x_{0_2}^2/200} = \frac{1}{2}$$

yields

$$x_{0_2} = 10\sqrt{2\ln 2}\,.$$

Thus, the FWHM of subsystem $h_2(x)$ is

$$\text{FWHM}_2 = 2x_{0_2} = 20\sqrt{2\ln 2} \approx 23.55\,.$$

(b) The PSF of the overall system is given by

$$\begin{aligned} h(x) &= h_1(x) * h_2(x) \\ &= \int_{-\infty}^{\infty} e^{-\xi^2/2} e^{-(x-\xi)^2/200}\, d\xi \\ &= \int_{-\infty}^{\infty} e^{-(x^2-2\xi x+\xi^2+100\xi^2)/200}\, d\xi \\ &= \int_{-\infty}^{\infty} e^{-101(\xi-x/101)^2/200} e^{-x^2/202}\, d\xi \\ &= Ce^{-x^2/202}\,, \end{aligned}$$

where $C = \displaystyle\int_{-\infty}^{\infty} e^{-101\xi^2/200} d\xi$ is a constant. Clearly,

$$\max_x h(x) = h(0) = C\,.$$

Thus, from $h(x_0) = e^{-x_0^2/202} = \frac{1}{2}$, we get the FWHM of the overall system as

$$\text{FWHM}_{\text{total}} = 2\sqrt{202\ln 2} \approx 23.67 \approx \text{FWHM}_2\,.$$

Alternatively, since the subsystems have PSFs that are in exponential form, one can directly compute the FWHM of the overall system as

$$\begin{aligned} \text{FWHM}_{\text{total}} &= \sqrt{\text{FWHM}_1^2 + \text{FWHM}_2^2} \\ &= \sqrt{\left(2\sqrt{2\ln 2}\right)^2 + \left(20\sqrt{2\ln 2}\right)^2} = \sqrt{808\ln 2} \\ &\approx 23.67\,. \end{aligned}$$

(c) From (a) and (b), we can see that the second subsystem mostly affects the FWHM of the overall system.

Solution 3.11

A bar phantom, with bars parallel to y-axis, can be modeled as

$$b(x,y) = \sum_k \text{rect}\left(\frac{x-2kw}{w}\right)\,,$$

where w is the width and the separation of bars. Since $b(x,y)$ is constant in y for any fixed x, it suffices to consider

the profile of the system and the phantom for $y = 0$:

$$\begin{aligned} b_{1D}(x) &= \sum_k \text{rect}\left(\frac{x - 2kw}{w}\right), \\ h_{1D}(x) &= \text{rect}\left(\frac{x}{\Delta}\right). \end{aligned}$$

The output of the system is the convolution of $b(x, y)$ and $h(x, y)$:

$$\begin{aligned} g(x,y) &= b(x,y) * h(x,y) \\ &= \iint b(x-\xi, y-\eta) h(\xi,\eta) d\xi d\eta \\ &= \int \text{rect}\left(\frac{\eta}{\Delta}\right) \left[\int b_{1D}(x-\xi)\,\text{rect}\left(\frac{\xi}{\Delta}\right) d\xi\right] d\eta \\ &= \int \text{rect}\left(\frac{\eta}{\Delta}\right) d\eta \int b_{1D}(x-\xi)\,\text{rect}\left(\frac{\xi}{\Delta}\right) d\xi \\ &= \Delta \int b_{1D}(x-\xi) h_{1D}(\xi) d\xi \\ &= \Delta b_{1D}(x) * h_{1D}(x)\,. \end{aligned}$$

(a) If $w = \Delta$, the separation of the bars is just wide enough to contain $f_{1D}(x)$. The minimal value of $g_{1D}(x) = b_{1D}(x) * h_{1D}(x)$ is 0, which occurs at $x = (2k+1)\Delta$ when $h_{1D}(\xi)$ completely overlaps with the separations of $b_{1D}(x - \xi)$. The maximal value of $g_{1D}(x)$ is Δ, which occurs at $x = 2k\Delta$ when $h_{1D}(\xi)$ completely overlaps with the bars of $b_{1D}(x - \xi)$. The values between extreme values change linearly from 0 to Δ. This situation is shown in Figure S3.3. Based on the above analysis, we have

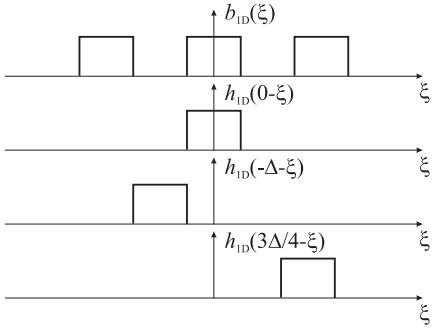

Figure S3.3 $w = \Delta$. See Problem 3.11(a).

$$g_{1D}(x) = \begin{cases} \Delta - (x - 2k\Delta), & 2k\Delta \le x < (2k+1)\Delta \\ x - (2k-1)\Delta, & (2k-1)\Delta \le x < 2k\Delta \end{cases}.$$

So,

$$\begin{aligned} g(x,y) &= b(x,y) * h(x,y) \\ &= \begin{cases} \Delta^2 - \Delta(x - 2k\Delta), & 2k\Delta \le x < (2k+1)\Delta \\ \Delta x - (2k-1)\Delta^2, & (2k-1)\Delta \le x < 2k\Delta \end{cases} . \end{aligned}$$

(b) If $w = 0.5\Delta$, no matter what x is, $h_{1D}(x - \xi)$ always overlaps with one complete bar (or parts of two adjacent bars that add up to 1 complete bar) of $b_{1D}(\xi)$ (see Figure S3.4). So, the output of the system is

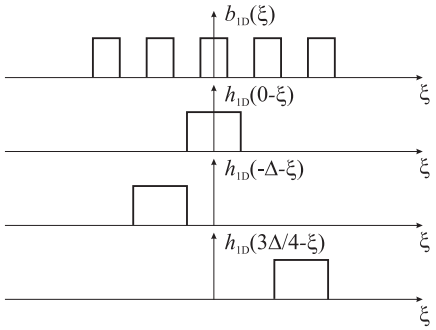

Figure S3.4 $w = 0.5\Delta$. See Problem 3.11(b).

$$g(x,y) = b(x,y) * h(x,y) = 0.5\Delta^2 .$$

(c) Now consider the range $0.5\Delta < w < \Delta$. With a similar figure as Figures S3.3 and S3.4, we can see that $h_{1D}(x - \xi)$ at most overlaps with one bar of $b_{1D}(\xi)$, and it at least overlaps with part of a bar of width $\Delta - w$. So the maximal value of $g(x,y)$ is Δw and the minimal value is $\Delta(\Delta - w)$. The contrast of the output image of the bar phantom is therefore

$$C(w) = \frac{2w - \Delta}{\Delta} .$$

RANDOM VARIABLES AND NOISE

Solution 3.12

Evaluate the expectation of M as follows:

$$\begin{aligned} E\{M\} &= E\left\{\frac{N-\mu_N}{\sigma_N}\right\} \\ &= \frac{E\{N-\mu_N\}}{\sigma_N} \text{ (because } \sigma_N \text{ is a constant)} \\ &= \frac{E\{N\}-\mu_N}{\sigma_N} \text{ (because } \mu_N \text{ is a constant)} \\ &= \frac{\mu_N-\mu_N}{\sigma_N} \\ &= 0\,. \end{aligned}$$

Evaluate the variance of M as follows:

$$\begin{aligned} \sigma_M^2 &\overset{①}{=} E\{M^2\}-(E\{M\})^2 \\ &= E\{M^2\}(\text{ because } E\{M\}=0 \text{ from above}) \\ &= E\left\{\frac{(N-\mu_N)^2}{\sigma_N^2}\right\} \\ &= \frac{E\{(N-\mu_N)^2\}}{\sigma_N^2} \\ &= \frac{\sigma_N^2}{\sigma_N^2} \\ &= 1\,. \end{aligned}$$

In order to get equality ①, we used the following property of variance:

$$\begin{aligned} \sigma_M^2 &= E\{(M-\mu_M)^2\} \\ &= E\{M^2-2\mu_M M+\mu_M^2\} \\ &= E\{M^2\}-2\mu_M E\{M\}+\mu_M^2 \\ &= E\{M^2\}-\mu_M^2\,. \end{aligned}$$

Solution 3.13

Let $X=\sum_{i=1}^{N} X_i$. The mean of X is

$$\mu = \mathrm{E}[X] = \mathrm{E}\left[\sum_{i=1}^{N} X_i\right] = \sum_{i=1}^{N} \mathrm{E}[X_i] = \sum_{i=1}^{N} \mu_i\,,$$

where we used the linearity of the expectation operator E. The variance of X is

$$\begin{aligned}\sigma^2 &= \mathrm{E}\left[(X-\mu)^2\right] \\ &= \mathrm{E}\left[\left(\sum_{i=1}^{N} X_i - \sum_{i=1}^{N}\mu_i\right)^2\right] = \mathrm{E}\left[\left(\sum_{i=1}^{N}(X_i-\mu_i)\right)^2\right] \\ &= \sum_{i=1}^{N}\mathrm{E}[(X_i-\mu_i)^2] + \sum_{i=1}^{N}\sum_{j=1,j\neq i}^{N}\mathrm{E}[(X_i-\mu_i)(X_j-\mu_j)]\end{aligned}$$

Since $X_i,\ i=1,\cdots,N$ are independent, $\mathrm{E}[(X_i-\mu_i)(X_j-\mu_j)]=0$ if $j\neq i$. Therefore,

$$\sigma^2 = \sum_{i=1}^{N}\mathrm{E}[(X_i-\mu_i)^2] = \sum_{i=1}^{N}\sigma_i^2\,.$$

Solution 3.14

If $X_i,\ i=1,\cdots,N$ are not independent, then

$$\mu = \mathrm{E}[X] = \sum_{i=1}^{N}\mu_i$$

still holds, since in deriving this equality, we used only the linearity of the expectation operator. The equality for the variance, however, does not hold because when $X_i,\ i=1,\cdots,N$ are not independent the statement $\mathrm{E}[(X_i-\mu_i)(X_j-\mu_j)]=0$ is not necessarily true.

Solution 3.15

The PDF of the uniform random variable is given by

$$p_X(x) = \begin{cases} \dfrac{1}{(b-a)}\,, & \text{for } a\leq x<b \\ \\ 0\,, & \text{otherwise}\end{cases}\,.$$

Thus,

$$\begin{aligned}\mu_X &= \int_{-\infty}^{\infty} x p_X(x)\,dx \\ &= \int_a^b x\frac{1}{b-a}\,dx = \frac{b^2-a^2}{2(b-a)} \\ &= \frac{a+b}{2}\end{aligned}$$

and

$$\begin{aligned}
\sigma_X^2 &= \int_{-\infty}^{\infty} (x-\mu_X)^2 p_X(x)\,dx \\
&= \int_a^b (x-\frac{a+b}{2})^2 \frac{1}{b-a}\,dx \\
&= \int_a^b (x-\frac{a+b}{2})^2 \frac{1}{b-a}\,d(x-\frac{a+b}{2}) \\
&= \frac{1}{b-a}\int_{a-(a+b)/2}^{b-(a+b)/2} t^2\,dt \\
&= \frac{1}{3(b-a)}\left[\left(\frac{b-a}{2}\right)^3 - \left(\frac{a-b}{2}\right)^3\right] \\
&= \frac{(b-a)^2}{12}\,.
\end{aligned}$$

Solution 3.16

For the system with PSF $h_1(x,y)$, the output power SNR is given by (3.63)

$$\text{SNR}_{p1} = \frac{\displaystyle\int_{-\infty}^{\infty}\int_{-\infty}^{\infty} |h_1(x,y) * f(x,y)|^2\,dx\,dy}{\displaystyle\int_{-\infty}^{\infty}\int_{-\infty}^{\infty} \text{NPS}(u,v)\,du\,dv}\,.$$

By applying Parseval's theorem, we have

$$\begin{aligned}
\text{SNR}_{p1} &= \frac{\displaystyle\int_{-\infty}^{\infty}\int_{-\infty}^{\infty} |h_1(x,y) * f(x,y)|^2\,dx\,dy}{\displaystyle\int_{-\infty}^{\infty}\int_{-\infty}^{\infty} \text{NPS}(u,v)\,du\,dv} \\
&= \frac{\displaystyle\int_{-\infty}^{\infty}\int_{-\infty}^{\infty} |H_1(u,v)F(u,v)|^2\,du\,dv}{\displaystyle\int_{-\infty}^{\infty}\int_{-\infty}^{\infty} \text{NPS}(u,v)\,du\,dv} \\
&= \frac{\displaystyle\int_{-\infty}^{\infty}\int_{-\infty}^{\infty} |H_1(u,v)|^2|F(u,v)|^2\,du\,dv}{\displaystyle\int_{-\infty}^{\infty}\int_{-\infty}^{\infty} \text{NPS}(u,v)\,du\,dv} \\
&= \frac{\displaystyle\int_{-\infty}^{\infty}\int_{-\infty}^{\infty} \text{MTF}_1^2(u,v)|F(u,v)|^2\,du\,dv}{\displaystyle\int_{-\infty}^{\infty}\int_{-\infty}^{\infty} \text{NPS}(u,v)\,du\,dv}\,.
\end{aligned}$$

Similarly, we have the output power SNR for the second system

$$\text{SNR}_{p2} = \frac{\displaystyle\int_{-\infty}^{\infty}\int_{-\infty}^{\infty} \text{MTF}_2^2(u,v)|F(u,v)|^2\,du\,dv}{\displaystyle\int_{-\infty}^{\infty}\int_{-\infty}^{\infty} \text{NPS}(u,v)\,du\,dv}\,.$$

Since $\text{MTF}_1(u,v) \le \text{MTF}_2(u,v)$, we have $\text{MTF}_1^2(u,v)|F(u,v)|^2 \le \text{MTF}_2^2(u,v)|F(u,v)|^2$. Therefore

$$\int_{-\infty}^{\infty}\int_{-\infty}^{\infty} \text{MTF}_1^2(u,v)|F(u,v)|^2\,du\,dv \le \int_{-\infty}^{\infty}\int_{-\infty}^{\infty} \text{MTF}_2^2(u,v)|F(u,v)|^2\,du\,dv\,.$$

So $\text{SNR}_{p1} \le \text{SNR}_{p2}$, the output power SNR of the second system, the one with larger MTF, is higher. Therefore, the second system is better in terms of image quality.

Solution 3.17

(a) The noise in the output $g(x,y)$ is $n'(x,y)$

$$n'(x,y) = h(x,y) * n(x,y)\,.$$

Its mean is

$$\begin{aligned} E\{n'(x,y)\} &= E\{h(x,y) * n(x,y)\} \\ &= E\left\{\int_{-\infty}^{\infty}\int_{-\infty}^{\infty} h(\xi,\eta)n(x-\xi,y-\eta)d\xi d\eta\right\} \\ &= \int_{-\infty}^{\infty}\int_{-\infty}^{\infty} h(\xi,\eta)E\{n(x-\xi,y-\eta)\}\,d\xi d\eta \\ &= 0\,. \end{aligned}$$

Its variance is

$$\begin{aligned}
E\left\{n'(x,y)n'(x,y)\right\} &= E\left\{[h(x,y)*n(x,y)]^2\right\} \\
&= E\left\{\int_{-\infty}^{\infty}\int_{-\infty}^{\infty} h(\xi,\eta)n(x-\xi,y-\eta)d\xi\,d\eta \right. \\
&\qquad \left. \int_{-\infty}^{\infty}\int_{-\infty}^{\infty} h(p,q)n(x-p,y-q)dp\,dq\right\} \\
&= E\left\{\int_{-\infty}^{\infty}\int_{-\infty}^{\infty}\int_{-\infty}^{\infty}\int_{-\infty}^{\infty} h(\xi,\eta)n(x-\xi,y-\eta) \right. \\
&\qquad \left. h(p,q)n(x-p,y-q)dp\,dq\,d\xi\,d\eta\right\} \\
&= \int_{-\infty}^{\infty}\int_{-\infty}^{\infty}\int_{-\infty}^{\infty}\int_{-\infty}^{\infty} h(\xi,\eta)h(p,q) \\
&\qquad E\left\{n(x-\xi,y-\eta)n(x-p,y-q)\right\}dp\,dq\,d\xi\,d\eta \\
&= \int_{-\infty}^{\infty}\int_{-\infty}^{\infty}\int_{-\infty}^{\infty}\int_{-\infty}^{\infty} h(\xi,\eta)h(p,q) \\
&\qquad \sigma_n^2\delta(p-\xi,q-\eta)dp\,dq\,d\xi\,d\eta \\
&= \sigma_n^2\int_{-\infty}^{\infty}\int_{-\infty}^{\infty} h^2(\xi,\eta)d\xi\,d\eta \\
&= \sigma_n^2 H_0\,,
\end{aligned}$$

where, $H_0 = \int_{-\infty}^{\infty}\int_{-\infty}^{\infty} h^2(\xi,\eta)d\xi\,d\eta$.

(b) The power SNR for the input image is

$$\text{SNR}_{\text{in}} = \frac{\int_{-\infty}^{\infty}\int_{-\infty}^{\infty} f^2(x,y)dx\,dy}{\sigma_n^2}\,.$$

The power SNR for the output image is

$$\text{SNR}_{\text{out}} = \frac{\int_{-\infty}^{\infty}\int_{-\infty}^{\infty}[h(x,y)*f(x,y)]^2dx\,dy}{H_0\sigma_n^2}\,.$$

(c) Since we assume that the system does not change $f(x,y)$, $h(x,y)*f(x,y) = f(x,y)$, we must have $H_0 < 1$ in order for the SNR to be improved by the system.

SAMPLING THEORY

Solution 3.18

(a) We have

$$\begin{aligned} f_s(t) &= f(t)\delta_s(t;\Delta T) \\ &= \sum_{m=-\infty}^{\infty} f(t)\delta(t-m\Delta T) \\ &= \sum_{m=-\infty}^{\infty} f(m\Delta T)\delta(t-m\Delta T)\,. \end{aligned}$$

Since

$$f(t) = \begin{cases} \sin\left(\dfrac{2\pi t}{T}\right), & 0 \le t \le T \\ \\ 0, & \text{otherwise} \end{cases}$$

and $\Delta T = 0.25T$, then

$$f_s(t) = \delta(t-0.25T) - \delta(t-0.75T)\,.$$

Also

$$f_d(m) = f(m\Delta T) = \begin{cases} 1, & m = 1 \\ -1, & m = 3 \\ 0, & \text{otherwise} \end{cases}\,.$$

(b) The signal $f_h(t)$ is referred to as a *zero-order hold*. By definition,

$$\begin{aligned} f_h(t) &= \begin{cases} 1, & 0.25T \le t < 0.5T \\ -1, & 0.75T \le t < T \\ 0, & \text{otherwise} \end{cases} \\ &= \text{rect}\left(\frac{t-0.375T}{0.25T}\right) - \text{rect}\left(\frac{t-0.875T}{0.25T}\right). \end{aligned}$$

Using the properties of the Fourier transform, we have

$$\begin{aligned} F_h(f) &= \mathcal{F}(f_h(t)) \\ &= \int_{-\infty}^{\infty} f_h(t)e^{-j2\pi ft}dt \\ &= 0.25T\text{sinc}(0.25Tf)e^{-j2\pi(0.375Tf)} - 0.25T\text{sinc}(0.25Tf)e^{-j2\pi(0.875Tf)} \\ &= 0.25T\text{sinc}(0.25Tf)\left[e^{-j2\pi(0.375Tf)} - e^{-j2\pi(0.875Tf)}\right]. \end{aligned}$$

(c) For $\Delta T = 0.5T$, we have

$$\begin{aligned} f_s(t) &= 0\,, \\ f_d(m) &= 0\,, \\ f_h(t) &= 0\,, \\ F_h(f) &= 0\,. \end{aligned}$$

Solution 3.19

Since the Nyquist sampling periods for 1-D band-limited signals $f(x)$ and $g(x)$ are Δ_f and Δ_g, the highest frequency of $f(x)$ and $g(x)$ are $\frac{1}{2\Delta_f}$ and $\frac{1}{2\Delta_g}$. In order to find the Nyquist sampling periods, we need to find the highest frequency for each of the signals.

(a) A shift in location does not change the frequency components of a signal, so the magnitude spectrum of $f(x - x_0)$ is the same as that of $f(x)$. The Nyquist sampling period of $f(x - x_0)$ is Δ_f.

(b) The Fourier transform of $f(x) + g(x)$ is $\mathcal{F}[f(x) + g(x)] = \mathcal{F}[f(x)] + \mathcal{F}[g(x)]$. The highest frequency of $f(x) + g(x)$ is $\max(\frac{1}{2\Delta_f}, \frac{1}{2\Delta_g})$, so the Nyquist sampling period of $f(x) + g(x)$ is $\min(\Delta_f, \Delta_g)$.

(c) The Fourier transform of $f(x) * f(x)$ is $\mathcal{F}[f(x)]^2$. The highest frequency of $f(x) * f(x)$ is $\frac{1}{2\Delta_f}$, The Nyquist sampling period of $f(x) * f(x)$ is Δ_f.

(d) The Fourier transform of $f(x)g(x)$ is $\mathcal{F}[f(x)] * \mathcal{F}[g(x)]$, The highest frequency of $f(x)g(x)$ is $\frac{1}{2\Delta_f} + \frac{1}{2\Delta_g}$, and the Nyquist sampling period is $\frac{\Delta_f \Delta_g}{\Delta_f + \Delta_g}$.

(e) If $f(x) \geq 0$, $\|f(x)\| = f(x)$, the Nyquist sampling period of $\|f(x)\|$ is Δ_f. But in general, the operation of taking absolute value will reverse part of the original signal $f(x)$, and therefore introduce high frequency component. In general case, $\|f(x)\|$ is no longer bandlimited, even though $f(x)$ is.

Solution 3.20

The sampling frequencies are $\frac{1}{\Delta x} = 1.5$ and $\frac{1}{\Delta y} = 1.5$. From the sampling theorem, in order to avoid aliasing, the cutoff frequencies of the low-pass filtered signal $f * h$ must satisfy:

$$U \leq \frac{1}{2\Delta x} = 0.75, \text{ and } V \leq \frac{1}{2\Delta y} = 0.75\,.$$

Thus, the ideal low-pass filter $h(x, y)$ that gives the maximum possible frequency content must have a frequency response as

$$H(u, v) = \begin{cases} 1\,, \text{if } |u| \leq 0.75 \text{ and } |v| \leq 0.75 \\ 0, \text{ otherwise} \end{cases}\,.$$

$H(u, v)$ is one inside a square region and zero outside. The PSF of the required anti-aliasing low-pass filter can be computed as:

$$\begin{aligned} h(x,y) &= \mathcal{F}_2^{-1}(H(u,v)) = \int_{-\infty}^{\infty}\int_{-\infty}^{\infty} H(u,v)e^{j2\pi(ux+vy)}\,dudv \\ &= \int_{-0.75}^{0.75}\int_{-0.75}^{0.75} e^{j2\pi(ux+vy)}\,dudv \\ &= \left(\int_{-0.75}^{0.75} e^{j2\pi ux}\,du\right)\cdot\left(\int_{-0.75}^{0.75} e^{j2\pi vy}\,dv\right) \\ &= \frac{\exp[j2\pi(0.75)x] - \exp[j2\pi(-0.75)x]}{j2\pi x}\cdot\frac{\exp[j2\pi(0.75)y] - \exp[j2\pi(-0.75)y]}{j2\pi y} \\ &= \frac{\sin(1.5\pi x)}{\pi x}\cdot\frac{\sin(1.5\pi y)}{\pi y}\,. \end{aligned}$$

From Table 2.1, we know that

$$\mathcal{F}_2(f)(u,v) = e^{-\pi(u^2+v^2)}\,.$$

Thus, the total spectrum energy of $f(x,y)$ is

$$\begin{aligned}
E_{\text{total}} &= \int_{-\infty}^{\infty}\int_{-\infty}^{\infty} |\mathcal{F}_2(f)(u,v)|^2\,du\,dv \\
&= \int_{-\infty}^{\infty}\int_{-\infty}^{\infty} e^{-2\pi(u^2+v^2)}\,du\,dv \\
&= \left(2\pi\sigma^2\right)\frac{1}{2\pi\sigma^2}\int_{-\infty}^{\infty}\int_{-\infty}^{\infty} e^{-(u^2+v^2)/2\sigma^2}\,du\,dv \text{ with } \sigma^2 = \frac{1}{4\pi} \\
&= 2\pi\cdot\frac{1}{4\pi} \\
&= 0.5\,.
\end{aligned}$$

The spectrum that is kept by the low pass filter has energy of

$$\begin{aligned}
E_{\text{preserve}} &= \int_{-0.75}^{0.75}\int_{-0.75}^{0.75} e^{-2\pi(u^2+v^2)}\,du dv \\
&= \int_{-0.75}^{0.75} e^{-2\pi u^2}\,du\cdot\int_{-0.75}^{0.75} e^{-2\pi v^2}\,dv \\
&= \left(\frac{1}{\sqrt{2\pi}}\int_{-0.75\sqrt{2\pi}}^{0.75\sqrt{2\pi}} e^{-t^2}\,dt\right)^2 \\
&= \left[\frac{1}{\sqrt{2\pi}}\frac{\sqrt{\pi}}{2}2\text{erf}\left(0.75\sqrt{2\pi}\right)\right]^2 \\
&= \frac{1}{2}\left[\text{erf}\left(0.75\sqrt{2\pi}\right)\right]^2 \\
&\approx \frac{1}{2}\left[0.992\right]^2 \\
&\approx 0.492\,,
\end{aligned}$$

where erf(·) is the error function. Thus, the percentage of the spectrum energy that is preserved is

$$\frac{E_{\text{preserve}}}{E_{\text{total}}} = \frac{0.492}{0.5} = 98.4\%\,.$$

Since the spectrum of $f(x,y)$, which is $\mathcal{F}_2(f)(u,v) = e^{-\pi(u^2+v^2)}$, is non-zero for all $(u,v) \in (-\infty,\infty)\times(-\infty,\infty)$, it is impossible to sample $f(x,y)$ free of aliasing without using an anti-aliasing filter.

Solution 3.21

(a) Impulse response: $h(x,y) = \text{rect}(\frac{x}{w})\text{rect}(\frac{y}{w})$.
MTF: $H(u,v) = w^2\text{sinc}(wu)\text{sinc}(wv)$ and $H(0,0) = w^2$.
Thus $\text{MTF}(u,v) = \frac{H(u,v)}{H(0,0)} = \text{sinc}(wu)\text{sinc}(wv)$.
Horizontal FWHM = w.

(b) Since $H(u,v) = w^2\text{sinc}(wu)\text{sinc}(wv)$ and $H(0,0) = w^2$, considering the main lobe of the sinc function

and from Nyquist sampling theory, $u_s \geq 2/w$, $v_s \geq 2/w$. Then $\Delta X \leq w/2$ and $\Delta Y \leq w/2$. This means that aliasing occurs in the sampling scheme using detectors of dimensions $w \times w$ and separation of w. Since $\Delta X = w$ and $\Delta Y = w$ then $u_s = 1/w, v_s = 1/w$ then the object must be limited to $-1/2w$ and $1/2w$. i.e the object must have width $\mathrm{W}_x = 1/w$ and $\mathrm{W}_y = 1/w$ so that no aliasing occurs.

(c) In order to eliminate the aliasing occurring from using the $w \times w$ size detectors as explained before, grouping of four of the small detectors is done so that the new detector size is $2w \times 2w$. That means that separation between detectors of $\Delta X \leq w$ and $\Delta Y \leq w$ will guarantee no aliasing (detectors must overlap). This can be achieved as in Figure S3.5 by using the fact that we can overlap the resultant detector by sequentially using the small detectors for overlap.

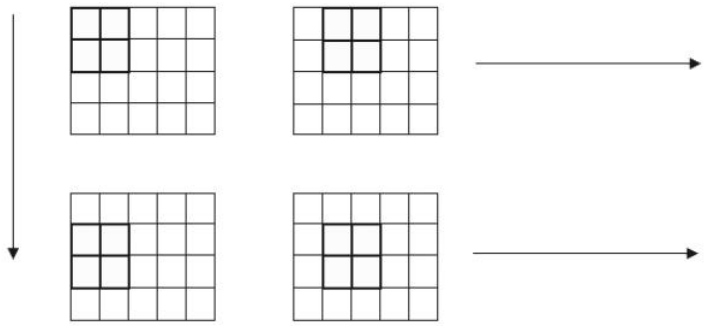

Figure S3.5 Overlapping of the detectors. See Problem 3.21.

(d) The impulse response function now is $h(x, y) = \mathrm{rect}(\frac{x}{2w})\mathrm{rect}(\frac{y}{2w})$ and the (horizontal) FWHM $= 2w$.

(e) Sequential grouping can be done after the image is acquired by the summation of 4 pixel values using the same scheme described in (c) to get an aliasing free image.

Solution 3.22

(a) System 1 has a PSF that is a rectangle of width 0.5. Its FWHM is therefore 0.5.

System 2's FWHM can be found by

$$\begin{aligned} \frac{1}{2} &= e^{-\pi x^2} \\ \implies -\log 2 &= -\pi x^2 \\ \implies x^2 &= \frac{\log 2}{\pi} \\ \implies x &= \pm\sqrt{\frac{\log 2}{\pi}}\,. \end{aligned}$$

Therefore the FWHM is $2\sqrt{\frac{\log 2}{\pi}} \sim 0.9394$.

System 1 has the better resolution.

(b) The MTF is defined by the absolute value of the transfer function divided by its value at zero frequency. The transfer function for system 1 is therefore given by

$$\begin{aligned}\mathrm{rect}(x) &\leftrightarrow \mathrm{sinc}(u)\,,\\ \mathrm{rect}(2x) &\leftrightarrow \frac{1}{2}\mathrm{sinc}\left(\frac{u}{2}\right)\,,\\ h_1(x) = \mathrm{rect}(2x) &\leftrightarrow H_1(u) = \frac{1}{2}\mathrm{sinc}\left(\frac{u}{2}\right)\,.\end{aligned}$$

And the transfer function for system 2 is given by

$$h_2(x) = e^{-\pi x^2} \leftrightarrow e^{-\pi u^2} = H_2(u)$$

The MTFs are then

$$\begin{aligned}\mathrm{MTF}_1(u) &= \frac{\frac{1}{2}\mathrm{sinc}\left(\frac{u}{2}\right)}{\frac{1}{2}}\\ &= \mathrm{sinc}\left(\frac{u}{2}\right)\,,\\ \mathrm{MTF}_2(u) &= e^{-\pi u^2}\,.\end{aligned}$$

(c) $f(x)$ is a sinusoidal signal at frequency 2 (i.e., $2\pi f x = 4\pi x \implies f = 2$). Since this is a LSI system, with a real/even transfer function, the only effect is to rescale the amplitude of the sinusoid by the transfer function at frequency $\frac{1}{4}$. Therefore

$$\begin{aligned}g_1(x) &= H_1(2)\cos(4\pi x)\\ &= \frac{1}{2}\mathrm{sinc}(2/2)\\ &= \frac{1}{2}\mathrm{sinc}(1)\\ &= 0\,,\end{aligned}$$

and

$$\begin{aligned}g_2(x) &= H_2(2)\cos(4\pi x)\\ &= e^{-\pi 2^2}\cos(4\pi x)\\ &\sim 3.4873\times 10^{-6}\cos(4\pi x)\,.\end{aligned}$$

Therefore you should use system 2 to image this signal because system 1 will not respond to it at all.

(d) We must sample at a rate greater than twice the highest frequency in our signal. The highest frequency (the only frequency) is 4. Therefore we must sample at a rate greater than 4. This corresponds to a period less than 1/4.

ARTIFACTS, DISTORTION, AND ACCURACY

Solution 3.23

Both noise and artifacts degrade the image, making correct detection and delineation of anatomical features difficult. The main technical difference between the two is that artifacts are reproducible scan after scan, whereas noise will come out differently with each scan. On the other hand, noise is well-modeled using probability and random variables, so that the broad characteristic of noise—for example, mean and variance—will be the same. Artifacts are deterministic, and can originate from a variety of sources that, in principle, can be modeled and removed. For example, some artifacts appear because of instrumentation failure or calibration problems. Artifacts can also appear because the image reconstruction method fails to adequately model the true physics of the imaging modality. Finally, artifacts might arise due to inadequacies in data collection—aliasing, for example.

Solution 3.24

Suppose the center of the ball has coordinates $(x, 0, 0)$. When the source is inside the ball or on the ball surface, i.e. $x \leq r$, the shadow of the ball will cover the entire detector plane. In this case, the radius of the image is ∞. When $x > r$, by simple geometry, we have the radius of the image on the detector plane, R:

$$R = d \tan\theta = \frac{r}{\sqrt{x^2 - r^2}} \quad \Rightarrow \quad R = \frac{dr}{\sqrt{x^2 - r^2}},$$

where θ is the angle between the x axis and the tangent plane of the ball through the source. The size distortion is measured by the ratio $R/r = d/\sqrt{x^2 - r^2}$. When d is fixed, we can increase x to reduce the ratio R/r. And the largest x we can get is $d - r$, in which case $R/r = d/\sqrt{d^2 - 2dr}$.

Solution 3.25

(a) If we take measurements on rectangular grids in the image plane, the locations of sample points are $(k\Delta x, l\delta y)$, where k, and l are integers, and $\Delta x, \delta y$ are spacing in x and y directions. The corresponding coordinates of the samples in the physical domain can be obtained by solving the equations above, yielding

$$\begin{aligned} \xi(k,l) &= \frac{k\Delta x}{1 + (l\Delta y)^2/50}\,, \\ \eta(k,l) &= l\Delta y\,. \end{aligned}$$

The (k,l)-th sample on the image plane needs to be placed at $(\xi(k,l), \eta(k,l))$ on the physical domain to correct the geometric distortion.

(b) If we take measurements on rectangular grids in the physical domain, the locations of sample points in the physical domain are $(k\Delta\xi, l\delta\eta)$. On the image plane, we need to sample points at

$$\begin{aligned} x(k,l) &= k\Delta\xi + \frac{1}{50} k\Delta\xi (l\Delta\eta)^2\,, \\ y(k,l) &= l\Delta\eta\,. \end{aligned}$$

Solution 3.26

(a) The pdf of the test value for normal and diseased subjects are

$$\begin{aligned} p_{\mathrm{N}}(t) &= \frac{1}{\sqrt{2\sigma_0^2}} e^{-(x-\mu_0)^2/2\sigma_0^2}, \\ p_{\mathrm{D}}(t) &= \frac{1}{\sqrt{2\sigma_1^2}} e^{-(x-\mu_1)^2/2\sigma_1^2}. \end{aligned}$$

(b) When the threshold is set to be $t_0 = (\mu_0 + \mu_1)/2$, the sensitivity and the specificity are

$$\begin{aligned} \text{sensitivity} &= \frac{a}{a+c} \\ &= \frac{\int_{t_0}^{\infty} p_{\mathrm{D}}(t)dt}{\int_{-\infty}^{t_0} p_{\mathrm{D}}(t)dt + \int_{t_0}^{\infty} p_{\mathrm{D}}(t)dt} \\ &= \frac{1}{2} + \text{erf}\left(\frac{\mu_1 - t_0}{\sigma_1}\right) \\ &= \frac{1}{2} + \text{erf}\left(\frac{\mu_1 - \mu_0}{2\sigma_1}\right), \\ \text{specificity} &= \frac{d}{b+d} \\ &= \frac{1}{2} + \text{erf}\left(\frac{\mu_1 - \mu_0}{2\sigma_0}\right). \end{aligned}$$

(c) The sensitivity as a function of threshold value is

$$\text{sensitivity}(t) = \begin{cases} \frac{1}{2} + \text{erf}\left(\frac{\mu_1 - t}{\sigma_1}\right), & t \le \mu_1 \\ \frac{1}{2} - \text{erf}\left(\frac{t - \mu_1}{\sigma_1}\right), & t > \mu_1 \end{cases}.$$

(d) The diagnostic accuracy is

$$\text{DA} = \frac{a+d}{a+b+c+d} = \begin{cases} \frac{1}{2}\left[1 - \text{erf}\left(\frac{\mu_0 - t}{\sigma_0}\right) + \text{erf}\left(\frac{\mu_1 - t}{\sigma_1}\right)\right], & t < \mu_0 \\ \frac{1}{2}\left[1 + \text{erf}\left(\frac{t - \mu_0}{\sigma_0}\right) + \text{erf}\left(\frac{\mu_1 - t}{\sigma_1}\right)\right], & \mu_0 \le t \le \mu_1 \\ \frac{1}{2}\left[1 + \text{erf}\left(\frac{t - \mu_0}{\sigma_0}\right) - \text{erf}\left(\frac{t - \mu_1}{\sigma_1}\right)\right], & t > \mu_1 \end{cases}.$$

APPLICATIONS, EXTENSIONS AND ADVANCED TOPICS

Solution 3.27

We consider image quality to be characterized by contrast and resolution. Since resolution is typically characterized using the FWHM, from (3.22) we know that the FWHM of the overall system can be determined approximately from the FWHMs of the individual subsystems according to

$$\text{FWHM}_{\text{total}} = \sqrt{\text{FWHM}_1^2 + \text{FWHM}_2^2 + \cdots + \text{FWHM}_K^2}\,.$$

It follows that

$$\text{FWHM}_{\text{total}} \geq \text{FWHM}_i, \text{ for all } 1 \leq i \leq K\,.$$

Thus the resolution of the overall system is worse than each of the individual subsystems.

Both contrast and resolution can be characterized using the MTF. The MTF of the overall system is given by

$$\text{MTF}(u,v) = \text{MTF}_1(u,v)\text{MTF}_2(u,v)\cdots\text{MTF}_K(u,v)\,,$$

in terms of the individual subsystem MTFs $\text{MTF}_i(u,v)$, $i = 1,2,...,K$. For most medical imaging systems, $\text{MTF}(u,v) \leq 1$ for all (u,v). Assuming this is true for all the subsystems, that is,

$$\text{MTF}_i(u,v) \leq 1, \text{ for } i = 1,2,\ldots,K\,,$$

then it follows that

$$\text{MTF}(u,v) \leq \text{MTF}_i(u,v), \text{ for } i = 1,2,\ldots,K\,.$$

Therefore, from this standpoint as well, the contrast and resolution of the overall system is inferior to each individual subsystem.

Solution 3.28

(a) Let $\lambda = (x - x_0)/(x_1 - x_0)$, and $\mu = (y - y_0)/(y_1 - y_0)$. Linear interpolation gives

$$\begin{aligned} f(E) &= (1-\lambda)f(A) + \lambda f(B)\,, \\ f(F) &= (1-\lambda)f(C) + \lambda f(D)\,. \end{aligned}$$

Then $f(P)$ can be obtained by linear interpolation of $f(E)$ and $f(F)$:

$$\begin{aligned} f(P) &= (1-\mu)f(F) + \mu f(E) \\ &= \mu(1-\lambda)f(A) + \mu\lambda f(B) + (1-\mu)(1-\lambda)f(C) + (1-\mu)\lambda f(D)\,. \end{aligned}$$

(b) Similarly,

$$\begin{aligned} f(G) &= (1-\mu)f(C) + \mu f(A)\,, \\ f(H) &= (1-\mu)f(D) + \mu f(B)\,, \end{aligned}$$

and

$$\begin{aligned} f(P) &= (1-\lambda)f(G) + \lambda f(H) \\ &= (1-\lambda)(1-\mu)f(C) + (1-\lambda)\mu f(A) + \lambda(1-\mu)f(D) + \lambda\mu f(B)\,. \end{aligned}$$

Comparing the coefficients for $f(A)$, $f(B)$, $f(C)$, and $f(D)$, we can see that the results from (a) and (b) are the same.

(c) The point $\xi = 3, \eta = 3.5$ locates at $x = 3.735, y = 3.5$ on the image plane, which is inside the cell with four corners $x_0 = 3, y_0 = 3$, $x_0 = 3, y_1 = 4$, $x_1 = 4, y_0 = 3$, and $x_1 = 4, y_1 = 4$. By our definition in Problem 3.25, $\lambda = 0.735, \mu = 0.5$. The value for $\xi = 3, \eta = 3.5$ is

$$f'(\xi = 3, \eta = 3.5) = 0.1325(f(3,4) + f(3,3)) + 0.3675(f(4,4) + f(4,3)),$$

where $f(m, n)$ are the measurements on the image plane.

Solution 3.29

(a) For a given threshold value t with $\mu_0 \le t \le \mu_1$, the sensitivity and the specificity are given as:

$$\begin{aligned} \text{sensitivity} &= \frac{1}{2} + \text{erf}\left(\frac{\mu_1 - t}{\sigma_1}\right)\,, \\ \text{specificity} &= \frac{1}{2} + \text{erf}\left(\frac{t - \mu_o}{\sigma_1}\right)\,. \end{aligned}$$

The ROC curve is shown in Figure S3.6.

(b) The perfect diagnostic test should have both sensitivity and specificity equal to 1. In this case, the ROC curve is a point $(0, 1)$ on the coordinate system of Figure S3.6.

(c) The point on the ROC curve that is closest to the point $(0, 1)$ is $(0.0179, 0.9744)$. In this case, 97.44% of the diseased patients will be diagnosed correctly, while 1.79% of the normal patients will be wrongfully

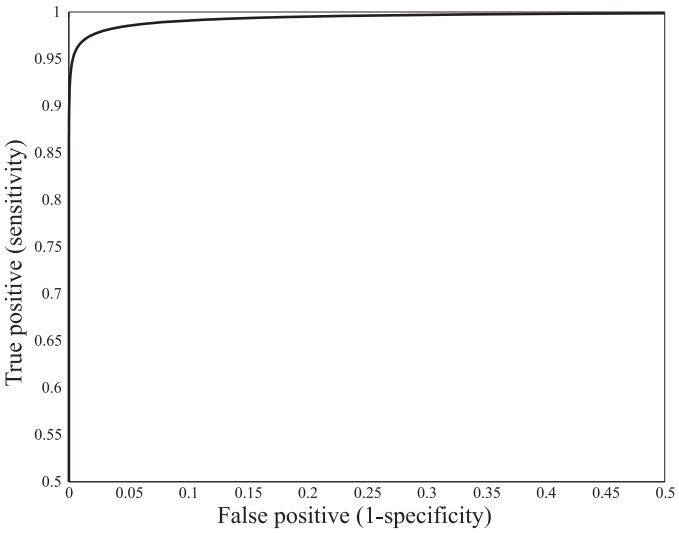

Figure S3.6 The ROC curve. See Problem 3.29.

diagnosed as diseased. Using the relationship between sensitivity and threshold, the corresponding threshold value is $t_{\text{opt}} = 5.24$, which is different from $(\mu_0 + \mu_1)/2$ because the two groups of subjects have different variances.

4

Physics of Radiography

PHYSICS OF ATOMS

Solution 4.1

(a) From tables (internet or physics or chemistry textbooks),

$$\text{mass of carbon-12} = 1.99264663 \times 10^{-26}\ \text{kg}\,.$$

From the information given in the problem statement, we calculate

$$\text{mass of (6p + 6n + 6e)} = 2.0090759569 \times 10^{-26}\ \text{kg}\,.$$

The mass defect is therefore

$$\begin{aligned} \text{mass defect of carbon atom} &= 2.0090759569 \times 10^{-26}\ \text{kg} - 1.99264663 \times 10^{-26}\ \text{kg} \\ &= 1.6429326956 \times 10^{-28}\ \text{kg}\,. \end{aligned}$$

To find this in atomic mass units

$$\begin{aligned} \text{mass defect of carbon atom} &= 1.6429326956 \times 10^{-28}\ \text{kg} \times 6.0221415 \times 10^{26}\ \text{u/kg} \\ &= 0.098939732\ \text{u}\,. \end{aligned}$$

(b) We have

$$\begin{aligned} E &= mc^2 \\ &= 1.6429326956 \times 10^{-28}\ \text{kg} \times (2.99792458 \times 10^{8}\ \text{m/s})^2 \\ &= 1.47659426 \times 10^{-11}\ \text{J}\,. \end{aligned}$$

Since $1\ \text{eV} = 1.60217653 \times 10^{-19}$ J, we also have

$$E = 9.21617711 \times 10^{7}\ \text{eV}\,.$$

Solution 4.2

(a) The mass-equivalent energy of an electron at rest is

$$E = m_0 c^2 \,.$$

Since $m_0 = 9.10938 \times 10^{-31}$ kg is the mass of an electron at rest and $c = 2.99792 \times 10^8$ m/s, we have

$$\begin{aligned} E &= 9.10938 \times 10^{-31} \times (2.99792 \times 10^8)^2 \text{ kg} - \text{m}^2/\text{s}^2 \\ &= 8.18697 \times 10^{-14} \text{ J} \\ &= 5.11 \times 10^5 \text{ eV} = 511 \text{ keV}. \end{aligned}$$

(b) Ignoring relativity the kinetic energy of an electron at speed $v = \frac{1}{10}c$ is

$$E_k = \frac{1}{2} m_0 v^2 = \frac{1}{200} m_0 c^2 = 2.558 \text{ keV} \,.$$

So when the effect of relativity is ignored, the potential needed to accelerate an electron to a speed equal to 1/10 the speed of light is 2.558 kV. This is not accurate since at 1/10 the speed of light, the effect of relativity cannot be ignored.

(c) The kinetic energy gained by an electron after it is accelerated across a 120 kV potential is

$$\text{KE} = mc^2 - m_0 c^2 = 120 \text{ keV} \,,$$

where m is the relativistic mass of the electron after acceleration, which is given by

$$m = \frac{m_0}{\sqrt{1 - (v/c)^2}} \,.$$

Therefore, we can carry out the following steps to find v:

$$\begin{aligned} 120 \text{ keV} &= mc^2 - m_0 c^2 \\ &= \frac{m_0}{\sqrt{1 - (v/c)^2}} c^2 - m_0 c^2 \\ &= m_0 c^2 \left(\frac{1}{\sqrt{1 - (v/c)^2}} - 1 \right) \\ \frac{120}{511} &= \frac{1}{\sqrt{1 - (v/c)^2}} - 1 \\ v &= 0.5867c. \end{aligned}$$

Thus, at 120 keV the speed of the electrons hitting the anode is over 1/2 that of the speed of light.

Solution 4.3

From Eq. (4.3), we have:

$$\begin{aligned} \text{KE} &= E - E_0 \\ &= mc^2 - m_0 c^2 \,, \end{aligned}$$

where m, m_0 are the mass and the rest mass of the particle, respectively. They are related by the following equation (Eq. (4.1) in the text):

$$m = \frac{m_0}{\sqrt{1 - v^2/c^2}} \, .$$

When $v \ll c$, v^2/c^2 is close to 0. By using Taylor's expansion of function $f(x) = \frac{1}{\sqrt{1-x}}$ in the neighborhood of $x = 0$, we have the following approximation for m:

$$m \approx m_0 \left(1 + \frac{1}{2}\frac{v^2}{c^2}\right) \, .$$

Using this approximation yields

$$\begin{aligned} \text{KE} &= mc^2 - m_0 c^2 \\ &\approx m_0 \left(1 + \frac{1}{2}\frac{v^2}{c^2}\right) c^2 - m_0 c^2 \\ &\approx \frac{1}{2} m_0 v^2 \, . \end{aligned}$$

Notice that when $v \ll c$, the mass m is approximately equal to the rest mass m_0, so we have:

$$\text{KE} \approx \frac{1}{2} m v^2 \, ,$$

which is the usual expression for kinetic energy of a mass in motion.

IONIZING RADIATION

Solution 4.4

Characteristic radiation is produced by electrons that drop to lower energy states (more inner orbits) after they have been excited to higher energy states (more outer orbits). The differential in energy lost by the electron is given off as an x-ray—characteristic radiation. Because electrons exist in discrete energy states that are specific to a given atom, characteristic radiation can only be emitted at a collection of discrete energy levels within the EM spectrum. Therefore, the intensity spectrum for characteristic radiation comprises a discrete spectrum—that is, spectral lines.

On the other hand, Bremsstrahlung radiation is caused by interaction of an energetic electron with a nucleus of an atom. Specifically, the nucleus, having a positive charge, will tend to attract the electron, having a negative charge, causing the electron to slow down and be deflected from its original path. The electron loses energy as a result, which is radiated away as an x-ray with energy equal to that lost by the electron. An electron can lose all its energy, by collision into the atomic nucleus, or any smaller amount, by smaller deflection. Therefore, unlike characteristic radiation, the energy spectrum of bremsstrahlung radiation is continuous. Since lower energy losses are more likely, and direct collision with a nucleus is very unlikely, the bremsstrahlung spectrum is zero at the incident energy of the electrons and grows larger with decreasing energy.

Solution 4.5

(a) Ionization is the *ejection* of an electron from an atom. In order to eject an electron, the incident radiation must have sufficient energy to overcome the binding energy of the electron. The smallest binding energy among atoms having smaller atomic numbers is that of the sole electron in the hydrogen atom. Its binding energy is 13.6 eV. Therefore, a radiation having energy above 13.6 eV is capable of ionizing the hydrogen

atom, which makes it ionizing radiation. If the radiation has energy smaller than 13.6 eV it is not capable of ionizing the hydrogen atom or any other atom (with smaller atomic number), and is therefore considered non-ionizing. (There are larger atoms having electrons with binding energy less than 13.6 eV, but these are rare in nature and even rarer in the human body.)

(b) Ionization is the *ejection* of an electron from an atom, while excitation is the process of raising the energy of an electron within the electron cloud, without causing ejection. Excitation rearranges the electrons within the shells, but this is only a temporary effect, since the electrons will seek a lower energy configuration, and in the process generate characteristic radiation.

Solution 4.6

(a) The frequencies and the wavelengths of EM waves are related by the formula:

$$\lambda = \frac{c}{\nu}\,,$$

where $c = 3.0 \times 10^8$ meters/sec is the speed of light. For $\lambda = 4$ nanometers, we have

$$\begin{aligned} \nu &= \frac{c}{\lambda} \\ &= \frac{3.0 \times 10^8 \text{ m/s}}{4 \times 10^{-9} \text{ m}} \\ &= 7.5 \times 10^{16} \text{ Hz}\,. \end{aligned}$$

Similarly, for $\lambda = 400$ nanometers we have $\nu = 7.5 \times 10^{14}$ Hz. So the frequency range for ultraviolet light is 7.5×10^{14} Hz $\sim 7.5 \times 10^{16}$ Hz.

(b) The energy of a photon is given by

$$E = h\nu\,,$$

where $h = 6.626 \times 10^{-34}$ Joule-sec is Planck's constant. So for ultraviolet light with frequency $\nu = 7.5 \times 10^{14}$ Hz, the energy is $E = h\nu = 6.626 \times 10^{-34} \times 7.5 \times 10^{14} = 4.97 \times 10^{-19}$ Joule. Since 1 eV $= 1.6 \times 10^{-19}$ Joule, we have that $E = 4.97 \times 10^{-19}$ Joule $= 3.1$ eV. Similarly, for ultraviolet light with frequency $\nu = 7.5 \times 10^{16}$ Hz, the energy is $E = 310$ eV. So the photon energy range for ultraviolet light is 3.1–310 eV.

(c) Radiation with energy greater than or equal to 13.6 eV is considered to be *ionizing radiation*. It is easy to calculate that when the frequency of the ultraviolet light is $\nu = 3.284 \times 10^{15}$ Hz, the photon energy is $E = h\nu = 13.6$ eV. So ultraviolet light is ionizing radiation when its frequency is greater or equal to $\nu_0 = 3.284 \times 10^{15}$ Hz. Ultraviolet light with a frequency lower than that is not ionizing radiation. Or equivalently, when the wavelength is larger than $\lambda_0 = \frac{c}{\nu_0} = 91.35$ nanometers, ultraviolet light is not ionizing radiation.

Solution 4.7

(a) Electron density is:

$$\text{EC} = \frac{N_A Z}{W_m}\,,$$

where

$$\begin{aligned} N_A &= 6.022 \times 10^{23}\,, \\ Z &= 1 \quad \text{(for hydrogen)}\,, \\ W_m &= 1 \text{ gram/mole (for hydrogen)}\,, \end{aligned}$$

where the last fact follows from the fact that the atomic weight of a hydrogen atom is approximately 1 u. Therefore,

$$\text{ED} = \frac{6.022 \times 10^{23} \times 1}{1 \text{ gram/mole(of electrons)}} \approx 6 \times 10^{23} \text{ electrons/g} = 6 \times 10^{26} \text{ electrons/kg}\,.$$

(b) Except for the hydrogen atom, all other low atomic number materials have nearly equal numbers of neutrons as protons. Therefore, since the weight of these other atoms is doubled, while the number of electrons remains tied to the number of protons, the electron density is approximately halved from that of hydrogen.

(c) The slight deviation can result from the ratio of neutrons to protons become larger than one with increasing atomic number and from the differing hydrogen content in various materials.

ATTENUATION OF EM RADIATION

Solution 4.8

(a) Let I_0 denote the incident intensity, and I_x the exiting intensity. Denote the thickness of the shielding material. From the problem specification, we know that

$$\frac{I_x}{I_0} = 1 - 99.5\% = 0.005.$$

Since I_x and I_0 are related by

$$I_x = I_0 e^{-\mu x}\,,$$

we have

$$e^{-\mu x} = \frac{I_x}{I_0} = 0.005\,.$$

Then, we solve for x as follows

$$x = -\frac{1}{\mu}\ln 0.005 = \frac{\ln 200}{\mu} \approx \frac{5.3}{\mu}\,,$$

which is the required thickness of the shielding material.

(b) The desired range of an ionizing beam in tissue would be centimeters to tens of centimeters, which is about the distance that the beam would have to travel through the body. If the range is larger, then the incident beam would travel through the body with almost no attenuation, and no contrast would be obtained. If the range is too short, all beam energy would be absorbed by the body, and no image can be formed.

Solution 4.9

Let $df = \frac{dN}{N} = -\mu dx$. By solving $\frac{df}{dN} = \frac{1}{N}$, we have $f = \ln N + c_1$, and by solving $\frac{df}{dx} = -\mu$, we have $f = -\mu x + c_2$, where c_1 and c_2 are two arbitrary constants. Therefore, $f = \ln N + c_1 = -\mu x + c_2$. This leads to $\ln N = -\mu x + c$, where c is an arbitrary constant. So we have $N = N_0 e^{-\mu x}$, with a constant N_0.

Solution 4.10

Suppose that the x-ray photons hit the phantom on a unit area is N_0. On the screen where it is not blocked by the bars, the photons detected on a unit area is also N_0. The thickness of the bars is 0.4 cm, which is 4 times the HVL, so the x-ray photons passing through the bars is $(1/2)^4 = 1/16$ of those entering the bars. So the screen that is blocked by the bars detects $N_0/16$ photons on a unit area. The contrast of the image on the screen is

$$C = \frac{N_0 - N_0/16}{N_0 + N_0/16} = \frac{15}{17}\,.$$

Solution 4.11

From Eq. (4.8), the energy of the scattered photon is given by

$$h\nu' = \frac{h\nu}{1 + \dfrac{h\nu}{m_0 c^2}(1 - \cos\theta)}\,,$$

where $m_0 c^2 = 511$ keV. Thus, the larger θ is, the smaller the energy of the scattered photon. Using the facts 1 Angstrom $= 10^{-10}$meter, $h = 6.626 \times 10^{-34}$joule-sec, and 1 joule $= 6.241 \times 10^{15}$ keV, we can compute the energy of the source x-ray photon as

$$\begin{aligned} h\nu &= hc/\lambda \\ &= \frac{6.626 \times 10^{-34}\text{joule-sec} \times 3 \times 10^{8}\text{m/s} \times 6.241 \times 10^{15}\ \text{keV/joule}}{8.9 \times 10^{-2} \times 10^{-10}\text{m}} \\ &\approx 139.4\ \text{keV}\,. \end{aligned}$$

The energy of a photon that has been scattered by 25° is

$$\begin{aligned} h\nu' &= \frac{h\nu}{1 + \dfrac{h\nu}{m_0 c^2}(1 - \cos 25^\circ)} \\ &= \frac{139.4\ \text{keV}}{1 + \dfrac{139.4\ \text{keV}}{511\ \text{keV}}(1 - \cos 25^\circ)} \\ &\approx 135.9\ \text{keV}\,. \end{aligned}$$

Thus, to eliminate all photons that have scattered more than 25 degrees, the system should only accept photon energy between 135.9 keV and 139.4 keV.

Solution 4.12

From Eq. (4.8), the energy of the scattered photon is given by:

$$h\nu' = \frac{h\nu}{1 + \dfrac{h\nu}{m_0c^2}(1 - \cos\theta)} ,$$

where $m_0c^2 = 511$ keV.

(a) We use the provided numbers and solve for θ as follows:

$$\begin{aligned} 99 &= \frac{100}{1 + (1 - \cos\theta)100/511} \\ \implies \theta &= \cos^{-1}\left(1 - \frac{511}{100 \times 99}\right) \\ &= 18.49^\circ . \end{aligned}$$

(b) We use the provided numbers to solve for E as follows:

$$\begin{aligned} E &= \frac{100}{1 + (1 - \cos(25^\circ))100/511} \\ &= 98.20\,\text{keV} . \end{aligned}$$

The range is therefore 98.20–100 keV.

Solution 4.13

(a) We use the provided linear attenuation coefficient and solve for HVL as follows:

$$\begin{aligned} \frac{N}{N_0} &= e^{-\mu\text{HVL}} = \frac{1}{2} , \\ \implies \mu\text{HVL} &= \ln 2 , \\ \implies \text{HVL} &= \frac{\ln 2}{\mu} = 0.3\ \text{cm} . \end{aligned}$$

Therefore, the HVL of the NaI crystal at 140 keV is 0.3 cm.

(b) Plugging in the provided numbers yields

$$\begin{aligned} E' &= \frac{E}{1 + (1 - \cos\theta)E/(511\ \text{keV})} \\ &= \frac{140\ \text{keV}}{1 + (1 - 0) \times 140/511} \\ &= \frac{140}{1 + 0.274} \\ &= 109.89\ \text{keV} . \end{aligned}$$

Therefore, the energy of the scattered photon is 109.89 keV.

(c) Since both energies are above the K-edge, the attenuation coefficient at the lower energy will be larger. Therefore, the scattered photons are more likely to be absorbed than the incident photons because the scattered photon has lower energy than the incident photon.

Solution 4.14

(a) We are not told the linear attenuation coefficient of the shielding material. But we know that it blocks 90% of the incident radiation. So

$$N = N_0 e^{-\mu \Delta x}$$
$$\frac{N}{N_0} = \frac{1 - 0.9}{1} = e^{-1.5 \text{ cm}\mu} .$$

Therefore,

$$\mu = \frac{-\ln 0.1}{1.5 \text{ cm}} .$$

The definition of HVL is

$$\frac{1}{2} = e^{-\text{HVL}\mu} ,$$

so

$$\text{HVL}\mu = -\ln 0.5 .$$

Plugging in our expression for μ derived above yields

$$\frac{\text{HVL}}{1.5 \text{ cm}} = \frac{\ln 0.5}{\ln 0.1} ,$$

which can be solved for HVL as follows

$$\text{HVL} = \frac{\ln 0.5}{\ln 0.1} \times 1.5 \text{ cm} = 0.45 \text{ cm} .$$

(b) From Eq. (4.8), the energy of the scattered photon is given by:

$$h\nu' = \frac{h\nu}{1 + \dfrac{h\nu}{m_0 c^2}(1 - \cos\theta)} ,$$

where $m_0 c^2 = 511$ keV. Therefore,

$$\begin{aligned} E' &= \frac{102.2}{1 + (1 - 0) \times 102.2/511} \\ &= \frac{102.2}{1 + 0.2} \\ &= 85.17 \text{ keV} . \end{aligned}$$

Solution 4.15

(a) Use of Beer's law yields

$$I = I_0 e^{-\mu d} = I_0 e^{-0.3\times 1} = 0.7408 I_0$$

(b) If 1/2 of the incident x-rays are blocked then $I = I_0/2$. Then using $I = I_0 e^{-\mu d}$ and solving for d yields

$$d = \frac{\ln 0.5}{-\mu} = 2.31 \text{ cm}\,.$$

(c) In the broad beam geometry, photons from outside the detector's line-of-sight might get scattered toward the detector because of Compton scattering. Those that were directed at the detector and scattered away will do so in both geometries, so they have no impact on the relative number of detected photons in the two geometries. Therefore more photons will be detected, in general.

RADIATION DOSIMETRY

Solution 4.16

From Example 4.7, we know that in order to keep the dose equivalent to be under 10 mrems, the lung should have an exposure less than 10.8 mR. Since the exposure follows an inverse square law for point sources, the smallest distance the patient should be away from the source should be

$$\sqrt{\frac{10}{10.8\times 10^{-3}}} \times 1 = 30.5 \text{ cm}\,.$$

Solution 4.17

The effective dose is given by (4.38):

$$D_{\text{effective}} = \sum_{\text{organs}} H_j w_j = 0.002 H_{\text{bone}} + 0.002 H_{\text{muscle}}\,.$$

From Sections 4.6.1-4.6.5, we have

$$\begin{aligned} D_{\text{effective}} &= 0.002 D_{\text{bone}} Q + 0.002 D_{\text{muscle}} Q \\ &= 0.002 f_{\text{bone}} X Q + 0.002 f_{\text{muscle}} X Q \\ &= 0.002 \times 0.87 \frac{(\mu/\rho)_{\text{bone}} + (\mu/\rho)_{\text{muscle}}}{(\mu/\rho)_{\text{air}}} X Q\,. \end{aligned}$$

For x-ray at 20 keV, $Q \approx 1$ (see http://physics.nist.gov/PhysRefData/XrayMassCoef/tab4.html) and

$$(\mu/\rho)_{\text{bone}} = 0.4 \text{cm}^2/\text{g},\ (\mu/\rho)_{\text{muscle}} = 0.82 \text{cm}^2/\text{g},\ (\mu/\rho)_{\text{air}} = 0.78 \text{cm}^2/\text{g}\,.$$

So,

$$D_{\text{effective}} = 0.00174 \frac{(\mu/\rho)_{\text{bone}} + (\mu/\rho)_{\text{muscle}}}{(\mu/\rho)_{\text{air}}} X = 2.06 \text{ mrems}\,.$$

5

Projection Radiography

INSTRUMENTATION

Solution 5.1

The system is shift variant in the z direction because of the divergence of the x-ray. The system is *shift invariant* in x and y directions if the object is infinitesimally thin in the z direction. Otherwise the system is shift variant in general.

The intensity of x-rays incident on the detector at (x, y) is given by

$$I(x,y) = \int_0^{E_{\max}} S_0(E')E' \exp\left\{-\int_0^{r(x,y)} \mu(s;E',x,y)ds\right\} dE' ,$$

where $S_0(E)$ is the spectrum of the incident x-rays. When two objects with linear attenuation coefficients $\mu_1(s;E',x,y)$ and $\mu_2(s;E',x,y)$ are presented, the intensity of x-rays on the detector is

$$I_{\text{sum}}(x,y) = \int_0^{E_{\max}} S_0(E')E' \exp\left\{-\int_0^{r(x,y)} \left(\mu_1(s;E',x,y) + \mu_2(s;E',x,y)\right) ds\right\} dE' .$$

In general, $I_{\text{sum}}(x,y) \neq I_1(x,y) + I_2(x,y)$, where $I_i(x,y)$ is the intensity of x-rays on the detector when only the i-th object is presented. So in general the system is not linear.

When monoenergetic x-rays are used, we can remove the outer integral and have

$$I_{\text{sum}}(x,y) = S_0(E_0)E_0 \exp\left\{-\int_0^{r(x,y)} \left(\mu_1(s;E_0,x,y) + \mu_2(s;E_0,x,y)\right) ds\right\} .$$

Once again, this is not a linear system.

Solution 5.2

(a) The highest energy is determined by the peak x-ray tube voltage. For example, if the peak voltage is p kV, then the peak x-ray energy will be p keV. The energy spectrum is determined by several factors. First, it will be zero above p keV. Second, it will be the sum of characteristic x-ray spectrum and a bremsstrahlung x-ray

spectrum. The characteristic x-ray spectrum depends on the atoms in the anode of the x-ray tube, and their relative proportions. The bremsstrahlung x-ray spectrum has a typical shape, linearly increasing from zero at the peak energy as energy decreases.

(b) Low energy photons are undesirable because they are usually completely absorbed by the body. Therefore, they contribute to dose but not image quality. Measures that can be taken to reduce the number of low energy photons entering the body include: restriction (which works on all photons regardless of energy) and filtering. Filtering occurs as x-rays pass through objects between the anode and the body, including the glass tube and surrounding oil and objects placed between the tube and the patient, typically containing plastics and metals. If copper is used, then aluminum usually follows because copper produces characteristic x-rays at 8 keV, which would otherwise form a new low energy x-ray source.

(c) Beam hardening is the increasing of an x-ray beam's effective energy as it propagates through tissues or materials. It is caused by the selective attenuation of low-energy x-rays in a polyenergetic x-ray beam. This occurs because most materials have larger attenuation coefficients at lower x-ray energies.

Solution 5.3

The mass attenuation coefficient of aluminum at 80 kVp is $\mu/\rho = 0.02015$ m^2/kg. The density of aluminum is $\rho = 2,699$ kg/m^3. Therefore,

$$\begin{aligned} \mu(\text{Al}) &= 0.02015 \text{ m}^2/\text{ kg} \times 2,699 \text{ kg/m}^3 \\ &= 54.38 \text{ m}^{-1} . \end{aligned}$$

For the new material at 80 kVp: $\mu/\rho = 0.08$ m^2/kg, $\rho = 5,000$ kg/m^3. So,

$$\begin{aligned} \mu(\text{new}) &= 0.08 \text{ m}^2/\text{kg} \times 5,000 \text{ kg/m}^3 \\ &= 400 \text{ m}^{-1} . \end{aligned}$$

Since attenuation is determined by the exponential factor $e^{-\mu x}$, the x-ray attenuation is equal if the exponents are equal. Hence, the following relation must be satisfied:

$$\mu(\text{Al})x(\text{Al}) = \mu(\text{new})x(\text{new}) .$$

The equivalent thickness of the new material to 2.5 mm of aluminum at 80 kVp is therefore given by

$$\begin{aligned} x(\text{new}) &= \frac{54.38 \text{ m}^{-1} \times 2.5 \text{ mm}}{400 \text{ m}^{-1}} \\ &= 0.34 \text{ mm} . \end{aligned}$$

From Example 5.1, we know that the copper thickness equivalent to 2.5 mm of aluminum at 80 kVp is $x(\text{Cu}) = 0.2$ mm. For the filter of same cross section area, the copper filter weighs $0.2 \times 10^{-3} A \times 8,960$ kg/m$^3 = 1.792A$ kg and the filter made of the new material weighs $0.34 \times 10^{-3} A \times 5,000$ kg/m$^3 = 1.7A$ kg. So the filter made of the new material is lighter.

Solution 5.4

(a) Iodine and barium are used as contrast agents for two reasons. First, they are bio-compatible—that is, they are both nontoxic and can be directed to a useful target in the body. Second, they exhibit K-edges in the

diagnostic x-ray range. Because of their K-edges, they are highly attenuating in the x-ray energy range immediately above the K-edge, far more attenuating than both tissues and bone. This means that they will provide exquisite contrast between the agent and the body.

(b) Figure S5.1(a) demonstrates the benefits of an airgap in scatter reduction. Scattering path ① shows a photon that, when scattered, would hit the standard detector but miss the detector in both cases of a small airgap and large airgap. Scattering path ② shows a photon that, when scattered, would hit both the standard detector and positions with a small airgap, but would miss the detector positioned with a large airgap. This example shows that larger airgaps reject scatter better.

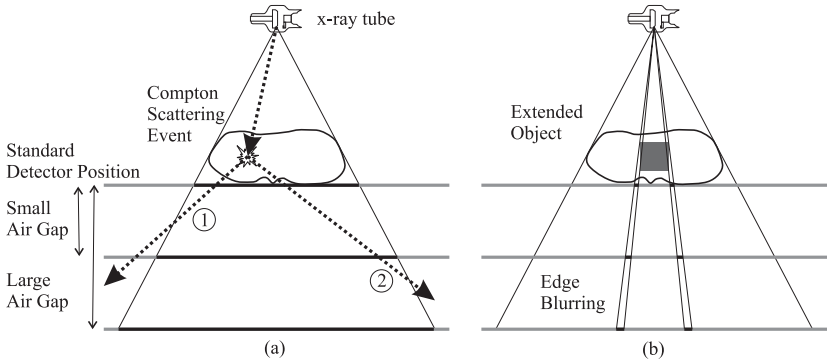

Figure S5.1 See Problem 5.4(b).

The problem with airgaps is demonstrated in Figure S5.1(b). In this figure, and extended object is projected onto the three detector positions, demonstrating edge blurring as the result of depth dependent magnification. Clearly, the blurring is smallest in the standard detector position and largest for the largest airgap. This shows that, when using a large airgap for scatter rejection, the objects will appear with more geometric distortion and/or edge blurring.

Solution 5.5

(a) Compton scattering is random phenomenon. Hence it will cause a random fog throughout the projection radiograph. It contributes to the loss in SNR and contrast in the resulting image.

(b) The H & D curve has a toe, shoulder and a linear region. When the x-ray exposures are in the toe or shoulder regions, the optical density of film remains constant; thereby reducing the contrast of the resulting image. So, it is better for the x-ray exposures to be in the linear portion of the H & D curve.

(c) The low energy x-ray photons are absorbed within the body and don't contribute to the image, thereby contributing to the dose. So, it is necessary to filter out the low energy photons coming out of the x-ray source.

(d) If w and h are the width and height of the lead strips in the grid, then the maximum scatter angle θ is given by $\theta = \tan^{-1}(w/h) = \tan^{-1}(1/8) = 0.1244$ radians.

IMAGE FORMATION

Solution 5.6

Let I_0 be the intensity of the incident beam. Let I_c be the intensity of the x-ray beam falling at the center of the imaging screen, while I_x be the intensity at a point on the screen where then intensity falls off to 95% of that at the center, thus giving a 5% variation in the image intensity. Thus, we have $I_x = 0.95 I_0$. If the linear attenuation of the slab is μ and its thickness is L, then

$$I_c = I_0 e^{-\mu L}\,,$$
$$I_x = I_0 \cos^3\theta e^{-\mu L/\cos\theta}\,.$$

Assuming θ is small, then $\mu L/\cos\theta \approx \mu L$ and

$$\begin{aligned} \frac{I_x}{I_0} &= \cos^3\theta\,, \\ \cos^3\theta &= 0.95\,, \\ \cos\theta &= 0.983\,, \\ \theta &= 10.56^\circ\,. \end{aligned}$$

The maximal size is $2d\tan\theta = 2 \times 2 \times 0.19 = 0.746$ m.

Solution 5.7

(a) Assume the source-to-object distance is z, and source-to-detector distance is d, then the magnification of the object is simply

$$M = \frac{d}{z}\,.$$

(b) One can reduce the magnification and distortion effects by either moving the object closer to the detector panel or moving the x-ray source further away from the object and the detector.

Solution 5.8

(a) The weighting aims to compensate for the $\cos^3\theta$ dependency and the path length factor. As we know, the image intensity is given by

$$I_d(x_d, y_d) = I_0 \cos^3\theta e^{-\frac{\mu L}{\cos\theta}}\,,$$

where $\cos\theta = 1/\sqrt{1 + r_d^2/d^2}$. We want to transform this relationship back to $I'_d = I_0 \exp(-\mu L)$ with a

weighting function that is independent of μ and L. The derivation can be done as follows:

$$\begin{aligned}
\frac{I_d}{I_0 \cos^3\theta} &= e^{-\mu L/\cos\theta}\,, \\
\left(\frac{I_d}{I_0 \cos^3\theta}\right)^{\cos\theta} &= e^{-\mu L}\,, \\
I_0\left(\frac{I_d}{I_0 \cos^3\theta}\right)^{\cos\theta} &= I_0 e^{-\mu L}\,, \\
I_d \cdot \frac{I_0}{I_d}\left(\frac{I_d}{I_0 \cos^3\theta}\right)^{\cos\theta} &= I_0 e^{-\mu L}\,.
\end{aligned}$$

Thus, the weighting function should be chosen as

$$w(\cos\theta) = \frac{I_0}{I_d}\left(\frac{I_d}{I_0 \cos^3\theta}\right)^{\cos\theta}\,,$$

where $\cos\theta = \dfrac{1}{\sqrt{1 + r_d^2/d^2}}$. Now substitute the expression for I_d into above expression and after some simplification we find

$$w(\cos\theta) = \frac{1}{\cos^3\theta} e^{-\frac{\cos\theta - 1}{\cos\theta}\mu L}\,.$$

This correction will hold as long as $\mu(x, y, z) = \mu(z)$. That is, we assume that we are imaging an object in which μ only varies in the z direction.

(b) Assume that the image of the object-of-interest lies in the center of the detector, i.e, it has small r_d while the background region has large r_d. Assume also that initially $I_t < I_b$. Then the image contrast will be improved after the correction. Under the same assumptions, the SNR is also improved because the image contrast is improved.

Solution 5.9

(a) Let us consider a 2-D cross section of the system through the y-z plane as shown in Figure S5.2.

The image on the screen will have 3 regions. In the center of the image, between points $-a$ and a, the appearance of the image is governed by the inverse square law, obliquity, and path length variations. So we have

$$I_d(x, y) = I_0 \cos^3\theta e^{-\mu L/\cos\theta}\,.$$

The value of a can be obtained as follows:

$$\begin{aligned}
\frac{a}{d} &= \frac{w/2}{z_0 + L/2}\,, \\
a &= \frac{wd}{2z_0 + L}\,.
\end{aligned}$$

When the x-rays are passing through the edges of the object, however, there is a loss of object path length, and corresponding reduction in attenuation. This corresponds to the region between a and b, and between

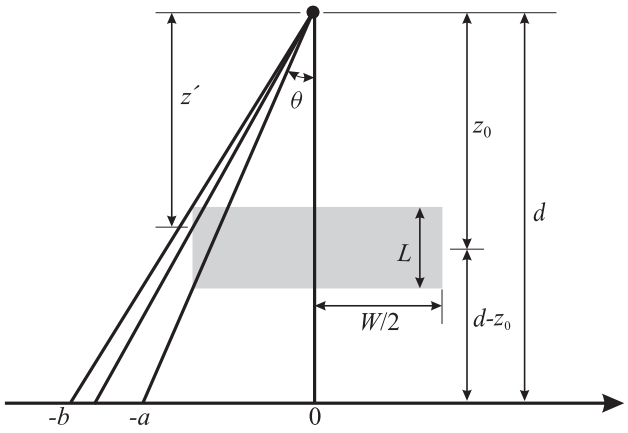

Figure S5.2 The cross section of the prism through y-z plane. See Problem 5.9(a).

$-b$ and $-a$ on the screen and the intensity is given as

$$I_d(x,y) = I_0 \cos^3\theta e^{-\mu_a(z'-z_0+L/2)/\cos\theta}\,.$$

The value of b and z' are obtained as follows:

$$\begin{aligned} \frac{b}{d} &= \frac{w/2}{z_0 - L/2}\,, \\ b &= \frac{wd}{2z_0 - L}\,, \\ z' &= \frac{wd}{2x}\,. \end{aligned}$$

Beyond, b and $-b$, the rays miss the prism completely. In this case,

$$I_d(x,y) = I_0 \cos^3\theta\,.$$

In summary, we have

$$I_d(x,y) = \begin{cases} I_0\cos^3\theta\exp(-\mu_a L/\cos\theta) \\ \qquad \text{if } 0 \le x \le \dfrac{wd}{2z_0+L} \text{ and } 0 \le y \le \dfrac{wd}{2z_0+L} \\ I_0\cos^3\theta\exp\left[-\mu_a\left(\frac{wd}{2\max(|x|,|y|)} - z_0 + L/2\right)/\cos\theta\right] \\ \qquad \text{if } \dfrac{wd}{2z_0+L} \le x \le \dfrac{wd}{2z_0-L} \text{ or } \dfrac{wd}{2z_0+L} \le y \le \dfrac{wd}{2z_0-L} \\ I_0\cos^3\theta \\ \qquad \text{if } x > \dfrac{wd}{2z_0-L} \text{ and } y > \dfrac{wd}{2z_0-L} \end{cases} . \tag{S5.1}$$

(b) The plot along $y = 0$, is shown in Figure S5.3.

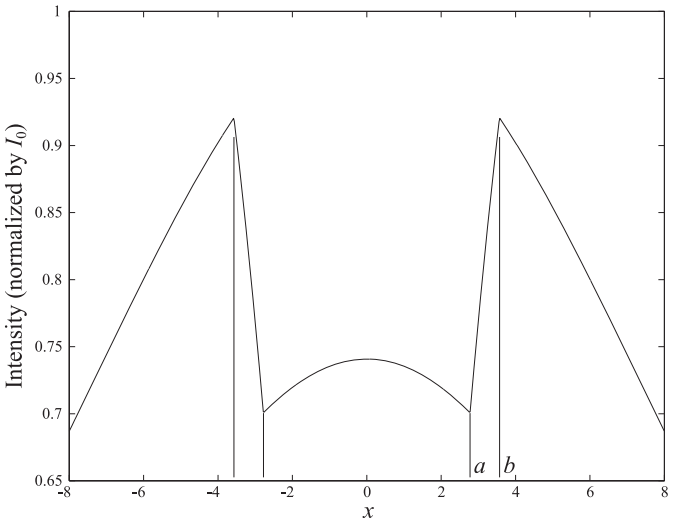

Figure S5.3 The intensity of the image in the detector plane along $y = 0$. See Problem 5.9(b).

(c) The x-ray intensity on the detector, $I_d(x, y)$ was determined in Part (b), and is given by Equation S5.1. From (5.32), we have

$$D = \Gamma \log_{10}(X/X_0)\,.$$

But X is exposure, not intensity. In a given material, however, the ratio of exposures is equal to the ratio of intensities. So, we also have

$$D = \Gamma \log_{10}(I_d/I_0)\,,$$

where it is understood that this applies only in the linear range of the H&D curve. Accordingly, I_0 must be the intensity at which $I_0\Delta t$ yields the "fog" level on the film, where Δt is the duration of the exposure. Therefore, the developed film will have optical density

$$D(x, y) = \Gamma \log_{10}(I_d(x, y)/I_0)\,.$$

Solution 5.10

Most of the derivation is included in the text preceding the equation. Here we provide a review, and fill in the missing details. Assume the intensity surrounding a given point on the source is I_S. Then the inverse square law predicts the following intensity at the center of the detector

$$I_0 = \frac{I_S}{4\pi d^2}\,.$$

Moving away from the center of the detector a distance r leads to an additional $\cos^2\theta$ loss of intensity; but while moving away, the unit area increases as well, leading to an additional $\cos\theta$ loss of intensity. Put together, we have

$$I_d = \frac{I_S \cos^3\theta}{4\pi d^2}\,.$$

We now incorporate an infinitesimally thin object $t_z(x, y)$, at range z (measured from the source) such that if $z = d$

it provides a further multiplicative attenuation of the source intensity, as follows

$$I_d = \frac{I_S \cos^3\theta}{4\pi d^2} t_d(x,y)\,.$$

If the object is moved away from the detector, it will cast a wider shadow on the detector. This fact is captured mathematically using the magnification $M = M(z) = d/z$, and by scaling the x and y axes as follows

$$I_d = \frac{I_S \cos^3\theta}{4\pi d^2} t_z(x/M, y/M)\,.$$

The last phenomenon that must be included is due to the extended source. Suppose that the source location is not a point but instead is a small area having a source intensity distribution given by $s(x,y)$. If this source were viewed through a small hole (which blocks all other transmission) on the z-axis (where $x = y = 0$) at range z, it would make an inverted and scaled image of the source intensity, as follows

$$I_d(x,y) = \frac{s(x/m, y/m)}{4\pi d^2 m^2}\,,$$

where $m = m(z) = 1 - M(z)$. This represents a response to the impulse transmittivity $\delta_z(x,y)$. If the transmittivity were not unity, then the response would be attenuated by the transmittivity as follows

$$I_d(x,y) = \frac{s(x/m, y/m)}{4\pi d^2 m^2} t_z(0,0)\,,$$

Now suppose the impulse transmittivity (hole) were moved to position $(\xi/M, \eta/M)$. Assume that θ is small so that both the source shape distortion due to obliquity and the difference in source magnification as compared to that at the detector origin can be ignored. Then the detected image is simply an inverted and scaled source intensity, shifted to a new position

$$I_d(x,y) = \frac{\cos^3\theta\, s((x-\xi)/m, (y-\eta)/m)}{4\pi d^2 m^2} t_z(\xi/M, \eta/M)\,,$$

This image represents an approximate impulse response to an impulse in transmittivity at $(\xi/M, \eta/M)$ within the thin object at range z. The whole response is the superposition of these individual responses:

$$\begin{aligned} I_d(x,y) &= \int_{-\infty}^{\infty}\int_{-\infty}^{\infty} \frac{\cos^3\theta\, s((x-\xi)/m, (y-\eta)/m)}{m^2} t_z(\xi/M, \eta/M)\, d\xi\, d\eta\,. \\ &= \frac{\cos^3\theta}{4\pi d^2 m^2} s(x/m, y/m) * t_z(x/M, y/M)\,, \end{aligned}$$

which is the desired expression.

IMAGE QUALITY

Solution 5.11

If m photons are incident on a detector and each one has a probability p of getting detected, independently from other photons, then the probability that n out of those m photons are detected has a binomial distribution and is

given as:

$$P\{n \text{ out of } m \text{ photons are detected}\} = \left(\begin{array}{c} m \\ n \end{array} \right) p^n (1-p)^{m-n} .$$

Now, the PMF of the number of photons detected $D(t)$ can be computed as follows:

$$\begin{aligned} P\{D(t)=n\} &= \sum_{m=n}^{\infty} P\{m\text{photons are fired by the x-ray tube}\} \cdot P\{n \text{ out of } m \text{ photons are detected}\} \\ &= \sum_{m=n}^{\infty} \frac{e^{-\mu t}(\mu t)^m}{m!} \left(\begin{array}{c} m \\ n \end{array} \right) p^n (1-p)^{m-n} \\ &= \sum_{m=n}^{\infty} \frac{e^{-\mu t}(\mu t)^m}{m!} \frac{m!}{n!(m-n)!} p^n (1-p)^{m-n} \\ &= \sum_{m=n}^{\infty} \frac{e^{-\mu t}(\mu t)^m}{n!(m-n)!} p^n (1-p)^{m-n} . \end{aligned}$$

Substituting $k = m - n$, we get

$$\begin{aligned} P\{D(t)=n\} &= \sum_{m=n}^{\infty} \frac{e^{-\mu t}(\mu t)^{n+k}}{n!k!} p^n (1-p)^k \\ &= \frac{e^{-\mu t}(\mu t)^n}{n!} p^n \sum_{k=0}^{\infty} \frac{(\mu t)^k}{k!} (1-p)^k \\ &= \frac{e^{-\mu t}(\mu t p)^n}{n!} \sum_{k=0}^{\infty} \frac{[\mu t(1-p)]^k}{k!} \\ &= \frac{e^{-\mu t}(\mu t p)^n}{n!} e^{\mu t(1-p)} . \end{aligned}$$

Here we have used the identity $e^t = \sum_{k=0}^{\infty} \frac{t^k}{k!}$. By simple rearrangement, we get the PMF of $D(t)$ as

$$P\{D(t)=n\} = \frac{e^{-\mu p t}(\mu p t)^n}{n!} .$$

Thus, $D(t)$ also follows a Poisson distribution.

Solution 5.12

(a) Since the object is located at $z = 3d/4$, the magnification of the object is

$$\begin{aligned} m &= -\frac{d-z}{z} \\ &= -\frac{d-3d/4}{3d/4} \\ &= -1/3 . \end{aligned}$$

The PSF of an extended source when the object is magnified by m is given by $h(x/m)$. Let the PSF for any

arbitrary magnification m be $h_1(x) = e^{-ax^2/m^2}$. Since $h_1(x) = e^{-x^2/5}$ is the PSF of the extended source, when $m = -1/3$ we have

$$\begin{aligned} ax^2/m^2 &= x^2/5\,, \\ \Longrightarrow\ a &= m^2/5 \\ &= (1/3)^2/5 \\ &= 1/45\,. \end{aligned}$$

Hence at any arbitrary range z, the PSF of the extended source is given by

$$h_1(x) = e^{-\frac{x^2}{45m^2}} = e^{-\frac{x^2z^2}{45(d-z)^2}}\,.$$

(b) Since the PSF is $h_1(x) = e^{-x^2/45m^2}$ the Fourier transform is

$$H_1(u) \quad = \quad e^{-45m^2/\pi^2u^2}\sqrt{45m^2}\,.$$

Hence, the transfer function of the overall blurring is

$$H(u) \quad = \quad \sqrt{450}me^{-(45m^2+10)\pi^2u^2}\,,$$

and the MTF is given by

$$\text{MTF}(u) \quad = \quad e^{-(45m^2+10)\pi^2u^2}\,.$$

(c) The inverse Fourier transform of $H(u) = \sqrt{450}me^{-(45m^2+10)\pi^2u^2}$ is

$$h(x) = m\sqrt{\frac{450(45m^2+10)}{\pi}}e^{-\frac{x^2}{45m^2+10}}\,.$$

At $x = \text{FWHM}/2$ we have $e^{-\frac{x^2}{45m^2+10}} = 1/2$, and therefore

$$\text{FWHM} \quad = \quad 2\sqrt{(45m^2+10)\ln 2}\,.$$

Solution 5.13

Scatter fraction, denoted by SF, is defined as

$$\text{SF} = \frac{I_s}{I_s + I_b},$$

where I_b denotes the background intensity and I_s denotes the intensity contributed by scattering. The new image contrast C' (with scattering) is related to the original scatter-free contrast C by

$$C' = \frac{I_t + I_s - (I_b + I_s)}{I_b + I_s} = C(1 - \text{SF})\,.$$

Thus, when SF $= 0.35$,

$$C'_{0.35} = C(1 - 0.35) = 0.08 \times 0.65 = 0.052\,,$$

and when SF $= 0.8$,

$$C'_{0.8} = C(1 - 0.8) = 0.08 \times 0.2 = 0.016\,.$$

Using the relationship SNR $= C\sqrt{\eta N}$, we can compute the SNR in both cases as follows (assuming $\eta = 1$)

$$\begin{aligned} \text{SNR}_{0.35} &= C_{0.35}\sqrt{\eta N} = 0.052\sqrt{1 \times 1,000} = 1.64; \quad \text{and} \\ \text{SNR}_{0.8} &= C_{0.8}\sqrt{\eta N} = 0.016\sqrt{1,000} = 0.51\,. \end{aligned}$$

If the detector absorption efficiency η is halved, the SNRs become

$$\text{SNR}'_{0.35} = 0.052\sqrt{0.5 \times 1,000} = 1.16\,;$$

$$\text{SNR}'_{0.35} = 0.016\sqrt{0.5 \times 1,000} = 0.36\,.$$

This problem shows that SNR can be altered in two ways:

- Increase the scatter fraction, which causes an increase in the noise level;
- Decrease the absorption efficiency, which causes a decrease in the signal amplitude.

Solution 5.14

Suppose an x-ray burst with an average of $\bar{N}$ photons is incident upon a detector having quantum efficiency QE. Then the average number of photons stopped by the detector is QE $\bar{N}$. The intrinsic SNR's of the stopped photons is $\sqrt{\text{QE}\,\bar{N}}$. By physical law, the signal itself—whatever measured and derived quantity that might be—must have an SNR lower than the intrinsic SNR. Therefore, we find that the maximum DQE is

$$\begin{aligned} \text{DQE}_{\max} &= \left(\frac{\sqrt{\text{QE}\,\bar{N}}}{\sqrt{\bar{N}}}\right)^2 \\ &= \text{QE}\,, \end{aligned}$$

which was to be proven.

Solution 5.15

By definition,

$$\text{DQE} = \frac{\hat{\lambda}}{\lambda}\,,$$

where $\hat{\lambda}$ is the *noise-equivalent quanta*,

$$\begin{aligned} \hat{\lambda} &= \widehat{\text{SNR}}_a^2 \\ &= \left[\frac{\lambda_d}{\sqrt{\sigma_N^2}}\right]^2\,, \end{aligned}$$

where λ_d is the number of photons detected at the detector every second and σ_N^2 is the variance of the noise. For this problem, $\lambda_d = 10,000$ and $\lambda = 10,000$. Now substitute these numbers into the above equations to get

$$\text{DQE} = \frac{\lambda_d^2}{\sigma_N^2 \lambda} = \frac{10,000}{\sigma_N^2} .$$

So, the variance of the noise as a function of DQE is:

$$\sigma_N^2 = \frac{10,000}{\text{DQE}} .$$

The function is plotted in Figure S5.4.

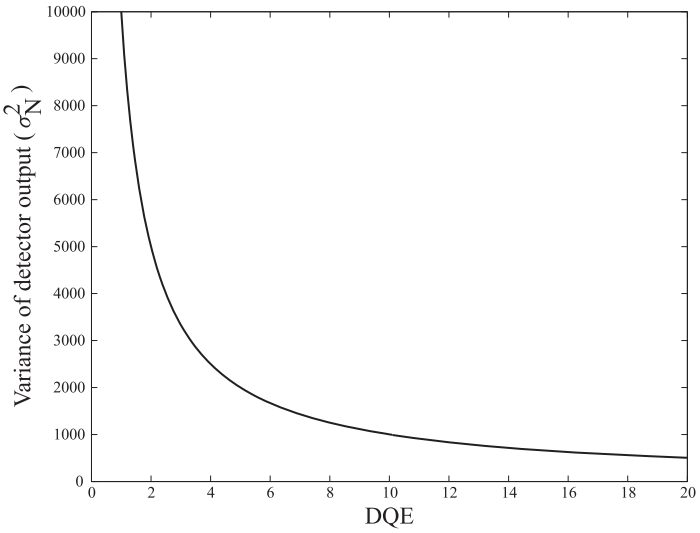

Figure S5.4 The variance of the detector's output (σ_N^2) as a function of DQE. See Problem 5.15.

If the variance of the output noise is 2,000, we require DQE $= \frac{10,000}{2,000} = 5$. This answer may look incorrect at the first glance, since in the text we say that "Clearly, $0 \leq$ DQE ≤ 1." But, let's think about what it means that the variance of the output noise is 2,000 in the setting of the problem. Given that we have detected 10,000 photons per second at the detector, the amplitude signal to noise ratio is, by definition,

$$\widehat{\text{SNR}}_a = \frac{10,000}{\sqrt{2,000}} = 223.6 .$$

But the output signal to noise ratio of an ideal detector is only $\text{SNR}_a = \sqrt{10,000} = 100 < \widehat{\text{SNR}}_a$, which means this detector does better than the ideal detector. This is impossible in reality, where $0 \leq$ DQE ≤ 1.

Solution 5.16

Assume that each point on the detector sees a Poisson random variable with parameter a. Since this input is white noise, it has a flat noise power spectrum, and is given by the variance of the random variable, a. Thus, the frequency dependent (power) SNR of the input is

$$\text{SNR}_p(\text{in}) = a .$$

From Table 2.1, we can determine the frequency response of the nonideal detector to be

$$H(u,v) = e^{-2\pi^2(u^2+v^2)}\,.$$

The frequency response of the detector will selectively filter out frequencies in the power spectrum according to the square of the transfer function. Therefore, the frequency dependent (power) SNR of the output is

$$\text{SNR}_p(\text{out}) = a|H(u,v)|^2\,.$$

Putting this together, and using (5.40), we find that the DQE is given by

$$\begin{aligned}
\text{DQE}(u,v) &= \frac{(\text{SNR}_{\text{out}})^2}{(\text{SNR}_{\text{in}})^2} \\
&= \frac{\text{SNR}_p(\text{out})}{\text{SNR}_p(\text{in})} \\
&= \frac{a|H(u,v)|^2}{a} \\
&= e^{-4\pi^2(u^2+v^2)}\,.
\end{aligned}$$

Solution 5.17

Figure S5.5 shows the orientation of the plastic hollow cylinder with respect to the source and detector. The distortion is due to depth dependent magnification. The circular cross section closest to the source gets magnified more than the other cross section.

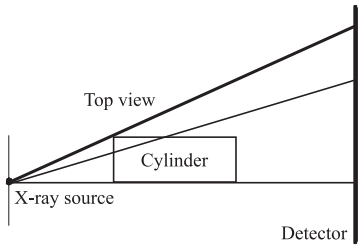

Figure S5.5 Off axis cylinder with depth dependent magnification artifact. See Problem 5.17.

Solution 5.18

From basic trigonometry,

$$\begin{aligned}
\tan\phi &= \frac{s_2 + d\tan\alpha_2}{d} && \text{(S5.2)}\\
&= \frac{s_1 + d\tan\alpha_1}{d} && \text{(S5.3)}\\
&= \frac{s + d_1\tan\alpha_1}{d_1} && \text{(S5.4)}\\
&= \frac{s + d_2\tan\alpha_2}{d_2}\,. && \text{(S5.5)}
\end{aligned}$$

So, we see that $s_2 + d\tan\alpha_2 = s_1 + d\tan\alpha_1$; therefore,

$$\begin{aligned}
\frac{s_2}{s_1} &= 1 + d\frac{\tan\alpha_1 - \tan\alpha_2}{s_1} && \text{(S5.6)}\\
&= 1 + \frac{\tan\alpha_1 - \tan\alpha_2}{\tan\phi - \tan\alpha 1} \;\; (\text{using } (S5.3)) && \text{(S5.7)}\\
&= 1 + d_1\frac{\tan\alpha_1 - \tan\alpha_2}{s} \;\; (\text{using } (S5.4))\,. && \text{(S5.8)}
\end{aligned}$$

Equating (S5.4) and (S5.5), we get $\tan\alpha_1 - \tan\alpha_2 = s(\frac{d_1 - d_2}{d_1 d_2})$. Substituting this back into (S5.8) yields

$$m = \frac{s_1}{s_2} = \frac{d_2}{d_1}\,.$$

Therefore, when $d1 = 40$ cm and $d2 = 80$ cm, $m = 2$.

Solution 5.19

(a) For $|y| \le r$, we have

$$I(d, y) = I_p e^{-\mu_A \cdot 2(r - \sqrt{r^2 - y^2}) - \mu_B \cdot 2\sqrt{r^2 - y^2}}\,.$$

For $r \le |y| \le a$, we have

$$I(d, y) = I_p e^{-\mu_A \cdot 2r}\,.$$

(b) From the definition of local contrast, with appropriate substitution we have

$$\begin{aligned}
C &= \frac{I_t - I_b}{I_b}\\
&= \frac{I_p e^{-\mu_B \cdot 2r} - I_p e^{-\mu_A \cdot 2r}}{I_p e^{-\mu_A \cdot 2r}}\\
&= e^{-(\mu_B - \mu_A)\cdot 2r} - 1\,.
\end{aligned}$$

(c) From the expression in (b), we see that C will be positive when

$$\mu_B < \mu_A \,.$$

(d) The boundary of B (a circle) can be represented as

$$(x-(z+r))^2 + y^2 = r^2 \,.$$

The line connecting the source $(0,0)$ and the point $(d, \frac{r}{\sqrt{z^2+2rz}}d)$ can be represented as

$$y = \frac{r}{\sqrt{z^2+2rz}}x \,.$$

The intersection (x_0, y_0) of the line and the circle satisfies

$$\begin{cases} (x_0-(z+r))^2 + y_0^2 = r^2 \\ y_0 = \frac{r}{\sqrt{z^2+2rz}}x_0 \end{cases} \,.$$

Thus,

$$\begin{aligned} & (x_0-(z+r))^2 + (\frac{r}{\sqrt{z^2+2rz}}x_0)^2 = r^2 \,, \\ \Longrightarrow \; & \frac{(z+r)^2}{z^2+2rz}x_0^2 - 2(z+r)x_0 + z^2 + 2rz = 0 \,. \end{aligned}$$

Since the quadratic discriminant is

$$\begin{aligned} \Delta &= 4(z+r)^2 - 4(z^2+2rz)\frac{(z+r)^2}{z^2+2rz} \,, \\ &= 0 \end{aligned}$$

the line is tangent to the circle. The geometry, where $\cos\theta = \frac{\sqrt{z^2+2rz}}{r+z}$, is shown in Figure S5.6. The intensity at $(d, \frac{r}{\sqrt{z^2+2rz}}d)$ is

$$\begin{aligned} I(d, \frac{r}{\sqrt{z^2+2rz}}d) &= I_0 \cos^3\theta e^{-\mu_A \cdot 2r/\cos\theta} \\ &= I_0 \left(\frac{\sqrt{z^2+2rz}}{r+z}\right)^3 e^{-\mu_A \cdot 2r \frac{r+z}{\sqrt{z^2+2rz}}} \,. \end{aligned}$$

(e) The magnification is $M(z) = \frac{d}{z+r}$. Thus, the point is $(z+r, \frac{z+r}{d}y_0)$.

APPLICATIONS

Solution 5.20

(a) You would change the peak tube voltage, or kVp. To generate the first film, you would use a tube voltage $= 30$ kVp, and to generate the second film, you would use a tube voltage $= 100$ kVp.

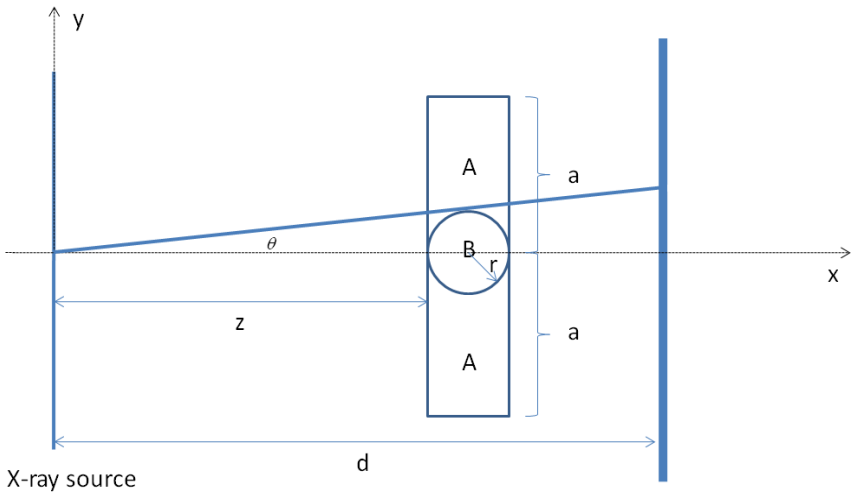

Figure S5.6 See Problem 5.19.

(b) If you did not change anything else, the second film, taken at 100 kVp, would be more exposed. That is because the body is more transparent at higher x-ray energies, so more x-rays would get through to expose the film. The high energy x-rays, when stopped by the intensifying screen, will generate more light output as well adding to the exposure. It is true that the intensifying screen is also more transparent at higher energies, but the x-ray spectrum at 100 kVp also contains lower energy x-rays that would contribute to the overall exposure.

(c) From Chapter 4, we know that Compton scattering events become an increasingly larger fraction of the events as the x-ray energy increases. Therefore, Compton scattering will be more of "a problem" at 100 keV versus 30 keV, yielding lower contrast images.

(d) This depends on what kind of filtration is used. Ordinarily, when using a 100 kVp source, filtration would remove lower energy x-rays. In this case, the higher energy source would be more penetrating and the dose for the 100 kVp source would be lower. However, if the complete 100 kVp spectrum is allowed to be incident on the patient, then the 100 kVp source would generate more dose to the patient.

(e) The subtracted optical density is

$$\begin{aligned} D(x,y) &= D(x,y;E_h) - D(x,y;E_l) \\ &= \Gamma \log_{10}(X_h/X_0) - \Gamma \log_{10}(X_l/X_0) \\ &= \Gamma \log_{10}\left(\frac{X_h}{X_l}\right) . \end{aligned}$$

Since $X_h > X_l$ (in general), $D(x,y)$ will be a nonnegative image revealing the relative additional "transparency" of tissues at the higher x-ray energies. (Note: If the two energies were used on "opposite sides" of the k-edge of a contrast agent, then the difference $D(x,y;E_l) - D(x,y;E_h)$ would be used instead, since the attenuation at the higher energy would be larger.)

Solution 5.21

(a) We have $b = 20$ cm and

$$t(E) = e^{-\mu d} = 10^{-\frac{(E-150)^2}{5,000}} .$$

So,

$$\mu d = \frac{(E-150)^2}{5,000} \ln 10 \quad \Longrightarrow \quad \mu(E) = \frac{(E-150)^2}{5,000d} \ln 10 .$$

(b) Intrinsic contrast is $C = \frac{\mu_t - \mu_b}{\mu_t + \mu_b}$. The object is shown in Figure S5.7. The two linear attenuation coefficients

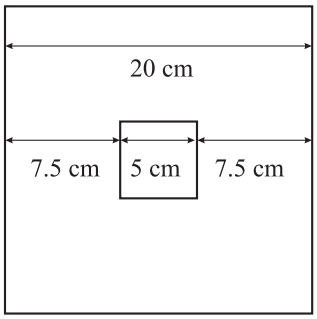

Figure S5.7 See Problem 5.21(b).

are

$$\begin{aligned} \mu_t &= 0.15 \text{ cm}^{-1} , \\ \mu_b &= \frac{(75-150)^2}{5,000d} \ln 10 = 0.13 \text{ cm}^{-1} . \end{aligned}$$

So, the intrinsic contrast is

$$C = \frac{0.15 - 0.13}{0.15 + 0.13} = 0.071 .$$

(c) Consider two paths, one through the new material, and one that misses it. Then

$$\begin{aligned} I_{\text{through}} &= I_0 \left(e^{-\mu_b \times 15 \text{ cm}}\right) \left(e^{-\mu_t \times 5 \text{ cm}}\right) \\ &= I_0 \left(e^{-0.13 \times 15 \text{ cm}}\right) \left(e^{-0.15 \times 5 \text{ cm}}\right) \\ &= 0.067 I_0 , \end{aligned}$$

and

$$\begin{aligned} I_{\text{miss}} &= I_0 \left(e^{-\mu_b \times 20 \text{ cm}}\right) \\ &= 0.074 I_0 . \end{aligned}$$

The contrast is therefore given by

$$C = \frac{0.067 - 0.074}{0.067 + 0.74} = -0.05 .$$

Solution 5.22

(a) The energy spectrum is shown in Figure S5.8. The spectrum is just the number of photons, viewed as a continuous plot. 10^4 and 10^5 represent *integrals* (area or mass) of spectrum, which has units photons-keV.

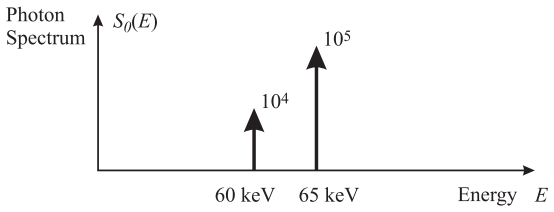

Figure S5.8 See Problem 5.22.

(b) Consider Figure S5.9. The total number of x-ray photons per cm that hit the detector as a function of position

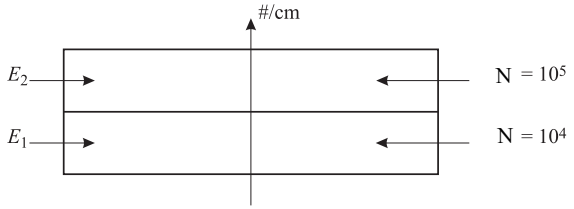

Figure S5.9 See Problem 5.22.

x is

$$\begin{aligned} A_1: \quad N_d^1 &= 0.5 \times 10^4 e^{-0.2\times 2} = 3,351\,, \\ N_d^2 &= 0.5 \times 10^5 e^{-0.4\times 2} = 22,466\,. \end{aligned}$$

The total is $= 25,817$. For the other parts we have

$$\begin{aligned} A_2: \quad N_h^1 &= 0.5 \times 10^4 e^{-0.3\times 1} = 3,704\,, \\ N_h^2 &= 0.5 \times 10^5 e^{-0.1\times 1} = 45,242\,. \end{aligned}$$

and

$$\begin{aligned} A_3: \quad N_d^1 &= 3,704 e^{-0.5\times 1} = 2,247\,, \\ N_d^2 &= 45,242 e^{-0.4\times 1} = 30,327\,. \end{aligned}$$

Therefore, the total is $= 32,574$.

(c) Consider Figure S5.10. The local contrast of the image observed at the detector as a function of position x assuming that A is the target and B is the background is $I = \alpha N$. Therefore

$$C = \frac{I_t - I_b}{I_b} = \frac{N_t - N_b}{N_b} = \frac{-6,757}{32,574} = -0.21\,.$$

(d) The optical density, given by $D = \Gamma \log \frac{X}{X_0}$, as a function of position x assuming x-ray film is shown in Figure S5.11.

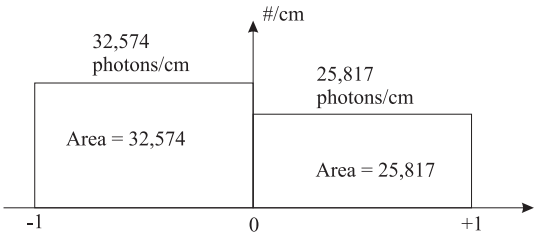

Figure S5.10 See Problem 5.22.

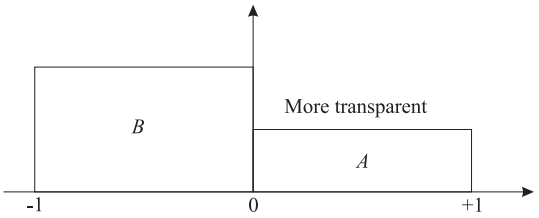

Figure S5.11 See Problem 5.22.

Solution 5.23

(a) The object magnification is

$$M = d/z = 60/40 = 1.5\,.$$

(b) The source magnification is

$$m = -\frac{d-z}{z} = 1 - M = -0.5\,.$$

(c) The image of the line phantom can be written as:

$$\begin{aligned} I_d(x_d, y_d) &= K[S_0 e^{-(x_d/m)^2}\delta(y_d/m)] * \left[\delta\left(\frac{x_d}{M} - \frac{w}{2}\right) + \delta\left(\frac{x_d}{M} + \frac{w}{2}\right)\right] \\ &= KS_0\left\{\left[e^{-(x_d/m)^2}\delta(y_d/m)\right] * \delta\left(\frac{x_d}{M} - \frac{w}{2}\right) + \left[e^{-(x_d/m)^2}\delta(y_d/m)\right] * \delta\left(\frac{x_d}{M} + \frac{w}{2}\right)\right\}\,. \end{aligned}$$

To evaluate this, we first compute the convolution

$$\left[e^{-(x_d/m)^2}\delta(y_d/m)\right] * \delta\left(\frac{x_d}{M} - \frac{w}{2}\right)$$

as follows:

$$\begin{aligned} \left[e^{-(x_d/m)^2}\delta(y_d/m)\right] * \delta\left(\frac{x_d}{M} - \frac{w}{2}\right) &= \int_{-\infty}^{\infty}\int_{-\infty}^{\infty} e^{-\left(\frac{x_d-u}{m}\right)^2}\delta\left(\frac{y_d - v}{m}\right)\delta\left(\frac{u}{M} - \frac{w}{2}\right)du\,dv \\ &= M|m|\int_{-\infty}^{\infty} e^{-\left(\frac{x_d - u'M}{m}\right)^2}\delta\left(u' - \frac{w}{2}\right)du' \int_{-\infty}^{\infty}\delta\left(\frac{y_d}{m} - v'\right)dv' \\ &= M|m|e^{-\left(\frac{x_d - \frac{wM}{2}}{m}\right)^2}\,. \end{aligned}$$

Similarly,

$$\left[e^{-(x_d/m)^2}\delta\left(y_d/m\right)\right] * \delta\left(\frac{x_d}{M}-\frac{w}{2}\right) = M|m|e^{-\left(\frac{x_d+\frac{wM}{2}}{m}\right)^2}.$$

Hence,

$$\begin{aligned} I_d(x_d,y_d) &= KM|m|S_0 e^{-\left(\frac{x_d-\frac{wM}{2}}{m}\right)^2} + KM|m|S_0 e^{-\left(\frac{x_d+\frac{wM}{2}}{m}\right)^2} \\ &= 0.75KS_0\left[e^{-4(x_d-0.75w)^2}+e^{-4(x_d+0.75w)^2}\right]. \end{aligned}$$

(d) As shown in (c), the image of the line phantom is the sum of two Gaussian-shaped functions that are centered at $wM/2$ and $-wM/2$ respectively, and both have a variance of $m^2/2$. With the same reasoning as in determining FWHM, we know that in order for the two Gaussians to be distinguishable, the following must be true

$$KM|m|S_0 e^{-\left(\frac{0-\frac{wM}{2}}{m}\right)^2} \le \frac{1}{2}\max_{x_d} KM|m|S_0 e^{-\left(\frac{x_d-\frac{wM}{2}}{m}\right)^2} = \frac{1}{2}KM|m|S_0.$$

Hence,

$$\left(\frac{wM}{2m}\right)^2 \ge \ln 2$$

and

$$w \ge \frac{2|m|\sqrt{\ln 2}}{M}.$$

Thus, the minimum value that w can take is $2|m|\sqrt{\ln 2}/M \approx 0.555$ cm.

Here is an alternative solution. Notice that the image of the line phantom $I_d(x_d,y_d)$ is simply its image under an ideal point source ($t'(x_d,y_d) = t(x_d/M, x_d/M)$) blurred (convoluted) by the magnified source distribution ($s'(x_d,y_d) = s(x_d/m, y_d/m)$) with a suitable scaling (K). The image of the phantom under a point source would still be two parallel lines with the same orientation, but the spacing is magnified to wM. The magnified source still has the same form, and can be computed as

$$s'(x_d,y_d) = s(x_d/m, y_d/m) = S_0 e^{-(x_d/m)^2}\delta(y_d/m) = |m|S_0 e^{-x_d^2/m^2}\delta(y_d).$$

By the definition of FWHM, we know that in order for the images of the two lines to be distinguishable, the spacing wM must be greater than the FWHM of $s'(x_d,y_d)$, which is computed to be $2|m|\sqrt{\ln 2}$. Hence the minimum value of w is $2|m|\sqrt{\ln 2}/M \approx 0.555$ cm.

Solution 5.24

(a) Since the number of photons are uniformly shed upon the side of the whole tissue, it is clear that $1/4(= 0.5/2.0)$ of the total incident photons will go through the blood vessel, and the remaining $3/4N_i$ photons only pass through the soft tissue. Hence the total number of photons can be computed as follows

$$\begin{aligned} N_t &= \frac{N_i}{4}e^{-\mu_{\text{vessel}}L_{\text{vessel}}-\mu_{\text{tissue}}(L_{\text{tissue}}-L_{\text{vessel}})} + \frac{3N_i}{4}N_i e^{-\mu_{\text{tissue}}L_{\text{tissue}}} \\ &= \frac{N_i}{4}e^{-0.5\mu_{\text{vessel}}}e^{-1.5\mu_{\text{tissue}}} + \frac{3N_i}{4}e^{-2\mu_{\text{tissue}}}. \end{aligned}$$

At 15 keV,

$$\begin{aligned} N_t &= \frac{4\times 10^6}{4} e^{-0.5\times 3.0} e^{-1.5\times 4.0} + \frac{3\times 4\times 10^6}{4} e^{-2\times 4.0} \\ &\approx 1,006 + 553 \\ &= 1,559. \end{aligned}$$

At 40 keV,

$$\begin{aligned} N_t &= \frac{4\times 10^6}{4} e^{-0.5\times 0.2} e^{-1.5\times 0.4} + \frac{3\times 4\times 10^6}{4} e^{-2\times 0.4} \\ &\approx 4.96\times 10^5 + 1.35\times 10^6 \\ &= 1.84\times 10^6. \end{aligned}$$

We see from this analysis that, at the lower energy level 15 keV, more photons are absorbed because the linear attenuation coefficients of the tissue and the blood vessel are both higher at 15 keV than at 40 keV.

(b) Since the incident photons are uniformly shed upon the tissue, the photon density p, that is, the number of photons per unit area, is a constant and can be computed as $p = N_i/A$, where A is the area of the side of the tissue. Notice that the value of p does not affect the local contrast computation, which can be shown as follows. The background intensity N_b is simply

$$N_b = pe^{-\mu_{\text{tissue}} L_{\text{tissue}}} = pe^{-2.0\mu_{\text{tissue}}}.$$

The object intensity N_o is given by

$$\begin{aligned} N_o &= pe^{-\mu_{\text{vessel}} L_{\text{vessel}} - \mu_{\text{tissue}}(L_{\text{tissue}} - L_{\text{vessel}})} \\ &= pe^{-0.5\mu_{\text{vessel}} - 1.5\mu_{\text{tissue}}}. \end{aligned}$$

Hence, the local contrast can be computed as

$$\begin{aligned} C &= \frac{N_o - N_b}{N_b} \\ &= \frac{pe^{-0.5\mu_{\text{vessel}} - 1.5\mu_{\text{tissue}}} - pe^{-2.0\mu_{\text{tissue}}}}{pe^{-2.0\mu_{\text{tissue}}}} \\ &= e^{-0.5(\mu_{\text{vessel}} - \mu_{\text{tissue}})} - 1. \end{aligned}$$

At 15 keV, the local contrast is

$$C_{15} = e^{-0.5\times(3.0-4.0)} - 1 \approx 0.649.$$

At 40 keV, the local contrast is

$$C_{40} = e^{-0.5\times(0.2-0.4)} - 1 \approx 0.105.$$

Hence, the local contrast is higher (better) at 15 keV.

Note: If you confused local contrast and contrast, the answer you would get differs. At 15 keV, the contrast

of the blood vessel is

$$\begin{aligned} C_{15} &= \frac{N_o - N_b}{N_o + N_b} \\ &= \frac{pe^{-0.5\mu_{\text{vessel}}}e^{-1.5\mu_{\text{tissue}}} - pe^{-2\mu_{\text{tissue}}}}{pe^{-0.5\mu_{\text{vessel}}}e^{-1.5\mu_{\text{tissue}}} - pe^{-2\mu_{\text{tissue}}}} \\ &= \frac{e^{-0.5\mu_{\text{vessel}}} - e^{-0.5\mu_{\text{tissue}}}}{e^{-0.5\mu_{\text{vessel}}} - e^{-0.5\mu_{\text{tissue}}}} \\ &= \frac{1 - e^{-0.5(\mu_{\text{tissue}} - \mu_{\text{vessel}})}}{1 + e^{-0.5(\mu_{\text{tissue}} - \mu_{\text{vessel}})}} \\ &= \frac{1 - e^{-0.5\times(4.0-3.0)}}{1 + e^{-0.5\times(4.0-3.0)}} \\ &\approx 0.2449. \end{aligned}$$

Similarly, at 40 keV the local contrast of the blood vessel is

$$C_{40} = \frac{1 - e^{-0.5\times(0.4-0.2)}}{1 + e^{-0.5\times(0.4-0.2)}} \approx 0.05\,.$$

In this case, the contrast is still higher at 15 keV.

(c) As we derived in part (b), the local contrast is totally determined by the difference between the linear attenuation coefficients of the soft tissue and the blood vessel. As can be seen from the table, at 15 keV this difference does not change much after the contrast agent is injected into the blood vessel. Hence, it would be expected that the local contrast (in its absolute value) does not change much. (The new contrast is actually 0.393 in absolute value.)

At 40 keV, the linear attenuation coefficient of the contrast agent is hugely different from that of the soft tissue and the original blood vessel. Thus, it can be expected that the local contrast of the blood vessel will be largely changed (improved) after the contrast agent is injected in. (The new contrast is actually 0.999 in absolute value.)

(d) The explanation is that the contrast agent material has K-shell electrons whose binding energy is slightly lower than 40 keV but higher than 15 keV. When x-ray photons with an energy of 40 keV enter the material, photoelectric interaction will cause electrons from the K-shell to be ejected and the x-ray photons will be completely absorbed. This effect, called K-edge absorption, significantly increases the attenuation coefficient of the contrast agent.

Solution 5.25

(a) The intensity of x-ray beam is given by

$$I(E) = \frac{NE}{A\Delta t}\,.$$

When the x-ray source is an ideal point source, we need to take the magnification into account. The distance between the source and the object is $2z_0$, the distance between the source and the detector is $3z_0$, so the object magnification is $M = \frac{d}{z} = 1.5$. The intensity profile on the detector along the x-axis is shown in Figure S5.12.

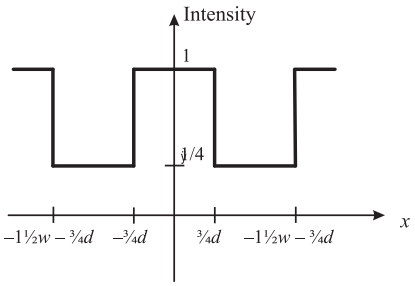

Figure S5.12 Intensity profile along x axis for ideal point x-ray source. See Problem 5.25.

(b) The dark bars on the phantom are treated as target. So, the contrast is

$$C = \frac{I_t - I_b}{I_b} = \frac{1/4 - 1}{1} = -\frac{3}{4}\,.$$

(c) The Fourier transform of the PSF of the system is:

$$\begin{aligned} H(u,v) &= \mathcal{F}\{h(x,y)\} \\ &= \mathcal{F}\{\mathrm{sinc}(\alpha x)\}\mathcal{F}\{\mathrm{sinc}(\beta y)\} \\ &= \frac{1}{\alpha}\,\mathrm{rect}\left(\frac{u}{\alpha}\right)\cdot\frac{1}{\beta}\,\mathrm{rect}\left(\frac{v}{\beta}\right)\,. \end{aligned}$$

The system is an ideal low pass filter. The highest frequencies of the output signal in x and y directions are $U_0 = \frac{\alpha}{2}$ and $V_0 = \frac{\beta}{2}$, respectively. According to the sampling theorem, the maximum sampling periods for the output signals of the system are $(\Delta x)_{\max} = \frac{1}{2U_0} = \frac{1}{\alpha}$, and $(\Delta y)_{\max} = \frac{1}{2V_0} = \frac{1}{\beta}$.

(d) The imaging equation of a projection radiography system is

$$I_d = I_0 \int_0^{E_{max}} S_0(E) E \exp\left[-\int_0^x \mu(s,E)ds\right] dE.$$

Since the x-ray photons are monochromatic, and the target in the phantom is homogeneous, the above equation can be simplified to

$$\frac{I_d}{I_0} = e^{-\mu(160\ \mathrm{keV})x} = \frac{1}{4}\,. \tag{S5.9}$$

Then

$$-\mu(160\ \mathrm{keV}) = \ln\left(\frac{640(\ \mathrm{keV})}{160(\ \mathrm{keV})}\right)\ \mathrm{cm}^{-1} = \ln(4)\ \mathrm{cm}^{-1}\,.$$

Solving for x in Equation (S5.9) yields

$$x = \frac{\ln(4)}{\ln(4)} = 1\ \mathrm{cm}\,.$$

Solution 5.26

(a) SNR decreases because the differences between the attenuation of different body tissues decreases as the energy increases.

(b) The dose is reduced due to the compensatory change in the exposure time.

(c)
- D
- I
- N
- I
- I

(d) The airgap is most effective in reducing the scatter fraction in case of small field size.

(e) The image noise ultimately limits the contrast sensitivity of an x-ray imaging system.

(f) The average photon energy is mainly determined by the material in the beam path.

Solution 5.27

(a) The best contrast agent to be used in this case is iodine because it has the k-shell energies within the energy of the source. This increases probability of photoelectric effect and hence higher linear attenuation coefficient that barium. Therefore the use of iodine will provide better contrast in the image.

(b) (i) *Contrast before contrast agent is applied*: Let I_0 be the intensity at the middle of the detector when nothing is put between the source and the detector. The intensity at the center of the tumor is

$$\begin{aligned} I_t &= I_0 e^{-(\mu_{\text{tumor}})(2R)} e^{-(\mu_{\text{tissue}})w} \\ &= I_0 e^{-(0.75\times 0.2)-(1\times 1)} = (0.3166) I_0 \,. \end{aligned}$$

The intensity at the edge of the tumor is

$$I_b = I_0 \cos^3\theta_1 e^{-(\mu_{\text{tissue}})\frac{w}{\cos\theta_1}} \,.$$

From Figure P5.8 we see that $\tan\theta_1 = R/(D - D_{td} - w - R)$. Therefore $\theta_1 = 2.5714 \times 10^{-4}$ radians and $\cos\theta_1 = 1$. This implies that we can neglect the $\cos^3\theta_1$ effect in this problem. Accordingly,

$$\begin{aligned} I_b &= I_0 e^{-(\mu_{\text{tissue}})w} \\ &= I_0 e^{(-1\times 1)} = (0.3679) I_0 \,, \end{aligned}$$

and

$$\text{Contrast before contrast agent is applied} = \frac{I_0(0.3166 - 0.3679)}{I_0(0.3679)} = -0.1394 \,.$$

(ii) *Contrast After contrast agent is applied*: The intensity at the center of the tumor is

$$\begin{aligned} I_t &= I_0 e^{-(\mu_{\text{tumor with contrast agent}})(2R)} e^{-(\mu_{\text{tissue}})w} \\ &= I_0 e^{-(10\times 0.2)-(1\times 1)} = (0.0498) I_0 \,. \end{aligned}$$

The intensity at the edge of the tumor remains the same since the photons do not pass through the tumor. Accordingly,

$$I_b = (0.3679)I_0\,,$$

and

$$\text{Contrast before contrast agent is applied} = \frac{I_0(0.0498 - 0.3679)}{I_0(0.3679)} = -0.8646\,.$$

(c) Assume that $w \approx 0$ in this part. The single Compton scattering event could take place either in the tissue or in the tumor. But, for the photon to have the lowest possible energy while hitting the detector, it should be scattered the most—that is, it should have the largest scattering angle.

The dashed line in Figure S5.13 shows the path that yields a Compton scattered photon, which will hit the detector at the lowest possible energy. Among all the Compton scattered photon trajectories (with single scattering events) the dashed line path will have the largest scatter angle.

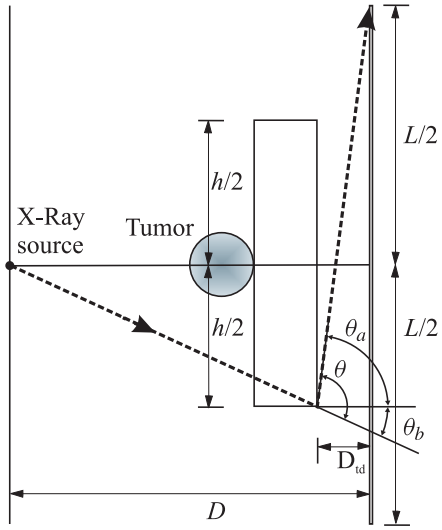

Figure S5.13 θ is the maximum Compton scattering angle. The dotted line shows the trajectory of the photon having the lowest possible energy reaching the detector. See Problem 5.27.

(d) In this part, we have to find the energy of the Compton scattered photon which follows the dashed line trajectory in part (c). To find the energy, we should find the scatter angle θ (see Figure S5.13). The angle θ can be written as sum of θ_a and θ_b. From the geometry of the setup,

$$\tan\theta_a = \frac{(l/2) + (h/2)}{D_{td}}\,,$$
$$\tan\theta_b = \frac{(h/2)}{D - D_{td}}\,.$$

Given the above relationships, and using the given values of l, h, D, and D_{td}, we find that $\theta_a = 1.3790$ radians and $\theta_b = 0.0038$ radians. Therefore, $\theta = 0.0038 + 1.3790 = 1.3828$ radians is the maximum scattering

angle. This implies that

$$\text{Minimum energy of Compton photon} \quad = \quad \frac{E}{1 + (1 - \cos(\theta))\frac{E}{m_o c^2}} \, .$$

Substituting, $E = 35$ keV (energy of incoming photon), $\theta = 1.3828$ radians, and $m_o c^2 = 511$ keV yields

$$\text{minimum energy} = 33.1536 \text{ keV} \, .$$

6

Computed Tomography

INSTRUMENTATION

Solution 6.1

(a) $(h^W - h^A) = a(h_m^W - h_m^A)$, hence

$$\begin{aligned} a &= (h^W - h^A)/(h_m^W - h_m^A)\,, \\ b &= h^W - h_m^W(h^W - h^A)/(h_m^W - h_m^A) \\ &= h^A - h_m^A(h^W - h^A)/(h_m^W - h_m^A)\,. \end{aligned}$$

(b) $h^W = 0$; h^A = -1,000.

(c) $a = 0.9$; $b = -9.01$.

Solution 6.2

(a) The x-ray source detector apparatus rotates at a speed of 4π radians/s, so it takes 0.5 s to rotate a full circle (2π). During this period of time, the patient table moves 2 cm/ s $\times$ 0.5 s $= 1$ cm. So the pitch of the helix is 1 cm.

(b) It takes 0.5 s for the imaging devices to rotate a full circle of 2π, and it takes 1 ms to measure a projection. So the system can measure at most 500 projections over a 2π angle.

(c) The imaging time for a torso is $60/2 = 30$ s.

RADON TRANSFORM

Solution 6.3

Proof: An operator $\mathcal{R}$ is linear if $\mathcal{R}(af_1 + bf_2) = a\mathcal{R}(f_1) + b\mathcal{R}(f_2)$. Let

$$\mathcal{R}f = \int_{-\infty}^{\infty}\int_{-\infty}^{\infty} f(x,y)\delta(x\cos\theta + y\sin\theta - \ell)\,dx\,dy.$$

Then we have

$$\begin{aligned}
\mathcal{R}(af_1 + bf_2) &= \iint [af_1(x,y) + bf_2(x,y)]\delta(x\cos\theta + y\sin\theta - \ell)\,dx\,dy \\
&= a\iint f_1(x,y)\delta(x\cos\theta + y\sin\theta - \ell)\,dx\,dy \\
&\qquad + b\iint f_2(x,y)\delta(x\cos\theta + y\sin\theta - \ell)\,dx\,dy \\
&= a\mathcal{R}f_1 + b\mathcal{R}f_2\,.
\end{aligned}$$

which was to be proved.

Solution 6.4

Let $u = x - x_0$, $v = y - y_0$, then $du = dx$, $dv = dy$. We get

$$\begin{aligned}
&\iint f(x - x_0, y - y_0)\delta(x\cos\theta + y\sin\theta - \ell)\,dx\,dy \\
&= \iint f(u,v)\,\delta\left[(u + x_0)\cos\theta + (v + y_0)\sin\theta - \ell\right]\,du\,dv \\
&= \iint f(u,v)\delta\left[u\cos\theta + v\sin\theta - (\ell - x_0\cos\theta - y_0\sin\theta)\right]\,du\,dv \\
&= g(\ell - x_0\cos\theta - y_0\sin\theta, \theta),
\end{aligned}$$

where $g(\ell,\theta)$ is the Radon transform of $f(x,y)$.

Solution 6.5

Since $f(x,y)$ is rotationally symmetric, $g(\ell,\theta) = g(\ell,0)$. Hence,

$$\begin{aligned}
g(\ell,\theta) &= \int_{L(\ell,\theta)} f(x,y)ds \\
&= \int_{-\infty}^{\infty}\int_{-\infty}^{\infty} e^{-x^2-y^2}\delta(x\cos(\theta) - \ell)\,dxdy \\
&= \int_{-\infty}^{\infty} e^{-\ell^2-y^2}\,dy \\
&= e^{-l^2}\int_{-\infty}^{\infty} e^{-y^2}\,dy\,.
\end{aligned}$$

Since

$$\frac{1}{\sqrt{2\pi\sigma^2}} \int_{-\infty}^{\infty} e^{-x^2/\sigma^2}\, dx = 1\,,$$

then

$$\int_{-\infty}^{\infty} e^{-y^2}\, dy = \sqrt{\pi}\,.$$

Thus,

$$g(\ell,\theta) = \sqrt{\pi} e^{-\ell^2}\,.$$

Solution 6.6

$$\begin{aligned}\int_{-\infty}^{\infty} g(\ell,\theta) d\ell &= \int_{-\infty}^{\infty} h_\ell(\ell) h_\theta(\theta)\, d\ell \\ &= h_\theta(\theta) \int_{-\infty}^{\infty} h_\ell(\ell)\, d\ell\,.\end{aligned}$$

On the other hand

$$\begin{aligned}\int_{-\infty}^{\infty} g(\ell,\theta) d\ell &= \int_{-\infty}^{\infty} \iint f(x,y)\delta(x\cos\theta + y\sin\theta - \ell)\, dx\, dy\, d\ell \\ &= \iint f(x,y) \int_{-\infty}^{\infty} \delta(x\cos\theta + y\sin\theta - \ell)\, d\ell\, dx\, dy \\ &= \iint f(x,y)\, dx\, dy\,.\end{aligned}$$

Thus,

$$h_\theta(\theta) \int_{-\infty}^{\infty} h_\ell(\ell) d\ell = \iint f(x,y)\, dx\, dy\,.$$

Since the right-hand side does not depend on θ, the left-hand side cannot depend on θ either. Hence, $h_\theta(\theta)$ must be a constant.

Solution 6.7

(a) The Fourier transform of $f(x,y)$ is

$$F(u,v) = 0.5(\delta(u - f_0, v) + \delta(u + f_0, v))\,.$$

In order to use the projection slice theorem, we must change to polar coordinates. We use the following steps

for a shifted impulse function:

$$\begin{aligned}\delta(u - f_0, v) &= \delta(u - f_0)\delta(v) \\ &= \delta(\varrho\cos\theta - f_0)\delta(\varrho\sin\theta) \\ &= \delta(\varrho[1 - \frac{\theta^2}{2!} + \cdots] - f_0)\delta(\varrho[\theta - \frac{\theta^3}{3!} + \cdots]) \\ &= \delta(\varrho - f_0)\delta(\varrho\theta) \\ &= \delta(\varrho - f_0)\frac{1}{|\varrho|}\delta(\theta)\,.\end{aligned}$$

In this derivation we have used a Taylor series approximation for cosine and sine and the scaling property of the impulse function. This derivation can be repeated for the impulse shifted in the opposite direction; then we apply the projection slice theorem, yielding

$$G(\varrho,\theta) = F(\varrho\cos\theta, \varrho\sin\theta) = \frac{0.5}{|\varrho|}[\delta(\varrho - f_0) + \delta(\varrho + f_0)]\delta(\theta)\,.$$

Now we write the expression for filtered backprojection, plug in this Radon transform, and simplify as follows:

$$\begin{aligned}f(x,y) &= \int_0^\pi \left[\int_{-\infty}^{\infty} |\varrho| G(\varrho,\theta) e^{j2\pi\varrho\ell} d\varrho\right]_{\ell = x\cos\theta + y\sin\theta} d\theta \\ &= \int_0^\pi \left[\int_{-\infty}^{\infty} |\varrho| \frac{0.5}{|\varrho|}[\delta(\varrho - f_0) + \delta(\varrho + f_0)]\delta(\theta) e^{j2\pi\varrho\ell} d\varrho\right]_{\ell = x\cos\theta + y\sin\theta} d\theta \\ &= \int_0^\pi \left[\int_{-\infty}^{\infty} 0.5[\delta(\varrho - f_0) + \delta(\varrho + f_0)]\delta(\theta) e^{j2\pi\varrho\ell} d\varrho\right]_{\ell = x\cos\theta + y\sin\theta} d\theta \\ &= \int_0^\pi \left[\int_{-\infty}^{\infty} 0.5[\delta(\varrho - f_0) + \delta(\varrho + f_0)] e^{j2\pi\varrho\ell} d\varrho\right]_{\ell = x\cos\theta + y\sin\theta} \delta(\theta) d\theta \\ &= \int_0^\pi [\cos(2\pi f_0 \ell)]_{\ell = x\cos\theta + y\sin\theta}\, \delta(\theta) d\theta \\ &= \int_0^\pi \cos(2\pi f_0 [x\cos\theta + y\sin\theta])\delta(\theta) d\theta \\ &= \cos(2\pi f_0 x)\,.\end{aligned}$$

The last step follows from the sifting property of the impulse function. This proves that filtered backprojection produces the correct result.

(b) i) Using the result from part (a) and the linearity of the Radon transform, it follows that the Radon transform of $f(x,y) = \cos 2\pi a x + \cos 2\pi b y$ is

$$G(\varrho,\theta) = \frac{0.5}{|\varrho|}[\delta(\varrho - a) + \delta(\varrho + a)]\delta(\theta) + \frac{0.5}{|\varrho|}[\delta(\varrho - b) + \delta(\varrho + b)]\delta(\theta)\,.$$

From the linearity of the inverse Radon transform (i.e., filtered backprojection), we can follow the same steps carried out in part (a) to prove that filtered backprojection will yield $f(x,y) = \cos 2\pi a x + \cos 2\pi b y$.

ii) The function $f(x,y) = \cos 2\pi(ax + by)$ is a rotated version of $\cos(2\pi f_0 x)$, which was solved in part (a). Although the math can be carried out in analogous fashion, it is easier to simply use the form found in (a)

and carefully apply it here. The frequency of this sinusoid (distance from the origin is $f_0 = \sqrt{a^2 + b^2}$ and its rotation from the x-axis is $\theta_0 = \tan^{-1}(b/a)$. Therefore, its Radon transform is given by

$$G(\varrho, \theta) = \frac{0.5}{|\varrho|}[\delta(\varrho - f_0) + \delta(\varrho + f_0)]\delta(\theta - \theta_0)\,.$$

In proving that filtered backprojection gives the right answer, it is only necessary to evaluate the last step differently.

$$\begin{aligned} f(x,y) &= \int_0^\pi [\cos(2\pi f_0 \ell)]_{\ell = x\cos\theta + y\sin\theta}\, \delta(\theta - \theta_0) d\theta \\ &= \int_0^\pi \cos(2\pi f_0 [x\cos\theta + y\sin\theta])\delta(\theta - \theta_0) d\theta \\ &= \cos(2\pi f_0 [x\cos\theta_0 + y\theta_0) \\ &= \cos(2\pi [xa + yb])\,. \end{aligned}$$

The last step follows from the facts that $a = f_0 \cos\theta_0$ and $b = f_0\theta_0$ from the geometry.

Solution 6.8

(a) We write

$$\begin{aligned} \mu(x,y) &= \mu_0 \,\mathrm{rect}(x)\,\mathrm{rect}(y) \\ &= \begin{cases} \mu_0 & \text{if } -1/2 \le x \le 1/2 \text{ and } -1/2 \le y \le 1/2; \\ 0 & \text{otherwise}\,. \end{cases} \end{aligned}$$

(b) $\mathcal{F}_{2\mathrm{D}}\{\mu\}(u,v) = \mu_0 \mathrm{sinc}(u)\mathrm{sinc}(v)$.

(c) The relationship is given by the Radon transform, which can be simplified by the form of the observed function

$$\begin{aligned} g(\ell,\theta) &= \int_{-\infty}^{\infty}\int_{-\infty}^{\infty} \mu(x,y)\delta(x\cos\theta + y\sin\theta - \ell)dx\,dy \\ &= \int_{-1/2}^{1/2}\int_{-1/2}^{1/2} \mu_0\delta(x\cos\theta + y\sin\theta - \ell)dx\,dy\,. \end{aligned}$$

(d) Writing the projection slice theorem yields

$$G(\varrho,\theta) = \mathcal{F}_{2\mathrm{D}}\{\mu\}(\varrho\cos\theta, \varrho\sin\theta) = \mu_0 \mathrm{sinc}(\varrho\cos\theta)\mathrm{sinc}(\varrho\sin\theta)\,.$$

(e) We want to find $g(\ell,\theta) = \mathcal{F}_{1\mathrm{D}}^{-1}\{G(\varrho,\theta)\}$. By symmetry, we have

$$\begin{aligned} G(\varrho, \theta + \frac{\pi}{2}) &= G(\varrho,\theta)\,, \\ G(\varrho, \theta + \pi) &= G(\varrho,\theta)\,, \\ G(\varrho, \frac{\pi}{2} - \theta) &= G(\varrho,\theta)\,, \end{aligned}$$

since $\mathrm{sinc}(-x) = \mathrm{sinc}(x)$. Hence, we only need to compute $g(\ell, \theta)$ for $0 \le \theta \le \pi/4$.

First, if $\theta = 0$, $G(\varrho, \theta) = \mu_0 \mathrm{sinc}(\varrho)$, and hence

$$g(\ell, 0^\circ) = \mathcal{F}_{1\mathrm{D}}^{-1}\{\mu_0 \mathrm{sinc}(\varrho)\} = \mu_0 \,\mathrm{rect}(\ell)\,.$$

If $0 < \theta \le \pi/4$,

$$\begin{aligned} g(\ell, \theta) &= \mathcal{F}_{1\mathrm{D}}^{-1}\{\mu_0 \mathrm{sinc}(\varrho\cos\theta)\mathrm{sinc}\varrho\sin\theta\} \\ &= \frac{\mu_0}{|\sin\theta\cos\theta|}\,\mathrm{rect}(\frac{\ell}{\cos\theta}) * \mathrm{rect}(\frac{\ell}{\sin\theta})\,. \end{aligned}$$

The convolution of two rect functions, $\mathrm{rect}(x/a) * \mathrm{rect}(x/b)$ for $0 < b \le a$, can be easily computed to be:

$$\mathrm{rect}(x/a) * \mathrm{rect}(x/b) = \begin{cases} x + \frac{1}{2}(a+b) & -\frac{1}{2}(a+b) \le x \le -\frac{1}{2}(a-b) \\ b & -\frac{1}{2}(a-b) \le x \le \frac{1}{2}(a-b) \\ -x + \frac{1}{2}(a+b) & \frac{1}{2}(a-b) \le x \le \frac{1}{2}(a+b) \\ 0 & \text{otherwise} \end{cases}.$$

Since $\cos\theta > \sin\theta$ for $\theta \in (0, \pi/4]$, hence

$$g(\ell, \theta) = \frac{\mu_0}{|\sin\theta\cos\theta|} \times \begin{cases} \ell + \frac{1}{2}(\cos\theta + \sin\theta) & -\frac{1}{2}(\cos\theta + \sin\theta) \le \ell \le -\frac{1}{2}(\cos\theta - \sin\theta) \\ \sin\theta & -\frac{1}{2}(\cos\theta - \sin\theta) \le \ell \le \frac{1}{2}(\cos\theta - \sin\theta) \\ -\ell + \frac{1}{2}(\cos\theta + \sin\theta) & \frac{1}{2}(\cos\theta - \sin\theta) \le \ell \le \frac{1}{2}(\cos\theta + \sin\theta) \\ 0 & \text{otherwise} \end{cases}$$

for $0 < \theta \le \pi/4$.

(f) $\theta = 30^\circ$, $\sin\theta = 1/2$, $\cos\theta = \sqrt{3}/2$. From (e), we get

$$g(\ell, 30^\circ) = \frac{4\mu_0}{\sqrt{3}} \times \begin{cases} \ell + \frac{1+\sqrt{3}}{4} & -\frac{1+\sqrt{3}}{4} \le \ell \le -\frac{\sqrt{3}-1}{4} \\ \frac{1}{2} & -\frac{\sqrt{3}-1}{4} \le \ell \le \frac{\sqrt{3}-1}{4} \\ -\ell + \frac{1+\sqrt{3}}{4} & \frac{\sqrt{3}-1}{4} \le \ell \le \frac{1+\sqrt{3}}{4} \\ 0 & \text{otherwise} \end{cases}$$

for $0 < \theta \le \pi/4$. Therefore,

$$\begin{aligned} b_{30^\circ}(x, y) &= g(x\cos 30^\circ + y\sin 30^\circ, 30^\circ) = g(\frac{\sqrt{3}x + y}{2}, 30^\circ) \\ &= \frac{4\mu_0}{\sqrt{3}} \times \begin{cases} \frac{\sqrt{3}x+y}{2} + \frac{1+\sqrt{3}}{4} & -\frac{1+\sqrt{3}}{4} \le \frac{\sqrt{3}x+y}{2} \le -\frac{\sqrt{3}-1}{4} \\ \frac{1}{2} & -\frac{\sqrt{3}-1}{4} \le \frac{\sqrt{3}x+y}{2} \le \frac{\sqrt{3}-1}{4} \\ -\frac{\sqrt{3}x+y}{2} + \frac{1+\sqrt{3}}{4} & \frac{\sqrt{3}-1}{4} \le \frac{\sqrt{3}x+y}{2} \le \frac{1+\sqrt{3}}{4} \\ 0 & \text{otherwise} \end{cases} \end{aligned}$$

The sketch is straightforward; note that $g(\ell, 30^\circ)$ is trapezoid shaped, not a triangle.

Solution 6.9

We start with the convolution integral

$$g(x,y) = \int_{\xi}\int_{\eta} f(\xi,\eta)h(x-\xi,y-\eta)\,d\xi\,d\eta\,.$$

Now, we perform the following steps:

$$\begin{aligned}
\mathcal{R}\{g\} &= \int_y\int_x\int_\eta\int_\xi f(\xi,\eta)h(x-\xi,y-\eta)\,d\xi d\eta\delta(x\cos\theta+y\sin\theta-\ell)\,dxdy\\
&= \int_\eta\int_\xi f(\xi,\eta)\int_y\int_x h(x-\xi,y-\eta)\delta(x\cos\theta+y\sin\theta-\ell)\,dxdy\,d\xi d\eta\\
&= \int_\eta\int_\xi f(\xi,\eta)\int_{y'}\int_{x'} h(x',y')\delta(x'\cos\theta+y'\sin\theta-[\ell-\xi\cos\theta-\eta\sin\theta])\,dx'dy'\,d\xi d\eta\\
&= \int_\eta\int_\xi f(\xi,\eta)\mathcal{R}\{h\}(\ell-\xi\cos\theta-\eta\sin\theta,\theta)\,d\xi d\eta\\
&= \int_\eta\int_\xi f(\xi,\eta)\int_{\ell'}\mathcal{R}\{h\}(\ell-\ell',\theta)\delta(\xi\cos\theta+\eta\sin\theta-\ell')\,d\ell'\,d\xi d\eta\\
&= \int_{\ell'}\mathcal{R}\{h\}(\ell-\ell',\theta)\int_\eta\int_\xi f(\xi,\eta)\delta(\xi\cos\theta+\eta\sin\theta-\ell')\,d\xi d\eta\,d\ell'\\
&= \int_{\ell'}\mathcal{R}\{h\}(\ell-\ell',\theta)\mathcal{R}\{f\}(\ell',\theta)d\ell'\\
&= \mathcal{R}\{h\}*\mathcal{R}\{f\}
\end{aligned}$$

which was to be proved.

CT RECONSTRUCTION

Solution 6.10

(a) We carry out the following steps:

$$\begin{aligned}
g_s(\ell,\theta+\pi/2) &= \iint s(x,y)\delta(x\cos(\theta+\pi/2)+y\sin(\theta+\pi/2)-\ell)\,dxdy\\
&= \iint s(x,y)\delta(-x\sin\theta+y\cos\theta-\ell)\,dxdy\\
&= \iint s(-v,u)\delta(u\cos\theta+v\sin\theta-\ell)\,dudv\ (u=y,v=-x)\\
&= \iint s(u,v)\delta(u\cos\theta+v\sin\theta-\ell)\,dudv\\
&= g_s(\ell,\theta)\,.
\end{aligned}$$

(b) We carry out the following steps:

$$\begin{aligned} g_s(\ell,-\theta) &= \iint s(x,y)\delta(x\cos(-\theta)+y\sin(-\theta)-\ell)\,dxdy \\ &= \iint s(x,y)\delta(x\cos\theta-y\sin\theta-\ell)\,dxdy \\ &= \iint s(u,-v)\delta(u\cos\theta+v\sin\theta-\ell)\,dudv \;(u=x,v=-y) \\ &= \iint s(u,v)\delta(u\cos\theta+v\sin\theta-\ell)\,dudv \\ &= g_s(\ell,\theta)\,. \end{aligned}$$

(c) Let

$$\tilde{g}_s(\ell,\theta)=\begin{cases} g_s(\ell,\theta) & 0\le\theta<\frac{\pi}{4} \\ g_s\left(\ell,\frac{\pi}{2}-\theta\right) & \frac{\pi}{4}\le\theta<\frac{\pi}{2} \end{cases},$$

which covers $0\le\theta<\pi/2$. Then

$$g_s(\ell,\theta)=\begin{cases} \tilde{g}_s(\ell,\theta) & 0\le\theta<\frac{\pi}{2} \\ \tilde{g}_s\left(\ell,\theta-\frac{\pi}{2}\right) & \frac{\pi}{2}\le\theta\le\pi \end{cases},$$

covers $0\le\theta<\pi$.

(d) See Figure S6.1.

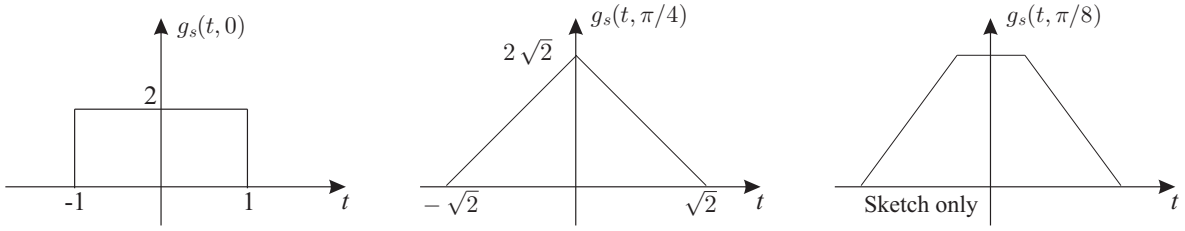

Figure S6.1 Sketch of projections at different angles. See Problem 6.10(d).

(e) See Figure S6.2. From simple rotations, we have $\ell_1=-\cos\theta-\sin\theta$, $\ell_2=-\cos\theta+\sin\theta$, $\ell_3=\cos\theta-\sin\theta$, and $\ell_4=\cos\theta+\sin\theta$. By similar triangles, we have:

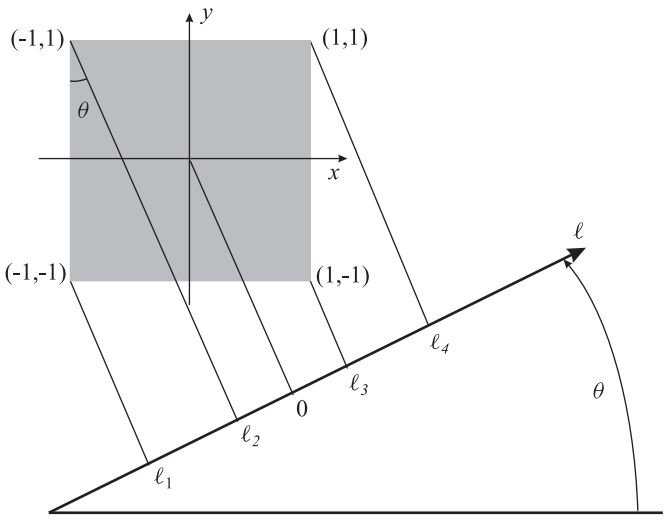

Figure S6.2 See Problem 6.10(e).

$$
\begin{aligned}
\underline{\ell_1 \le \ell \le \ell_2\text{:}} \quad \frac{\ell - \ell_1}{\ell_2 - \ell_1} &= \frac{g(\ell,\theta)}{\left(\frac{2}{\cos\theta}\right)} \\
\Rightarrow g(\ell,\theta) &= \frac{2}{\cos\theta}\left(\frac{\ell + \cos\theta + \sin\theta}{2\sin\theta}\right) \\
&= \frac{\ell + \cos\theta + \sin\theta}{\cos\theta\sin\theta} \\
\\
\underline{\ell_2 \le \ell \le \ell_3\text{:}} \quad g(\ell,\theta) &= \frac{2}{\cos\theta} \\
\\
\underline{\ell_3 \le \ell \le \ell_4\text{:}} \quad \frac{\ell_4 - \ell}{\ell_4 - \ell_3} &= \frac{g(\ell,\theta)}{\left(\frac{2}{\cos\theta}\right)} \\
\Rightarrow g(\ell,\theta) &= \frac{\cos\theta + \sin\theta - \ell}{\cos\theta\sin\theta}\,.
\end{aligned}
$$

and $g(\ell,\theta) = 0$ elsewhere.

Solution 6.11

(a) Carry out the following steps:

$$\begin{aligned} m_p(\theta) &= \int g(\ell,\theta)d\ell \\ &= \iiint f(x,y)\delta(x\cos\theta + y\sin\theta - \ell)dxdydt \\ &= \iint f(x,y)\int \delta(x\cos\theta + y\sin\theta - \ell)d\ell dxdy \\ &= \iint f(x,y)dxdy \\ &= m\,. \end{aligned}$$

(b) Carry out the following steps:

$$\begin{aligned} c_p(\theta) &= \frac{1}{m}\int \ell g(\ell,\theta)\,d\ell \\ &= \frac{1}{m}\int \ell \iint f(x,y)\delta(x\cos\theta + y\sin\theta - \ell)\,dxdyd\ell \\ &= \frac{1}{m}\iint f(x,y)\int \ell\delta(x\cos\theta + y\sin\theta - \ell)\,d\ell dxdy \\ &= \frac{1}{m}\iint f(x,y)\left[x\cos\theta + y\sin\theta\right]\,dxdy \\ &= \cos\theta\frac{1}{m}\iint f(x,y)x\,dxdy \\ &\qquad + \sin\theta\frac{1}{m}\iint f(x,y)y\,dxdy \\ &= c_x\cos\theta + c_y\sin\theta\,. \end{aligned}$$

(c) We have $m_p\left(\frac{\pi}{4}\right) = m = 1$ and $c_x = 0$ since $f(x,y)$ is symmetric about the y-axis.

$$\begin{aligned} c_y &= \iint yf(x,y)\,dxdy \\ &= \int_{-1}^{0}\int_{0}^{1+x} y\,dxdy + \int_{0}^{1}\int_{0}^{1-x} y\,dxdy \\ &= \int_{-1}^{0}\frac{(1+x)^2}{2}\,dx + \int_{0}^{1}\frac{(1-x)^2}{2}\,dx \\ &= \frac{1}{3}\,. \end{aligned}$$

Hence,

$$c_p\left(\frac{\pi}{4}\right) = c_y\sin\theta = \frac{1}{3}\frac{\sqrt{2}}{2} \approx 0.2357.$$

Solution 6.12

(a) The object is shown in Figure S6.3.

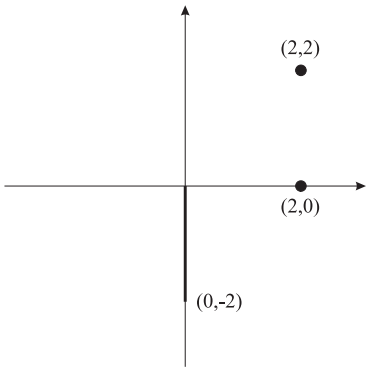

Figure S6.3 See Problem 6.12(a).

(b) The number of photons as a function of ℓ for $\theta = 0^\circ$ and $\theta = 90^\circ$ are shown in Figures S6.4 and S6.5.

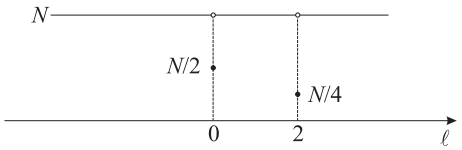

Figure S6.4 $\theta = 0^\circ$. See Problem 6.12(b).

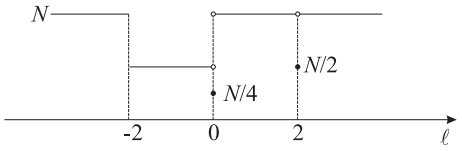

Figure S6.5 $\theta = 90^\circ$. See Problem 6.12(b).

(c) The projections at $\theta = 0^\circ$ and $\theta = 90^\circ$ are shown in Figures S6.6 and S6.7.

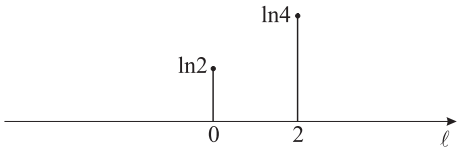

Figure S6.6 $\theta = 0^\circ$. See Problem 6.12(c).

(d) The backprojection image at $\theta = 0^\circ$ is shown in Figure S6.8. In the shaded area, the value is zero, on $x = 0$, the value is $\ln 2$, and on $x = 2$, the value is $\ln 4$.

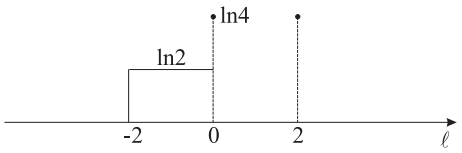

Figure S6.7 $\theta = 90^\circ$. (See Problem 6.12(c).)

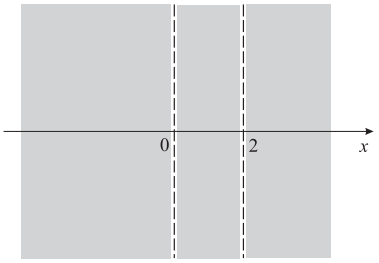

Figure S6.8 See Problem 6.12(d).

Solution 6.13

(a) We have

$$g(\ell, 60^\circ) = \begin{cases} \sqrt{3}\mu\left(\frac{a}{2} + \ell\right), & -\frac{a}{2} \le \ell \le 0 \\ \sqrt{3}\mu\left(\frac{a}{2} - \ell\right), & 0 \le \ell \le \frac{a}{2} \\ 0, & \text{otherwise} \end{cases}.$$

The projection $g(\ell, 60^\circ)$ is shown in Figure S6.9.

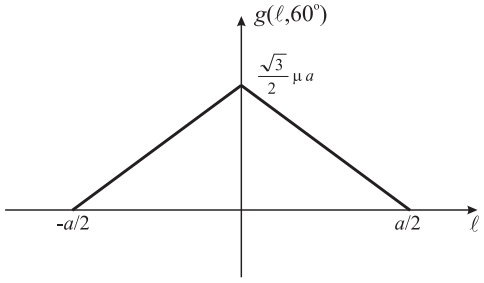

Figure S6.9 See Problem 6.13(a).

(b) We have

$$\begin{aligned} b_{60^\circ}\left(0, \frac{a}{4}\right) &= g\left(0\cos 60^\circ + \frac{a}{4}\sin 60^\circ, 60^\circ\right) \\ &= g\left(\frac{\sqrt{3}a}{8}, 60^\circ\right) \\ &= \sqrt{3}\mu\left(\frac{a}{2} - \frac{\sqrt{3}a}{8}\right) \\ &= \frac{\sqrt{3}\mu a}{8}(4-\sqrt{3})\,. \end{aligned}$$

(c) Let function $f(t)$ be defined by scaling a rect function as:

$$f(t) = \begin{cases} K, & -\frac{p}{2} \le t \le \frac{p}{2} \\ 0, & \text{otherwise} \end{cases}\,.$$

The convolution $f(t) * f(t)$ is given by:

$$f(t) * f(t) = \begin{cases} K^2(p+t), & -p \le t \le 0 \\ K^2(p-t), & 0 \le t \le p \\ 0, & \text{otherwise} \end{cases}\,.$$

Comparing with $g(\ell, 60^\circ)$, we see that it is a convolution of function $f(\ell)$ with itself, where $K^2 = \sqrt{3}\mu$, and $p = a/2$:

$$g(\ell, 60^\circ) = \sqrt{\sqrt{3}\mu}\,\text{rect}\left(\frac{2\ell}{a}\right) * \sqrt{\sqrt{3}\mu}\,\text{rect}\left(\frac{2\ell}{a}\right).$$

By the projection slice theorem, we get $F(\varrho\cos\theta, \varrho\sin\theta) = G(\varrho,\theta) = \mathcal{F}\{g(\ell,\theta)\}$. Since $g(\ell, 60^\circ)$ is expressed as a convolution of a rect function with itself, we have:

$$\mathcal{F}\{g(\ell, 60^\circ)\} = \left[\mathcal{F}\{\sqrt{\sqrt{3}\mu}\,\text{rect}\left(\frac{2\ell}{a}\right)\}\right] = \frac{\sqrt{3}\mu a^2}{4}\,\text{sinc}^2\left(\frac{a\varrho}{2}\right).$$

Therefore,

$$F(\varrho\cos 60^\circ, \varrho\sin 60^\circ) = \frac{\sqrt{3}\mu a^2}{4}\,\text{sinc}^2\left(\frac{a\varrho}{2}\right).$$

Solution 6.14

(a) Define $\wedge(x) = \text{rect}(x) * \text{rect}(x)$. By the convolution theorem, its Fourier transform is

$$\mathcal{F}\{(\wedge(x)\}(\varrho) = \text{sinc}^2(\varrho)\,.$$

We see that $W(\varrho) = \wedge(\varrho/\varrho_0)$. So by the duality of the Fourier transform and the scaling theorem, we have

$$\mathcal{F}^{-1}\{W(\varrho/\varrho_0)\}(\ell) = \varrho_0 \text{sinc}^2(\varrho_0\ell)\,.$$

Multiplying $|\varrho|$ by $W(\varrho) = \wedge(\varrho/\varrho_0)$ corresponds to convolving $c(\ell) = \mathcal{F}^{-1}\{|\varrho|\}(\ell)$ by $\mathcal{F}^{-1}\{W(\varrho/\varrho_0)\}(\ell)$,

which yields

$$\tilde{c}(\ell) = c(\ell) * \varrho_0 \mathrm{sinc}^2(\varrho_0 \ell)\,.$$

(b) We have

$$\lim_{\varrho_0 \to \infty} \varrho_0 \mathrm{sinc}^2 \varrho_0 \ell = \delta(\ell)\,,$$

Therefore,

$$\lim_{\varrho_0 \to \infty} \tilde{c}(\ell) = c(\ell)\,,$$

which means that the exact solution is produced.

Solution 6.15

First expand the integral:

$$\begin{aligned}&\int_0^{2\pi} \int_0^{\infty} \varrho G_\theta(\varrho) e^{+j2\pi\varrho\boldsymbol{\omega}\cdot\mathbf{x}}\, d\varrho\, d\theta \\ &\quad = \underbrace{\int_0^{\pi} \int_0^{\infty} \varrho G_\theta(\varrho) e^{+j2\pi\varrho\boldsymbol{\omega}\cdot\mathbf{x}}\, d\varrho\, d\theta}_{I_1} + \underbrace{\int_{\pi}^{2\pi} \int_0^{\infty} \varrho G_\theta(\varrho) e^{+j2\pi\varrho\boldsymbol{\omega}\cdot\mathbf{x}}\, d\varrho\, d\theta}_{I_2}\,.\end{aligned}$$

Now make the substitution $\phi = \theta - \pi$ in I_2:

$$I_2 = \int_0^{\pi} \int_0^{\infty} \varrho G_{\phi+\pi}(\varrho) e^{+j2\pi\varrho[x\cos(\phi+\pi)+y\sin(\phi+\pi)]}\, d\varrho\, d\phi\,.$$

From the geometry, $g_{\phi+\pi}(\ell) = g_\theta(-\ell)$, which implies $G_{\phi+\pi}(\varrho) = G_\theta(-\varrho)$. Therefore,

$$I_2 = \int_0^{\pi} \int_0^{\infty} \varrho G_\theta(-\varrho) e^{+j2\pi\varrho[-x\cos(\phi)-y\sin(\phi)]}\, d\varrho\, d\phi\,.$$

Now let $q = -\varrho$ and $\theta = \phi$ to yield:

$$I_2 = -\int_0^{\pi} \int_0^{\infty} -q G_\theta(q) e^{+j2\pi q\boldsymbol{\omega}\cdot\mathbf{x}}\, dq\, d\theta\,.$$

Now let $\varrho = q$ and switch around the limits with the minus sign:

$$I_2 = \int_0^{\pi} \int_{-\infty}^{0} -\varrho G_\theta(\varrho) e^{+j2\pi\varrho\boldsymbol{\omega}\cdot\mathbf{x}}\, d\varrho\, d\theta\,.$$

Now, I_1 and I_2 can be added together to yield the desired result.

Solution 6.16

(a) We have $\mathcal{F}\{\delta(x,y)\} = 1$, so $G(\varrho,\theta) = 1$. Therefore, $g(\ell,\theta) = \mathcal{F}^{-1}\{G(\varrho,\theta)\} = \delta(\ell)$.

(b) We write

$$\begin{aligned} f_b^\delta &= \int_0^\pi \delta(x\cos\theta + y\sin\theta)\,d\theta \\ &= \int_0^\pi \delta(r\cos\phi\cos\theta + r\sin\phi\sin\theta)\,d\theta \\ &= \int_0^\pi \delta(r\cos(\theta-\phi))\,d\theta \\ &= \int_{-\pi/2}^{\pi/2} \delta(r\sin(\theta-\phi))\,d\theta\,. \end{aligned}$$

Since $\sin\theta \approx \theta$ for small θ, $\sin(\theta-\phi) \approx \theta-\phi$ for $\theta \approx \phi$. Hence

$$f_b^\delta \approx \int_{-\pi/2}^{\pi/2} \delta(r(\theta-\phi))d\theta, \text{ for } \theta \approx \phi\,.$$

Since $\delta(at) = \frac{\delta(t)}{|a|}$ (this is the scaling theorem for the impulse function), we have

$$\begin{aligned} f_b^\delta &= \int_{-\pi/2}^{\pi/2} \frac{1}{|r|}\delta(\theta-\phi)d\theta, \text{ for } \theta \approx \phi \\ &= \frac{1}{|r|} \text{ if } \phi \in \left(-\frac{\pi}{2}, \frac{\pi}{2}\right)\,. \end{aligned}$$

If $\phi \notin \left(-\frac{\pi}{2}, \frac{\pi}{2}\right)$, it still works by noticing that

$$\begin{aligned} \int_{-\pi/2}^{\pi/2} g(x\cos\theta + y\sin\theta, \theta)\,d\theta &= \int_{\pi/2}^{3\pi/2} g(x\cos(\theta-\pi) + y\sin(\theta-\pi), \theta-\pi)\,d\theta \\ &= \int_{\pi/2}^{3\pi/2} g(-x\cos\theta - y\sin\theta, \theta-\pi)\,d\theta \\ &= \int_{\pi/2}^{3\pi/2} g(x\cos\theta + y\sin\theta, \theta)\,d\theta\,, \end{aligned}$$

since $g(\ell, \theta-\pi) = g(-\ell, \theta)$.

(c) We have

$$\frac{1}{|r|} = \frac{1}{\sqrt{x^2+y^2}}\,.$$

By the Fourier shift theorem, we know that $\mathcal{F}\{\delta(x-x_0, y-y_0)\} = e^{-j2\pi(ux_0+vy_0)}$. Hence,

$$G(\varrho, \theta) = e^{-j2\pi\varrho(\cos\theta x_0 + \sin\theta y_0)}$$

and

$$g(\ell, \theta) = \mathcal{F}^{-1}\{G(\varrho, \theta)\} = \delta(\ell - x_0\cos\theta - y_0\sin\theta)\,.$$

We have

$$\begin{aligned} f_b^\delta &= \int_0^\pi \delta(x\cos\theta + y\sin\theta - x_0\cos\theta - y_0\sin\theta)d\theta \\ &= \int_0^\pi \delta((x-x_0)\cos\theta + (y-y_0)\sin\theta)d\theta\,. \end{aligned}$$

Let $r = \sqrt{(x-x_0)^2+(y-y_0)^2}$ and $\phi = \tan^{-1}((y-y_0)/(x-x_0))$—i.e., the radius and angle are measured from (x_0, y_0). Then

$$f_b^\delta = \int_0^\pi \delta(r\cos(\theta-\phi))d\theta = \frac{1}{|r|}\,.$$

Therefore,

$$f_b^\delta = \frac{1}{\sqrt{(x-x_0)^2+(y-y_0)^2}}\,.$$

(d) Define $\mathcal{R}$ as the Radon transform operator and $\mathcal{B}$ as the backprojection operator. Both are linear operators and the composition $\mathcal{BR}$ was shown in part (c) to be shift-invariant. Therefore convolution still holds. The impulse response was found in part (b) to be $1/\sqrt{x^2+y^2}$. Therefore,

$$f_b = f * \frac{1}{\sqrt{x^2+y^2}}\,.$$

(e) In principle, all one needs to do is find the Fourier transform of $1/\sqrt{x^2+y^2}$ and apply its inverse to f_b.

Define $H(u,v) = \mathcal{F}\left\{\frac{1}{\sqrt{x^2+y^2}}\right\}$, then $F_b(u,v) = F(u,v)H(u,v)$. Hence, $F(u,v) = F_b(u,v)/H(u,v)$ provided that $H(u,v) \neq 0$.

The problem is that the Fourier Transform of $1/r$ is $1/g$ where $g = \sqrt{u^2+v^2}$. Therefore, the inverse filter is $q = \sqrt{u^2+v^2}$, which has infinite gain at infinite frequencies. In other words, it is the worst type of high-pass filter.

Solution 6.17

(a) $b_\theta(x,y) = g(x\cos\theta + y\sin\theta, \theta)$.

(b) We have

$$\begin{aligned} \ell &= x\cos\theta + y\sin\theta = 1\cos 30^\circ + 2\sin 30^\circ \\ &= 0.866 + 1 = 1.866\,. \end{aligned}$$

Therefore,

$$b_{30^\circ}(1,2) = g(1.866, 30^\circ) \approx 0.155\,.$$

(c) No, because $g(\ell, 30^\circ)$ does not say anything about $g(\ell, 45^\circ)$.

(d) Since $210^\circ = 30^\circ + 180^\circ$, this is the "opposite" projection, and therefore

$$g(\ell, 210^\circ) = g(-\ell, 30^\circ) = 0.155\,.$$

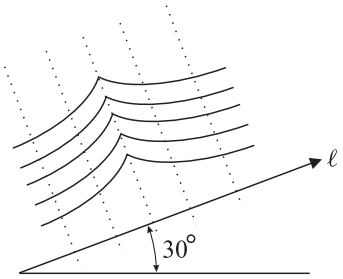

Figure S6.10 See Problem 6.17(e).

(e) See Figure S6.10. The image always has the same value along the lines with a slope of $\tan 120^\circ = -\sqrt{3}/3$.

(f) No, because to determine $b_{30^\circ}(1,2)$, we need $\ell = 1.866$ as shown in (b), which is not an integer. An approximate value might be to choose $\ell = 2$, which yields 0.135.

(g) We have that $\ell = 2 \times 0.866 + 1 \times 0.5 = 2.232$, which, again, is not an integer. Thus, the exact value still cannot be determined. As an approximation, we might choose $\ell = 2$, and the approximate value is again 0.135.

Solution 6.18

The ramp filter is defined as

$$c(\ell) = \int_{-\infty}^{\infty} |\varrho| e^{+j2\pi\varrho\ell}\, d\varrho\,.$$

Letting

$$\ell = D' \sin\gamma\,,$$

yields

$$c(D'\sin\gamma) = \int_{\infty}^{\infty} |\varrho| e^{+j2\pi\varrho D'\sin\gamma}\, d\varrho\,.$$

Now let

$$\varrho' = \frac{\varrho D'\sin\gamma}{\gamma} = \varrho a\,,$$

which yields

$$c(D'\sin\gamma) = \int_{\infty}^{\infty} |\frac{\varrho'}{a}| e^{+j2\pi\varrho'\gamma} \frac{1}{|a|}\, d\varrho'\,.$$

Rearranging terms yields

$$c(D'\sin\gamma) = \frac{1}{a^2}\int_{\infty}^{\infty} |\varrho'| e^{+j2\pi\varrho'\gamma}\, d\varrho'\,,$$

which yields the correct result after substituting the following

$$a = \frac{D'\sin\gamma}{\gamma}\,.$$

IMAGE QUALITY

Solution 6.19

Beam width W has the effect of convolving projection with $\text{rect}\left(\frac{\ell}{W}\right)$. Ignoring sampling (at first) and pretending that we don't know about the distortion, CBP yields

$$\tilde{f}(x,y) = \int_0^\pi \left[(g_\theta(\ell) * \text{rect}\left(\frac{\ell}{W}\right) * c(\ell) \right]_{\ell = x\cos\theta + y\sin\theta} d\theta$$

or

$$\tilde{f}(x,y) = \int_0^\pi \int_{-\infty}^{\infty} \left[(g_\theta(\ell) * \text{rect}\left(\frac{\ell}{W}\right) * c(\ell) \right] \delta(x\cos\theta + y\sin\theta - \ell)\, d\ell\, d\theta.$$

We let $g_\theta(\ell) = \delta(\ell) =$ 2-D Radon transform of $\delta(x,y)$ to find the impulse response. But $\delta(\ell) * \text{rect}\left(\frac{\ell}{W}\right) * c(\ell) = \text{rect}\left(\frac{\ell}{W}\right) * c(\ell)$. Therefore, the impulse response in the inverse 2-D Radon transform of $g_\theta(\ell) = \text{rect}\left(\frac{\ell}{W}\right)$, or the function $h(x,y)$ whose 2-D Radon transform is $\text{rect}\left(\frac{\ell}{W}\right)$. The function has support on the disk with diameter W centered at the origin, but is not constant within, as shown in Figure S6.11.

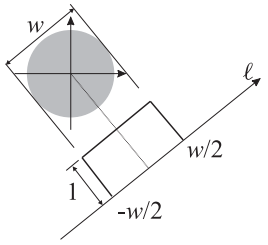

Figure S6.11 See Problem 6.19.

The easiest way to determine $h(x,y)$ is via the projection-slice theorem. Since

$$\mathcal{F}\left\{\text{rect}\left(\frac{\ell}{W}\right)\right\} = |W|\,\text{sinc}(W\varrho)$$

and since all projections are the same, we conclude that

$$H(\varrho) = |W|\,\text{sinc}(W\varrho) = |W|\frac{\sin(\pi W\varrho)}{\pi W\varrho}\,.$$

$H(\varrho)$ is the radial part of $\mathcal{F}(h(x,y))$. The inverse transform of $H(\varrho)$ also has circular symmetry and is given by the inverse Hankel transform:

$$h(r) = 2\pi \int_0^\infty H(\varrho) J_0(2\pi\varrho r)\varrho\, d\varrho\,.$$

where J_0 is the Bessel function of order 0. From the Hankel transform table we find

$$\frac{\text{rect}\left(\frac{r}{2a}\right)}{\sqrt{a^2 - r^2}} \longleftrightarrow \frac{\sin(2\pi a\varrho)}{\varrho}\,.$$

Hence

$$h(r) = \left(\frac{1}{\pi W}\right) \frac{\text{rect}\left(\frac{r}{W}\right)}{\sqrt{\left(\frac{W}{2}\right)^2 - r^2}},$$

which gives

$$h(x,y) = \left(\frac{1}{\pi W}\right) \frac{\text{rect}\left(\frac{\sqrt{x^2+y^2}}{W}\right)}{\sqrt{\left(\frac{W}{2}\right)^2 - (x^2+y^2)}}.$$

Finally, we conclude that

$$\tilde{f}(x,y) = f(x,y) * h(x,y).$$

Additional comments: $h(x,y)$ is a low-pass filter since its Fourier transform decays as a sinc in ϱ. Hence, $\tilde{f}(x,y)$ is a blurred version of $f(x,y)$ as expected. However, $h(x,y)$ has finite support, so that the blurring is strictly local-in fact contributions occur only from over the disk of radius $\frac{W}{2}$. But $h(x,y)$ approaches asymptotically at $r = \frac{W}{2}$, which means that the contribution to blurring at exactly the radius $\frac{W}{2}$ can be very strong and one might expect to see circular artifacts of radius $\frac{W}{2}$ near bright point objects. In a real system CBP is done for sampled data. The convolution $g_\theta(\ell) * \text{sinc}(\ell/W)$ is a continuous convolution, however, followed by discrete sampling. Therefore we might write

$$\tilde{f}(x,y) = \frac{\pi}{M} \sum_{j=1}^{M} T \sum_{i=1}^{N} \left[g_\theta(s) * \text{sinc}\left(\frac{s}{w}\right) \right]_{s=iT} C(x\cos\theta_j + y\sin\theta_j - iT).$$

But there is not more we can say analytically about $\hat{f}(x,y)$ versus $f(x,y)$.

Solution 6.20

Assume a rectangular windowed ramp filter is used. The SNR can be computed using Equation (6.74). By assumption, $M = 100$, $C = 0.05$, $\bar{\mu} = 0.15\ \text{cm}^{-1}$. Since the detectors are touching each other, $k = 1$. Since the cylinder has a diameter of 20 cm, and the detector dimension is 2.0 mm $\times$2.0 mm, the number of measurements per projection is

$$\frac{20\ \text{cm}}{2\ \text{mm}} = 100.$$

Hence,

$$0.1\ \text{R/projection} \times \frac{1}{100}\ \text{projection/measurement} = 0.001\ \text{R/ measurement}.$$

The worst-case intersection length of a beam with the water is 20 cm. Therefore, the worst-case $\bar{N}$ is

$$\begin{aligned} \bar{N} &= 2.5 \times 10^{10}\ \frac{\text{photons}}{\text{cm}^2\text{R}} \times 0.04\ \text{cm}^2 \times 0.001\ \frac{\text{R}}{\text{measurement}} e^{-0.15\times 10} \\ &\approx 50 \times 10^3\ \text{photons/measurement}. \end{aligned}$$

Thus,

$$\begin{aligned}\text{SNR} &\approx 0.4kC\bar{\mu}\sqrt{\bar{N}M}w \\ &= 0.4 \times 1 \times 0.05 \times 0.15\ \text{cm}^{-1}\sqrt{50 \times 10^3 \times 100} \times 0.2 \\ &\approx 1.3\,.\end{aligned}$$

Also, $\text{SNR} = 20\log_{10} 1.3 \approx 2.5$ dB, since the SNR is not a power ratio as defined.

Solution 6.21

(a) Since SNR-in-dB = $20\log_{10}\text{SNR}$, from assumption we get

$$\text{SNR} = 10^{20\ \text{dB}/20} = 10\,.$$

Since SNR $= \frac{C\bar{\mu}}{\sigma_\mu} = 10$, we have

$$\sigma_\mu = \frac{0.005}{10} \times 0.15\ \text{cm}^{-1} = 1.5 \times 10^{-5}\ \text{cm}^{-1}\,.$$

Thus,

$$\sigma_\mu^2 = 5.625 \times 10^{-9}\ \text{cm}^{-2} = \frac{2\pi^2}{3}\frac{\varrho_0^3 T}{M\bar{N}}\,.$$

Since $\varrho_0 = 1/d$, and $T = d$, we have

$$\sigma_\mu^2 = \frac{2\pi^2}{3}\frac{1}{d^2}\frac{1}{M\bar{N}}\,.$$

Furthermore, since $d = 100\ \text{cm}/D$ and $M = D$, then

$$\sigma_\mu^2 = \frac{2\pi^2 D}{3(100)^2\bar{N}}\,.$$

Thus, the photons-per-projection is

$$\begin{aligned}P_p &= \bar{N}D = \frac{2\pi^2}{3(100)^2}\frac{D^2}{\sigma_\mu^2} \\ &= \frac{2\pi^2}{3(100)^2}\frac{300^2}{5.625 \times 10^{-9}} \\ &= 1.053 \times 10^{10}(\text{minimum})\,.\end{aligned}$$

(b) Photons-per-scan is

$$P_s = DP_p = \frac{2\pi^2}{3(100)^2}\frac{D^3}{5.625 \times 10^{-9}}\,.$$

Since

$$2.5 \times 10^{10}\ \frac{\text{photons}}{\text{cm}^2\text{R}} \times 0.125\ \text{m}^2 \times 10,000\ \frac{\text{cm}^2}{\text{m}^2} \times 2\text{R} = 6.25 \times 10^{13}\ (\text{maximum})\,,$$

then

$$D^3 = \frac{(6.25 \times 10^{13})(5.625 \times 10^{-9})(3)(100)^2}{2\pi^2} \approx 5.34311 \times 10^8\,.$$

Then, $D \approx 811.455$, and hence $D_{\max} = 811$.

Solution 6.22

(a) SNR is given by

$$\text{SNR} = \frac{C\bar{\mu}}{\pi}\varrho_0^{-3/2}\sqrt{\frac{3}{2}(\bar{N}/T)M}\,.$$

Since $T = d$, $d = L/D$, and $\bar{N} = \bar{N}_f/D$, we have

$$\frac{\bar{N}}{T} = \frac{\bar{N}}{d} = \frac{\bar{N}}{L/D} = \frac{\bar{N}_f/D}{L/D} = \frac{\bar{N}_f}{L}\,.$$

Let

$$K = \frac{C\bar{\mu}}{\pi}\sqrt{\frac{3}{2}}\sqrt{\frac{\bar{N}_f}{L}},$$

then $\text{SNR} = K\varrho_0^{-3/2}\sqrt{M}$. But $M = 1.5D$, then $\text{SNR} = \sqrt{1.5}K\varrho_0^{-3/2}D^{1/2}$. Since $\varrho_0 = \min\{d^{-1}, \varrho_{\max}\} = \min\{D/L, \varrho_{\max}\}$, there can be two cases:

When $D \le L\varrho_{\max}$,

$$\text{SNR} = \sqrt{1.5}K\left(\frac{D}{L}\right)^{-3/2}D^{1/2} = \sqrt{1.5}KL^{3/2}D^{-1}\,,$$

or when $D \ge L\varrho_{\max}$,

$$\text{SNR} = \sqrt{1.5}K\varrho_{\max}^{-3/2}D^{1/2}\,.$$

(b) SNR increases away from $L\varrho_{\max}$ in either direction. Thus, either $D = 1$ or $D = J$ gives the maximum SNR, but not $D \approx L\varrho_{\max}$. At $D = 1$, SNR=$\sqrt{1.5}KL^{3/2}$; at $D = J$, SNR=$\sqrt{1.5}K[J/(2L)]^{-3/2}J^{1/2}$. (Note that $L\varrho_{\max} = LJ/(2L) = J/2$, which lies between 1 and J.) So,

$$R = \frac{\sqrt{1.5}KL^{3/2}}{\sqrt{1.5}K(2L)^{3/2}J^{-1}} = \frac{J}{2^{3/2}} = \frac{J}{2.8}\,.$$

Since J is an image pixel size, $R \gg 1$, hence SNR is biggest at $D = 1$. SNR may be maximum but resolution is poor. SNR can be improved at large D's by lowering $\varrho_{\max}$.

Solution 6.23

(a) Every projection looks the same, like that shown in Figure S6.12(a). Accordingly, the sinogram looks like that shown in Figure S6.12(b).

(b) The observed sinogram can be modeled as

$$\begin{aligned} y(\ell,\theta) &= g(\ell,\theta)(1 - \text{rect}(\ell/h)) \\ &= g(\ell,\theta) - g(\ell,\theta)\,\text{rect}(\ell/h)\,, \end{aligned}$$

where h is some small distance, equal to the width of a detector. The inverse Radon transform is a linear operator, so the reconstruction will be

$$\hat{f}(x,y) = f(x,y) - \mathcal{R}^{-1}\{g(\ell,\theta)\,\text{rect}(\ell/h)\}\,.$$

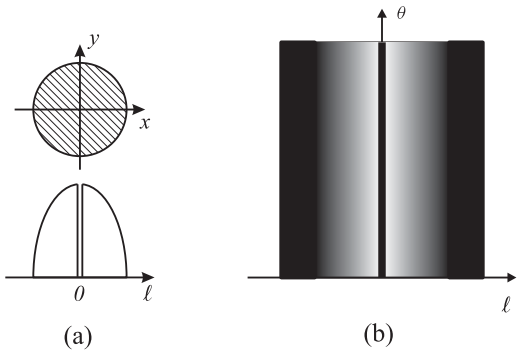

Figure S6.12 See Problem 6.23.

Assume the width of the detector h is small, so that we can approximate the above equation by

$$\hat{f}(x,y) = f(x,y) - \mathcal{R}^{-1}\{g(0,\theta)\,\mathrm{rect}(\ell/h)\}\,.$$

Now, we need to find $f_{\mathrm{rect}}(x,y) = \mathcal{R}^{-1}\{g(0,\theta)\,\mathrm{rect}(\ell/h)\}$. All the projections are the same rect function. The 1-D Fourier transform of any projection is a sinc function, independent of θ:

$$\begin{aligned} G_{\mathrm{rect}}(\varrho) &= \mathcal{F}_{1\mathrm{D}}\{g(0,\theta)\,\mathrm{rect}(\ell/h)\} \\ &= hg(0,\theta)\,\mathrm{sinc}(h\varrho)\,. \end{aligned}$$

By using the projection slice theorem, the 2-D Fourier transform of $f_{\mathrm{rect}}(x,y)$ is circularly symmetric. In this case, $f_{\mathrm{rect}}(x,y)$ and $G_{\mathrm{rect}}(\varrho)$ is related by Hankel transform (Section 2.7). With some abuse of notation, we have

$$\begin{aligned} f_{\mathrm{rect}}(r) &= \mathcal{H}^{-1}\{G_{\mathrm{rect}}(\varrho)\} \\ &= \mathcal{H}\{hg(0,\theta)\,\mathrm{sinc}(h\varrho)\} \\ &= \frac{g(0,\theta)}{h}\frac{2\,\mathrm{rect}(r/h)}{\pi\sqrt{1-4r^2/h^2}}\,. \end{aligned}$$

So the reconstructed image looks like that shown in Figure S6.13. The disk in the center has a diameter h, the intensity is $-f_{\mathrm{rect}}(r)$.

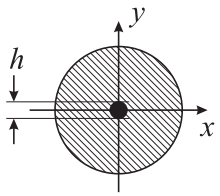

Figure S6.13 See Problem 6.23(b).

(c) If the scanner always skips measurement at $\ell = \ell_0$, the sinogram can be modeled as:

$$\begin{aligned} z(\ell,\theta) &= g(\ell,\theta)(1 - \operatorname{rect}\left(\frac{\ell-\ell_0}{h}\right) \\ &= g(\ell,\theta) - g(\ell,\theta)\operatorname{rect}\left(\frac{\ell-\ell_0}{h}\right). \end{aligned}$$

Again, assume h is small, we have

$$z(\ell,\theta) = g(\ell,\theta) - g_0 \operatorname{rect}\left(\frac{\ell-\ell_0}{h}\right),$$

where $g_0 = g(\ell_0,\theta)$. Let $f'_{\text{rect}} = \mathcal{R}^{-1}\left\{g_0 \operatorname{rect}\left(\frac{\ell-\ell_0}{h}\right)\right\}$. So the 1-D Fourier transform of a projection is:

$$\begin{aligned} G'_{\text{rect}}(\varrho) &= \mathcal{F}_{1\text{D}}\left\{g_0 \operatorname{rect}\left(\frac{\ell-\ell_0}{h}\right)\right\} \\ &= hg_0 \operatorname{sinc}(h\varrho)e^{-j2\pi\varrho\ell_0}. \end{aligned}$$

The inverse Hankel transform of $G'_{\text{rect}}(\varrho)$ is:

$$\begin{aligned} f'_{\text{rect}}(r) &= \mathcal{H}^{-1}\{G'_{\text{rect}}(\varrho)\} \\ &= 2\pi\int_0^\infty hg_0 \operatorname{sinc}(h\varrho)e^{-j2\pi\varrho\ell_0}J_0(2\pi\varrho r)\,\varrho\,d\varrho. \end{aligned}$$

The function $f'_{\text{rect}}(r)$ is a complex function, which means that the sinogram $g_0 \operatorname{rect}\left(\frac{\ell-\ell_0}{h}\right)$ is not a valid radon transform of a real image. The explicit expression of $f'_{\text{rect}}(r)$ is hard to obtain. Numerical simulation shows that the reconstructed image will have parts of a circle with radius ℓ_0 around the image center.

APPLICATIONS AND ADVANCED TOPICS

Solution 6.24

(a) Plugging the form of $f(x,y)$ into the observation equation yields

$$g_i = \int_{L_i}\sum_{j=1}^n f_j\phi_j(x,y)\,ds = \sum_{j=1}^n f_j\int_{L_i}\phi_j(x,y)\,ds, \quad i = 1,\ldots,m\,.$$

Therefore,

$$H_{ij} = \int_{L_i}\phi_j(x,y)\,ds\,.$$

So,

$$\begin{bmatrix} g_1 \\ g_2 \\ \vdots \\ g_m \end{bmatrix} = \begin{bmatrix} H_{11} & H_{12} & \cdots & H_{1n} \\ H_{21} & H_{22} & & \\ \vdots & & \ddots & \\ H_{m1} & & & H_{mn} \end{bmatrix} \begin{bmatrix} f_1 \\ f_2 \\ \vdots \\ f_n \end{bmatrix}$$

(b) Consider each case:

(1) H^{-1} exists but $v \neq 0$: Since $y = Hf + v$, $Hf = y - v$ and $H^{-1}Hf = H^{-1}(y - v)$ or

$$f = H^{-1}y - H^{-1}v\,.$$

This provides a reconstruction formula but will give a noisy solution.

(2) $v = 0$ but $m < n$: We have $y = Hf$, but there are fewer measurements than unknowns. Therefore, $y = H(f + \tilde{f})$ for any $\tilde{f}$ in the nullspace of H. Hence, there is no unique solution to the inverse problem.

(3) $v = 0$ but $m > n$: We have $y = Hf$, but there are more measurements than unknowns. If the system is truly noise-free, then some of thee extra measurements will be redundant. In this case, if H^{-1} exists, there will be a unique solution.

(c) The solution is given by the normal equations:

$$\hat{f} = (H^T H)^{-1} H^T y\,,$$

which is a standard result of least squares minimization from linear algebra.

(d) The image vector has the dimensions $256^2 \times 1$. The output vector has dimensions $(360 \times 512) \times 1$. Therefore, we will be required to invert a matrix of dimensions $256^2 \times 256^2$, which is too large to solve directly.

Solution 6.25

(a) There are four important points ℓ_1, ℓ_2, ℓ_3, and ℓ_4, and three ranges (see Fig. S6.14).

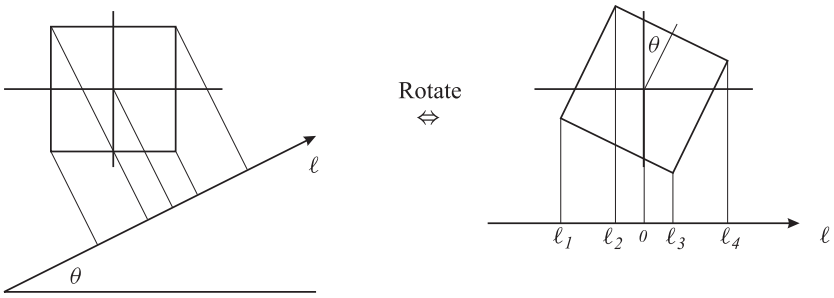

Figure S6.14 See Problem 6.25(a).

- $\ell_1 \leq \ell \leq \ell_2$: From similar triangles:

$$g_\theta(\ell) = \frac{(\ell - \ell_1)/(\ell_2 - \ell_1)}{\cos\theta}$$

- $\ell_2 \leq \ell \leq \ell_3$:

$$g_\theta(\ell) = \frac{1}{\cos\theta}$$

which is independent of ℓ.

- $\ell_3 \leq \ell \leq \ell_4$:

$$g_\theta(\ell) \frac{(\ell_4 - \ell)/(\ell_4 - \ell_3)}{\cos\theta}$$

Rotation by θ gives the values:

$$\begin{aligned}
\ell_1 &= -\frac{1}{2}\cos\theta - \frac{1}{2}\sin\theta\,, \\
\ell_2 &= -\frac{1}{2}\cos\theta + \frac{1}{2}\sin\theta\,, \\
\ell_3 &= \frac{1}{2}\cos\theta - \frac{1}{2}\sin\theta\,, \\
\ell_4 &= \frac{1}{2}\cos\theta - \frac{1}{2}\sin\theta\,.
\end{aligned}$$

(b) A projection is shown in Figure S6.15.

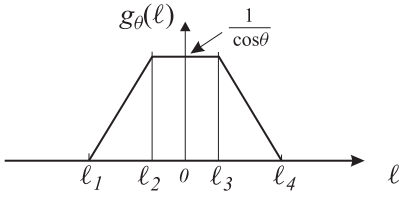

Figure S6.15 See Problem 6.25(b).

(c) This is straightforward

$$\int_{-\infty}^{\infty} g_\theta(\ell)\,d\ell = 1 = \int_{-\infty}^{\infty}\int_{-\infty}^{\infty} f(x,y)\,dx\,dy$$

(d) We have $g_0(\ell) = g_{90^\circ}(\ell)$, as shown in Figure S6.16(a). Therefore,

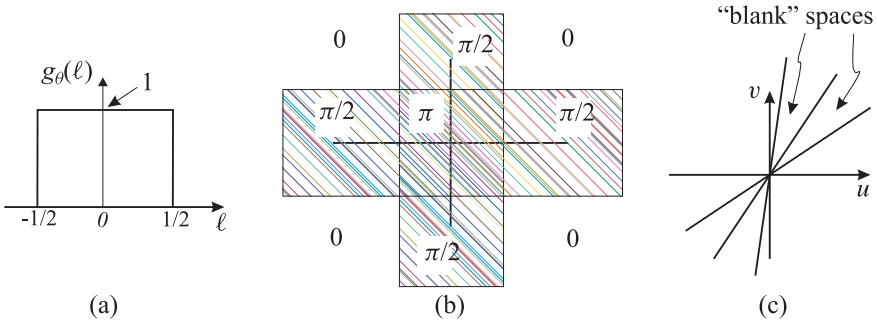

Figure S6.16 See Problem 6.25(d) and (e).

$$\begin{aligned}
f_b(x,y) &= \int_0^\pi g_\theta(x\cos\theta + y\sin\theta)\,d\theta \\
\hat{f}_b(x,y) &= \frac{\pi}{V}\sum_{i=1}^{V} g_{\theta_i}(x\cos\theta_i + y\sin\theta_i)
\end{aligned}$$

Here $V = 2$; therefore,

$$\hat{f}_b(x,y) = \begin{cases} \pi & -1/2 \le x, y \le 1/2 \\ \pi/2 & -1/2 \le y \le 1/2, \quad x > 1/2 \\ \pi/2 & -1/2 \le y \le 1/2, \quad x < -1/2 \\ \pi/2 & -1/2 \le x \le 1/2, \quad y > 1/2 \\ \pi/2 & -1/2 \le x \le 1/2, \quad y < -1/2 \\ 0 & \text{otherwise} \end{cases} .$$

(e) No, it is generally not possible. From the projection slice theorem, we know that, given a finite number of slices, there is always some "blank" space between the central slices passing radially through the origin. See Figure S6.16(c).

Solution 6.26

For the given two energy photons, we have

$$\begin{aligned} \mu_1(100 \text{ keV}) &= 1.0e^{-1} \approx 0.3679 \text{ cm}^{-1} , \\ \mu_1(140 \text{ keV}) &= 1.0e^{-1.4} \approx 0.2466 \text{ cm}^{-1} , \\ \mu_2(100 \text{ keV}) &= 2.0e^{-1} \approx 0.7358 \text{ cm}^{-1} , \\ \mu_2(140 \text{ keV}) &= 2.0e^{-1.4} \approx 0.4932 \text{ cm}^{-1} . \end{aligned}$$

(a) The incident intensity of the x-ray burst is

$$I_0 = 10^6 \times 100 \text{ keV} + 0.5 \times 10^6 \times 140 \text{ keV} = 1.7 \times 10^8 \text{ photon keV} .$$

(b) For $-30 \text{ cm} \le x \le -10 \text{ cm}$, the photons are only attenuated by μ_1,

$$I_d(x) = 10^6 \times 100e^{-60\times 0.3679} + 0.5 \times 10^6 \times 140e^{-60\times 0.2466} \approx 26.285 \text{ photon keV} .$$

For $-10 \text{ cm} \le x \le 10 \text{ cm}$, the photons are attenuated by 40 cm of μ_1 and 20 cm of μ_2,

$$I_d(x) = 10^6 \times 100e^{-40\times 0.3679 - 20\times 0.7358} + 0.5 \times 10^6 \times 140e^{-40\times 0.2466 - 20\times 0.4932} \approx 0.1894 \text{ photon keV} .$$

For $10 \text{ cm} \le x \le 10 \text{ cm}$, the photons are also only attenuated by μ_1, as previously,

$$I_d(x) \approx 26.285 \text{ photon keV} .$$

(c) The local contrast is

$$\begin{aligned} C &= \frac{I_{\text{do}} - I_{\text{db}}}{I_{\text{db}}} \\ &= \frac{0.1894 - 26.285}{26.285} \\ &\approx -0.9928 . \end{aligned}$$

The projection $g(x,0) = -\ln \frac{I_d(x)}{I_0}$. Hence,

For $-30\text{ cm} \le x \le -10\text{ cm}$,

$$g(x,0) = -\ln(\frac{26.285}{1.7 \times 10^8}) \approx 15.682\,.$$

For $-10\text{ cm} \le x \le 10\text{ cm}$,

$$g(x,0) = -\ln(\frac{0.1894}{1.7 \times 10^8}) \approx 20.615\,.$$

For $10\text{ cm} \le x \le 10\text{ cm}$,

$$g(x,0) \approx 15.682\,.$$

The local contrast computed by $g(x,0)$ is

$$\begin{aligned} C &= \frac{g_\text{o} - g_\text{b}}{g_\text{b}} \\ &= \frac{20.615 - 15.682}{15.682} \\ &\approx 0.3146\,. \end{aligned}$$

(d) The detector is of finite length so its response is no longer a delta function; instead, the response is a rect function. The measured projection $I'_d(x)$ is equal to the previous projection convolved with the detector response:

$$I'_d(x) = I_d(x) * \text{rect}(x)\,.$$

Since the detector width is still quite small relative to the object size, the local contrast remains the same in most parts, but is reduced near $x = -10$ and $x = 10$, where the original step transition is blurred to a ramp.

Solution 6.27

(a) $\theta_0 = 0$, $\theta_1 = \pi/4$, $\theta_2 = 2\pi/4 = \pi/2$, and $\theta_3 = 3\pi/4$. See Figure S6.17.

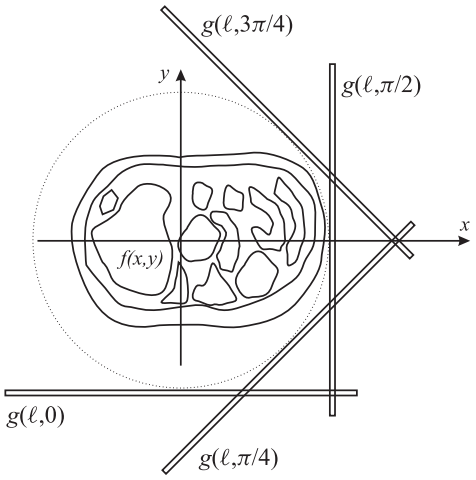

Figure S6.17 See Problem 6.27(a).

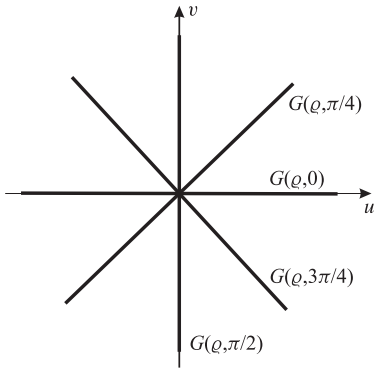

Figure S6.18 See Problem 6.27(b).

(b) See Figure S6.18.

(c) Let $g_2(\ell,\theta_j) \in G_2$. Then $\mathcal{F}\{g_2(\ell,\theta_j)\} = G_2(\varrho,\theta_j) = F_1(\varrho\cos\theta_j, \varrho\sin\theta_j) + F_2(\varrho\cos\theta_j, \varrho\sin\theta_j)$ (by the projection slice theorem and by the linearity of the Radon transform. Hence, the fact that $G_2 = G_1$ means that $F_2(\varrho\cos\theta_j, \varrho\sin\theta_j) = 0$ for θ_j, $j = 0,\ldots,M-1$. Then

$$\begin{aligned} F_2(u,v) &= \mathcal{F}_2\{\cos 2\pi f_x x \cos 2\pi f_y y\} \\ &= \mathcal{F}_1\{\cos 2\pi f_x x\}\mathcal{F}_1\{\cos 2\pi f_y y\} \\ &= \frac{1}{4}[\delta(u-f_x)+\delta(u+f_x)][\delta(v-f_y)+\delta(v+f_y)] \\ &= \frac{1}{4}[\delta(u-f_x,v-f_y)+\delta(u-f_x,v+f_y)+\delta(u+f_x,v-f_y)+\delta(u+f_x,v+f_y)]\,. \end{aligned}$$

But (f_x, f_y) is a unit vector pointing in the $\theta = 3\pi/16$ direction. A picture of this 2-D Fourier transform is shown in Figure S6.19. Since $F_2(u,v)$ does not intersect the lines over which we sample the Fourier

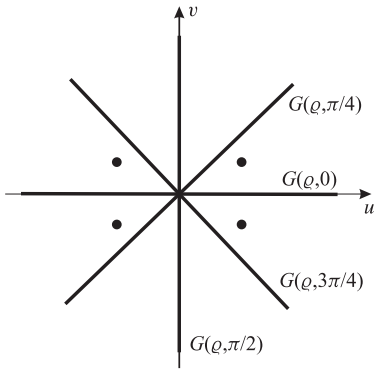

Figure S6.19 See Problem 6.27(c).

transform of f_1, the value of $D_4 f_2$ will be zero. Hence, $G_2 = G_1$.

(d) $3\pi/16 = \pi i/16$ for $i = 3$ and 3 does not go into 16 without a remainder. Hence $M = 16$.

(e) No, at least in theory. Sampling the plane with a finite number of lines will always permit us to place delta functions in the appropriate spots to define ghost functions. In practice, functions of infinite extent are not

available. Therefore, F_2 will always have some spread and a line will hit it. Because of this, "nearly" ghost functions will have to be high frequency functions in order to "fit between the sampling lines."

(f) Yes. f_2 will still be a ghost function. Low-pass filtering a projection does not change the geometry over which F is sampled. It would just filter along the sampled lines.

Solution 6.28

(a) We have

$$g(\ell, 0^\circ) = \begin{cases} \mu_1 \times 20 = 2 & -30 \text{ cm} \le \ell \le -10 \text{ cm} \\ \mu_2 \times 20 = 4 & -10 \text{ cm} \le \ell \le 10 \text{ cm} \\ \mu_3 \times 20 = 6 & 10 \text{ cm} \le \ell \le 30 \text{ cm} \\ 0 & \text{otherwise} \end{cases} .$$

which is shown in Figure S6.20.

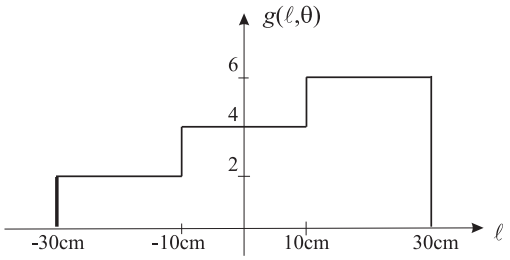

Figure S6.20 See Problem 6.28(a).

(b) We have

$$g(\ell, 90^\circ) = \mu_1 \times 20 + \mu_2 \times 20 + \mu_3 \times 20 = 12, \quad -10 \text{ cm} \le \ell \le 10 \text{ cm},$$

which is shown in Figure S6.21.

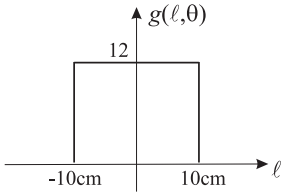

Figure S6.21 See Problem 6.28(b).

(c) We have

$$g(\ell, 45^\circ) = \begin{cases} \frac{1}{5}\ell + 4\sqrt{2} & -20\sqrt{2} \text{ cm} \le \ell \le 10\sqrt{2} \text{ cm} \\ -\frac{3}{5}\ell + 12\sqrt{2} & 10\sqrt{2} \text{ cm} \le \ell \le 20\sqrt{2} \text{ cm} \\ 0 & \text{otherwise} \end{cases} ,$$

which is shown in Figure S6.22.

(d) We have

$$b_{45^\circ}(x, y) = g(x \cos 45^\circ + y \sin 45^\circ, 45^\circ)$$

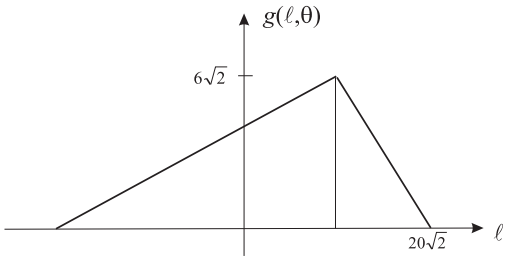

Figure S6.22 See Problem 6.28(c).

$$\begin{aligned} b_{45^\circ}(1,1) &= g(1\cos 45^\circ + 1\sin 45^\circ, 45^\circ) \\ &= g(\sqrt{2}, 45^\circ) \\ &= \frac{1}{5}\sqrt{2} + 4\sqrt{2} \\ &= \frac{21}{5}\sqrt{2} \\ &\approx 5.94\,, \end{aligned}$$

which is shown in Figure S6.23.

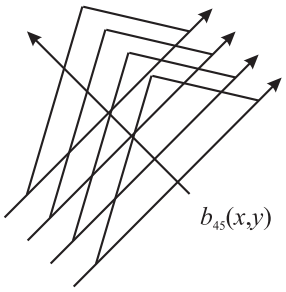

Figure S6.23 See Problem 6.28(d).

(e) The FOV should cover the object in any angle. Thus the smallest possible circular FOV will have the diameter equal to the diagonal of the object:

$$d = \sqrt{20^2 + 60^2} = \sqrt{4,000} = 63.2 \text{ cm}$$

$$r = \frac{d}{2} = 31.6 \text{ cm}\,.$$

The geometry is shown in Figure S6.24. We can solve for x as follows

$$\begin{aligned} m = \sqrt{(1.5-r)^2 - r^2} &= \sqrt{(1.5-0.316)^2 - 0.316^2} = 1.14 \text{ m} \\ \frac{m}{1.5} &= \frac{r}{x} \\ \Longrightarrow\ x &= \frac{r \times 1.5}{m} = 0.415 \text{ m} \end{aligned}$$

The length of detector array should be $2x = 0.83$ m.

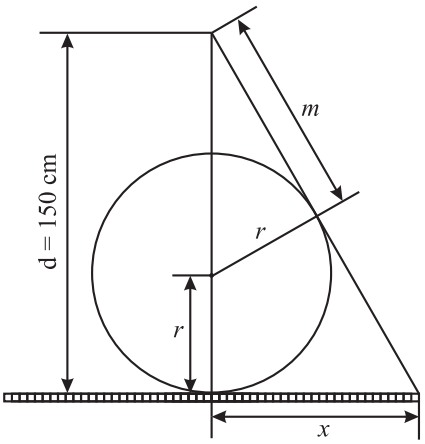

Figure S6.24 See Problem 6.28(e).

(f) From the "rule of thumb" of CT, $M = D = J = 256$. Therefore,

$$\frac{d}{M} = \frac{63.2 \text{ cm}}{256} = 0.25 \text{ cm}$$

So, the pixel size is 0.25 cm $\times$ 0.25 cm.

Solution 6.29

(a) Since this is a first-generation CT scanner, collimation is technically not required. However, it is best to collimate the source to a pencil beam in order that (1) radiation dose to regions not affecting the measurements is reduced, (2) single Compton scattering events cannot be detected (and thereby contribute to measurement errors).

(b) A circle with diameter 56.57 cm will contain the square.

(c) Since 180° is needed to acquire a complete CT data set, and there is 0.25° angular increment, 720 projections will be acquired. The CT "rule of thumb" says that $M = D = J$. Therefore, since $M = 720$, there should be $D = 720$ line integrals per projection. The reconstructed image should cover the FOV, which was determined in Part (a) to be a circle with diameter $d = 56.57$ cm. By the CT "rule of thumb," $J = 720$. Therefore, the pixel size is square with side dimension equal to $565.7 \text{ mm}/720 = 0.78 \text{ mm}$.

(d) The most fundamental expression for SNR given the present scenario is

$$\text{SNR} = \frac{C\bar{\mu}}{\pi} \varrho_0^{-3/2} \sqrt{\frac{3}{2}(\bar{N}/T)M} \, .$$

By problem assumption, we will not violate the "rule of thumb." Therefore, T and M will remain unchanged. This still leaves some flexibility in selection of $\bar{N}$ and ϱ_0. We could, for example, keep ϱ_0 unchanged and quadruple the number of incident x-rays. This would quadruple the number of x-rays $\bar{N}$ incident on the detector array,

$$\bar{N}' = 4\bar{N} \, .$$

This solution would increase the dose to the patient. We could, on the other hand, keep the number of incident x-rays constant and use a cutoff frequency equal to

$$\varrho_0' = \frac{1}{\sqrt[3]{4}}\varrho_0 = 0.63\varrho_0 \,.$$

This solution would reduce the resolution of the resultant scan.

(e) The sketch of $g(\ell, 45^\circ)$ is shown in Figure S6.25(a).

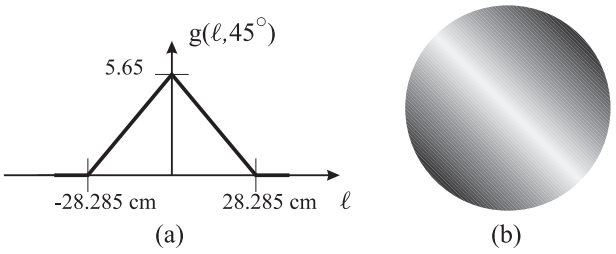

Figure S6.25 See Problem 6.29.

(f) The sketch of $b_{45^\circ}(x, y)$ is shown in Figure S6.25(b). Assume that $(10, 10)$ is in units of cm. Then this point projects to

$$\begin{aligned} \ell &= 10\cos 45^\circ + 10\sin 45^\circ \\ &= 20\frac{\sqrt{2}}{2} \\ &= 14.14 \text{ cm} \,. \end{aligned}$$

This is halfway between the origin and the corner at $\ell = 28.285$ cm. Therefore, the projection value will be 1/2 of that at the origin, that is, $b_{45^\circ}(10, 10) = 2.825$.

Solution 6.30

(a) We have $M = D = J$ and $\varrho_0 = 1/d$. Therefore, $k = 1$. In order to resolve two point source separated by 1 mm, the pixel size can not be bigger than 0.707 mm. See Figure S6.26. We also have $\frac{60 \text{ cm}}{0.707 \text{ mm/pixel}} = 848.6$ pixels, so the minimum number of pixels is 849. See Figure S6.27.

(b) The detector length is 925×0.8 mm $= 740$ mm, and $180 = d + 30 \Rightarrow d = 150$ cm.

$$\tan\theta = \frac{37}{180} \Rightarrow \theta = 11.6156^\circ$$

$$\sin\theta = \frac{x}{150} \Rightarrow x = 30.2 \text{ cm}.$$

Since $x = 30.2$ cm, the circular FOV with radius 30 cm fits.

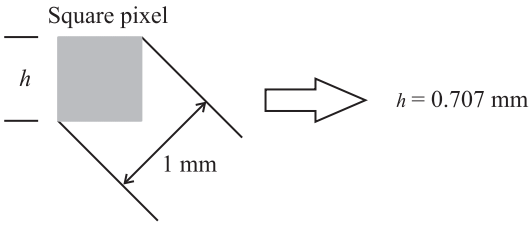

Figure S6.26 See Problem 6.30(a).

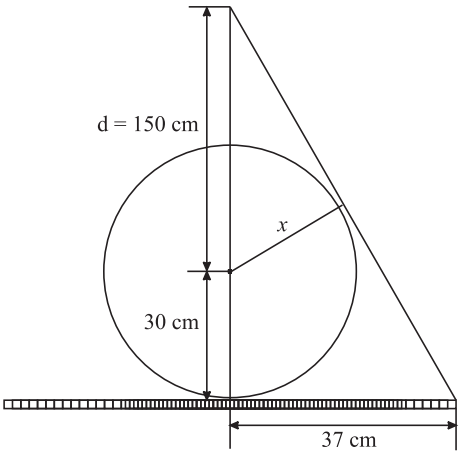

Figure S6.27 See Problem 6.30(b).

(c) For fan beam geometry,

$$\begin{aligned}
\text{SNR} &= 0.4kC\bar{\mu}LD^{-3/2}\sqrt{\bar{N}_f m} \\
k &= 1 \text{ since } \varrho_0 = 1/d \\
C &= \frac{0.25 - 0.2}{0.2} = 0.25 \\
\bar{\mu} &= 0.2 \text{ cm}^{-1} \\
L &= 74 \text{ cm} \\
D &= 925 \\
\bar{N}_f &= 1.5 \times 10^{11} \\
m &= 925 \,.
\end{aligned}$$

Plugging these numbers in yields

$$\begin{aligned}
\text{SNR} &= 619.677 \\
\text{SNR(dB)} &= 20 \log_{10} 619.677 = 55.84 \text{ dB} \,.
\end{aligned}$$

Solution 6.31

(a) The radius of the circular FOV is 25 cm. Therefore, a right triangle can be formed for which the hypotenuse is 70 cm and the side opposite 1/2 of the fan angle is 25 cm. Therefore,

$$\theta_{1/2} = \sin^{-1}\frac{25}{70} = 20.925^\circ\,.$$

The fan angle is therefore $2 \times 20.925 = 41.85^\circ$.

(b) The distance between source and detector is $Q = 105$ cm and the total circumference of a circle with radius Q is $C = 2\pi Q = 2\pi \times 105$ cm $= 659.7$ cm. Therefore, the arclength of the detector array is

$$L = \frac{41.85^\circ}{360^\circ}659.7 \text{ cm} = 76.69 \text{ cm}\,.$$

Since there are 703 detectors over this range, we have that the spacing between detectors is

$$\Delta_d = \frac{766.9 \text{ mm}}{703} = 1.09 \text{ mm}\,.$$

(c) There is 1 pulse/ms and 1 rev/s. Therefore, there are 1,000 pulses over a single revolution. The angular increment is therefore $\Delta\theta = 360^\circ/1,000 = 0.36^\circ$. Since each line will pass through the origin, the value of the lateral position of each of these lines is $\ell = 0$. Therefore, the following line integrals are acquired:

$$g(0, 0.36^\circ m)\,, \quad m = 0, \ldots, 999\,.$$

The acquired data are shown in Figure S6.28(a). One half of the lines are repeated.

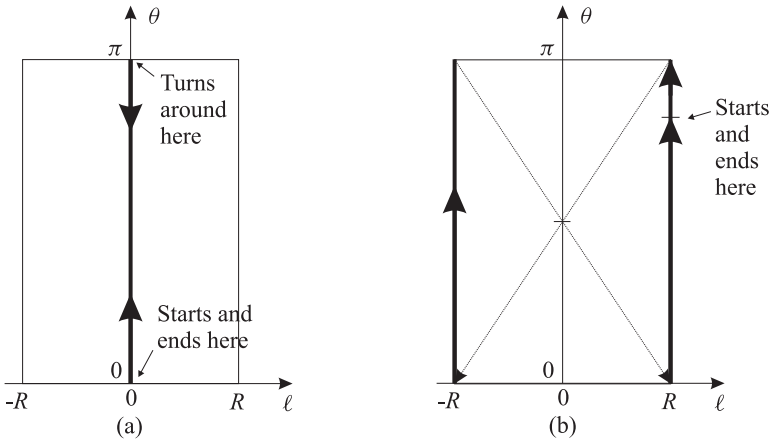

Figure S6.28 See Problem 6.31.

(d) From the work we did in Part (a), we see that the starting angle is -20.925° and the lateral displacement is -25 cm. The angles increment exactly as in Part (c) and the lateral displacement never changes. Therefore, the following line integrals are acquired

$$g(-25, -20.925^\circ + 0.36^\circ m)\,, \quad m = 0, \ldots, 999\,.$$

These are at the limits of the lateral displacement in the sinogram. But, rather than repeating, these acquire both the positive and negative max displacements, as shown in Figure S6.28(b).

(e) Cycle through each of the detectors in order from left to right. The sinogram will be filled in vertical columns as shown in Figure S6.28(b). When scanning the central detector, turn off the tube for the second half of the rotation to avoid redundancy.

(f) This scanner has a fanbeam source collimation but only acquires information from one detector at a time. Therefore, the patient is getting irradiated repeatedly in a slice, and the vast majority of that radiation is not getting used to image the slice. This is like having 703 CT scans, just to obtain one image.

Solution 6.32

(a) Use the following steps:

$$\begin{aligned} g(\ell,\theta) &= \mathcal{R}\delta(x,y) \\ &= \int_{-\infty}^{\infty}\int_{-\infty}^{\infty} \delta(x,y)\delta(x\cos\theta + y\sin\theta - \ell)dxdy \\ &= \delta(x\cos\theta + y\sin\theta - \ell)|_{x=0,\,y=0} \\ &= \delta(-\ell) = \delta(\ell) \quad \delta(\ell) \text{ is an even function .} \end{aligned}$$

The sinogram is shown in Figure S6.29.

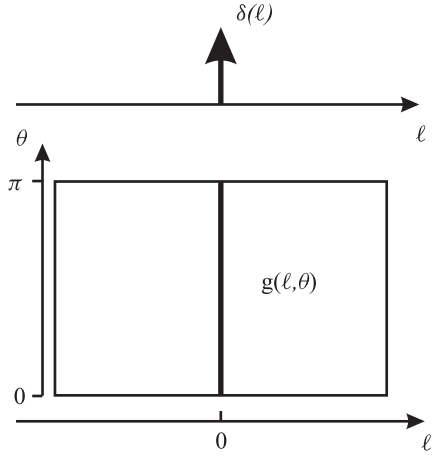

Figure S6.29 The Radon transform of $\delta(x,y)$. See Problem 6.32.

(b) The shift theorem is proven as follows:

$$\begin{aligned}
\mathcal{R}f(x-x_0, y-y_0) &= \int_{-\infty}^{\infty}\int_{-\infty}^{\infty} f(x-x_0, y-y_0)\delta(x\cos\theta + y\sin\theta - \ell)dxdy \\
&\quad \text{Let } \xi = x - x_0,\ \eta = y - y_0 \\
&\quad (x = \xi + x_0, y = \eta + y_0, dx = d\xi, dy = d\eta)\,. \\
\mathcal{R}f(x-x_0, y-y_0) &= \int_{-\infty}^{\infty}\int_{-\infty}^{\infty} f(\xi,\eta)\delta((\xi + x_0)\cos\theta + (\eta + y_0)\sin\theta - \ell)d\xi d\eta \\
&= \int_{-\infty}^{\infty}\int_{-\infty}^{\infty} f(\xi,\eta)\delta(\xi\cos\theta + \eta\sin\theta - (\ell - x_0\cos\theta - y_0\sin\theta))d\xi d\eta \\
&= g(\ell - x_0\cos\theta - y_0\sin\theta, \theta)\,.
\end{aligned}$$

(c) From the results of parts (a) and (b), we have

$$\mathcal{R}\delta(x-1, y) = \delta(\ell - \cos\theta)\,.$$

The trajectory is plotted in Figure S6.30.

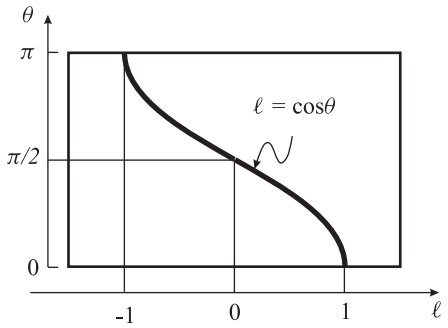

Figure S6.30 The Radon transform of $\delta(x-1, y)$. See Problem 6.32.

(d) The acquired sinogram is shown in Fig. S6.31.

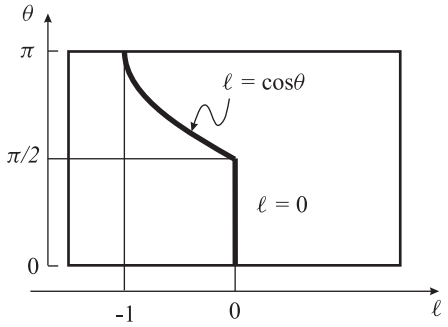

Figure S6.31 Acquired sinogram. See Problem 6.32.

(e)

$$\begin{aligned}
\int_{-\infty}^{\infty} \ell g(\ell,\theta) d\ell &= \int_{-\infty}^{\infty} \ell \left[\int_{-\infty}^{\infty}\int_{-\infty}^{\infty} f(x,y)\delta(x\cos\theta + y\sin\theta - \ell) dxdy \right] d\ell \\
&= \int_{-\infty}^{\infty}\int_{-\infty}^{\infty} f(x,y) \left[\int_{-\infty}^{\infty} \ell\delta(x\cos\theta + y\sin\theta - \ell) d\ell \right] dxdy \\
&= \int_{-\infty}^{\infty}\int_{-\infty}^{\infty} f(x,y)(x\cos\theta + y\sin\theta) dxdy \\
&= \int_{-\infty}^{\infty}\int_{-\infty}^{\infty} f(x,y) x\cos\theta dxdy + \int_{-\infty}^{\infty}\int_{-\infty}^{\infty} f(x,y) y\sin\theta dxdy \\
&= \cos\theta \int_{-\infty}^{\infty}\int_{-\infty}^{\infty} f(x,y) x dxdy + \sin\theta \int_{-\infty}^{\infty}\int_{-\infty}^{\infty} f(x,y) y dxdy \\
&= q_x \cos\theta + q_y \sin\theta \,.
\end{aligned}$$

(f) The sinogram acquired can be expressed as

$$g(\ell,\theta) = \begin{cases} \delta(\ell) & 0 \le \theta \le \pi/2 \\ \delta(\ell - \cos\theta) & \pi/2 < \theta \le \pi \end{cases}$$

Let us calculate the first moment of each projection:

$$\begin{aligned}
\int_{-\infty}^{\infty} \ell g(\ell,\theta) d\ell &= \begin{cases} \int_{-\infty}^{\infty} \ell\delta(\ell) d\ell & 0 \le \theta \le \pi/2 \\ \int_{-\infty}^{\infty} \ell\delta(\ell - \cos\theta) d\ell & \pi/2 < \theta \le \pi \end{cases} \\
&= \begin{cases} 0 & 0 \le \theta \le \pi/2 \\ \cos\theta & \pi/2 < \theta \le \pi \end{cases}
\end{aligned}$$

From the results in part (e) we have

$$\begin{aligned}
q_x \cos\theta + q_y \sin\theta = 0 \quad &\text{for } 0 \le \theta \le \pi/2 \quad \Rightarrow q_x = q_y = 0 \\
q_x \cos\theta + q_y \sin\theta = \cos\theta \quad &\text{for } \pi/2 < \theta \le \pi \quad \Rightarrow q_x = 1,\ q_y = 0
\end{aligned}$$

Since q_x and q_y are quantities calculated from $f(x,y)$, they do not depend on θ. The above two results contradict. So the acquired sinogram cannot be the Radon transform of any object.

Solution 6.33

(a) The energy spectrum of the x-ray beam after it passes through the material is shown in Figure S6.32

(b) The two measurements should ideally be identical because the basic measurement of CT is the line integral of the linear attenuation coefficient. If the x-ray was perfectly monochromatic, then both the measurements will be exactly the same, since the line integrals in $\theta = 90^\circ$ projection and $\theta = 270^\circ$ projection are the same. But in practice, we have polychromatic x-ray source and because of beam hardening, the effective energy of the x-ray beam and hence the linear attenuation coefficient is different for different projection. So the two measurements are different in practice.

(c) One way to change the input spectra of the x-ray tube is to add filters in the x-ray tube.

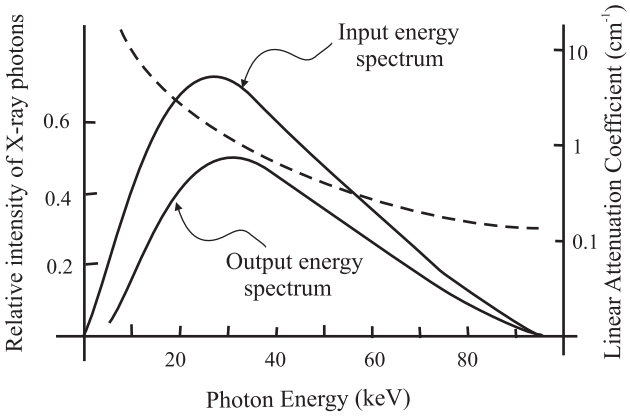

Figure S6.32 See Problem 6.33(a).

(d) $g_{t_1}^L$ = line integral of μ at lower photon energy,
$g_{t_1}^H$ = line integral of μ at higher photon energy.

At lower energy, μ is larger and therefore the line integral is larger. At higher energy, μ is smaller and therefore the line integral is smaller.

(e)

$$\mu(\text{Al}, 75\text{ keV}) = 0.7\text{ cm}^{-1} \quad \mu(\text{H}_2\text{O}, 75\text{ keV}) = 0.1866\text{ cm}^{-1}.$$

$$g_{t_1}^{75} = 0.7 \times 2 + 0.1866 \times 8 = 2.8928,$$

$$g_{t_2}^{75} = 0.7 \times 8 + 0.1866 \times 2 = 5.9732.$$

(f) The set of linear equations we get is

$$\begin{aligned} 2.8928 &= a^L(3.16) + a^H(2.2)\,, \\ 5.9732 &= a^L(6.79) + a^H(4.3)\,. \end{aligned}$$

Solving the equations, we have

$$a^L = 0.52, \quad a^H = 0.568\,.$$

(g)

$$\mu(\text{object}, 75\text{ keV}) = \int_0^\pi \left[\left(0.52 g^L(\ell,\theta) + 0.568 g^H(\ell,\theta)\right) * \tilde{c}(\ell)\right] d\theta\,.$$

7

The Physics of Nuclear Medicine

FUNDAMENTALS OF ATOMS

Solution 7.1

The mass of an electron m_e is 0.000548 u. So 1u = $\frac{1}{0.000548} m_e$. The equivalent energy of an electron is 511 keV. So the equivalent energy of 1 u is $\frac{1}{0.000548} \times 511$ keV = 931 MeV.

Solution 7.2

The mass defect of a deuteron is $1.007276+1.008665-2.01355 = 0.002391$u. Its binding energy is 0.002391 u$\times$ 931 MeV/u$= 2.228$ MeV.

RADIOACTIVE DECAY AND ITS STATISTICS

Solution 7.3

The PMF of a Poisson distribution with parameter a is given by

$$\Pr[N = k] = \frac{a^k e^{-a}}{k!} .$$

Its mean is given by

$$\begin{aligned} \mu_N &= \sum_{k=0}^{\infty} k \Pr[N = k] \\ &= \sum_{k=0}^{\infty} k \frac{a^k e^{-a}}{k!} = \sum_{k=1}^{\infty} \frac{a^k e^{-a}}{(k-1)!} \\ &= a \sum_{k=1}^{\infty} \frac{a^{(k-1)} e^{-a}}{(k-1)!} = a \sum_{k=0}^{\infty} \frac{a^k e^{-a}}{k!} \\ &= a . \end{aligned}$$

The variance is

$$\sigma_N^2 = \sum_{k=0}^{\infty} k^2 \text{Pr}[N=k] - a^2 \quad \text{because } \sigma^2 = E[X^2] - (E[X])^2 \,.$$

Evaluate the summation as follows:

$$\begin{aligned}
\sum_{k=0}^{\infty} k^2 \text{Pr}[N=k] &= a \sum_{k=1}^{\infty} k \frac{a^{(k-1)} e^{-a}}{(k-1)!} \\
&= a \left[1 + \sum_{k=2}^{\infty} (k-1) \frac{a^{(k-1)} e^{-a}}{(k-1)!} \right] \\
&= a \left[1 + a \right] \\
&= a + a^2 \,.
\end{aligned}$$

So the variance of a Poisson random variable with parameter a is

$$\sigma_N^2 = a \,.$$

Solution 7.4

(a) Using (7.8), the decay constant λ is found as

$$\lambda = \frac{0.693}{T_{1/2}} = \frac{0.693}{13 \times 3,600 \text{ sec}} \approx 1.4808 \times 10^{-5} \text{ sec}^{-1}.$$

The radioactivity A is then

$$A = \lambda N = 1.4808 \times 10^{-5} \times 10^9 = 1.4808 \times 10^4 \text{ dps}.$$

(b) Since $N_t = N_0 e^{-\lambda t}$, then

$$N_{24 \text{ h}} = 10^9 \times \exp(-1.4808 \times 10^{-5} \times 24 \times 3,600) \approx 2.78 \times 10^8 \text{ atoms}.$$

(c) The number of radioactive atoms left follows a Poisson distribution with a mean as computed in (b). For large mean value, the Poisson distribution can be well approximated by a Gaussian distribution with the same mean and variance.

Thus,

$$P_{N=10^8} = \frac{1}{\sqrt{2\pi \times 2.78 \times 10^8}} \exp\left[-\frac{(10^8 - 2.78 \times 10^8)^2}{2 \times 2.78 \times 10^8} \right] \approx 0.$$

Solution 7.5

At $t = 0$, the number of technetium-99m atoms is 1×10^{12}. Since the half-life of technetium-99m is 6 hours (Table 7.1), the decay constant is

$$\lambda = \frac{0.693}{t_{1/2}} = \frac{0.693}{6 \times 3,600 \text{ sec}} = 3.21 \times 10^{-5} \text{ sec}^{-1} \,.$$

The radioactivity at $t = 0$ is

$$A_0 = 1 \times 10^{12} \times 3.2 \times 10^{-5} \text{ sec}^{-1} = 3.2 \times 10^7 \text{Bq} = 0.86 \text{mCi} \,.$$

The intensity measured is:

$$I_0 = 8.91 \times 10^9 \frac{\text{keV}}{\text{sec} \cdot \text{m}^2} \,.$$

One hour later, the radioactivity becomes

$$A_1 = A_0 e^{-\lambda t} = A_0 e^{-0.693/6} = 0.89 A_0 \,.$$

So the intensity measured at $t = 1$ hour is

$$I_1 = 7.94 \times 10^9 \frac{\text{keV}}{\text{sec m}^2} \,.$$

Solution 7.6

(a) A_0 =1 Ci= 3.7×10^{10}Bq and $A_t = A_0 e^{-\lambda t} = 1$Bq. So

$$e^{-\lambda t} = \frac{1}{3.7 \times 10^{10}} = 2.7 \times 10^{-11} \,,$$

which is solved as

$$-\lambda t = \ln\left(2.7 \times 10^{-11}\right) = -24.334$$
$$\Longrightarrow \; t = \frac{24.334}{\lambda}$$

Since $T_{1/2} = \frac{0.693}{\lambda} = \tau$, we have $\lambda = \frac{0.693}{\tau}$, and $t = 35.114\tau$. It takes $t = 35.114\tau$ for a radioactive sample with activity 1 Ci to decay to activity 1 Bq if the half-life is τ.

(b) The radioactive tracers used in nuclear medicine should have a half-life on the order of minutes to hours, about the time it takes to perform study. If longer, activity remains in patient. If shorter, activity disappears before scan is completed.

Solution 7.7

(a) The radioactive source decays according to

$$A_t = A_0 e^{-\lambda t} \,.$$

The intensity at range r from this source is

$$I_t = \frac{A_t E}{4\pi r^2} \,,$$

where the time-dependency is made explicit using a subscript t and E is the gamma-ray energy. A point (x, y) on the detector is at a distance

$$r = \sqrt{R^2 + x^2 + y^2}$$

from the source. Therefore, the intensity on the detector face is

$$I_t(x,y) = \frac{A_t E}{4\pi(R^2+x^2+y^2)}\,, \quad |x|,|y| < D/2\,.$$

(b) The average intensity is

$$\begin{aligned} I_t^{\text{av}} &= \frac{1}{D^2}\int_{-D/2}^{D/2}\int_{-D/2}^{D/2} I_t(x,y)\,dx\,dy \\ &= \frac{1}{D^2}\int_{-D/2}^{D/2}\int_{-D/2}^{D/2} \frac{A_t E}{4\pi(R^2+x^2+y^2)}\,dx\,dy \\ &\approx \frac{A_t E}{4\pi R^2}\,, \end{aligned}$$

where the last approximation holds if $R \gg D$.

Solution 7.8

(a) DF is defined as DF $= e^{-\lambda t}$. And decay constant λ is given by

$$\frac{A_{1/2}}{A_0} = \frac{1}{2} = e^{-\lambda T_{1/2}}\,.$$

Taking the natural logarithm of the above equation yields $-\lambda T_{1/2} = -\ln 2 = -0.693$ and $\lambda = \frac{0.693}{T_{1/2}}$. So the decay factor is

$$\text{DF} = e^{-0.693t/T_{1/2}}\,.$$

(b) From above, we have $\tau = \frac{1}{\lambda} = \frac{T_{1/2}}{0.693} = 1.443T_{1/2}$.

Solution 7.9

(a) The half-life of ^{99m}Tc is 6 hours. It is 8 hours from 8 a.m. to 4 p.m. Therefore, using the relation between the decay constant and the half-life,

$$\lambda = \frac{0.693}{T_{1/2}}$$

we can write

$$A_{4\text{p.m.}} = A_{8\text{a.m.}} e^{-\lambda t} = 2e^{-0.693\times 8/6} \approx 0.7939 \text{ mCi/ml}\,.$$

(b) To get 1.5 mCi radioactivity, we need a volume of

$$V = \frac{1.5 \text{ mCi}}{0.7939 \text{ mCi/ml}} \approx 1.89 \text{ ml}\,.$$

Solution 7.10

(a) First we find the decay constant as follows

$$\begin{aligned} N_t &= N_0 e^{-\lambda t} \\ 9.9212 \times 10^6 &= 10^8 e^{-\lambda 864{,}000} \\ \lambda &= -\ln((9.9212 \times 10^6)/10^8)/864{,}000 \\ \lambda &= 2.6742 \times 10^{-6}\ \text{sec}^{-1}\,. \end{aligned}$$

Using the relationship between the half-life and the decay constant, we find

$$\begin{aligned} t_{1/2} &= \ln(2)/\lambda \\ &= 259{,}198 \approx 259{,}200\ \text{sec (or 3 days)} \end{aligned}$$

(b) For $\Delta t << t_{1/2}$, the average number of disintegrations = Poisson rate $\times \Delta t = N_0 \lambda \Delta t = 2.6742$ disintegrations.

(c) Using Equation (7.11) and $a = 2.6742$ disintegrations (from part (b)), we have:

$$\begin{aligned} \text{Prob}(\Delta N > 2) &= 1 - \text{Prob}(\Delta N = 2) - \text{Prob}(\Delta N = 1) - \text{Prob}(\Delta N = 0) \\ &= 1 - \frac{(a)^2 e^{-a}}{2!} - \frac{(a)^1 e^{-a}}{1!} - \frac{(a)^0 e^{-a}}{0!} \\ &= 1 - (\frac{a^2}{2} + a + 1)e^{-a} \\ &= 1 - (\frac{2.6742^2}{2} + 2.6742 + 1)e^{-2.6742} \\ &= 0.50003\,. \end{aligned}$$

Solution 7.11

Determine the decay constant of $^{21}_{11}$Ms as follows:

$$\begin{aligned} 1/2 &= e^{\lambda t_{1/2}}\,, \\ t_{1/2} &= 2\ \text{hours}\,, \\ \lambda &= \frac{\ln(1/2)}{-2} = 0.347\ \text{hr}^{-1}\,. \end{aligned}$$

Determine the amount of $^{21}_{11}$Ms left at 5 pm as follows:

$$\begin{aligned} \Delta t &= 4\ \text{hours}\,, \\ N &= N_0 e^{\lambda t} \\ &= 8\ \text{g} \times e^{-0.347 \times 4} \\ &= 2\ \text{g}\,. \end{aligned}$$

Subtract to determine the amount that has decayed:

$$8\ \text{g} - 2\ \text{g} = 6\ \text{g}\,.$$

Solution 7.12

(a) First determine the decay constant:

$$\begin{aligned} A_t &= A_0 e^{-\lambda t}\,, \\ 1\ \mathrm{mCi/ml} &= 3\ \mathrm{mCi/ml}\, e^{-\lambda 3{,}600}\,, \\ \lambda &= -\ln\frac{1}{3}\times\frac{1}{3{,}600} = 3.05\times 10^{-4}\mathrm{s}^{-1}\,. \end{aligned}$$

Then find the half-life:

$$t_{1/2} = \frac{\ln 2}{\lambda} = \frac{\ln 2}{3.05\times 10^{-4}s^{-1}} = 2{,}271.3\ \mathrm{s} = 0.63\ \mathrm{h} = 37.86\ \mathrm{min}\,.$$

(b) Compute the radioactivity:

$$\begin{aligned} A_t &= 3\ \mathrm{mCi/ml}\, e^{-\lambda\times 4\times 3{,}600} \\ &= 3\ \mathrm{mCi/ml}\, e^{-3.05\times 10^{-4}s^{-1}\times 4\times 3{,}600\ s} \\ &= 0.037\ \mathrm{mCi/ml}\,. \end{aligned}$$

(c) Calculate the volume:

$$V = \frac{1.5\ \mathrm{mCi}}{0.6371\ \mathrm{mCi/ml}} = 2.3544\ \mathrm{ml}\,.$$

RADIOTRACERS

Solution 7.13

(a) Explanation for each:
(i) $E_\gamma = 30$ Kev, $t_{1/2} = 7$ hours: This is a bad choice for medical imaging because the energy of the gamma rays is low and the body will absorb most of the emitted gamma rays.
(ii) $E_\gamma = 150$ Kev, $t_{1/2} = 5$ hours: This is a good choice for medical imaging purposes because its half-life is long enough to enable imaging and short enough to weaken strongly before the patient leaves the hospital. The gamma ray energy is high so that it is somewhat transparent in the body but still detectable by conventional detectors.
(iii) $E_\gamma = 200$ Kev, $t_{1/2} = 10$ days: The energy would be a pretty good choice for this one. The half-life would be good for biological processes that take a week or so for the radiotracer to reach its destination. It is too long, however, for most processes.

(b) Activity follows the radioactive decay law. If activity reduces to 1/4 after 5 hours then 5 hours is twice the

half-life. Accordingly,

$$
\begin{aligned}
t_{1/2} &= 2.5 \text{ hours}\,, \\
\lambda &= \frac{0.693}{t_{1/2}} = 7.7 \times 10^{-5}\ \text{s}^{-1}\,, \\
N_0 &= \frac{A_0}{\lambda} = \frac{4.4 \times 10^{10}}{7.7 \times 10^{-5}} = 5.19 \times 10^{14}\,.
\end{aligned}
$$

Solution 7.14

A radiotracer is chosen first for its properties of biodistribution and then by its physical imaging properties. The two radiotracers are not equivalent if they distribute in the body in different ways and most likely they cannot be interchanged.

8

Planar Scintigraphy

INSTRUMENTATION

Solution 8.1

(a) For the diagrams of an Anger gamma camera, see Figures 8.1, 8.2, 8.3, and 8.4. An Anger gamma camera consists of a multi-hole lead collimator, a sodium iodide scintillation crystal, an array of PMTs on the crystal, a positioning logic network, a pulse height analyzer, a gating circuit, and a computer. The functions of each of these parts are:

The collimator provides an interface between the patient and the scintillation crystal, by allowing only those photons traveling in an appropriate direction (i.e., those that can pass through the holes without being absorbed in the lead) to interact with the crystal;

The scintillation crystal emits light photons after deposition of energy in the crystal of ionizing radiation;

The photomultiplier tubes do two things: converting light signals into electrical signals and amplifying these signals;

The positioning logic network determines both where the event occurred on the face of the crystal and the combined output of all the tubes, which represents the light output of the crystal (which in turn represents the energy deposited by the gamma photon). These output signals are denoted as X and Y for the estimated two-dimensional position of the event and Z for the total light output. The amplitude of a given tube's output is directly proportional to the amount of light (number of scintillation photons) its photocathode receives. The tubes closest to the scintillation event will have the largest output pulses, while those farther away will have smaller output pulses. By analyzing the spatial distribution of pulse heights, the location of a single scintillation event (X, Y) can be determined quite accurately.

The pulse height analyzer is used to distinguish photons been Compton scattered from those are not by analyzing the energy deposited in the crystal via the Z-pulse whose height is proportional to the total energy deposited in the crystal. The pulse height analyzer is used to set an acceptable window around the *photopeak* in the spectrum of the Z-pulse.

The gating circuit is used to compensate for the imperfect photopeak localization and further reduce the scattered photons being accepted as a valid event.

The computer is used to record the location of each event and form images.

(b) When we select radionuclides in nuclear medicine, the following issue must be considered:

- The radionuclides must be "clean" gamma ray emitters, which means that they do not emit alpha or beta particles.
- The radionuclides must emit gamma rays with appropriate energy. The energy cannot be too low because low-energy gamma rays are more likely to be absorbed by the body; therefore, increase patient dose without contributing to the images. Also, the energy cannot be too high since high-energy gamma rays are less likely to be detected.
- The radionuclides should have a half-life on the order of minutes to hours.
- The radionuclides should be useful and safe to trace in the body.
- The radionuclides should emit gamma rays as monochromatic as possible.

Solution 8.2

(a) Use Beer's law for calculating the path length w in the septa to allow less than 60% incident photons to pass through. If μ is the linear attenuation coefficient for lead at 140 keV, then $e^{-\mu w} \leq 0.60$. This gives $w \geq 0.51/\mu$. From geometry, the collimator septa thickness h is related to path length w for gamma-rays incident at 45° by $h = w/\sqrt{2} = 0.36/\mu$.

(b) Here, using the above two equations to find d and , the values of l are found by the roots of a quadratic equation to be $l = 8$ mm, 30 mm. Choose $l = 30$ mm, then $d = 0.22$ mm.

(c) Increasing l, the length of the holes, improves rejection of scattered photons, thereby improves resolution. Sensitivity decreases too, as less photons reach the detector. Also collimators with large l may be heavy.

(d) Increasing the thickness of the scintillator will increase the sensitivity and compensate to some extent its decrease due to long holes. The disadvantage of increasing crystal thickness is that the intrinsic resolution of the crystal degrades.

Solution 8.3

(a) Note that 20% pulse-height window is 10% on either side.

$$150 \text{ keV} \times 0.1 = 15 \text{ keV}\,,$$

$$150 \text{ keV} - 15 \text{ keV} = 135 \text{ keV}\,.$$

Since

$$h\nu' = \frac{h\nu}{1 + \frac{h\nu}{m_0 c^2}(1 - \cos\theta)}\,,$$

we have

$$135 \text{ keV} = \frac{140 \text{ keV}}{1 + \frac{140 \text{ keV}}{511 \text{ keV}}(1 - \cos\theta)}\,.$$

Solving for θ, we get $\theta = 30.14°$.

(b) For a window centered at the photopeak, the maximum acceptable scattering angle for a 140 keV photon is 53.54°, as shown in Example 8.2. Do a similar computation, we can see that photons with energy $h\nu = 364$ keV can be scattered by an angle $\theta = 32.43°$ and still be accepted by a 20% window centered at the photopeak.

(c) From (b), we conclude that as the frequency goes up, the directional selectivity gets better. Compare (a) and (b), we can see that an offset window centered at a higher energy can further reduce scatter.

Solution 8.4

(a) The intensity at radius r from the source is

$$I = \frac{AE}{4\pi r^2}\,,$$

where E is the gamma ray photon energy.

(b) Hole size does not matter since "per unit area" is already figured into the intensity. Therefore, the intensity is the same as in part (a).

(c) Doubling the source−camera distance yields

$$I = \frac{AE}{4\pi(2r)^2} = \frac{AE}{16\pi r^2}\,.$$

This is 1/4 the intensity of part (a).

Solution 8.5

The septal thickness of a collimator depends on the minimum required path length for adequate attenuation. That is, the septa must be thick enough that photons traveling through them have a high probability of being absorbed. From a geometric point of view, we can define a minimum septal thickness from a minimum path length as

$$h = \frac{2dw}{l-w}\,. \tag{S8.1}$$

If septal penetration is to be less than 5%, the transmission factor from Beer's Law [(4.24)]for the minimum path length is:

$$e^{-\mu w} \leq 0.05\,. \tag{S8.2}$$

We note that $e^{-3} \approx 0.05$, so this implies $\mu w \geq 3$. We can thus substitute this definition into (S8.1) for septal thickness:

$$h \geq \frac{6d}{\mu l - 3}\,. \tag{S8.3}$$

The μ for lead at 140 keV is 21.43 cm^{-1}. For comparison, at 511 keV, it is 1.746 cm^{-1}.

Solution 8.6

(a) Energy of 30° Compton scattered 140 keV photon.

$$E' = \frac{140\text{ keV}}{1+(1-\cos(30^\circ))140\text{ Kev}/511\text{ Kev}} = 135.04\text{ keV} \tag{S8.4}$$

Acceptance window $= 2\frac{140-135.04}{140}100 = 7.08\%$.

(b) See Figure S8.1.

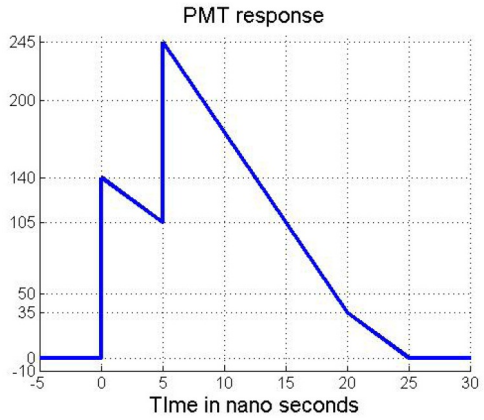

Figure S8.1 Plot of response. See Problem 8.6(b).

(c) The detection circuit is on until the response falls below 80% of the photo peak. So the second photon should not arrive while the response from the first is at 80%. Time for the response to fall to 80% is $t = 20/140 \times 140 \times 0.2 = 4$ ns.

The acceptance window is 20% this means that second photon should not arrive while the response from the first photon is above 10%. Otherwise the net response will be over 110% and the acceptance window will reject the second photon. Time for the response to fall to 10% is $t = 20/140 \times 140 \times 0.9 = 18$ ns.

This means that arrival of two photons should be 18 ns apart so that both the photons are accepted as separate event.

(d)

$$\begin{aligned}\text{Probability of at least one disintegration} &= 1 - \text{Probability of no disintegration} \\ &= 1 - e^{-\lambda N_0 \Delta t} \\ &= 1 - e^{-A_0 \Delta t}\,.\end{aligned}$$

Plug in the known numbers as follows

$$0.5 = 1 - e^{-0.25 \times A \times 3.7 \times 10^{10}\ \text{dps} \times 18 \times 10^{-10}\ \text{s}}\,,$$

and solve the equation to get $A = 0.0416$ Ci $= 41.6$ mCi.

(e) The height of the Z-pulse is $80 + 30 + 20 + 5 = 135$. Find the center of mass as follows:

x location $= (-1.5 \times 80 + 1.5 \times 30 + (-1.5) \times 20 + 1.5 \times 5)/135 = -0.722$ cm ,

y location $= (1.5 \times 80 + 1.5 \times 30 + (-1.5) \times 20 + (-1.5) \times 5)/135 = 0.9442$ cm .

IMAGE FORMATION

Solution 8.7

Refer to Figure S8.2.

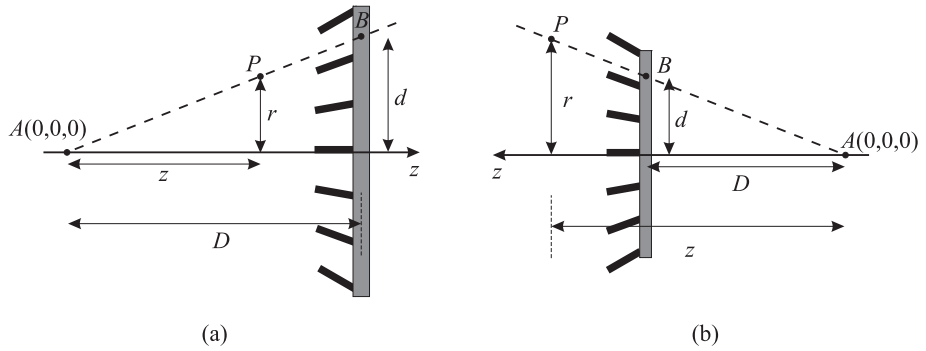

Figure S8.2 Converging and diverging collimators. See Problem 8.7.

(a) Let the converging collimator have a focal point located at A, which is at a distance D on the left side of the detector, as shown in the Figure S8.2(a). Let the coordinate system be such that the origin is located at the focal point A. Consider a point B on the detector at a distance d, as shown and at an angle θ. The coordinates of this point B are $(d\cos\theta, d\sin\theta, D)$. The photons reaching this point will travel along a line passing through the focal point A and the point on the detector B. Hence, these photons will experience an attenuation obtained by integrating the linear attenuation coefficient $\mu(x, y, z)$ along this line. Consider a point P on this line, at a distance z' from the origin, as shown in the figure. The coordinates of P are $(r\cos\theta, r\sin\theta, z') = (z'd\cos\theta/D, z'd\sin\theta/D, z')$. Hence the intensity at B, due to an event occurring at a location z, is given as:

$$I_d = \frac{AE}{4\pi l^2} \exp\left\{ -\int_z^D \mu(z'd\cos\theta/D, z'd\sin\theta/D, z')dz' \right\} ,$$

where, $l = \sqrt{(zd\cos\theta/D - d\cos\theta)^2 + (zd\sin\theta/D - d\sin\theta)^2 + (z-D)^2}$. This is the intensity due to a single event occurring at a depth z, along the line. Integrating the activity over all possible events along the line, we get

$$\begin{aligned} I(d\cos\theta, d\sin\theta) &= \int_{-\infty}^{D} \frac{A(zd\cos\theta/D, zd\sin\theta/D, z)E}{4\pi l^2} \\ &\qquad \exp\left\{ -\int_z^D \mu(z'd\cos\theta/D, z'd\sin\theta/D, z')dz' \right\} dz \, . \end{aligned}$$

(b) Let the diverging collimator have a focal point located at A, which is at a distance D on the right side of the detector as shown in Figure S8.2(b). Let the coordinate system be such that the origin is located at the focal point A. Consider a point B on the detector at a distance d, as shown and at an angle θ. The coordinates of this point B are $(d\cos\theta, d\sin\theta, D)$. The photons reaching this point will travel along a line colinear with the focal point A and the point on the detector B. Hence, these photons will experience an attenuation obtained by integrating the linear attenuation coefficient $\mu(x, y, z)$ along this line. Consider a point P on this line, at a distance z' from the origin, as shown in the figure. The coordinates of P are

$(r\cos\theta, r\sin\theta, z') = (z'd\cos\theta/D, z'd\sin\theta/D, z')$. Hence the intensity at B, due to an event occurring at a location z, is given as:

$$I_d = \frac{AE}{4\pi l^2}\exp\left\{-\int_z^{-D}\mu(z'd\cos\theta/D, z'd\sin\theta/D, z')dz'\right\}.$$

This is the intensity due to a single event occurring at a depth z, along the line. Integrating the activity over all possible events along the line, we get

$$\begin{aligned} I(d\cos\theta, d\sin\theta) &= \int_{-\infty}^{-D}\frac{A(zd\cos\theta/D, zd\sin\theta/D, z)E}{4\pi l^2} \\ &\qquad \exp\left\{-\int_z^{-D}\mu(z'd\cos\theta/D, z'd\sin\theta/D, z')dz'\right\}dz\,. \end{aligned}$$

Solution 8.8

(a) By simple computation, we have the outputs of the PMTs are:

$$\begin{aligned} a_1 &= 21.10 \quad a_2 = 21.10 \quad a_3 = 12.13 \\ a_4 &= 21.10 \quad a_5 = 21.10 \quad a_6 = 12.13 \\ a_7 &= 12.13 \quad a_8 = 12.13 \quad a_9 = 8.13\,. \end{aligned}$$

(b) The Z-pulse is

$$Z = \sum_{i=1}^{9} a_i = 141.05\,.$$

The estimated position is

$$\begin{aligned} \bar{X} &= \frac{1}{Z}\sum_{i=1}^{9} a_i x_i = -0.16 \text{ cm}\,, \\ \bar{Y} &= \frac{1}{Z}\sum_{i=1}^{9} a_i y_i = 0.16 \text{ cm}\,. \end{aligned}$$

(c) The estimated position is different from the true position of the scintillation event. The reason is that the event position estimation uses a linear model, while (P8.1) is nonlinear.

Solution 8.9

(a) From Figure P8.3(a), when pulse height is 180, the energy deposited is 160 keV. Therefore, we have

$$\begin{aligned} h\nu' &= \frac{h\nu}{1+\frac{h\nu}{mc_0^2}(1-\cos\theta)} \\ &= \frac{160}{1+\frac{160}{511}(1-\cos 50^\circ)} \\ &= 143.9 \text{ keV}\,. \end{aligned}$$

Suppose the acceptance window is centered at the photo peak at 160 keV, the upper bound of the energy window is $160+(160-143.9)=176.1$ keV. So the acceptance window can be set to be $143.9-176.1$ keV.

(b) The Z-pulse $= 40+5+15+15+20+45+30 = 170$. The corresponding energy deposited is 150 keV. It will be accepted by the acceptance window.

(c) The coordinates of the 7 tubes and pulse heights are:

tube	1	2	3	4	5	6	7
(x,y) in mm	(0,0)	$(-2,0)$	$(-1,\sqrt{3})$	$(1,\sqrt{3})$	(2,0)	$(1,-\sqrt{3})$	$(-1,-\sqrt{3})$
pulse height	40	5	15	15	20	45	30

and

$$X = \frac{1}{Z}\sum_{k=1}^{7} a_k x_k = 0.26 \text{ mm}, \quad Y = \frac{1}{Z}\sum_{k=1}^{7} a_k y_k = -0.46 \text{ mm}$$

(d) If (X,Y) is set equal to the location of the PMT that has the largest amplitude, this will give a less accurate estimation of the location of an event. The resolution of the resulting image will be on the order of the size of tubes.

Solution 8.10

(a) See Figure S8.3.

(b) Note that a 10 percent pulse height window is 5 percent on either side. So the lowest energy that can be accepted is $140 \text{ keV} \times (1-0.05) = 133$ keV.

$$\begin{aligned} h\nu' &= \frac{h\nu}{1+\frac{h\nu}{m_0c^2}(1-\cos\theta))}\,, \\ 133 \text{ keV} &= \frac{140 \text{ keV}}{1+\frac{140 \text{ keV}}{511 \text{ keV}}(1-\cos\theta))}\,. \end{aligned}$$

And we get $\theta = 36.11^\circ$.

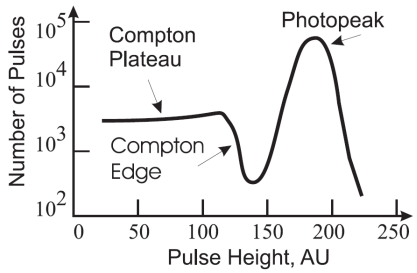

Figure S8.3 Pulse height spectrum. See Problem 8.10(a).

(c) The Z-pulse is $Z = 5 + 15 + 25 + 10 + 20 + 45 + 5 + 10 + 40 = 175$ AU.

(d) The position of the event $(X, Y) = (0.91, -1.14)$ is

$$X = \frac{1}{Z}\sum x_k a_k = \frac{0\times5+2\times15+4\times25-2\times10+0\times20+2\times45-4\times5-2\times10+0\times40}{175} = \frac{160}{175} = 0.91\,,$$

$$Y = \frac{1}{Z}\sum y_k a_k = \frac{4\times5+2\times15+0\times25+2\times10+0\times20-2\times45+0\times5-2\times10-4\times40}{175} = \frac{-200}{175} = -1.14\ .$$

(e) Causes of event localization error include edge effects, badly calibrated PMTs, and gamma rays passing through septa (scattering).

IMAGE QUALITY
Solution 8.11

(a) The overall system response is given by the convolution of the system responses of all its subsystems. In this case, it is the convolution of three rect functions. By assumption, $f_I(x) = a\,\mathrm{rect}(x/r_I)$, $f_C(x) = b\,\mathrm{rect}(x/r_C)$, and $f_P(x) = c\,\mathrm{rect}(x/r_P)$, where a, b, c denote the individual amplitude (actually, they can be assumed to be one when computing FWHM). Let's assume $r_I \le r_C \le r_P$ and $r_I \le r_P - r_C$.

$$\begin{aligned} f_{CP}(x) &= f_C(x) * f_P(x) = \int_{-\infty}^{\infty} bc\,\mathrm{rect}(\frac{x-t}{r_C})\,\mathrm{rect}(\frac{t}{r_P})dt \\ &= bc\int_{-r_P/2}^{r_P/2} \mathrm{rect}(\frac{x-t}{r_C})dt \\ &= \begin{cases} bc(x+\frac{r_C+r_P}{2}) & \text{if } -\frac{r_P+r_C}{2} \le x \le -\frac{r_P-r_C}{2}; \\ bcr_C & \text{if } -\frac{r_P-r_C}{2} \le x \le \frac{r_P-r_C}{2}; \\ bc(\frac{r_C+r_P}{2}-x) & \text{if } \frac{r_P-r_C}{2} \le x \le \frac{r_P+r_C}{2}; \\ 0 & \text{otherwise.} \end{cases} \end{aligned}.$$

Then, $f_{\mathrm{total}}(x) = f_I(x) * f_C(x) * f_P(x) = f_I(x) * f_{CP}(x)$ can be similarly computed to be: $f_{\mathrm{total}}(x) =$

$$\begin{cases} \frac{abc}{2}\left(x+\frac{r_I+r_C+r_P}{2}\right)^2 & \text{if } -\frac{r_P+r_C+r_I}{2} \le x \le -\frac{r_P+r_C-r_I}{2}, \\ abcr_I\left(x+\frac{r_C+r_P}{2}\right) & \text{if } -\frac{r_P+r_C-r_I}{2} \le x \le -\frac{r_P-r_C+r_I}{2}, \\ abc\left(-\frac{x^2}{2}-\frac{r_P-r_C-r_I}{2}x+\frac{(r_P-r_C-r_I)(r_I-3r_C-r_P)}{8}+\frac{r_C(r_P-r_C+r_I)}{2}\right) & \text{if } -\frac{r_P-r_C+r_I}{2} \le x \le -\frac{r_P-r_C-r_I}{2}, \\ abcr_Ir_C & \text{if } -\frac{r_P-r_C-r_I}{2} \le x \le \frac{r_P-r_C-r_I}{2}, \\ abc\left(-\frac{x^2}{2}+\frac{r_P-r_C-r_I}{2}x+\frac{(r_P-r_C-r_I)(r_I-3r_C-r_P)}{8}+\frac{r_C(r_P-r_C+r_I)}{2}\right) & \text{if } \frac{r_P-r_C-r_I}{2} \le x \le \frac{r_P-r_C+r_I}{2}, \\ abcr_I\left(-x+\frac{r_C+r_P}{2}\right) & \text{if } \frac{r_P-r_C+r_I}{2} \le x \le \frac{r_P+r_C-r_I}{2}, \\ \frac{abc}{2}\left(x+\frac{r_I+r_C+r_P}{2}\right)^2 & \text{if } \frac{r_P+r_C-r_I}{2} \le x \le \frac{r_P+r_C+r_I}{2}, \\ 0 & \text{otherwise.} \end{cases}$$

The maximum value of $f_{\mathrm{total}}(x)$ is $abcr_Ir_C$. Thus, we need to solve for x_0 such that $f_{\mathrm{total}}(x_0) = \frac{abcr_Ir_C}{2}$, which can be easily computed to be $x_0 = \pm\frac{r_P}{2}$. Hence the FWHM of the overall system is equal to r_P, which is the largest width of the three sub-systems.

(b) In the case of Gaussian cascade we know that

$$\mathrm{FWHM}_{total} = \sqrt{\mathrm{FWHM}_I^2 + \mathrm{FWHM}_C^2 + \mathrm{FWHM}_P^2},$$

and for each subsystem the FWHM is equal to $2\sqrt{2\ln 2}\sigma_.$. Hence,

$$\text{FWHM}_{total} = 2\sqrt{2\ln 2}\sqrt{\sigma_I^2 + \sigma_C^2 + \sigma_P^2}\,.$$

Solution 8.12

(a) The half-life of technetium-99m is 6 h $= 360$ min. Therefore the radioactive decay formula is

$$A = A_0 e^{-t/360}\,.$$

Our images will be acquired over 2 h $= 120$ min. There are 6 images per hour for 2 hours, which makes 12 images total.The counts in the last image are the integration of the activity over the interval $110 < t < 120$:

$$\begin{aligned} N_{12} &= \int_{110}^{120} A_0 e^{-t/360} \\ &= A_0(-360)e^{-t/360}\Big|_{110}^{120} \\ &= -360A_0(e^{-120/360} - e^{-110/360}) \\ &= 7.265759A_0\,. \end{aligned}$$

This is then solved for A_0

$$A_0 = \frac{2,000,000}{7.265759} = 275,263 \text{ counts/min}\,.$$

(b) The total count in image n is

$$\begin{aligned} N_n &= \int_{10(n-1)}^{10n} A_0 e^{-t/\tau}\,dt \\ &= A_0(-\tau)e^{-t/\tau}\Big|_{10(n-1)}^{10n} \\ &= A_0\tau(e^{-10(n-1)/\tau} - e^{-10n/\tau})\,. \end{aligned}$$

The count per pixels is

$$N_n^p = \frac{N_n}{J^2}\,.$$

and the SNR per pixel is

$$\begin{aligned} \text{SNR}_p &= \sqrt{N_N^p} \\ &= \frac{\sqrt{N_n}}{J} \\ &= \frac{\sqrt{A_0\tau(e^{-10(n-1)/\tau} - e^{-10n/\tau})}}{J} \\ &= \frac{\sqrt{275,263 \times 360}}{J}\sqrt{e^{-10(n-1)/\tau} - e^{-10n/\tau}} \\ &= 77\sqrt{e^{-10(n-1)/\tau} - e^{-10n/\tau}}\,. \end{aligned}$$

This is calculated for $n = 1, \ldots, 12$, yielding 12.74, 12.57, 12.40, 12.22, 12.06, 11.89, 11.72, 11.56, 11.40, 11.25, 11.09, 10.94.

(c) The tumor has contrast $C = 0.1$. The local SNR is

$$\text{SNR}_l = C\sqrt{\bar{N}_b}\,.$$

In decibels this is

$$\text{SNR}_l(\text{dB}) = 20\log_{10} C\sqrt{\bar{N}_b} = 5 \text{ dB}\,.$$

Therefore,

$$\begin{aligned} \log_{10} C\sqrt{\bar{N}_b} &= 5/20\,, \\ C\sqrt{\bar{N}_b} &= 1.778\,, \\ \sqrt{\bar{N}_b} &= 17.78\,, \\ \bar{N}_b &= 316\,. \end{aligned}$$

This implies that there must be approximately 5 M counts in the last image. From the result in part (a), we can deduce that there are approximately 6.8 M counts in the first image.

Solution 8.13

(a) The counting rate is at most 128K dps (disintegration per second). Each frame last for 75 ms during each heart beat, and there are $64 \times 64 = 4,096$ pixels on each frame. So, during one heart beat, each pixel can get at most

$$\frac{128,000 \text{ dps} \times 0.075 \text{ s}}{4,096} = 2.34 \frac{\text{disintegration}}{\text{pixel} \cdot \text{heartbeat}}.$$

In order to get the required counts, we need

$$N = \frac{1,000}{2.34} = 427 \text{ heartbeat}\,.$$

(b) The heart rate is 50 bpm, so the study will take

$$T = \frac{427}{50} = 8.54 \text{ minutes}\,.$$

(c) The intrinsic SNR for each pixel is

$$\text{SNR} = \sqrt{1,000} = 31.62\,.$$

(d) If we want to double the SNR, we need to have 4,000 counts per pixel for each frame. Therefore, the study will be 4 times as long as the one described in parts (a) and (b). The time it takes is

$$T_2 = 4 \times T = 34.16 \text{ minutes}\,.$$

Solution 8.14

Consider a source positioned at distance r from the collimator (as in Figure S8.4). Because of the collimator's geometry, this source will only be "seen" by the scintillation crystal over a certain (horizontal) extent. We will take 1/2 of this range to be the collimator resolution, R_c. This result would be exactly the FWHM if the response to the point source were a triangle function—a bold assumption, and one that is necessary for this geometric derivation. By similar triangles, we have

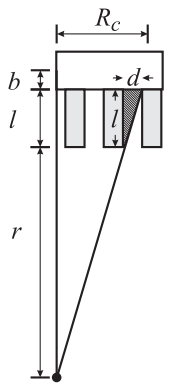

Figure S8.4 See Problem 8.14.

$$\frac{d}{l} = \frac{R_c}{l+b+r}\,.$$

Rearranging yields the desired result.

Solution 8.15

(a) The radioactivities of A and B are

$$\begin{aligned} A_t^A &= \frac{N_0^A}{10}\left(\frac{\ln 2}{t_{1/2}^A}\right)\exp\{-t\ln 2/t_{1/2}^A\} \\ &= \frac{N_0}{10}\left(\frac{\ln 2}{3}\right)\exp\{-t\ln 2/3\}\,, \\ A_t^B &= \frac{N_0^B}{10}\left(\frac{\ln 2}{t_{1/2}^B}\right)\exp\{-t\ln 2/t_{1/2}^B\} \\ &= \frac{N_0}{20}\left(\frac{\ln 2}{6}\right)\exp\{-t\ln 2/6\}\,. \end{aligned}$$

The projection is

$$\phi(x,t) = \left[A_t^A \mathrm{rect}\left(\frac{x+5}{10}\right) + A_t^B \mathrm{rect}\left(\frac{x-5}{10}\right)\right] e^{\mu_R l_R}\,.$$

At time $t = 0$, we have

$$\begin{aligned}\phi(x,0) &= \left[\frac{N_0}{10}\left(\frac{\ln 2}{3}\right)\text{rect}\left(\frac{x+5}{10}\right) + \frac{N_0}{20}\left(\frac{\ln 2}{6}\right)\text{rect}\left(\frac{x-5}{10}\right)\right]e^{-1} \\ &= 8.5\times 10^{-3}N_0\text{rect}\left(\frac{x+5}{10}\right) + 2.12\times 10^{-3}N_0\text{rect}\left(\frac{x-5}{10}\right).\end{aligned}$$

At time $t = 3$ hours, we have

$$\begin{aligned}\phi(x,3) &= \left[\frac{N_0}{10}\left(\frac{\ln 2}{3}\right)e^{-\ln 2}\text{rect}\left(\frac{x+5}{10}\right) + \frac{N_0}{20}\left(\frac{\ln 2}{6}\right)e^{-\ln 2}\text{rect}\left(\frac{x-5}{10}\right)\right]e^{-1} \\ &= 4.25\times 10^{-3}N_0\text{rect}\left(\frac{x+5}{10}\right) + 1.5\times 10^{-3}N_0\text{rect}\left(\frac{x-5}{10}\right).\end{aligned}$$

(b) $t_{\max} = 0$.

(c)

$$\begin{aligned}\epsilon &= \left(\frac{Kd^2}{l_e(d+h)}\right)^2 = \left(\frac{0.25\times 4}{35\times 2.2}\right)^2 = 1.69\times 10^{-4}, \\ R_C &= \frac{d}{l}(l+b+|z|) = \frac{2}{35}(35+b+110) = \frac{2}{35}(b+145).\end{aligned}$$

(d) $\phi_d = [4.25\times 10^{-3} - 1.50\times 10^{-3}]\times 1.69\times 10^{-4} = 4.6\times 10^{-7}$.

(e) $\text{Width}(P) = 10 + R_c$.

Solution 8.16

(a) We have

$$R_C = \frac{d}{l}(l+b+|z|) = \frac{3}{100}(10+2.5+50) = 1.875\text{ cm}.$$

(b) We have

$$R_C = 18.75\text{ mm} = 2\sigma_c\sqrt{2\ln 2}\ \Rightarrow\ \sigma_c = \frac{18.75}{2\sqrt{2\ln 2}} = 7.96.$$

Assuming that the PSF is Gaussian, then

$$h_C = e^{-\frac{x^2}{2\sigma_C^2}}.$$

Similarly,

$$R_I = 0.2\text{ mm}\ \Rightarrow\ \sigma_I = \frac{0.2}{2\sqrt{2\ln 2}} = 0.0849,$$

and

$$h_I = e^{-\frac{x^2}{2\sigma_I^2}}.$$

Then the overall PSF is

$$h = h_C * h_I.$$

Notice that

$$\mathcal{F}\{e^{-\frac{x^2}{2\sigma_c^2}}\} = \sqrt{2\pi}\sigma_c e^{-\pi(2\pi\sigma_c^2 u^2)}\,,$$
$$\mathcal{F}\{e^{-\frac{x^2}{2\sigma_I^2}}\} = \sqrt{2\pi}\sigma_I e^{-\pi(2\pi\sigma_I^2 u^2)}\,.$$

So

$$\mathcal{F}\{h\} = 2\pi\sigma_c\sigma_I e^{-\pi\{2\pi(\sigma_c^2+\sigma_I^2)u^2\}}\,,$$

and from the inverse Fourier transformation we get

$$h = \sqrt{\frac{2\pi}{\sigma_c^2+\sigma_I^2}}\sigma_c\sigma_I e^{-\frac{x^2}{2(\sigma_c^2+\sigma_I^2)}}\,.$$

(c) The shortest penetration path is depicted in Figure S8.5. It goes from the left top corner of the primary hole to the right bottom of the adjacent hole, the angle is denoted by θ. From the geometry, $\tan\theta = \frac{l}{h+2d} = 8.33$ and $w = h/\cos\theta = h/\frac{h+2d}{\sqrt{l^2+(h+2d)^2}} = 50.36$ mm.

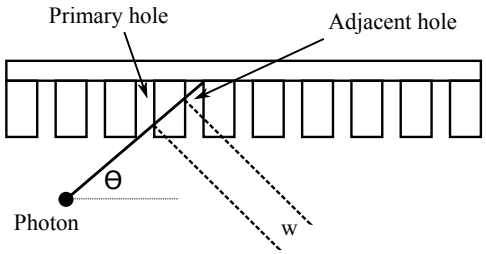

Figure S8.5 See Problem 8.16(c).

(d) If the septal penetration is to be less than 5%, the transmission factor for the minimum path length is $e^{-\mu w} \leq 0.05 \;\Rightarrow\; \mu w \geq 3.0$. For fixed l and d, $\frac{\mu h\sqrt{l^2+(h+2d)^2}}{h+2d} \geq 3.0$. Simplify the expression by the fact that $l \gg h+2d$, then $h \geq \frac{6d}{\mu l - 3}$.

(e) The septal penetration degrades the collimator resolution because it blurs the image.

(f) No. Because the attenuation in the septa lead doesn't change the energy of the photon, so the energy window wouldn't help.

(g) Compton scattering.

Solution 8.17

(a) Rate of photons emitted = $0.54 \times 10^{-3} \times 3.7 \times 10^{10} = 2 \times 10^{7}$ photons/s.
Assuming uniform emission, rate of photons hitting the detector is given by:

$$\frac{2\arctan(\frac{0.5}{0.8})}{2\pi} \times 2 \times 10^{7} = 0.355 \times 10^{7} \text{ photons/s}\,.$$

(b) Detector efficiency (DE) is defined as

$$\text{DE} = \frac{I_0 - I}{I_0}\,,$$

where $I = I_0 e^{-\mu b}$. $b = 2$ cm and $\mu = 0.64\text{cm}^{-1}$ gives:

$$\text{DE} = 1 - e^{-0.64\times 2} = 0.7220\,.$$

Thus, detector efficiency is 72.2%.

(c) Using similar triangles, we have:

$$R_C = \frac{d}{l}(|y| + b) = \frac{5 \text{ mm}}{80 \text{ mm}}(800 \text{ mm} + 20 \text{ mm}) = 51.25 \text{ mm}\,.$$

R_C is labeled on Figure S8.6.

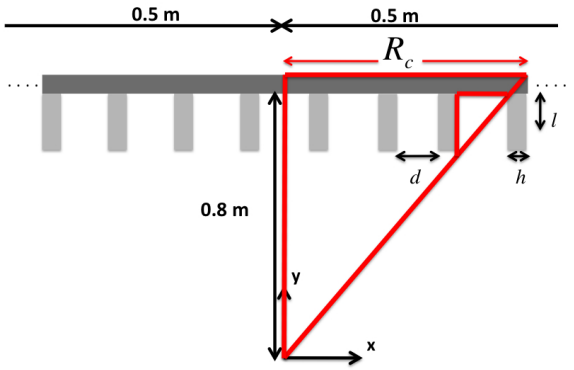

Figure S8.6 See Problem 8.17(c).

(d) We have

$$\begin{aligned} R_C &= 51.25 \text{ mm} = 2\sigma_c\sqrt{2\ln 2}\,, \\ R_I &= 1 \text{ mm} = 2\sigma_I\sqrt{2\ln 2}\,. \end{aligned}$$

Therefore, $\sigma_c = \frac{51.25}{2\sqrt{2\ln 2}} = 21.65$ and $\sigma_I = \frac{1}{2\sqrt{2\ln 2}} = 0.42$. Assuming that the PSF is Gaussian, we have

$$\begin{aligned} h_C &= e^{-\frac{x^2}{2{\sigma_c}^2}}\,, \\ h_I &= e^{-\frac{x^2}{2{\sigma_I}^2}}\,. \end{aligned}$$

The overall PSF is

$$h = h_C * h_I \, .$$

Using properties of the Fourier transform, $\mathcal{F}\{e^{-\frac{x^2}{2\sigma_c{}^2}}\} = \sqrt{2\pi}\sigma_c e^{-2\pi\sigma_c{}^2 u^2}$ and $\mathcal{F}\{e^{-\frac{x^2}{2\sigma_I{}^2}}\} = \sqrt{2\pi}\sigma_I e^{-2\pi\sigma_I{}^2 u^2}$, and knowing $\mathcal{F}\{h = h_c * h_I\} = \mathcal{F}\{h_c\}\mathcal{F}\{h_I\}$, we have

$$\mathcal{F}\{h\} = 2\pi\sigma_c\sigma_I e^{-2\pi(\sigma_I{}^2+\sigma_I{}^2)u^2} \, .$$

From the inverse Fourier transform,

$$h = \sqrt{\frac{2\pi}{\sigma_I{}^2 + \sigma_I{}^2}}\sigma_c\sigma_I e^{-\frac{x^2}{2(\sigma_I{}^2+\sigma_I{}^2)}} \, .$$

(e) Using similar triangles, $d/l = |x|/|y|$ thus the maximum distance from the center of the detector will be 50 mm. We need to find number of holes which will get the ray so $d/2 + nh + md = 50$ mm. Using $d = 5$ mm and $h = 2.5$ mm, detector will get through six holes each side which will be 13 holes in total (including the middle one).

(f) First guess can be $|y| = 80$ cm where collimator is as long as the distance of source to detector, but the following figure shows the geometry for shortest length. Using similar triangles:

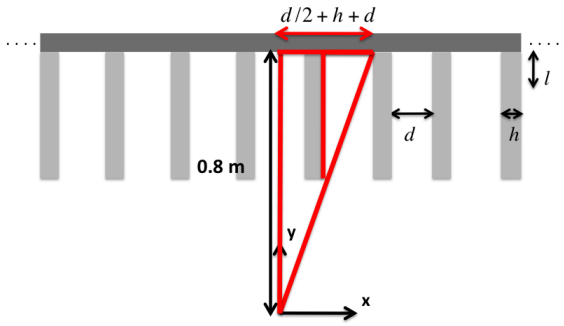

Figure S8.7 See Problem 8.17(f).

$$\frac{d/2 + h + d}{|y|} = \frac{d}{l_0} \, .$$

Solving the equation yields $l_0 = 40$ cm. For this l_0, we find that $R_c = 10.25$.

(g) The sensitivity of a collimator is $(\frac{Kd^2}{l_e(d+h)^2})^2$. For simplicity, $l_e = l$. Thus $\epsilon \propto 1/l^2$. If sensitivity is ϵ at $l = 8$ cm then, new sensitivity ϵ_{new} at $l_0 = 40$ cm will be:

$$\epsilon_{new} = \epsilon(\frac{l}{l_0})^2 = \frac{e}{25} \, .$$

APPLICATIONS

Solution 8.18

(a) 1. The photon goes through the hole;

2. It enters the scintillation crystal;
3. It has a photoelectric event producing an ejected electron;
4. Collapsing electrons (in this atom and many others) cause light photons to be emitted;
5. The light bounces around in the crystal and exits out the back face;
6. The light enters a PMT;
7. Its energy causes electrons to be emitted at the cathode and enhanced by dynode cascades;
8. The current at the anode is recoded as a small pulse;
9. The total height of all pulses, summed up over all tubes is the Z-pulse;
10. Weighted combinations of the pulse heights give the X^-, X^+, Y^-, and Y^+ signals;
11. $X = \frac{X^+ - X^-}{2}$, and $Y = \frac{Y^+ - Y^-}{2}$.

(b) See Figures S8.8 and S8.9.

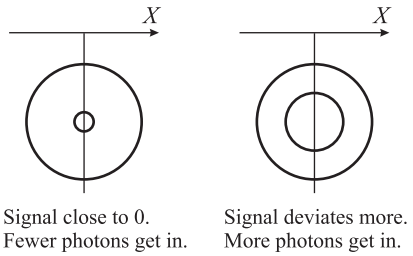

Figure S8.8 See Problem 8.18(b).

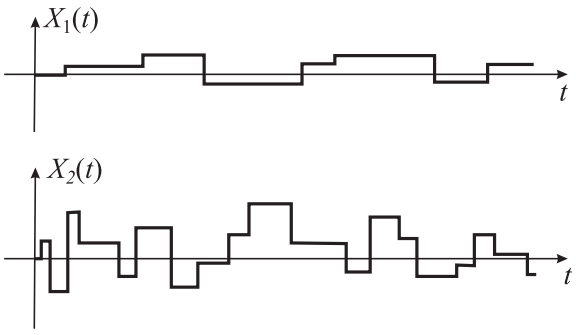

Figure S8.9 See Problem 8.18(b).

(c) With the larger hole we may get multiple photons occasionally—pulse pileup. Also, their rate will be higher for same reason as X-signal.

(d) The sensitivity is given by

$$\text{sensitivity} = \left(\frac{kd^2}{l(d+h)} \right)^2 .$$

If we double the hole diameter and keep the sensitivity unchanged, we have

$$\left(\frac{kd^2}{l(d+h)} \right)^2 = \left(\frac{k(2d)^2}{l_2(2d+h)} \right)^2 \Rightarrow l_2 = \frac{4l(d+h)}{2d+h} \Rightarrow l_2 \approx 4l \,,$$

where d is the original diameter and $d \ll h$.

Solution 8.19

(a) A straightforward calculation yields

$$T = \frac{2,000,000 \text{ photons}}{64 \times 64 \text{ pixels} \times 4 \text{ photons/pixel s}} = 122.07 \text{ s} \,.$$

(b) The Z-pulse of two photons is shown in Figure S8.10. The output of the pulse height analyzer is shown in Figure S8.11.

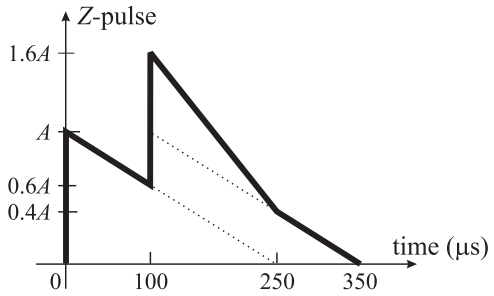

Figure S8.10 Z-pulse arising from two photons. See Problem 8.19(b).

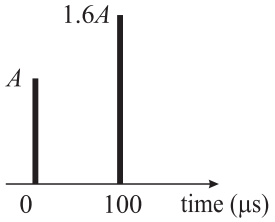

Figure S8.11 Output of the pulse height analyzer. See Problem 8.19(b).

(c) If the second photon arrives too soon after the first one, due to the pulse pileup, the output of the pulse height analyzer at the arrival time of the second photon will be larger than $1.2A$. Therefore, the second pulse will be rejected and will not result in an acceptable event.

In order for the second photon to be detectable, the peak voltage at the time when the second photon arrives cannot exceed $1.2A$, the voltage resulted from the first photon must be less than $0.2A$. Since the voltage drops linearly from the peak value A to 0 in 250 μs, it takes 200 μs for the voltage to drop to a value of $0.2A$. The time separation required in order for the second photon to be detected as a separate event is 200 μs.

(d) From part (c), we know that two successive photons must be separated by at least 200 μs in order to be detected as two events. So the maximal rate of arrival of photons is $\frac{1}{200\ \mu\ \mathrm{s}} = 5,000$ photons/s. This arrival rate is for the entire image (recall how Z-pulse is generated.) For each pixel, the arrival rate is at most $\frac{5{,}000}{64\times 64} = 1.22$ photons/s·pixel. This rate is smaller than 4 photons/s·pixel we used in part (a). So it is not possible to complete the experiment in the time we compute in part (a).

An alternative is as follows: we have a maximum rate of arrival of 5,000 photons/s. In 122.07 s, we can have at most $5,000 \times 122.07 \approx 610,000$ photons, which is less than the required number of photons to complete the experiment. So not possible.

(e) When an incident photon has undergone Compton scatter, it loses some energy. Under this condition, the photon might be rejected because its Z-pulse height is too small.

(f) On average each pixel is hit by $N = \frac{2{,}000{,}000\ \text{photons}}{64\times 64} = 488.28$ photons. So the intrinsic SNR in a single pixel is SNR $= \sqrt{N} = 22.1$.

Solution 8.20

(a) Rate of photons emitted from O $= 0.27 \times 10^{-3} \times 3.7 \times 10^{10} = 10^7$ photons/s. Assuming that the photons fly uniformly in the x-y plane, the rate of photons hitting the detector is

$$\frac{2\tan^{-1}(\frac{0.5}{0.5})}{2\pi} \times 10^7 = 0.25 \times 10^7 \text{ photons/s}\,.$$

(b) A straightforward calculation yields

$$\begin{aligned}
\text{detector efficiency} &= \text{fraction of photons blocked by the detector} \\
&= \frac{I_0 - I}{I_0} \\
&= \frac{I_0 - I_0 e^{-\mu b}}{I_0} \\
&= 1 - e^{-0.644\times 2.5} \\
&= 80.01\%\,.
\end{aligned}$$

(c) The Anger camera, on average, registers $0.8001 \times 0.25 \times 10^7$ events/s $= 0.2002 \times 10^7$ events/s. Hence, the time to register is 2×10^5 counts $= \frac{2\times 10^5}{0.2002\times 10^7} = 0.1$ s. Neglecting the time required to rotate the camera, 10 orientations can be captured in 1 s.

(d) The collimator resolution is

$$R_c = \frac{d}{l}\,(l + b + |z|) = \frac{0.005}{0.12}\,(0.12 + 0.025 + |0.5 - 0.12|) = 0.0219\ \mathrm{m} = 21.9\ \mathrm{mm}\,.$$

(e) Let x_n be the span on the detector within which photons can reach in the nth hole. For the central collimator hole, that is, $n = 0$, we have $x_0 = d$, since the photons can fall upon the entire detector length d. So the rate of photons hitting the central hole is

$$r_0 = \frac{2\tan^{-1}(\frac{0.005/2}{0.5})}{2\pi} \times 10^7 = 1.6 \times 10^4 \text{ photons/s}\,.$$

For $n > 0$, by the geometry we have the following relation

$$\begin{aligned}
\frac{d - x_n}{l} &= \frac{(n-1)(d+h) + h + 0.5d + (d - x_n)}{0.5}\,, \\
\frac{d - x_n}{l} &= 2[(n - 0.5)d + nh + d - x_n]\,, \\
d - x_n &= 2l[(n + 0.5)d + nh] - 2lx_n\,, \\
x_n(2l - 1) &= 2l[(n + 0.5)d + nh] - d\,, \\
x_n &= \frac{2l[(n + 0.5)d + nh] - d}{(2l - 1)}\,.
\end{aligned}$$

When $n = 1$, $x_1 = 2.63$ mm. So the rate of photons hitting the hole $n = 1$ is

$$r_1 = \frac{\tan^{-1}(\frac{d/2+h+d}{0.5}) - \tan^{-1}(\frac{d/2+h+d-x_1}{0.5})}{2\pi} \times 10^7 = 8.37 \times 10^3 \text{ photons/s}\,.$$

It is the same answer for $n = -1$.

(f) Evaluating x_n at $n = 2$, we get $x_2 = -0.5$ mm. So the collimator shadow completely covers the hole, that is, no photon is able to hit the detector from this hole. Therefore, the photons can enter only in the central three holes. Since the photons from a point source at the origin are spreading out into the central three collimator holes, the resolution, as defined by FWHM value, is $\hat{R}_c = \frac{3d+2h}{2} = 12.5$ mm. $\hat{R}_c$ is smaller than $R_c = 21.9$ mm computed in part (d), since R_c is computed with ideal geometry, neglecting the effects of septa.

Solution 8.21

(a) It is a straightforward calculation:

$$\begin{aligned}
R_c &= \frac{d}{l}(l + b + z) \\
&= \frac{3}{100}(100 + 25 + 0.5 \times 10^3) \\
&= 18.75 \text{ mm}\,.
\end{aligned}$$

(b) The intrinsic PSF is a Gaussian function with σ computed as follows

$$R_I = 0.2 \text{ mm} = 2\sigma\sqrt{2\ln 2} \quad \Rightarrow \quad \sigma = \frac{0.2}{2\sqrt{2\ln 2}} = 0.0849\,.$$

(c) The overall resolution is due to a cascade of systems; therefore,

$$R_{\text{overall}} = \sqrt{R_c^2 + R_I^2} = 18.75\,.$$

(d) The total count is 120×10^6.

(e) The local contrast is

$$C = \frac{\bar{N}_t - \bar{N}_b}{\bar{N}_b} = \frac{8-3}{3} = 1.667\,,$$

where $\bar{N}_t$ and $\bar{N}_b$ are mean target and background counts. The SNR is

$$\text{SNR}_{\text{local}} = C\sqrt{\bar{N}_b} = 2.89\,.$$

9

Emission Computed Tomography

SPECT

Solution 9.1

(a) For $|\ell| < 2$, we have

$$\begin{aligned}
g_{\mathrm{SPECT}}(\ell, 0^\circ) &= \int_{-\sqrt{4-\ell^2}}^{\sqrt{4-\ell^2}} f\exp\{-(\int_y^{\sqrt{4-\ell^2}} \mu_2 \mathrm{d}y' + \int_{\sqrt{4-\ell^2}}^{5} \mu_1 \mathrm{d}y')\}\mathrm{d}y \\
&= \int_{-\sqrt{4-\ell^2}}^{\sqrt{4-\ell^2}} f\exp\{-(\mu_2(\sqrt{4-\ell^2} - y) + \mu_1(5 - \sqrt{4-\ell^2}))\}\mathrm{d}y \\
&= f\exp\{-\mu_2(\sqrt{4-\ell^2})\}\exp\{-\mu_1(5 - \sqrt{4-\ell^2})\} \int_{-\sqrt{4-\ell^2}}^{\sqrt{4-\ell^2}} \exp\{\mu_2 y\}\mathrm{d}y \\
&= f\exp\{-\mu_2(\sqrt{4-\ell^2})\}\exp\{-\mu_1(5 - \sqrt{4-\ell^2})\}(\exp\{\mu_2\sqrt{4-\ell^2}\} - \exp\{-\mu_2\sqrt{4-\ell^2}\})/\mu_2 \\
&= \frac{f}{\mu_2}\exp\{-\mu_1(5 - \sqrt{4-\ell^2})\}(1 - \exp\{-\mu_2\sqrt{4-\ell^2}\})\,.
\end{aligned}$$

Thus,

$$g_{\mathrm{SPECT}}(\ell, 0^\circ) = \begin{cases} \frac{f}{\mu_2}\exp\{-\mu_1(5 - \sqrt{4-\ell^2})\}(1 - \exp\{-\mu_2\sqrt{4-\ell^2}\}) & |\ell| < 2 \\ 0 \quad \text{otherwise} \end{cases}$$

Similarly,

$$g_{\mathrm{SPECT}}(\ell, 180^\circ) = \begin{cases} \frac{f}{\mu_2}\exp\{-\mu_3(5 - \sqrt{4-\ell^2})\}(1 - \exp\{-\mu_2\sqrt{4-\ell^2}\}) & |\ell| < 2 \\ 0 \quad \text{otherwise} \end{cases}$$

(b) For $|\ell| < 2$, $g_{\rm PET}(\ell, 0^\circ) = g_{\rm PET}(-\ell, 180^\circ)$ and

$$\begin{aligned} g_{\rm PET}(\ell, 0^\circ) &= \int_{-\sqrt{4-\ell^2}}^{\sqrt{4-\ell^2}} f\exp\{-(\int_{-\sqrt{4-\ell^2}}^{\sqrt{4-\ell^2}} \mu_2 \mathrm{d}y' + \int_{\sqrt{4-\ell^2}}^{5} \mu_1 \mathrm{d}y' + \int_{-5}^{-\sqrt{4-\ell^2}} \mu_3 \mathrm{d}y')\}\mathrm{d}y \\ &= 2f\sqrt{4-\ell^2}\exp\{-\mu_3(5-\sqrt{4-\ell^2})\}\exp\{-\mu_1(5-\sqrt{4-\ell^2})\}\exp\{-2\mu_2\sqrt{4-\ell^2})\}\,. \end{aligned}$$

Thus,

$$g_{\rm PET}(\ell, 0^\circ) = \begin{cases} 2f\sqrt{4-\ell^2}\exp\{-\mu_3(5-\sqrt{4-\ell^2})\}\exp\{-\mu_1(5-\sqrt{4-\ell^2})\}\exp\{-2\mu_2\sqrt{4-\ell^2})\} & |\ell| < 2 \\ 0 \quad \text{otherwise} \end{cases}$$

$$g_{\rm PET}(\ell, 180^\circ) = \begin{cases} 2f\sqrt{4-\ell^2}\exp\{-\mu_3(5-\sqrt{4-\ell^2})\}\exp\{-\mu_1(5-\sqrt{4-\ell^2})\}\exp\{-2\mu_2\sqrt{4-\ell^2})\} & |\ell| < 2 \\ 0 \quad \text{otherwise} \end{cases}$$

(c) Substituting numerical values in the formulas found in (a) yields

$$\begin{aligned} g_{\rm SPECT}(0, 0^\circ) &= 0.2799\,\text{mCi/cm}^2\,, \\ g_{\rm SPECT}(0, 180^\circ) &= 0.3022\,\text{mCi/cm}^2\,. \end{aligned}$$

(d) Substituting numerical values in the formulas found in (b) yields

$$g_{\rm PET}(0, 0^\circ) = g_{\rm PET}(0, 180^\circ) = 0.0901\,\text{mCi/cm}^2\,.$$

Solution 9.2

(a) For $\theta = 180^\circ$, we see that will be a $g(\ell, 180^\circ)$ rect function with a magnitude determined from the SPECT imaging equation. The photon energy is 150KeV. For $|\ell| < 1$,

$$\begin{aligned} g(\ell, 180^\circ) &= \int_2^3 0.2e^{-\int_0^y \mu_s \mathrm{d}s}\mathrm{d}y + \int_0^2 0.4e^{-\int_0^y \mu_s \mathrm{d}s}\mathrm{d}y \\ &= \int_2^3 0.2e^{-\int_2^y 0.2\mathrm{d}s - \int_0^2 0.4\mathrm{d}s}\mathrm{d}y + \int_0^2 0.4e^{-\int_0^y 0.4\mathrm{d}s}\mathrm{d}y \\ &= 0.2 \times e^{-0.8} \times e^{0.4} \times \frac{1}{0.2}(e^{-0.4} - e^{-0.6}) + 0.4 \times \frac{1-e^{-0.8}}{0.4} \\ &= 0.0814 + 0.5507 \\ &= 0.6321\,. \end{aligned}$$

So $g(\ell, 180^\circ) = 0.6321 \times \text{rect}(\frac{\ell}{2})$.

Similarly, $g(\ell, 90^\circ)$ will be two rect functions, and magnitudes are to determined from SPECT equations.

$$\begin{aligned} g_1(\ell, 90^\circ) &= \int_{-1}^{1} 0.2e^{-\int_x^1 \mu_s \mathrm{d}s}\mathrm{d}x \\ &= \int_{-1}^{1} 0.2e^{-0.2(1-x)}\mathrm{d}x \\ &= 0.2 \times e^{-0.2}\int_{-1}^{1} e^{0.2x}\mathrm{d}x \\ &= 0.3297\,. \end{aligned}$$

$$\begin{aligned} g_2(\ell, 90^\circ) &= \int_{-1}^{1} 0.4e^{-\int_x^1 \mu_s \mathrm{d}s}\mathrm{d}x \\ &= \int_{-1}^{1} 0.4e^{-0.4(1-x)}\mathrm{d}x \\ &= 0.4 \times e^{-0.4}\int_{-1}^{1} e^{0.4x}\mathrm{d}x \\ &= 0.5507\,. \end{aligned}$$

So $g(\ell, 90^\circ) = 0.3297 \times \mathrm{rect}(\frac{\ell-1}{2}) + 0.5507 \times \mathrm{rect}(\ell - 2.5)$.

(b) For PET, the energy of photons is 511 keV. The magnitude of projection is given by

$$\begin{aligned} g(\ell, 0^\circ) &= \int_0^3 f(y)e^{-\int_0^3 \mu \mathrm{d}s}\mathrm{d}y \\ &= \int_0^3 f_1(y)e^{-\int_0^3 \mu \mathrm{d}s}\mathrm{d}y + \int_0^3 f_2(y)e^{-\int_0^3 \mu \mathrm{d}s}\mathrm{d}y \\ &= (0.2 \times 1 + 0.4 \times 2) + e^{-\int_0^3 \mu \mathrm{d}s}\mathrm{d}y \\ &= e^{-1\times 0.1 - 2\times 0.3} \\ &= 0.4966\,. \end{aligned}$$

So $g(\ell, 0^\circ) = 0.4966 \times \mathrm{rect}(\frac{\ell}{2})$.

(c) PET and SPECT imaging equations are given by

$$g_{\mathrm{SPECT}}(\ell, \theta) = \int_{-\infty}^{R} \frac{f(x(s), y(s))}{4\pi(s-R)^2}\exp\{-\int_y^R \mu(x(t), y(t); E)\mathrm{d}t\}\mathrm{d}s\,,$$

$$g_{\mathrm{PET}}(\ell, \theta) = K\int_{-R}^{R} f(x(s), y(s))\mathrm{d}s \times \exp\{-\int_{-R}^{R} \mu(x(s), y(s); E)\mathrm{d}s\}\,.$$

It is seen that the attenuation term containing μ is separable from activity term $f(x, y)$ in PET while it is not separable in SPECT. So prior to PET imaging, a CT scan of the patient is done and $\mu(x, y)$ is found by CT reconstruction. Then PET imaging is done to obtain $g(\ell, \theta)$. Thus, the line integral of activity is obtained by

dividing the PET projection by attenuation coefficients and Radon transform of A is given by

$$\begin{aligned} G(\ell,\theta) &= \int_{-R}^{R} f(x(s),y(s))\mathrm{d}s = \frac{g_{\mathrm{PET}}(\ell,\theta)}{\exp\{-\int_{-R}^{R}\mu(x(s),y(s);E)\mathrm{d}s\}}\,, \\ \Rightarrow f(x,y) &= \mathcal{R}^{-1}\{G(\ell,\theta)\}\,. \end{aligned}$$

where $\mathcal{R}$ denotes Radon transform. μ being not separable from SPECT equation, this technique is not applicable for attenuation correction of SPECT.

(d) If real collimators are used, the efficiency will be $< 100\%$. So less number of photons will be detected. So the height of the rect functions will be decreased.

Solution 9.3

(a) We have

$$\begin{aligned} \frac{1}{3}N_0 &= N_0 \cdot e^{-1\lambda_P}\,, \\ \frac{2}{3}N_0 &= N_0 \cdot e^{-1\lambda_Q}\,. \end{aligned}$$

Therefore,

$$\begin{aligned} \lambda_P &= \ln 3 \text{ hour}^{-1}\,, \\ \lambda_Q &= \ln 1.5 \text{ hour}^{-1}\,, \end{aligned}$$

and

$$\begin{aligned} t_{\frac{1}{2},P} &= \frac{0.693}{\ln 3} = 0.631 \text{ hour}\,, \\ t_{\frac{1}{2},Q} &= \frac{0.693}{\ln 1.5} = 1.709 \text{ hour}\,. \end{aligned}$$

(b) We have

$$\begin{aligned} A_P &= \frac{1}{3}N_0 \cdot \lambda_P = 0.366N_0 = 0.366 \times 10^{15}/3,600 \text{ dps} = 2.75 \text{ Ci}\,, \\ A_Q &= \frac{2}{3}N_0 \cdot \lambda_Q = 0.270N_0 = 0.270 \times 10^{15}/3,600 \text{ dps} = 2.03 \text{ Ci}\,. \end{aligned}$$

(c) Suppose the 180° projection in the object and the background are g_o and g_b, respectively. Then

$$\begin{aligned} g_o &= A_Q \cdot 2 + A_P \cdot 4 = 0.270 \times 2N_0 + 0.366 \times 4N_0 = 2.004N_0\,, \\ g_b &= A_P \cdot 6 = 0.366 \times 6N_0 = 2.196N_0\,. \end{aligned}$$

Therefore, the local contrast is

$$C = \frac{g_o - g_b}{g_b} = \frac{2.004N_0 - 2.196N_0}{2.196N_0} = -0.0874\,.$$

(d) Suppose the 180° projection in the object and the background considering linear attenuation are g'_o and g'_b, respectively. Then

$$\begin{aligned}
g'_o &= \int_3^6 A_P \cdot (e^{-(y-3)\cdot 1} \cdot e^{-1\cdot 1} \cdot e^{-2\cdot 2})\mathrm{d}y + \int_1^3 A_Q \cdot (e^{-(y-1)\cdot 2} \cdot e^{-1\cdot 1})\mathrm{d}y + \int_0^1 A_P \cdot (e^{-y\cdot 1})\mathrm{d}y \\
&= \int_3^6 A_P \cdot e^{-y-2}\mathrm{d}y + \int_1^3 A_Q \cdot e^{-2y+1}\mathrm{d}y + \int_0^1 A_P \cdot e^{-y}\mathrm{d}y \\
&= A_P \cdot e^{-2} \cdot (e^{-3} - e^{-6}) + A_Q \cdot e \cdot \frac{1}{2} \cdot (e^{-2} - e^{-6}) + A_P \cdot (e^0 - e^{-1}) \\
&= A_P \cdot (e^{-5} - e^{-8} + 1 - e^{-1}) + 0.5A_Q \cdot (e^{-1} - e^{-5}) \\
&= 0.366N_0 \cdot 0.639 + 0.5 \cdot 0.270N_0 \cdot 0.361 \\
&= 0.283N_0\,, \\
g'_b &= \int_0^6 A_P \cdot e^{-y\cdot 1}\mathrm{d}y \\
&= 0.366N_0 \cdot (1 - e^{-6}) \\
&= 0.365N_0\,.
\end{aligned}$$

Therefore, the local contrast is

$$C = \frac{g'_o - g'_b}{g'_b} = \frac{0.283N_0 - 0.365N_0}{0.365N_0} = -0.225\,.$$

(e) The absolute value of the local contrast would be bigger in 180° than that in 0°. First of all g'_b are the same on both projections. Second, $A_Q < A_P$ and $\mu_{\text{circle}} > \mu_{\text{square}}$. Therefore, inside the object, the radioactivity gets more attenuated in 180° than that in 0°. Thus g'_o in 180° is smaller than that in 0°, meaning g'_o is farther away from g'_b on 180° than that in 0°. Since we are considering the absolute value of the local contrast, $|C|$ would be bigger in 180° than that in 0°.

Solution 9.4

(a) First, we write

$$f(x,y) = \begin{cases} 0.5\ \mathrm{mCi/cm}^3 & |x| \le 1, y \le -x, \\ 0 & \text{otherwise.} \end{cases}$$

And

$$\mu(x,y) = \begin{cases} 0.1\ \mathrm{cm}^{-1} & |x| \le 1, |y| \le 1, y + x \le 0, \\ 0.2\ \mathrm{cm}^{-1} & |x| \le 1, |y| \le 1, y + x > 0, \\ 0 & \text{otherwise.} \end{cases}$$

For $|l| \leq 1$, the projection can be computed as

$$\begin{aligned} g_{\text{SPECT}}(l, 0^\circ) &= \int_{-1}^{-l} f\exp\{-\int_{y}^{-l} \mu_1 dy' - \int_{-l}^{1} \mu_2 dy'\} dy \\ &= \int_{-1}^{-l} f\exp\{-(-l-y)\mu_1 - (1+l)\mu_2\} dy \\ &= e^{-(1+l)\mu_2 + l\mu_1} \int_{-1}^{-l} f e^{\mu_1 y} dy \\ &= \frac{f}{\mu_1} e^{-(1+l)\mu_2 + l\mu_1} (e^{-l\mu_1} - e^{-\mu_1}) \\ &= 5e^{-0.1(2+l)} (e^{-0.1l)} - e^{-0.1)}) \\ &= 5(e^{-0.2(1+l)} - e^{-0.3-0.1l)}) \,. \end{aligned}$$

The final answer is

$$g_{\text{SPECT}}(l, 0^\circ) = 5(e^{-0.2(1+l)} - e^{-0.3-0.1l)}) \text{rect}(\frac{l}{2}) \,.$$

Similarly, for $|l| \leq 1$, $g_{\text{SPECT}}(l, 180^\circ)$ can be found as:

$$\begin{aligned} g_{\text{SPECT}}(l, 180^\circ) &= \int_{-1}^{l} f \exp\{-\int_{-1}^{y} \mu_1 dy'\} dy \\ &= \int_{-1}^{l} f e^{-(y+1)\mu_1} dy \\ &= f e^{-\mu_1} \int_{-1}^{l} e^{-\mu_1 y} dy \\ &= \frac{f}{\mu_1} e^{-\mu_1} (e^{\mu_1} - e^{-l\mu_1}) \\ &= 5(1 - e^{-(l+1)\mu_1}) \\ &= 5(1 - e^{-0.1(l+1)}) \,. \end{aligned}$$

The final answer is $g_{\text{SPECT}}(l, 180^\circ) = 5(1 - e^{-0.1(l+1)}) \text{rect}(\frac{l}{2})$.

(b) For $|l| \leq 1$,

$$\begin{aligned} g_{\text{PET}}(l, 0^\circ) &= \int_{-1}^{-l} f exp\{-\int_{-1}^{-l} \mu_1 dy' - \int_{-l}^{1} \mu_2 dy'\} dy \\ &= \int_{-1}^{-l} f e^{-(-l+1)\mu_1 - (1+l)\mu_2} dy \\ &= f e^{-((1-l)\mu_1 + (1+l)\mu_2)} \int_{-1}^{-l} dy \\ &= f(1-l) e^{-((1-l)\mu_1 + (1+l)\mu_2)} \\ &= 0.5(1-l) e^{-0.1(3+l)} \,. \end{aligned}$$

Thus, $g_{\rm PET}(l, 0^\circ) = 0.5(1-l)e^{-0.1(3+l)}{\rm rect}(\frac{l}{2})$. By the principle of PET imaging $g_{\rm PET}(l, 180^\circ) = g_{\rm PET}(-l, 0^\circ)$,

$$g_{PET}(l, 180^\circ) = 0.5(1+l)e^{-0.1(3-l)}{\rm rect}(\frac{l}{2})$$

(c) The attenuation term is separable from activity term in PET. And the attenuation term can be estimated by applying a CT scan prior to PET scan to get the activity term. Then the standard CT reconstruction method can be applied to correctly reconstruct the radioactivity distribution.

Solution 9.5

(a) Since N_{ij} is a Poisson random variable, the variance of N_{ij} is also $\bar{N}_{ij}$. The mean and the variance of g_{ij} are $k\bar{N}_{ij}$ and $k^2\bar{N}_{ij}$, respectively. Therefore,

$$\begin{aligned}
{\rm mean}[\hat{f}(x,y)] &= \frac{k\pi T}{M}\sum_{j=1}^{M}\sum_{i=-N/2}^{N/2}\bar{N}_{ij}\tilde{c}(x{\rm cos}\theta_j + y{\rm sin_j}\theta - iT)\,, \\
{\rm var}[\hat{f}(x,y)] &= \frac{k^2\pi^2T^2}{M^2}\sum_{j=1}^{M}\sum_{i=-N/2}^{N/2}\bar{N}_{ij}[\tilde{c}(x{\rm cos}\theta_j + y{\rm sin_j}\theta - iT)]^2\,.
\end{aligned}$$

(b) Carry out the following steps:

$$\begin{aligned}
& \frac{\pi}{M}\sum_{j=1}^{M}T\sum_{i=-N/2}^{N/2}[\tilde{c}(x{\rm cos}\theta_j + y{\rm sin_j}\theta - iT)]^2 \\
\approx\ & \int_0^\pi\int_{-\infty}^{\infty}[\tilde{c}(x{\rm cos}\theta + y{\rm sin}\theta - \ell)]^2{\rm d}\ell{\rm d}\theta \\
=\ & \pi\int_{-\infty}^{\infty}[\tilde{c}(\ell)]^2{\rm d}\ell \\
=\ & \pi\int_{-\infty}^{\infty}|C(\varrho)|^2{\rm d}\varrho \\
=\ & \pi\int_{-\varrho_0}^{\varrho_0}\varrho^2{\rm d}\varrho \\
=\ & \frac{2\pi\varrho_0^3}{3}\,.
\end{aligned}$$

(c) Substituting the result in (b) and simplifying yields

$$\begin{aligned}
{\rm var}[\hat{f}(x,y)] &= \frac{k^2\pi^2T^2\bar{N}}{M^2}\sum_{j=1}^{M}\sum_{i=-N/2}^{N/2}[\tilde{c}(x{\rm cos}\theta_j + y{\rm sin_j}\theta - iT)]^2 \\
&= \frac{2\pi^2k^2\varrho_0^3\bar{N}T}{3M}\,.
\end{aligned}$$

(d) ${\rm SNR} = \frac{{\rm mean}[\hat{f}(x,y)]}{\sqrt{{\rm var}[\hat{f}(x,y)]}} \propto \frac{\bar{N}}{\sqrt{\bar{N}}} = \sqrt{\bar{N}}$. So the ratio is $\sqrt{2}$.

PET

Solution 9.6

(a) Let the coordinate system be such that the upper left corner of the matrix is the origin. Consider a left-handed Cartesian coordinate system, so that the y axis is positive below the origin. Now the coordinates of the center of PMT(i,j) in inches are $(2(j-1)+1, 2(i-1)+1)$. Similarly, the coordinates of the center of subcrystal C(k,l) are $(0.5(l-1)+1, 0.5(k-1)+0.25)$. Hence, the distance between the centers of PMT(i,j) and subcrystal (k,l) is:

$$\begin{aligned} r &= \sqrt{[2(j-1)+1-0.5(l-1)-0.25]^2 + [2(i-1)+1-0.5(k-1)-0.25]^2}, \\ &= \sqrt{(2j-0.5l-0.75)^2 + (2i-0.5k-0.75)^2}. \end{aligned}$$

Hence, The PMT response is

$$\text{PMT}(i,j) = e^{-\sqrt{(2j-0.5l-0.75)^2+(2i-0.5k-0.75)^2}}.$$

(b) Given that $k=4$ and $l=5$, the above equation simplifies to:

$$\text{PMT}(i,j) = e^{-\sqrt{(2j-3.25)^2+(2i-2.75)^2}}.$$

Hence,

$$\begin{aligned} \text{PMT}(1,1) &= e^{-\sqrt{2.125}}, \\ \text{PMT}(1,2) &= e^{-\sqrt{1.125}}, \\ \text{PMT}(2,1) &= e^{-\sqrt{3.125}}, \\ \text{PMT}(2,2) &= e^{-\sqrt{2.125}}. \end{aligned}$$

(c) The responses in the 4 PMTs due to an event in crystal C(k,l) can be written as:

$$\begin{aligned} \text{PMT}(1,1) &= e^{-\sqrt{(1.25-0.5l)^2+(1.25-0.5k)^2}}, \\ \text{PMT}(1,2) &= e^{-\sqrt{(3.25-0.5l)^2+(1.25-0.5k)^2}}, \\ \text{PMT}(2,1) &= e^{-\sqrt{(1.25-0.5l)^2+(3.25-0.5k)^2}}, \\ \text{PMT}(2,2) &= e^{-\sqrt{(3.25-0.5l)^2+(3.25-0.5k)^2}}. \end{aligned}$$

Rearranging the equations:

$$\begin{aligned}
(1.25-0.5l)^2+(1.25-0.5k)^2 &= \left[\log\frac{1}{\text{PMT}(1,1)}\right]^2,\\
(3.25-0.5l)^2+(1.25-0.5k)^2 &= \left[\log\frac{1}{\text{PMT}(1,2)}\right]^2,\\
(1.25-0.5l)^2+(3.25-0.5k)^2 &= \left[\log\frac{1}{\text{PMT}(2,1)}\right]^2,\\
(3.25-0.5l)^2+(3.25-0.5k)^2 &= \left[\log\frac{1}{\text{PMT}(2,2)}\right]^2.
\end{aligned}$$

Subtracting the equations, we get:

$$\begin{aligned}
(3.25-0.5k)^2-(1.25-0.5k)^2 &= \left[\log\frac{1}{\text{PMT}(2,1)}\right]^2-\left[\log\frac{1}{\text{PMT}(1,1)}\right]^2,\\
9-2k &= \left[\log\frac{1}{\text{PMT}(2,1)}\right]^2-\left[\log\frac{1}{\text{PMT}(1,1)}\right]^2,\\
k &= 4.5-\frac{1}{2}\left\{\left[\log\frac{1}{\text{PMT}(2,1)}\right]^2-\left[\log\frac{1}{\text{PMT}(1,1)}\right]^2\right\}.
\end{aligned}$$

Similarly, an estimate of k can be obtained from PMT(1,2) and PMT(2,2) as:

$$k=4.5-\frac{1}{2}\left\{\left[\log\frac{1}{\text{PMT}(2,2)}\right]^2-\left[\log\frac{1}{\text{PMT}(1,2)}\right]^2\right\}.$$

Averaging the above two estimates of k, we get:

$$k=4.5-\frac{1}{4}\left\{\left[\log\frac{1}{\text{PMT}(2,1)}\right]^2-\left[\log\frac{1}{\text{PMT}(1,1)}\right]^2+\left[\log\frac{1}{\text{PMT}(2,2)}\right]^2-\left[\log\frac{1}{\text{PMT}(1,2)}\right]^2\right\}.$$

Similarly, an estimate of l can be obtained as:

$$l=4.5-\frac{1}{4}\left\{\left[\log\frac{1}{\text{PMT}(1,2)}\right]^2-\left[\log\frac{1}{\text{PMT}(1,1)}\right]^2+\left[\log\frac{1}{\text{PMT}(2,2)}\right]^2-\left[\log\frac{1}{\text{PMT}(2,1)}\right]^2\right\}.$$

(d) The worst-case scenario occurs when the event occurs very close to the boundary between two PMTs, for example, if an event occurs very close to the boundary between C(2,4) and C(2,5) but occurs in crystal C(2,4), then under noiseless condition, PMT(1,1) will be slightly greater than PMT(1,2). However if a small additive noise cause the signal $\text{PMT}(1,2) > \text{PMT}(1,1)$, then the event will be attributed to C(2,5).

Solution 9.7

(a) Since the detectors are designed to stop 75% of the photons, we have $0.75 = e^{-\mu d}$ where d is the detector

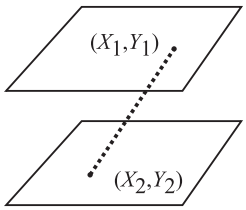

Figure S9.1 See Problem 9.8(c).

thickness. Hence we have

$$\begin{aligned} \text{for NaI(Tl)}: \quad d &= \ln 0.75/(-\mu) \\ &= (\ln 0.75)/(-0.343) \\ &= 0.8387 \text{ cm}, \\ \text{for BGO}: \quad d &= \ln 0.75/(-\mu) \\ &= (\ln 0.75)/(-0.964) \\ &= 0.2984 \text{ cm}. \end{aligned}$$

(b) The gamma rays photon burst is a random phenomena and can be modeled as a Poisson process. Let the average gamma ray photons arriving at the detector be λ. Let k be the fraction of these gamma ray photons converted into light photons by NaI(Tl). Since, BGO is 13% efficient, the fraction of gamma rays converted into light photons by BGO is 0.13k. Hence the intrinsic SNRs are:

$$\begin{aligned} \text{SNR}_{\text{NaI(tl)}} &= \sqrt{\lambda k}, \\ \text{SNR}_{\text{BGO}} &= \sqrt{0.13\lambda k}. \end{aligned}$$

The ratio of intrinsic SNR's is $\sqrt{1/0.13}$.

Solution 9.8

(a) No collimators. In a PET scanner, one must be able to detect coincidences at diverse angles.

(b) You would have to add a coincidence detector.

(c) Coincidence detections would be localized on each camera face using their X and Y pulses as shown in Figure S9.1. The line between the two detections would be calculated to show where the decay took place. The Z-pulse will be used in the calculation of the X and Y pulses. It could also be used for energy discrimination, as in a conventional PET scanner.

(d) From the geometry in Figure S9.2,

$$\alpha = \tan^{-1} \frac{0.15 \text{ m}}{0.75 \text{ m}} = 11.31^\circ.$$

(e) Consider reconstruction on a "central plane." There are many gamma rays that are "lost" between the two detectors in this geometry. In a conventional PET scanner, the plane is completely surrounded by detectors. Therefore, on this basis alone, we can expect that the total number of coincidence detections in a given time

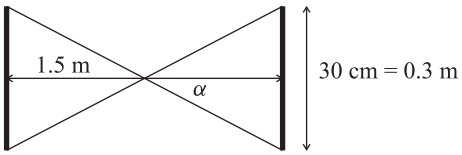

Figure S9.2 See Problem 9.8(d).

frame will be smaller given the same dose. Therefore, for the same quality, we would have to increase the dose. In addition to this argument, there is the fact that PET detectors are more efficient at stopping 511 keV photons. Therefore, the Anger-based camera will also be less efficient and also require a higher dose.

Solution 9.9

(a) Removing the constants in Eq. 9.6 but keeping the attenuation gives

$$g_{\rm SPECT}(\ell,\theta) = \int_{-\infty}^{\infty} f(x(s),y(s)) \exp\{-\int_{s}^{\infty} \mu(x(s'),y(s')ds'\}ds\,.$$

In this problem,

$$f(x,y) = \begin{cases} 0.3 \text{ mCi/cm}^3 & \text{if } 0 \le x \le 1, -3 \le y \le 3\,, \\ 0 & \text{otherwise}\,. \end{cases}$$

And,

$$\mu(x,y) = \begin{cases} 0.2 \text{ cm}^{-1} & \text{if } -3 \le x \le 0, -3 \le y \le 3\,, \\ 0.3 \text{ cm}^{-1} & \text{if } 0 \le x \le 1, -3 \le y \le 3\,, \\ 0.1 \text{ cm}^{-1} & \text{if } 1 \le x \le 3, -3 \le y \le 3\,, \\ 0 & \text{otherwise}\,. \end{cases}$$

When $\theta = 90°$, $x(s) = \ell\cos\theta - s\sin\theta = -s$, and $y(s) = \ell\sin\theta + s\cos\theta = \ell$. Hence,

$$\begin{aligned} g_{\rm SPECT}(\ell,90°) &= \int_0^1 0.3 \exp\{-\int_x^1 0.3dx' - \int_1^3 0.1dx'\}dx \\ &= e^{-0.1\times 2}\int_0^1 0.3e^{-0.3(1-x)}dx \\ &= e^{-0.5}(e^{0.3} - e^0) \\ &\approx 0.2122 \text{ mCi/cm}^2, \end{aligned}$$

for -3 cm $\le \ell \le 3$ cm. $g_{\rm SPECT}(\ell,90°) = 0$ if $\ell < -3$ cm, or $\ell > 3$ cm. Similarly,

$$\begin{aligned} g_{\rm SPECT}(\ell,270°) &= e^{-0.2\times 3}\int_0^1 f(x,\ell)e^{-0.3x}dx \\ &= e^{-0.2\times 3}\int_0^1 0.3e^{-0.3x}dx \\ &= e^{-0.6}(-e^{-0.3} + e^0) \\ &\approx 0.1422 \text{ mCi/cm}^2, \end{aligned}$$

for -3 cm $\leq \ell \leq 3$ cm. $g_{\rm SPECT}(\ell, 270^\circ) = 0$ if $\ell < -3$ cm, or $\ell > 3$ cm. Note that $g_{\rm SPECT}(\ell, 90^\circ) \neq g_{\rm SPECT}(\ell, 270^\circ)$.

(b) We have

$$\begin{aligned} g_{\rm PET}(\ell, 90^\circ) &= e^{-0.2\times 3} e^{-0.1\times 2} \int_0^1 f(x,\ell) e^{-0.3\times 1} dx \\ &= e^{-0.2\times 3 - 0.1\times 2 - 0.3\times 1} \int_0^1 0.3 dx \\ &= 0.3 e^{-1.1} \\ &\approx 0.0999 \text{ mCi/cm}^2, \end{aligned}$$

for -3 cm $\leq \ell \leq 3$ cm. $g_{\rm PET}(\ell, 90^\circ) = 0$ if $\ell < -3$ cm, or $\ell > 3$ cm. By the principle of PET imaging, $g_{\rm PET}(\ell, 270^\circ) = g_{\rm PET}(\ell, 90^\circ)$.

(c) It is clear that in PET imaging the attenuation factor does not depend on the location of the activity along the imaging line. Thus, to compensate for the attenuation effect of the object, one can image the object using a separate source to acquire the line integrals of $\mu(x, y)$. Then, the data can be corrected using

$$g^c_{\rm PET}(\ell, \theta) = \frac{g_{\rm PET}(\ell, \theta)}{\exp\{-\int_{-\infty}^{\infty} \mu(\ell\cos\theta - s\sin\theta, \ell\sin\theta - s\cos\theta) ds\}}.$$

The standard CT reconstruction method can then be applied on $g^c_{\rm PET}(\ell, \theta)$ to correctly reconstruct the radioactivity distribution. This compensation approach is not applicable for the SPECT scan.

Solution 9.10

(a) The perimeter of the circle is

$$\pi D = 1.5\pi \approx 4.712 \text{ m}.$$

The approximate detector width is thus

$$4.712 \text{ m}/1,000 = 4.712 \text{ mm}.$$

Shallow detectors are less efficient to stop the gamma photons, but incoming gamma photons from all directions can be equally detected. Deep detectors are more efficient, but they are more direction selective.

(b) Coincidence detection in PET is used to determine the direction of travel of the two back-to-back gamma photons, and hence to decide on which line the radioactivity occurs. Coincidence is assumed if two events occur within 2–12 ns in typical PET scanners. Since the radioactivity is not always occur at the center of the PET scanner, the traveling times of the two back-to-back gamma photons are not the same.

(i) If the time interval is too small, off-the-center radioactivities will not be detected.

(ii) If the time interval is too large, scattered photons will still be counted. Also, two or more distinct positron decays might be mixed together, and the line of coincidence can no longer be correctly determined.

(c) In the center of the scanner, $1,000/2 = 500$ detectors cover a range of $D = 1.5$m. Hence, the sampling interval is

$$T = D/500 = 1,500 \text{ mm}/500 = 3 \text{ mm}.$$

By the "rule of thumb", the number of pixels on one side of the image should be approximately equal to the number of samples for each projection angle. Since the number of samples is $1,000/2 = 500$ for the PET scanner, the PET image should have at least $500^2 = 250,000$ pixels. A "wobbling" motion of the PET gantry can reduce the effective spacing of the detectors and thus increase the resolution of the system.

(d) "Parallax errors" cause degradation of resolution farther away from the center. This is because events can be detected from oblique angles within the detector body (instead of end-on) which creates uncertainty about the actual line on which the event occurred.

Solution 9.11

(a) Suppose s_0 represents the center of the circle.

$$\exp\{-\int_{s_0}^{R}\mu(x(s'),y(s');E)\mathrm{d}s'\} = \frac{N^+}{N_0}\,,$$
$$\exp\{-\int_{-R}^{s_0}\mu(x(s'),y(s');E)\mathrm{d}s'\} = \frac{N^-}{N_0}\,.$$

The number of coincidence events N_c arising from positron annihilations at the center of the circle that will be detected is

$$\begin{aligned} N_c(s_0) &= N_0\exp\{-\int_{s_0}^{R}\mu(x(s'),y(s');E)\mathrm{d}s'\}\exp\{-\int_{-R}^{s_0}\mu(x(s'),y(s');E)\mathrm{d}s'\} \\ &= N_0\frac{N^+}{N_0}\frac{N^-}{N_0} = \frac{N^+N^-}{N_0}\,. \end{aligned}$$

(b) Carry out the following steps

$$\begin{aligned} g(\ell_1,0^\circ) &= \frac{2}{3}g(0,0^\circ)\,, \\ \int_0^6 f(\ell_1,y)e^{-6\mu_{\mathrm{square}}} &= \int_0^6 f(0,y)e^{-4\mu_{\mathrm{square}}-2\mu_{\mathrm{circle}}}\,, \\ -6\mu_{\mathrm{square}} &= -4\mu_{\mathrm{square}} - 2\mu_{\mathrm{circle}} + \ln\frac{2}{3}\,, \\ \mu_{\mathrm{square}} - \mu_{\mathrm{circle}} &= \frac{1}{2}\ln\frac{3}{2}\,. \end{aligned}$$

(c) Carry out the following steps

$$\begin{aligned} \frac{g(\ell_2,0^\circ)}{g(0,0^\circ} &= \frac{\int_0^6 f(\ell_2,y)e^{-5\mu_{\mathrm{square}}-\mu_{\mathrm{circle}}}}{\int_0^6 f(0,y)e^{-4\mu_{\mathrm{square}}-2\mu_{\mathrm{circle}}}} \\ &= e^{-\mu_{\mathrm{square}}+\mu_{\mathrm{circle}}} \\ &= e^{-\frac{1}{2}\ln\frac{3}{2}} \\ &= \sqrt{\frac{2}{3}} \\ &= 0.8165\,. \end{aligned}$$

(d) The local contrast is

$$\begin{aligned} C &= \frac{f_t - f_b}{f_b} \\ &= \frac{g(0,0^\circ) - g(\ell_1, 0^\circ)}{g(\ell_1, 0^\circ)} \\ &= \frac{g(0,0^\circ) - \frac{2}{3}g(0,0^\circ)}{\frac{2}{3}g(0,0^\circ))} \\ &= \frac{1/3}{2/3} \\ &= \frac{1}{2}\,. \end{aligned}$$

10

The Physics of Ultrasound

THE WAVE EQUATION

Solution 10.1

By taking the derivatives of $w_1(z,t)$ with respect to z and t, we have

$$\frac{\partial^2 w_1}{\partial z^2} = \xi''(z-ct), \quad \frac{\partial^2 w_1}{\partial t^2} = c^2\xi''(z-ct)\,.$$

It is obvious that

$$\frac{\partial^2 w_1}{\partial z^2} = \frac{1}{c^2}\frac{\partial^2 w_1}{\partial t^2}\,,$$

which is Equation (10.6). For $w_2(z,t) = \xi(z-ct) + \xi(z+ct)$, we have:

$$\frac{\partial^2 w_2}{\partial z^2} = \xi''(z-ct) + \xi''(z+ct)\,, \quad \frac{\partial^2 w_2}{\partial t^2} = c^2\xi''(z-ct) + c^2\xi''(z+ct)\,.$$

So, $w_2(z,t) = \xi(z-ct)+\xi(z+ct)$ is also a solution to the wave equation (10.6). $w_2(z,t) = \xi(z-ct)+\xi(z+ct)$ is the general solution to (10.6). It has two components, a forward-traveling wave $\xi(z-ct)$ and a backward-traveling wave $\xi(z+ct)$.

Solution 10.2

A sinusoidal plane wave is given as

$$p(z,t) = \cos[k(z-ct)]\,.$$

The wavelength is the spacing between crest. Suppose z_1, and z_2 are positions of two adjacent crests for a given time t, we have:

$$k(z_1 - ct) = 2n\pi, \quad k(z_2 - ct) = 2(n+1)\pi\,,$$

where n is an arbitrary integer. Then it is obvious

$$\lambda = z_2 - z_1 = 2\pi/k\,.$$

Solution 10.3

(a) The acoustic pulse is

$$\phi(t) = (1 - e^{-t/\tau_1})e^{-t/\tau_2}\,.$$

It reaches a peak when its derivative goes to zero; that is,

$$\frac{d\phi(t)}{dt} = e^{-t/\tau_2}(- - (t/\tau_1)e^{-t/\tau_1}) + (1 - e^{-t/\tau_1})(-t/\tau_2)e^{-t/\tau_2} = 0\,.$$

This leads to

$$\begin{aligned}(1 - e^{-t/\tau_1})(1/\tau_2) &= (1/\tau_1)e^{-t/\tau_1}\,,\\ 1 - e^{-t/\tau_1} &= (\tau_2/\tau_1)e^{-t/\tau_1}\,,\\ 1 &= (\tau_2/\tau_1 + 1)e^{-t/\tau_1}\,.\end{aligned}$$

Solving for t yields the time delay

$$t_d = -\tau_1 \ln \frac{1}{\tau_2/\tau_1 + 1}\,.$$

Plugging in $\tau_2 = \tau_1 = 5\ \mu$s yields $t_d = 3.5\ \mu$s. Therefore, the peak pressure will return to the transducer at $3.5 + 64.9 = 68.4\ \mu$s.

(b) The "generic" backward traveling wave is

$$\phi_b(z,t) = (1 - e^{-(t+z/c)/\tau_1})e^{-(t+z/c)/\tau_2}\,.$$

At time $t = 64.9\ \mu$s, this wave will be (begin) at position $z = 0.1$ m heading in the $-z$ direction. Incorporating both the temporal and spatial shift yields

$$\phi_b(z,t) = (1 - e^{-(t-64.9\ \mu\text{s}+(z-0.1\ \text{m})/c)/\tau_1})e^{-(t-64.9\ \mu\text{s}+(z-0.1\text{m}z)/c)/\tau_2}\,.$$

(c) It will take twice the time that it took to arrive at that range:

$$2 \times 64.9\ \mu\text{s} = 129.8\ \mu\text{s}\,.$$

Solution 10.4

The 3-D wave equation is

$$\nabla^2 = \frac{1}{c}\frac{\partial^2 p}{\partial t^2} \quad \text{where} \quad \nabla^2 = \frac{\partial^2 p}{\partial x_1^2} + \frac{\partial^2 p}{\partial x_2^2} + \frac{\partial^2 p}{\partial x_3^2}\,.$$

We have that

$$r^2 = x_1^2 + x_2^2 + x_3^2\,,$$

so

$$2r\frac{dr}{dx_i} = 2x_i \quad \Rightarrow \frac{dr}{dx_i} = \frac{x_i}{r}\,.$$

The new pressure function is $p = p(r, t)$. We have

$$\frac{\partial p}{\partial x_i} = \frac{\partial p}{\partial r}\frac{\partial r}{\partial x_i} = \frac{\partial p}{\partial r}\frac{x_i}{r},$$

and

$$\begin{aligned}
\frac{\partial^2 p}{\partial x_i^2} &= \frac{\partial}{\partial x_i}\left(\frac{\partial p}{\partial r}\frac{x_i}{r}\right) \\
&= \frac{\partial}{\partial x_i}\left(\frac{\partial p}{\partial r}\frac{1}{r}\right)x_i + \frac{1}{r}\frac{\partial p}{\partial r} \\
&= \frac{\partial}{\partial r}\left(\frac{1}{r}\frac{\partial p}{\partial r}\right)\frac{\partial r}{\partial x_i}x_i + \frac{1}{r}\frac{\partial p}{\partial r} \\
&= \frac{x_i^2}{r}\frac{\partial}{\partial r}\left(\frac{1}{r}\frac{\partial p}{\partial r}\right) + \frac{1}{r}\frac{\partial p}{\partial r}.
\end{aligned}$$

Therefore, using the fact that $r^2 = x_1^2 + x_2^2 + x_3^2$, we have

$$\nabla^2 p = \frac{3}{r}\frac{\partial p}{\partial r} + r\frac{\partial}{\partial r}\left(\frac{1}{r}\frac{\partial p}{\partial r}\right).$$

Now

$$\frac{\partial}{\partial r}(rp) = r\frac{\partial p}{\partial r} + p$$

and

$$\frac{\partial^2}{\partial r^2}(rp) = r\frac{\partial^2 p}{\partial r^2} + \frac{\partial p}{\partial r} + \frac{\partial p}{\partial r} = r\frac{\partial^2 p}{\partial r^2} + 2\frac{\partial p}{\partial r}.$$

So,

$$r\frac{\partial}{\partial r}\left(\frac{1}{r}\frac{\partial p}{\partial r}\right) = r\left[-\frac{1}{r^2}\frac{\partial p}{\partial r} + \frac{1}{r}\frac{\partial^2 p}{\partial r^2}\right] = \frac{-1}{r}\frac{\partial p}{\partial r} + \frac{\partial^2 p}{\partial r^2}.$$

Therefore,

$$\nabla^2 p = \frac{3}{r}\frac{\partial p}{\partial r} - \frac{1}{r}\frac{\partial p}{\partial r} + \frac{\partial^2 p}{\partial r^2} = \frac{2}{r}\frac{\partial p}{\partial r} + \frac{\partial^2 p}{\partial r^2} = \frac{1}{r}\frac{\partial^2}{\partial r^2}(rp).$$

This is the spherical wave equation.

Solution 10.5

Taking the derivatives of $w(r, t) = \xi(r - ct)/r$ with respect to t, we have:

$$\begin{aligned}
\frac{\partial w}{\partial t} &= -c\frac{\xi'(r - ct)}{r}, \\
\frac{\partial^2 w}{\partial t^2} &= c^2\frac{\xi''(r - ct)}{r}.
\end{aligned}$$

Taking the derivatives of $rw(r,t)$ with respect to r, we have:

$$\begin{aligned}\frac{\partial(rw)}{\partial r} &= \xi'(r-ct)\,,\\ \frac{\partial^2(rw)}{\partial r^2} &= \xi''(r-ct)\,.\end{aligned}$$

It can be seen that

$$\frac{1}{r}\frac{\partial^2}{\partial r^2}(rw) = \frac{1}{c^2}\frac{\partial^2 w}{\partial t^2}\,.$$

Solution 10.6

Substitute $p(r,t)$ into Equation 10.13, we have:

$$\frac{\partial^2}{\partial r^2}(rp) = \frac{1}{c^2}f''(t-c^{-1}r) + \frac{1}{c^2}g''(t+c^{-1}r)\,,$$

and

$$\frac{\partial^2 p}{\partial t^2}. = \frac{1}{r}f''(t-c^{-1}r) + \frac{1}{r}g''(t+c^{-1}r)\,.$$

So

$$\frac{1}{r}\frac{\partial^2}{\partial r^2}(rp) = \frac{1}{rc^2}(f''(t-c^{-1}r) + \frac{1}{r}g''(t+c^{-1}r)) = \frac{1}{c^2}\frac{\partial^2 p}{\partial t^2}\,,$$

and $p(r,t) = \frac{1}{r}f(t-c^{-1}r) + \frac{1}{r}g(t+c^{-1}r)$ is a solution to Equation 10.13.

WAVE PROPAGATION

Solution 10.7

$I(x,t) = v(x,t)p(x,t)$ and $I(0,t) = \text{Re}\{Ve^{j\omega t}\}\text{Re}\{Pe^{j\omega t}\}$. Let $V = V_m e^{j\phi}$ and $P = P_m e^{j\theta}$. Then

$$\begin{aligned}I(0,t) &= V_m\cos(\omega t+\phi)P_m\cos(\omega t+\theta)\\ &= \frac{V_m P_m}{2}[\cos(\phi-\theta)+\cos(2\omega t+\phi+\theta)]\end{aligned}$$

Therefore, since high frequency oscillations disappear,

$$I_{\text{av}} = \frac{V_m P_m}{2}\cos(\phi-\theta)\,.$$

But $VP^* = V_m P_m e^{j(\phi-\theta)}$. Therefore,

$$\frac{1}{2}\text{Re}\{VP^*\} = \frac{V_m P_m}{2}\cos(\phi-\theta) = I_{\text{av}}\,.$$

Solution 10.8

(a) Equations (10.25) and (10.26) are repeated here for convenience:

$$\frac{\cos\theta_t}{z_2}p_t + \frac{\cos\theta_r}{z_1}p_r = \frac{\cos\theta_i}{z_1}p_i\,,$$

$$p_t - p_r = p_i\,.$$

From these two equations, we can form a matrix equation as:

$$\begin{bmatrix} \frac{\cos\theta_t}{z_2} & \frac{\cos\theta_r}{z_1} \\ 1 & -1 \end{bmatrix} \begin{bmatrix} p_t \\ p_r \end{bmatrix} = \begin{bmatrix} \frac{\cos\theta_i}{z_1} \\ 1 \end{bmatrix} p_i\,.$$

Then we have

$$\begin{aligned} \begin{bmatrix} p_t \\ p_r \end{bmatrix} &= \begin{bmatrix} \frac{\cos\theta_t}{z_2} & \frac{\cos\theta_r}{z_1} \\ 1 & -1 \end{bmatrix}^{-1} \begin{bmatrix} \frac{\cos\theta_i}{z_1} \\ 1 \end{bmatrix} p_i \\ &= \frac{\begin{bmatrix} -1 & -\frac{\cos\theta_r}{z_1} \\ -1 & \frac{\cos\theta_t}{z_2} \end{bmatrix}}{\left(-\frac{\cos\theta_t}{z_2} - \frac{\cos\theta_r}{z_1}\right)} \begin{bmatrix} \frac{\cos\theta_i}{z_1} \\ 1 \end{bmatrix} p_i \\ &= \begin{bmatrix} \frac{z_2\cos\theta_i + z_2\cos\theta_r}{z_1\cos\theta_t + z_2\cos\theta_r} \\ \frac{z_2\cos\theta_i - z_1\cos\theta_t}{z_1\cos\theta_t + z_2\cos\theta_r} \end{bmatrix} p_i\,. \end{aligned}$$

Since $\theta_r = \theta_i$, we have

$$\begin{bmatrix} p_t \\ p_r \end{bmatrix} = \begin{bmatrix} \frac{2z_2\cos\theta_i}{z_1\cos\theta_t + z_2\cos\theta_i} \\ \frac{z_2\cos\theta_i - z_1\cos\theta_t}{z_1\cos\theta_t + z_2\cos\theta_i} \end{bmatrix} p_i\,.$$

The pressure reflectivity R and pressure transmittivity T are given by

$$\begin{aligned} R &= \frac{p_r}{p_i} = \frac{z_2\cos\theta_i - z_1\cos\theta_t}{z_1\cos\theta_t + z_2\cos\theta_i} \\ T &= \frac{p_t}{p_i} = \frac{2z_2\cos\theta_i}{z_1\cos\theta_t + z_2\cos\theta_i}\,. \end{aligned}$$

(b) We write

$$R_I = \frac{I_r}{I_i} = \frac{p_r^2/z_1}{p_i^2/z_1} = \frac{p_r^2}{p_i^2} = R^2 = \left(\frac{z_2\cos\theta_i - z_1\cos\theta_t}{z_1\cos\theta_t + z_2\cos\theta_i}\right)^2\,,$$

which is Equation (10.29). Also,

$$T_I = \frac{I_t}{I_i} = \frac{p_t^2/z_2}{p_i^2/z_1} = \frac{z_1 p_t^2}{z_2 p_i^2} = \frac{z_1}{z_2}T^2 = \frac{4z_1 z_2\cos^2\theta_i}{(z_2\cos\theta_i + z_1\cos\theta_t)^2}\,,$$

which is Equation (10.30).

Solution 10.9

(a) We have

$$P_1 = \frac{1}{r_1} f(t - c^{-1} r_1)\,,$$
$$P_2 = \frac{1}{r_2} f(t - c^{-1} r_2)\,,$$

where

$$r_1 = \sqrt{x^2 + y^2 + (z+d)^2}\,,$$
$$r_2 = \sqrt{x^2 + y^2 + (z-d)^2}\,.$$

From the geometry, we see that for large r, $r_1 \approx r + d\cos\theta$ and $r_2 \approx r - d\cos\theta$, where θ is the angle off the z-axis to the line connecting the origin with (x, y, z), and r is the length of that line. But $\cos\theta = z/r$. Therefore,

$$P = P_1 + P_2 \approx \frac{1}{r_1} f\left(t - c^{-1}\left(r + \frac{dz}{r}\right)\right) - \frac{1}{r_2} f\left(t - c^{-1}\left(r - \frac{dz}{r}\right)\right)\,.$$

But

$$f(t) = \mathrm{Re}\{\tilde{n}(t) e^{j2\pi f_0 t}\}\,,$$

and $r_1 \approx r_2$ (for amplitude). Hence, the complete waveform is

$$P_c \approx \frac{1}{r}\tilde{n}(t - c^{-1}r) e^{j2\pi f_0 (t - c^{-1}r)} (e^{-jk\frac{dz}{r}} - e^{+jk\frac{dz}{r}}),$$

where we have used the steady-state approximation for $\tilde{n}$.

But $e^{j\Phi} - e^{-j\Phi} = 2j\sin\Phi$, so

$$e^{-jk\frac{dz}{r}} - e^{+jk\frac{dz}{r}} = -2j\sin k\frac{dz}{r}\,.$$

As d gets very small, $\sin(kdz/r) \approx kdz/r$, therefore, since $-j = e^{-j\pi/2}$,

$$P_c \approx 2kde^{-j\pi/2}\frac{z}{r^2}\tilde{n}(t - c^{-1}r) e^{j2\pi f_0 (t - c^{-1}r)}\,.$$

One can see that the new pressure is given by

$$P = \frac{z}{r^2} f_n(t - c^{-1}r)\,,$$

where

$$f_n(t - c^{-1}r) = \mathrm{Re}\{2kde^{-j\pi/2}\tilde{n}(t - c^{-1}r) e^{j2\pi f_0 (t - c^{-1}r)}\}\,.$$

(b) See Figure S10.1.

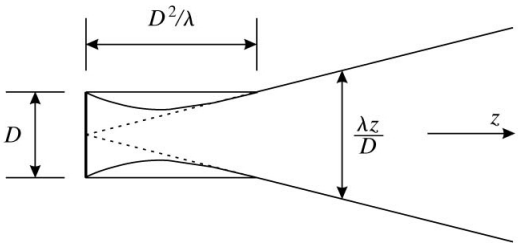

Figure S10.1 Field pattern. See Problem 10.9(b).

Solution 10.10

(a) The acoustic pressure of an outward propagating spherical wave is expressed as:

$$p(r,t) = \frac{A_0}{r}\phi_0(t - c^{-1}r)\,,$$

where $r = \sqrt{x^2 + y^2 + z^2}$. When there is attenuation, the expression becomes:

$$p(r,t) = e^{-\mu_a r}\frac{A_0}{r}\phi_0(t - c^{-1}r)\,.$$

(b) Let

$$d = \sqrt{x^2 + y^2 + z^2}$$

be the distance between the wave source and the scatter. Assume the reflection coefficient of the scatter is R. The scatter acts like a new point source. So the scattered wave can be expressed as

$$p_s(x', y', z', t) = \frac{Re^{-\mu_a r'}}{r'}A_0 e^{-\mu_a d}\phi_0(t - c^{-1}r - c^{-1}d),$$

where $r' = \sqrt{(x' - x)^2 + (y' - y)^2 + (z' - z)^2}$ is the distance between the scatter and any point (x', y', z') in space.

(c) For a point source located at (x_0, y_0, z_0), the acoustic pressure is:

$$p(x', y', z', t) = e^{-\mu_a r}\frac{A_0}{r}\phi_0(t - c^{-1}r)\,,$$

where $r = \sqrt{(x' - x_0)^2 + (y' - y_0)^2 + (z' - z_0)^2}$. The scattered wave by a scatter at (x, y, z) is

$$p_s(x', y', z', t) = \frac{Re^{-\mu_a r'}}{r'}A_0 e^{-\mu_a d}\phi_0(t - c^{-1}r - c^{-1}d)\,,$$

where $r' = \sqrt{(x' - x)^2 + (y' - y)^2 + (z' - z)^2}$ and $d = \sqrt{(x_0 - x)^2 + (y_0 - y)^2 + (z_0 - z)^2}$ is the distance between the wave source and the scatter.

Solution 10.11

(a) The acoustic intensity is related to the acoustic pressure by

$$I = p^2/Z\,.$$

So the acoustic intensity for the incident wave, the reflected wave, and the transmitted wave are:

$$\begin{aligned} I_i &= p_i^2/Z_1\,, \\ I_r &= p_r^2/Z_1\,, \\ I_t &= p_t^2/Z_2\,. \end{aligned}$$

The intensity reflectivity and intensity transmittivity are:

$$R_I = \frac{I_r}{I_i} = \frac{p_r^2 Z_1}{p_i^2 Z_1} = \left(\frac{Z_2\cos\theta_i - Z_1\cos\theta_t}{Z_2\cos\theta_i + Z_1\cos\theta_t}\right)^2\,,$$

$$T_I = \frac{I_t}{I_i} = \frac{p_t^2 Z_2}{p_i^2 Z_1} = \frac{4Z_1Z_2\cos^2\theta_i}{\left(Z_2\cos\theta_i + Z_1\cos\theta_t\right)^2}\,.$$

(b) Carry out the following steps:

$$\begin{aligned} T - R &= \frac{2Z_2\cos\theta_i - (Z_2\cos\theta_i - Z_1\cos\theta_t)}{Z_2\cos\theta_i + Z_1\cos\theta_t} \\ &= \frac{Z_2\cos\theta_i + Z_1\cos\theta_t}{Z_2\cos\theta_i + Z_1\cos\theta_t} = 1\,. \end{aligned}$$

(c) The pressure must be continuous across the interface

$$p_t - p_r = p_i\,.$$

Therefore, $T - R = 1$. But the relationship between acoustic pressure and acoustic intensity is a nonlinear relationship and $Z_2 \neq Z_1$. So $T_I \neq 1 + R_I$ in general. From the above derivation, we have:

$$R_I = R^2, \quad T_I = T^2 Z_1/Z_2, \quad \text{and} \quad T = R + 1\,.$$

So the relationship between T_I and R_I is

$$T_I = \frac{Z_1}{Z_2}\left(\sqrt{R_I} + 1\right)^2\,.$$

DOPPLER EFFECT

Solution 10.12

The frequency f_R of the sound received by the moving receiver can be derived by considering the time it takes for the receiver to observe two successive crests. If the source is producing a sinusoid with frequency f_0, the distance separating two adjacent crests is $\lambda = c/f_0$. Since the receiver is moving towards the source, the time it takes for

the receiver to observe two successive crests is $T = \lambda/(c+v) = c/(c+v)f_0$, which is the observed period. So the frequency observed is $f_R = (c+v)f_0/c$.

When the receiver moves away from the source with speed v, the frequency observed is $f_R = (c-v)f_0/c$.

Solution 10.13

(a) The observed frequency will be $f_R = (c+v)f_0/c$ and $f_R = (c-v)f_0/c$ for receivers moving towards and away from the source, respectively.

(b) When the receivers moves towards the source, the observed frequency will be $f_R = 2f_0$. When the receivers moves away from the source, the observed frequency is 0. In this situation, the receiver will sit on a point with constant phase, therefore will not observe the wave.

(c) When the receivers moves towards the source, the observed frequency will be $f_R = (c+v)f_0/c$. When the receivers moves away from the source, the observed frequency is $f_R = (c-v)f_0/c < 0$. In this situation, the receiver will observe a wave from the opposite direction with frequency $f_R = |c-v|f_0/c$.

ULTRASOUND FIELD PATTERN

Solution 10.14

By using the properties of Fourier transform, we have:

$$\mathcal{F}\{\tilde{n}(t)\} = e^{j\phi}N_e(\omega)\,,$$

$$\text{Re}\{\tilde{n}(t)e^{-j\omega_0 t}\} = \frac{1}{2}\left[\tilde{n}(t)e^{-j\omega_0 t} + \tilde{n}^*(t)e^{j\omega_0 t}\right]\,,$$

where * denotes complex conjugate. The Fourier transform of $n(t)$ is:

$$\mathcal{F}\{n(t)\} = \frac{1}{2}\left[e^{j\phi}N_e(\omega+\omega_0) + e^{-j\phi}N_e^*(-\omega+\omega_0)\right]\,.$$

Solution 10.15

(a) We have

$$\begin{aligned}\alpha_{5\text{ MHz}} &= 8.7\mu_a = 8.7\times 0.04\text{ cm}^{-1}\cdot\text{ MHz}^{-1}\times 5\text{ MHz} = 1.74\text{ dB}\cdot\text{ cm}^{-1}\,,\\ \alpha_{12\text{MHz}} &= 8.7\mu_a = 8.7\times 0.04\text{ cm}^{-1}\cdot\text{ MHz}^{-1}\times 12\text{ MHz} = 4.176\text{ dB}\cdot\text{ cm}^{-1}\,.\end{aligned}$$

(b) It is considered as far field when range is greater than D^2/λ. The speed of sound is 1,560 m/s. At 5 MHz, the wavelength is $\lambda_{5\text{ MHz}} = 0.312$ mm. At 12 MHz, the wavelength is $\lambda_{12\text{ MHz}} = 0.13$ mm.

For the 5 MHz transducer, when range is greater than $\frac{2\text{cm}\times 2\text{cm}}{0.312\text{ mm}} = 128.2$ cm, it is considered as far field. For the 12 MHz transducer, the range is $\frac{0.4\text{ cm}\times 0.4\text{ cm}}{0.13\text{ mm}} = 12.3$ cm.

Solution 10.16

(a) The time it takes to travel from $(x_0, y_0, 0)$ to d and back is

$$t = \frac{2}{c}\sqrt{x_0^2 + y_0^2 + d^2}\,.$$

Therefore, the time delay is

$$\tau = \frac{2}{c}\sqrt{x_m^2 + y_m^2 + d^2} - \frac{2}{c}\sqrt{x_0^2 + y_0^2 + d^2}\,.$$

In this way, the scattering from d will be integrated over the (flat) transducer face at the same time upon reception. Using the binomial approximation,

$$\begin{aligned}
\tau &= \frac{2}{c}\left[d\sqrt{1 + \frac{x_m^2 + y_m^2}{d^2}} - d\sqrt{1 + \frac{x_0^2 + y_0^2}{d^2}}\right] \\
&\approx \frac{2}{c}\left[d[1 + \frac{x_m^2 + y_m^2}{d^2}] - d[1 + \frac{x_0^2 + y_0^2}{d^2}]\right] \\
&\approx \frac{2}{dc}\left[r_m^2 - (x_0^2 + y_0^2)\right]\,.
\end{aligned}$$

(b) The narrowband assumption is

$$n(t) = \mathrm{Re}\{\tilde{n}(t)e^{-j2\pi f_0 t}\}\,.$$

When shifted in time, and using the steady-state approximation:

$$\begin{aligned}
n(t-\tau) &= \mathrm{Re}\{\tilde{n}(t-\tau)e^{-j2\pi f_0(t-\tau)}\} \\
&\approx \mathrm{Re}\{\tilde{n}(t)e^{-j2\pi f_0(t-\tau)}\}\,.
\end{aligned}$$

Therefore, after some simplification

$$\begin{aligned}
&n(t - \tau - c^{-1}r_0 - c^{-1}r_0') \\
&\quad\approx \mathrm{Re}\{\tilde{n}(t - 2c^{-1}z)e^{j\frac{k}{d}r_m^2}e^{-j\frac{k}{d}(x_0^2+y_0^2)}e^{jk(r_0-z)}e^{jk(r_0'-z)}\}\,.
\end{aligned}$$

$e^{j\frac{k}{d}r_m^2}$ is just a fixed phase, which can be "thrown" into $\tilde{n}(t - 2c^{-1}z)$. Now split up terms:

$$\underbrace{e^{-j\frac{k}{2d}(x_0^2+y_0^2)}e^{jk(r_0-z)}}_{\mathrm{transmitpattern}}\underbrace{e^{-j\frac{k}{2d}(x_0^2+y_0^2)}e^{jk(r_0'-z)}}_{\mathrm{receivepattern}}\,,$$

which leads to the field pattern

$$q(x,y,z) \approx \iint \frac{s(x_0,y_0)}{z}e^{-j\frac{k}{2d}(x_0^2+y_0^2)}e^{j\frac{k}{2d}[(x-x_0)^2+(y-y_0)^2]}\,dx_0\,dy_0\,,$$

where the the paraxial approximation was also used. Expanding the terms as follows

$$(x-x_0)^2 = x^2 - 2xx_0 + x_0^2 \quad \text{and} \quad (y-y_0)^2 = y^2 - 2yy_0 + y_0^2\,,$$

and setting $z = d$, yields

$$\begin{aligned} q(x,y,d) &= \iint \frac{s(x_0,y_0)}{z} e^{j\frac{k}{2d}(x^2+y^2)} e^{-j\frac{k}{d}(xx_0+yy_0)}\, dx_0\, dy_0 \\ &= \frac{1}{z} e^{j\frac{k}{2d}(x^2+y^2)} S\left(\frac{x}{\lambda d}, \frac{y}{\lambda d}\right), \end{aligned}$$

which is the desired result.

(c) The far-field pattern exists at d now. When d is made smaller, the pattern gets tighter; therefore, we can increase our resolution at the focal point over that of a flat transducer. The spread, after the focal point, however, will increase. Therefore, we need to choose the focal distance carefully.

Solution 10.17

(a) We have

$$q_0(x,y,z) = \frac{1}{z} e^{jk(x^2+y^2)/(2z)} S(\frac{x}{\lambda z}, \frac{y}{\lambda z}).$$

And

$$s(x,y) = \mathrm{rect}(\frac{x}{w})\,\mathrm{rect}(\frac{y}{h}),$$

$$S(u,v) = \mathcal{F}\{s(x,y)\} = wh\,\mathrm{sinc}(wu)\,\mathrm{sinc}(hv).$$

Thus,

$$q_0(x,y,z) = \frac{wh}{z} e^{jk(x^2+y^2)/(2z)}\,\mathrm{sinc}(\frac{wx}{\lambda z})\,\mathrm{sinc}(\frac{hy}{\lambda z}).$$

(b) We have

$$\mathrm{sinc}(v) = \frac{\sin \pi v}{\pi v},$$

and the first zero is when $v = 1$. Hence, $\frac{wx}{\lambda z} = 1$, $x = \lambda z/w = s$, and thus

$$z_0 = \frac{sw}{\lambda}.$$

(c) $z_0 \geq D^2/\lambda$, where D is maximum dimension of the transducer. Since $h > w$, $D \approx h$, and $z_0 \geq h^2/\lambda$, or $sw/\lambda \geq h^2/\lambda$. Hence,

$$s \geq \frac{h^2}{w}.$$

If one says $D = \sqrt{h^2 + w^2}$, then $s \geq (w^2 + h^2)/w$.

(d) The field pattern simply shifts in x for each of the five elements and adds (since everything is linear).

$$\begin{aligned} q(x,y,z) &= \sum_{n=-2}^{+2} q_0(x - ns, y, z) \\ &= \sum_{n=-2}^{+2} \frac{wh}{z} e^{j\frac{k}{2z}((x-ns)^2+y^2)}\,\mathrm{sinc}\left(\frac{w(x-ns)}{\lambda z}\right)\mathrm{sinc}\left(\frac{hy}{\lambda z}\right). \end{aligned}$$

(e) Because the central pattern goes to zero at $\pm s$, it also goes to zero at $\pm ns$ for $n \neq 0$. Hence beam-width in the x direction is $6s$. In the y direction, $\mathrm{sinc}(hy/\lambda z)$ gives the pattern. The first zero is at

$$\frac{hy}{\lambda z} = 1\,,$$

which gives $y = \lambda z/h$. The beam-width is twice that, and hence the beam-width in y direction is

$$\frac{2\lambda z_0}{h} = \frac{2\lambda}{h}\frac{sw}{\lambda} = \frac{2sw}{h}\,.$$

11

Ultrasound Imaging Systems

ULTRASOUND IMAGE FORMATION AND IMAGING MODES

Solution 11.1

(a) From Table 10.1, we know that $Z_1 = 1.52 \times 10^{-6}$ kgm^{-2}s^{-1} and $Z_2 = 1.35 \times 10^{-6}$ kgm^{-2}s^{-1}. Assume z_0 is far away. Therefore the only return is from point $(0, 0, z_0)$ on the interface. Therefore, $\theta_r = \theta_i = \theta_t = 0$; $\cos\theta_r = \cos\theta_i = \cos\theta_t = 1$.

$$P_r = \frac{Z_2 - Z_1}{Z_2 + Z_1} P_i \approx -0.06 P_i \,.$$

We can neglect the minus sign because of envelope detection. When transducer axis is in direction θ, the strength of P_i at $(0, 0, z_0)$ depends on the field pattern. The transducer face in the x-z plane is $s(x) = \text{rect}(\frac{x}{L})$. Therefore,

$$S(u) = L\,\text{sinc}(Lu)\,,$$

and

$$S\left(\frac{z_0 \sin\theta}{\lambda z_0 \cos\theta}\right) = S\left(\frac{\tan\theta}{\lambda}\right) = L\,\text{sinc}\left(\frac{L\tan\theta}{\lambda}\right)$$

describes off-axis field pattern. Pulse-echo squares this; hence, the strength of the return is

$$P_r(\theta) = 0.06 A_0 \left[S(\frac{\tan\theta}{\lambda})\right]^2 = 0.06 A_0 L^2\,\text{sinc}^2(L\tan\theta/\lambda)\,.$$

(b) The signal P_r is above threshold when

$$20\log_{10}\left(\frac{0.06 A_0\,\text{sinc}^2(L\tan\theta/\lambda)}{A_0}\right) \geq -80\text{dB}\,,$$

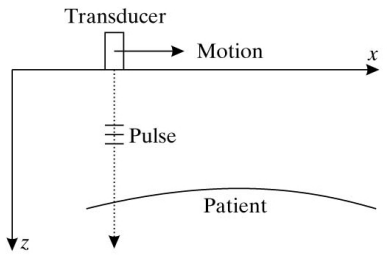

Figure S11.1 B-mode image. See Problem 11.1(b).

or $\text{sinc}^2(L\tan\theta/\lambda) \geq 0.001667$. Letting $u = \frac{L\tan\theta}{\lambda}$ we get

Sidelobe	$u =$	$\text{sinc}^2(u) =$
Main lobe	0	1
1st	1.5	0.045
2nd	2.5	0.0162
3	3.5	0.00827
4	4.5	0.005004
5	5.5	0.0033
6	6.5	0.0023
7	7.5	0.0018
8	8.5	0.0014
9	9.5	0.0011
10	10.5	0.0009

Thus, the system will "see" 7 sidelobes on each side. Since

$$\begin{aligned} u &= \frac{L\tan\theta}{\lambda} = \frac{Lz_0\tan\theta}{\lambda z_0} \\ &= \frac{2Lx'}{\lambda z_0}, \end{aligned}$$

the sidelobe separation is $x' = \frac{\lambda z_0}{2L}$. See Figure S11.1 for a sketch of the B-mode image.

Solution 11.2

(a) The echo is received at

$$t = \frac{2x}{c} = \frac{2 \times 10 \text{ cm}}{1,500 \text{ m/s}} \approx 1.33 \times 10^{-4} \text{ s}\,.$$

The round trip distance is 20 cm. Since $\alpha = 1$ dB/cm, there is a loss of 20 dB:

$$-20 \text{ dB} = 20\log_{10}\frac{A_z}{A_0}\,.$$

Thus, $A_z = 0.1A_0 = 1.225$ N/cm^2. See Figure S11.2 for a sketch of the A-mode signal.

(b) See Figure S11.3 for a sketch of the M-mode signal.

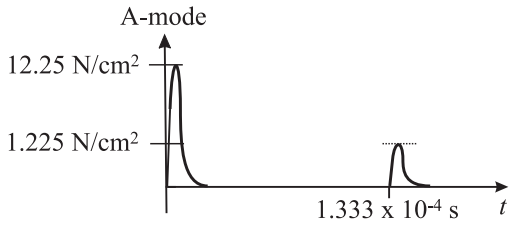

Figure S11.2 A-mode signal. See Problem 11.2(a).

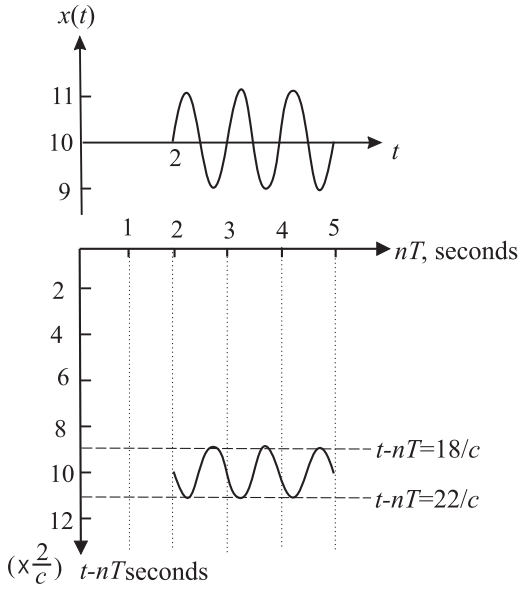

Figure S11.3 M-mode image. See Problem 11.2(b).

(c) See Figure S11.4 for a sketch of the B-mode image and Figure S11.5 for a sketch of the peak-height of the returning signal.

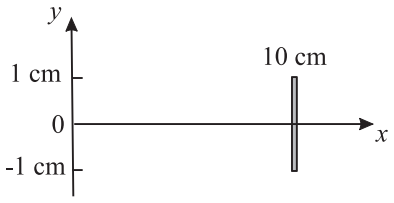

Figure S11.4 B-mode image. See Problem 11.2(c).

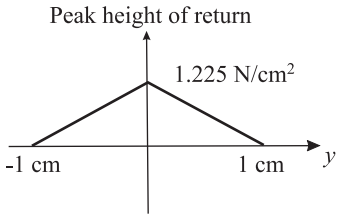

Figure S11.5 Peak-height plot. See Problem 11.2(c).

Solution 11.3

(a) See Figure S11.6.

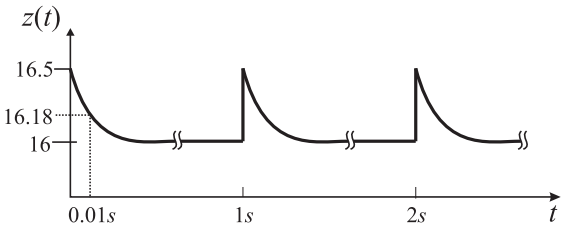

Figure S11.6 $z(t)$. See Problem 11.3(a).

(b) The pulse will be at range $z = ct$ at time t. The valve will be at range $z = 16 + 0.5e^{-t/\tau}$ at time t. At time $t = t_0$, they coincide. So we have:

$$\begin{aligned} ct &= 16 + 0.5e^{-t/\tau}\,, \\ 154,000t &= 16 + 0.5e^{-t/0.01}\,. \end{aligned}$$

Ignore the motion effect, we have $t_0 \approx \frac{16}{154,000} = 0.104$ ms. See Figure S11.7.

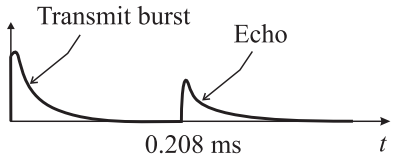

Figure S11.7 A-mode signal. See Problem 11.3(b).

(c) See Figure S11.8.

(d) Each scan line takes about 0.208 ms and ten scan lines take about 2.08 ms. Since the time constant is 10 ms, there will be five images in this time. So the time is adequate to make a B-mode image. (However, we won't be able to see this real time.)

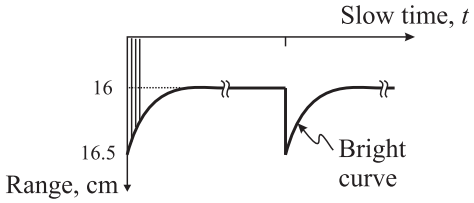

Figure S11.8 M-mode signal. See Problem 11.3(c).

Solution 11.4

Ignore the field pattern in x and y directions and assume the scatterers are ideal point scatterers, $R(x,y,z) = \delta(z-z_1) + \delta(z-z_2)$. In Fraunhofer field, the approximation of the received field is given by (11.20):

$$\hat{R}(x,y,z) = \left| R(x,y,z)e^{j2kz} \ast\ast\ast \left[S\left(\frac{x}{\lambda z}, \frac{y}{\lambda z}\right)\right]^2 n_e\left(\frac{z}{c/2}\right)\right| .$$

Ignoring $S\left(\frac{x}{\lambda z}, \frac{y}{\lambda z}\right)$, we have

$$\begin{aligned}
\hat{R}(x,y,z) &= \left| R(x,y,z)e^{j2kz} \ast\ast\ast\ n_e\left(\frac{z}{c/2}\right)\right| \\
&= \left| \left[\delta(z-z_1)e^{j2kz_1} + \delta(z-z_2)e^{j2kz_2}\right] \ast\ast\ast\ \mathrm{rect}\left(\frac{z}{\lambda}+\frac{1}{2}\right)\right| \\
&= \left| \mathrm{rect}\left(\frac{z-z_1}{\lambda}+\frac{1}{2}\right)e^{j2kz_1} + \mathrm{rect}\left(\frac{z-z_2}{\lambda}+\frac{1}{2}\right)e^{j2kz_2}\right| .
\end{aligned}$$

(a) Since $z_2 - z_1 = \lambda/2$, we have

$$\begin{aligned}
\hat{R}(x,y,z) &= \left| \mathrm{rect}\left(\frac{z-z_1}{\lambda}+\frac{1}{2}\right)e^{j2kz_1} + \mathrm{rect}\left(\frac{z-z_2}{\lambda}+\frac{1}{2}\right)e^{j2k(z_1+\lambda/2)}\right| \\
&= \left| e^{j2kz_1}\left[\mathrm{rect}\left(\frac{z-z_1}{\lambda}+\frac{1}{2}\right) + \mathrm{rect}\left(\frac{z-z_2}{\lambda}+\frac{1}{2}\right)e^{jk\lambda}\right]\right| \\
&= \mathrm{rect}\left(\frac{z-z_1}{\lambda}+\frac{1}{2}\right) + \mathrm{rect}\left(\frac{z-z_2}{\lambda}+\frac{1}{2}\right) .
\end{aligned}$$

(b) If $z_2 - z_1 = \lambda/8$, we have

$$\begin{aligned}
\hat{R}(x,y,z) &= \left| \mathrm{rect}\left(\frac{z-z_1}{\lambda}+\frac{1}{2}\right)e^{j2kz_1} + \mathrm{rect}\left(\frac{z-z_2}{\lambda}+\frac{1}{2}\right)e^{j2k(z_1+\lambda/8)}\right| \\
&= \left| \mathrm{rect}\left(\frac{z-z_1}{\lambda}+\frac{1}{2}\right) + \mathrm{rect}\left(\frac{z-z_2}{\lambda}+\frac{1}{2}\right)e^{jk\lambda/4}\right| \\
&= \left| \mathrm{rect}\left(\frac{z-z_1}{\lambda}+\frac{1}{2}\right) + j\,\mathrm{rect}\left(\frac{z-z_2}{\lambda}+\frac{1}{2}\right)\right| .
\end{aligned}$$

The estimated reflectivities are shown in Figure S11.9.

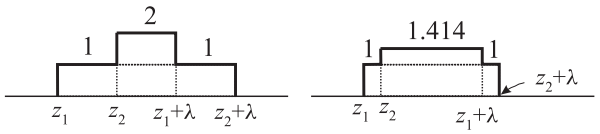

(a) $z_2 - z_1 = 1/2$ (b) $z_2 - z_1 = 1/8$

Figure S11.9 Estimated reflectivities. See Problem 11.4.

ULTRASOUND TRANSDUCER ARRAY

Solution 11.5

(a) From the geometry in Figure 10.5, the widest angle (from the axis) at which an ultrasound transducer will generate sound is defined by

$$\tan\theta = \frac{d/2}{d^2/\lambda}\,.$$

Using the relation $\lambda = c/f$ and the fact that $\theta = 30^\circ$ yields

$$\begin{aligned}\tan\theta = 0.5773502 &= \frac{1,540\text{ m/s}}{f\,0.2\text{ mm}}\,.\\ f &= \frac{1,540\text{ m/s}}{0.5773502 \times 0.0002\text{ m}}\\ &= 13.336\text{ MHz}\,.\end{aligned}$$

Any frequency higher than this will be more directive and incapable of generating a wave at $\theta = 30^\circ$.

(b) The zeroth transducer fires at time 0. The first transducer fires at

$$\begin{aligned}t_1 &= \frac{d\sin\theta}{c}\\ &= \frac{0.0002\text{ m} \times \sin 30^\circ}{1,540\text{ m/s}}\\ &= 64.9 \times 10^{-9}\text{ s}\,.\end{aligned}$$

This is the same time delay between each pair of transducers. Since there are 100 delays needed to fire 101 transducers the total time is

$$\text{time to fire array} = 100 \times 64.9 \times 10^{-9}\text{ s} = 6.49 \times 10^{-6}\text{ s}\,.$$

Solution 11.6

(a) We have

$$\begin{aligned} t_i &= \frac{id\sin\theta}{c} \\ &= \frac{0.6 \text{ mm}}{1,540 \times 10^3 \text{ mm/s}} i \sin\theta \\ &= (0.39\,\mu\text{s}) i \sin\theta\,. \end{aligned}$$

(b) The time it takes for one pulse to go to range R and back is the pulse repetition interval:

$$T_R = \frac{0.40 \text{ m}}{1,540 \text{ m/s}} = 260\,\mu\text{s}\,.$$

The total angle of the sector is 90°, and given $\Delta\theta = 1°$, we require 90 pulses in order to cover the field. Therefore, the total time it takes to acquire a frame is

$$T_F = 90 \times T_R = 23.4 \times 10^{-3}\text{s}\,.$$

The frame rate is therefore 42.8 frames/s, which will be flicker-free.

Solution 11.7

A diagram of the described transducer is given in Figure S11.10(a).

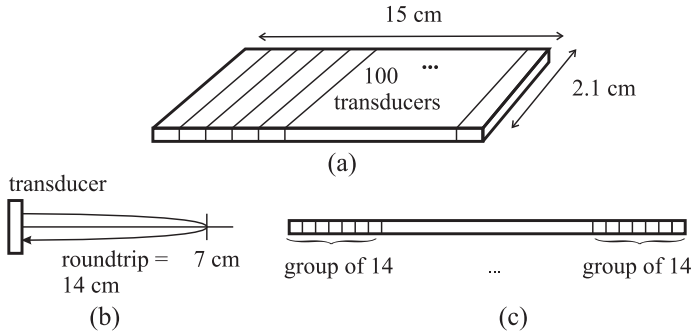

Figure S11.10 See Problem 11.7.

(a) Ranges $> D^2/\lambda$. Evaluate as follows

$$\begin{aligned} D &= 14 \times 1.5 \text{ mm} = 21 \text{ mm (same as width of transducer)}\,, \\ \lambda &= \frac{c}{f} = \frac{1,500 \text{ m/s}}{3.0 \times 10^6 s^{-1}} = 500 \times 10^{-6} \text{ m} = 0.5 \text{ mm}\,, \\ \frac{D^2}{\lambda} &= \frac{21^2 \text{ mm}^2}{0.5 \text{ mm}} = 882 \text{ mm}\,. \end{aligned}$$

Therefore,

$$\text{Ranges} > 0.882 \text{ m}\,.$$

(b) As shown in Figure S11.10(b), the total travel is 14 cm $= 0.14$ m. Therefore,

$$\Delta t = \frac{0.14 \text{ m}}{1,500 \text{m/s}} = 93.3 \mu \text{s} \, .$$

(c) The situation is depicted in Figure S11.10(c). The total number of distinct groups (which is therefore the number of lines of acquisition) is $100 - 14 + 1 = 87$. One A-mode burst takes this long:

$$\Delta t = \frac{40 \text{ cm}}{1,500 \text{ m/s}} = \frac{0.4 \text{ m}}{1,500 \text{ m/s}} = 266.7 \ \mu \text{s} \, .$$

Therefore, the total time to acquire one image is

$$87 \times 266.7 \ \mu \text{s} = 23.2 \text{ ms/frame} \, ,$$

and the frame rate is

$$\text{Frame Rate } = \frac{1}{23.2 \text{ ms}} = 43.1 \text{ frames/s} \, .$$

(d) One can increase the frequency of the transducer or acquire fewer lines—e.g., just acquire 40 lines from the center of the transducer.

Solution 11.8

(a) The transmit pulse is shown in Figure S11.11(a). An echo from a silicone-skin interface assuming normal incidence is shown in Figure S11.11(b). The amplitude of this echo is

$$\text{Amplitude } = \frac{Z_{\text{skin}} - Z_{\text{silicone}}}{Z_{\text{skin}} + Z_{\text{silicone}}} = \frac{1.5 \times 10^6 - 1.4 \times 10^6}{1.5 \times 10^6 + 1.4 \times 10^6} = 0.0345 \, .$$

The time of echo is:

$$\text{Time of Echo } = \frac{2 \times 2 \times 10^{-3}}{1,500} = 2.666 \times 10^{-6} \text{ s} = 2.6 \ \mu \text{s} \, .$$

Figure S11.11(c) shows the superposition of these two signal envelopes on the same graph. The A-mode signal is not simply the sum of the two A-mode signals since the underlying signals are sinusoidal. In general, there will be constructive or destructive interference. In the region of overlap, the actual signal is:

$$\cos(2\pi f t) + 0.0345 \cos(2\pi f (t - t_1)) \, ,$$

where $f = 2.0 \times 10^6$ Hz and $t_1 = 2.666 \times 10^{-6}$ s. Using the complex representation of sinusoids (phasors), it can be shown that the amplitude of this signal is 1.011. The corresponding A-mode signal is shown in Figure S11.11(d).

(b) $C(\text{gel}) = C(\text{skin}) = 1,550$ m/s for no refraction at the gel-skin interface.

(c) The pressure transmittivity at the silicone-gel interface assuming normal incidence is

$$T_1 = \frac{2Z(\text{gel})}{Z(\text{gel}) + Z(\text{silicone})} \, ,$$

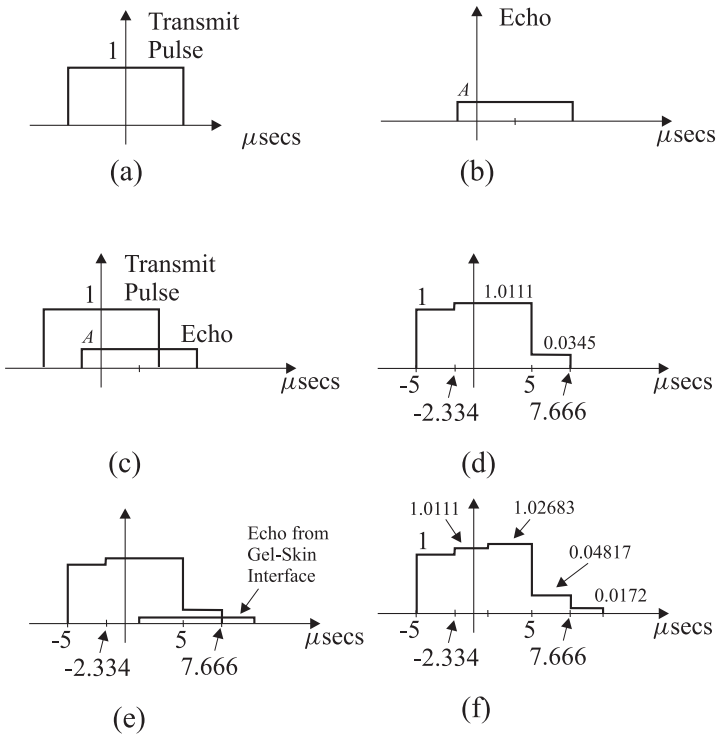

Figure S11.11 See Problem 11.8.

where

$$Z(\text{gel}) = 10^6\sqrt{1.5 \times 1.4} = 1.4491 \times 10^6\,.$$

This wave gets reflected at the gel-skin interface, where the pressure reflectivity is

$$R_2 = \frac{Z(\text{skin}) - Z(\text{gel})}{Z(\text{skin}) + Z(\text{gel})}\,.$$

The above reflected wave gets transmitted back through the gel-silicone interface where the pressure transmittivity is

$$T_3 = \frac{2Z(\text{silicone})}{Z(\text{gel}) + Z(\text{silicone})}\,.$$

The amplitude of the echo from the gel-skin interface (and incident on the transducer) is

$$1 \times T_1 \times R_2 \times T_3 = 0.0172\,.$$

The time of this echo is

$$t_2 = \frac{2s}{c(\text{silicone})} + \frac{2g}{c(\text{gel})} = 6.537\ \mu\text{s}\,.$$

This echo is superposed on the previous composite signal in Figure S11.11(e). The A-mode signal magnitude

for two new overlapping intervals needs to be worked out. The first interval has three overlapping signals:

$$\cos(2\pi ft) + 0.0345\cos(2\pi f(t-t_1)) + 0.0172\cos(2\pi f(t-t_2))\,,$$

where t_2 is given above. The magnitude of this wave is 1.02683. In the second overlapping region, the wave is given by

$$0.0345\cos(2\pi f(t-t_1)) + 0.0172\cos(2\pi f(t-t_2))\,,$$

and the resulting magnitude is 0.04817.

(d) The amplitude of the echo from the skin is 0.0172, while the initial amplitude is 1. Therefore,

$$\begin{aligned} L &= 20\log_{10} 0.0172 \\ &= -35.289 \text{ dB}\,. \end{aligned}$$

The sign of L is negative because it is an attenuation or loss. Normally, we say that the system is sensitive to $L = 35.289$ dB loss.

(e) $c = f\lambda$. So,

$$\lambda = \frac{c(\text{skin})}{2 \text{ MHz}} = \frac{1,550 \text{ m/s}}{2\times 10^6 \text{ s}^{-1}} = 7.75\times 10^{-4} \text{ m}\,.$$

Then,

$$\frac{D^2}{\lambda} = \frac{(3\times 10^{-3} \text{ m})^2}{7.75\times 10^{-4} \text{ m}} = 0.0116 \text{ m} = 1.16 \text{ cm}\,.$$

Therefore, point F is in the far field because 5 cm $>$ 1.16 cm.

(f) There are three relevant distances, d_L, d_C, and d_R, corresponding to the distances from point F to the left, center, and right transducers, respectively. These are:

$$\begin{aligned} d_L &= \sqrt{(5\times 10^{-2} + 8\times 10^{-3})^2 + (10\times 10^{-2})^2}\,, \\ d_C &= \sqrt{(5\times 10^{-2})^2 + (10\times 10^{-2})^2}\,, \\ d_R &= \sqrt{(5\times 10^{-2} - 8\times 10^{-3})^2 + (10\times 10^{-2})^2}\,. \end{aligned}$$

Now define:

$$\begin{aligned} \tau_L &= \frac{d_C - d_L}{c(\text{skin})} = \frac{0.1118 - 0.1156}{1,550} = -2.435\ \mu\text{s}\,, \\ \tau_C &= 0\,, \\ \tau_R &= \frac{d_C - d_R}{c(\text{skin})} = \frac{0.1118 - 0.1085}{1,550} = 2.129\ \mu\text{s}\,. \end{aligned}$$

Since we can't have negative times, add $-\tau_L$ to all values, yielding

$$\begin{aligned} \tau_L &= 0\,, \\ \tau_C &= 2.45\ \mu\text{s}\,, \\ \tau_R &= 4.579\ \mu\text{s}\,. \end{aligned}$$

ULTRASOUND IMAGING SYSTEM DESIGN AND IMAGE QUALITY

Solution 11.9

(a) Assuming the reflection coefficient of the line object is R_0, the mathematical expression for the scatter is

$$R(x,y,z) = R_0\delta(x, z-5)\,.$$

(b) The wavelength in the media at $f = 2.5$ MHz is

$$\lambda = c/f = 0.062\,\text{cm}\,.$$

The range at which the beam changes from geometric/Fresnel to far field is

$$z_0 = D^2/\lambda = 16.2\,\text{cm}\,.$$

Since the transducer face is a square, the transition between geometric field and the Fresnel field occurs at $D^2/2\lambda = 8.1$ cm. The scatter is located at a range of $z = 5$ cm. So the geometric assumption applies here. The estimated reflectivity is:

$$\begin{aligned}
\hat{R}(x,y,z) &= K\left|R_0\delta(x,z-5)e^{j2kz} * * * \tilde{s}(x,y)n_e\left(\frac{z}{c/2}\right)\right| && \text{(S11.1)}\\
&= K\left|R_0e^{j2k5}\delta(x,z-5) * * * \text{rect}(x,y)n_e\left(\frac{z}{c/2}\right)\right| && \text{(S11.2)}\\
&= KR_0\left|\delta(x,z-5) * * * \text{rect}(x,y)n_e\left(\frac{z}{c/2}\right)\right| && \text{(S11.3)}\\
&= KR_0\left|\text{rect}(x)n_e\left(\frac{z-5}{c/2}\right)\right|\,, && \text{(S11.4)}
\end{aligned}$$

where $\tilde{s}(x,y) = s(-x,-y) = \text{rect}(x,y)$ is the transducer face indicator function and $n_e\left(\frac{z}{c/2}\right)$ is the envelop of the narrowband pulse.

(c) From above, we see that at range $z = 5$ cm, in order to distinguish two line scatters at same range that are parallel to the y-axis, we need to have them separated by at least 1 cm, which is the width of the transducer.

(d) At range $z = 20$ cm, the scatter is in the far field, we need to use Fraunhofer assumption. The estimated reflectivity is:

$$\begin{aligned}
\hat{R}(x,y,z) &= \left|R(x,y,z)e^{j2kz} * \left[S\left(\frac{x}{\lambda z},\frac{y}{\lambda z}\right)\right]^2 n_e\left(\frac{z}{c/2}\right)\right| && \text{(S11.5)}\\
&= \left|R_0\delta(x,z-20)e^{j2kz} * \left[S\left(\frac{x}{\lambda z},\frac{y}{\lambda z}\right)\right]^2 n_e\left(\frac{z}{c/2}\right)\right| && \text{(S11.6)}\\
&= R_0\left|\delta(x,z-20) * \left[S\left(\frac{x}{\lambda z},\frac{y}{\lambda z}\right)\right]^2 n_e\left(\frac{z}{c/2}\right)\right|\,, && \text{(S11.7)}
\end{aligned}$$

where $S(u,v)$ is the Fourier transform of the face shape indicator function $s(x,y) = \text{rect}(x,y)$:

$$S(u,v) = \text{sinc}(u)\,\text{sinc}(v)\,.$$

We have:

$$\hat{R}(x,y,z) = R_0 \,\mathrm{sinc}^2\left(\frac{x}{\lambda(z-20)}\right) n_e\left(\frac{z-20}{c/2}\right) \int_{-\infty}^{\infty} \mathrm{sinc}^2\left(\frac{y}{\lambda(z-20)}\right) dy\,.$$

From the above, for a fixed z, the term that determines the minimal separation of two parallel line scatters at same range is

$$\mathrm{sinc}^2\left(\frac{x}{\lambda(z-20)}\right).$$

In order to resolve two line scatters, they must be separated by at least a distance $2d$, such that

$$\mathrm{sinc}^2\left(\frac{d}{\lambda(z-20)}\right) < 0.5\,.$$

The resolution depends on the depth.

Solution 11.10

Issues: Depth of penetration, Azimuth resolution, Speckle. First,

$$d_p = \frac{L}{2af} = \frac{100\mathrm{dB}}{2\times 1\times f} = \frac{50}{f(\mathrm{MHz})}.$$

If $f = 5$ MHz, $d_p = 10$ cm. Hence $f = 5$ MHz is ruled out. Let d_G denote the depth for geometric imaging. Then $d_G = D^2/\lambda$.

Let BW denote the beamwidth at 20 cm. In particular, BW_G denotes the beamwidth from the geometric approximation, BG_S beamwidth when using a square transducer, and BG_C is the beamwidth if using a circular transducer. Then,

$$BW_G = \begin{cases} D & \text{if } z \le D^2/\lambda \\ \frac{\lambda z}{D} & \text{if } z > D^2/\lambda. \end{cases}$$

$$BW_S = \begin{cases} D & \text{if } z \le D^2/2\lambda \\ \frac{\lambda z}{D} & \text{if } z > D^2/2\lambda. \end{cases}$$

$$BW_C = \begin{cases} D & \text{if } z \le D^2/4\lambda \\ \frac{\lambda z}{D} & \text{if } z > D^2/4\lambda. \end{cases}$$

Put these results into a chart:

	$f = 1$ MHz	$f = 2$ MHz
$D = 1$ cm	$d_p = 50$ cm	$d_p = 25$ cm
	$\lambda = 0.15$ cm	$\lambda = 0.075$ cm
	$d_G = 6.67$ cm	$d_G = 13.33$ cm
	$BW_G = 3.0$ cm	$BW_G = 1.5$ cm
	$BW_S = 3.0$ cm	$BW_S = 1.5$ cm
	$BW_C = 3.0$ cm	$BW_C = 1.5$ cm
$D = 2$ cm	$d_p = 50$ cm	$d_p = 25$ cm
	$\lambda = 0.15$ cm	$\lambda = 0.075$ cm
	$d_G = 26.67$ cm	$d_G = 53.33$ cm
	$BW_G = 2.0$ cm	$BW_G = 2.0$ cm
	$BW_S = 1.5$ cm	$BW_S = 2.0$ cm
	$BW_C = 1.5$ cm	$BW_C = 0.75$ cm

There can be several choices:

- To get the best resolution for geometric imaging, one should choose $D = 1$ cm, $f = 2$ MHz;
- To get the best resolution if using circular transducer, one should choose $D = 2$ cm, $f = 2$ MHz;
- To get the best resolution if using square transducer, one should choose $D = 1$ cm, $f = 2$ MHz.

Solution 11.11

(a) Given an $L \times L$ transducer, we have:

$$s(x, y) = \text{rect}\left(\frac{x}{L}\right) \text{rect}\left(\frac{y}{L}\right) .$$

For, the first point scatter, we have,

$$R(x, y, z) = \delta(x)\delta(y)\delta(z - z0) .$$

Hence, in the region, where geometric assumptions hold, we have

$$\begin{aligned} R'(x, y, z) &= K\left[R(x, y, z)e^{j2kz} * * * s(x, y)n_e\left(\frac{z}{c/2}\right)\right] \\ &= KR\left[\delta(x) * \text{rect}\left(\frac{x}{L}\right)\right]\left[\delta(y) * \text{rect}\left(\frac{y}{L}\right)\right]\left[e^{j2kz}\delta(z - z_0) * \text{sinc}\left(\frac{2\pi z}{c\Delta T}\right)\right] \\ &= KRe^{j2kz_0} \text{rect}\left(\frac{x}{L}\right) \text{rect}\left(\frac{y}{L}\right) \text{sinc}\left(\frac{2\pi(z - z_0)}{c\Delta T}\right) . \end{aligned}$$

Similarly, for the second scatter we have:

$$R'(x, y, z) = KRe^{j2kz_0} \text{rect}\left(\frac{x}{L}\right) \text{rect}\left(\frac{y}{L}\right) \text{sinc}\left(\frac{2\pi(z - z_0 - \Delta Z)}{c\Delta T}\right) .$$

(b) This part involves computing FWHM of a sinc function, which cannot be solved analytically. It involves transcendental equations, which require numerical solutions. But, note that the FWHM of the sinc can be approximated by the distance from the origin to the first zero the sinc.

(c) If $S(u,v)$ is the Fourier transform of $s(x,y)$, we have

$$S(u,v) = L^2 \operatorname{sinc}(Lu) \operatorname{sinc}(Ly) .$$

Using the far field approximation, we have:

$$\begin{aligned} R'(x,y,z) &= R\delta(x)\delta(y)\delta(z-z_0)e^{j2kz} * * * \left[S\left(\frac{x}{\lambda z}, \frac{y}{\lambda z}\right)\right]^2 \operatorname{sinc}\left(\frac{2\pi z}{c\Delta T}\right) \\ &= R\delta(z-z_0)e^{j2kz} * \left[S\left(\frac{x}{\lambda z}, \frac{y}{\lambda z}\right)\right]^2 \operatorname{sinc}\left(\frac{2\pi z}{c\Delta T}\right) \\ &= RL^4 e^{j2kz_0} \operatorname{sinc}^2\left(L\frac{x}{\lambda z}\right) \operatorname{sinc}^2\left(L\frac{y}{\lambda z}\right) \operatorname{sinc}\left(\frac{2\pi(z-z_0)}{c\Delta T}\right) . \end{aligned}$$

(d) This part involves computing FWHM of a sinc function.

Solution 11.12

(a) From the absorption coefficients in part (a) of Problem 10.15, we have

$$\begin{aligned} L_{5\text{MHz}} &= 40 \text{ cm} \times 1.74 \text{ dB} \cdot \text{cm}^{-1} = 69.6 \text{ dB} , \\ L_{12\text{MHz}} &= 40 \text{ cm} \times 4.176 \text{ dB} \cdot \text{cm}^{-1} = 167.04 \text{ dB} . \end{aligned}$$

(b) From the results of part (b) in Problem 10.15, range $z = 20$ cm is in the geometric region for the 5 MHz transducer, while it is in the far field for the 12 MHz transducer. So for the 5 MHz transducer, the beamwidth at 20-cm range equals the dimension of the transducer face, which is $w = 2$ cm. For the 12 MHz transducer, the beam width is $w = \frac{\lambda z}{D} = \frac{0.013 \text{ cm} \times 20 \text{ cm}}{0.4 \text{ cm}} = 0.65 \text{ cm}$.

(c) The depth of penetration is 20 cm, the speed of sound is 1,560 m/s, so the pulse repetition rate $T_R \geq \frac{2 \times 20 \text{ cm}}{156{,}000 \text{ cm/s}} = 256\mu\text{s}$. Therefore the maximal repetition rate is $\frac{1}{256\mu\text{S}} = 3,906$ Hz.

(d) $F = \frac{1}{T_R N} = \frac{1}{256\,\mu\text{S} \times 128} = 30$ frames/s.

(e) This will cause geometric distortion since the estimated ranges are wrong due to the poor uniform speed assumption.

Solution 11.13

(a) The depth of penetration in oil is

$$d_p = \frac{L}{2\alpha} = \frac{65\text{dB}}{2 \times 0.95\text{dB/cm}} \approx 34.2 \text{ cm} .$$

(b) The wavelength of sound in oil is

$$\lambda = \frac{c_{\text{oil}}}{f} = \frac{1,500\text{m/s}}{10^6\text{s}^{-1}} = 1.5 \times 10^{-3}\text{m} = 0.15 \text{ cm}\,.$$

Therefore,

$$\frac{D^2}{\lambda} = \frac{1^2}{0.15} \approx 6.67 \text{ cm}\,.$$

Since $z_0 = 20$ cm > 6.67 cm, the interface lies in the far-field. The beamwidth is approximately

$$w(z_0) = \frac{\lambda z_0}{D} = \frac{0.15 \times 20}{1} = 3 \text{ cm}\,.$$

(c) $Z = \rho c$. Hence, the characteristic impedances of oil and fat are

$$Z_{\text{oil}} = \rho_{\text{oil}} c_{\text{oil}} = 950 \times 1,500 \text{ kg m}^{-2}\text{s}^{-1} = 1.425 \times 10^6 \text{ kg m}^{-2}\text{s}^{-1}\,,$$

and

$$Z_{\text{fat}} = \rho_{\text{fat}} c_{\text{fat}} = 920 \times 1,450 \text{ kg m}^{-2}\text{s}^{-1} = 1.334 \times 10^6 \text{ kg m}^{-2}\text{s}^{-1}\,,$$

respectively. Thus, the pressure reflectivity at the interface is

$$R = \frac{1.334 - 1.425}{1.334 + 1.425} \approx -0.033\,.$$

We can ignore the negative sign since it only indicates a phase change. The amplitude attenuation coefficient inside oil is

$$\mu_a = \frac{\alpha}{8.686 \text{ dB}} = \frac{0.95\text{dB/cm}}{8.686 \text{ dB}} \approx 0.1094 \text{ cm}^{-1}\,.$$

Thus, the amplitude of the returned pulse is

$$p_r = R p_i e^{-2 z_0 \mu_a} = 0.033 \times 20 \times e^{-2 \times 20 \times 0.1094} \approx 0.0083(\text{N/cm}^2)\,.$$

The amplitude gain is

$$20\log_{10}\frac{p_r}{p_i} = 20\log_{10}\frac{0.0083}{20} \approx -67.639(\text{dB})\,.$$

Since the amplitude loss, which is 67.6 dB, is beyond the sensitivity of the system, the returning echo is undetectable by the system. This does not conflict with (a), since the depth-of-penetration is computed by assuming a perfect reflection from a target.

(d) The interface position is oscillating between 15 cm and 25 cm, with a period of $f_0^{-1} = 0.01\text{s} = 10$ ms. The time needed for the sound to travel 25 cm is

$$\frac{25 \text{ cm}}{1,500\text{m/s}} \approx 0.167 \text{ ms}\,,$$

which is negligible compared to the slow motion of the interface.

$$\cos(2\pi \times 100\text{Hz} \times 0.167 \times 10^{-3}\text{s}) \approx 0.9945 \approx 1\,.$$

Hence, the pulse at $t = 0$ will hit the interface at $z_1 = 20 - 5 = 15$cm. The amplitude loss for a return at

15 cm will be

$$0.95 \times 2 + 20 \log_{10} R \approx -58.1(\text{dB}) .$$

Hence, there will be signal shown on the A-mode scan, with a time of return about

$$t_r = \frac{2 \times 15 \text{ cm}}{1,500 \text{m/s}} = 0.2 \text{ ms} .$$

(e) The transducer fires with the same period as the oscillation of the interface. Hence, each pulse hits the interface at the same depth. The M-mode signal is a horizontal line at approximately 15 cm parallel to the time axis.

Solution 11.14

(a) The speed of sound in the media is

$$c = \frac{Z}{\rho} = \frac{1.35 \times 10^6 \text{ kg/m}^2 \cdot \text{s}}{920 \text{ kg/m}^3} = 1,500 \text{ m/s} .$$

At frequency of $f = 2.5$ MHz, the wavelength is:

$$\lambda = c/f = 0.06 \text{ cm} .$$

The far field begins at range of

$$z = D^2/\lambda = 0.5 \text{ cm} \times 0.5 \text{ cm}/0.06 \text{ cm} = 4.17 \text{ cm} .$$

(b) Assume the transmitter/preamplifier can handle at most an 80 dB loss (this is typical in ultrasound systems), then we have

$$2\alpha d_p = L .$$

So, $\alpha = L/2d_p = 80 \text{ dB}/2 \times 20 \text{ cm} = 2 \text{ dBcm}^{-1}$.

(c) At a range $z = 10$ cm, the far field approximation holds. From the derivations in Problem 11.9 part (d), we see that the lateral resolution of the transducer is related to

$$\text{sinc}^2\left(\frac{x}{\lambda z}\right) = \text{sinc}^2\left(\frac{x}{0.6 \text{ cm}^2}\right) .$$

The FWHM is

$$\text{FWHM} = 0.88 \times 0.6 = 0.53 \text{ cm} .$$

(d) With the depth of penetration of 20 cm, the time it takes for the ultrasound wave to make a round trip is:

$$T_R = 2 \times 20\text{cm}/1,500\text{m/s} = 2.67 \times 10^{-4}\text{s} .$$

There are N =12 cm/1 mm = 120 scans in one frame. So the maximum frame rate is

$$F = 1/T_R N = 31\text{frames/s} .$$

(e) Because the interface is perpendicular to the transducer axis, the incident wave, the reflected wave, and the

transmitted wave all travel in the direction of transducer axis. So $\theta_i = \theta_r = \theta_t = \pi/2$. The pressure reflectivity is:

$$R = \frac{Z_2 - Z_1}{Z_2 + Z_1} = \frac{1.7 - 1.35}{1.7 + 1.35} = 0.11\,.$$

The amplitude of the reflected acoustic pressure is

$$A = 0.11 \times A_0 10^{-\frac{20\times 1.5}{20}} = 0.0035 A_0\,.$$

Solution 11.15

(a) All quantities are in the appropriate units to apply the following equation $d_p = \frac{L}{2af} = \frac{80}{2\cdot 2} = 20$ cm.

(b) The pulse repitition rate is given by $f_r = \frac{1}{T_R} = \frac{c}{2d_p} = \frac{c}{2\cdot 20} = \frac{148{,}000}{40} = 3,700$ per second. Remember to convert from m/s into cm/s. So the frame rate is given by $F = f_r/256 = 14.4$ frames per second.

(c) The distance between elements is $d = \frac{1}{128}$ cm. The delays are given by

$$\begin{aligned}\tau_i &= \frac{r_0 - r_i}{c} \\ &= \frac{\sqrt{5^2 + 10^2} - \sqrt{(id-5)^2 + 10^2}}{148,000}\,.\end{aligned}$$

For $i = 64$ we get

$$\begin{aligned}\tau_{64} &= \frac{11.18 - \sqrt{(64/128 - 5)^2 + 10^2}}{148,000} \\ &= \frac{11.18 - \sqrt{20.25 + 100}}{148,000} \\ &= \frac{11.18 - 10.96}{148,000} \\ &= 0.00015 \text{ s}\,.\end{aligned}$$

(d) We can now use the pulse repetition rate, $3,700$ frames per second. The heart has frequency 500 cycles per min $= 8.3333$ Hz. In M-mode we can sample a signal up to $3,700/2 = 1,850$ per second without aliasing. So there is no aliasing here. However, there is aliasing in the B-mode image, because we cannot sample a signal with frequency higher than $14.4/2 = 7.2$ per second without introducing aliasing.

Solution 11.16

(a) Carry out the following math:

$$\begin{aligned} d_p &= \frac{L}{2af}\,, \\ d_{p,3\text{ MHz}} &= \frac{90\text{ dB}}{(2\frac{\text{dB}}{\text{cm MHZ}})(3\text{ MHz})} = 15\text{ cm} \\ d_{p,6\text{ MHz}} &= \frac{90\text{ dB}}{(2\frac{\text{dB}}{\text{cm MHZ}})(6MHz)} = 7.5\text{ cm}\,. \end{aligned}$$

(b) Focusing at a depth of $z = 5$ cm and $\theta = 20^\circ$ gives us $x_f = 5\tan(20^\circ) = 1.82$ and $z_f = 5$.

If we set the transducer distance to be $2d$, then we find the firing time for each i as follows:

$$\begin{aligned} t_i^{(6)} &= \frac{\sqrt{x_f^2 + z_f^2} - \sqrt{(i(2d) - x_f)^2 + z_f^2}}{c} \\ &= \frac{\sqrt{(1.82\text{ cm})^2 + (5\text{ cm})^2} - \sqrt{(i(2(0.04\text{ cm})) - 1.82\text{ cm})^2 + (5\text{ cm})^2}}{154,000\text{ cm/s}} \end{aligned}$$

$$\begin{aligned} t_1^{(6)} &= .174\,\mu\text{s} \\ t_{\min} &= t_{-2}^{(6)} = -.369\,\mu\text{s} \end{aligned}$$

$$\begin{aligned} \tau_i^{(6)} &= t_i^{(6)} - t_{min} \\ \tau_i^{(6)} &= t_i^{(6)} + .369\,\mu\text{s} \\ \tau_1^{(6)} &= .543\,\mu\text{s} \end{aligned}$$

(c) The solution is the same as (b) except i is shifted over left one detector if i is positive, and right one detector if i is negative. Also, we are focusing at a depth of $z = 10$ cm. So $x_f = 10\tan(20^\circ) = 3.64$ and $z_f = 10$.

$$\begin{aligned} t_i^{(3)} &= \frac{\sqrt{x_f^2 + z_f^2} - \sqrt{((2i - \text{sign}(i))(d) - x_f)^2 + z_f^2}}{c} \\ &= \frac{\sqrt{(3.64\text{ cm})^2 + (10\,cm)^2} - \sqrt{((2i - \text{sign}(i))(0.04\text{ cm}) - 3.64\text{ cm})^2 + (10\text{ cm})^2}}{154,000\text{ cm/s}} \end{aligned}$$

$$t_2^{(3)} = .262\,\mu\text{s}$$

$$\begin{aligned} \tau_i^{(3)} &= t_i^{(3)} - t_{\min} \\ \tau_i^{(3)} &= t_i^{(3)} + .369\,\mu\text{s} \\ \tau_2^{(3)} &= .631\,\mu\text{s} \end{aligned}$$

(d) Since the two transducer types are identical outside of the frequency. The main value we will be comparing

is when the amplitude of the traveling wave is larger for the 3MHz than for the 6Mhz. This amplitude is described by the decay function (Equation 10.32), $A_z = A_0 e^{-\mu_a z}$.

We know that the attenuation coefficient, μ_a, is directly related to frequency in our case by $\mu_a = \alpha/8.7 = af/8.7$. Hence:

$$\begin{aligned} \mu_a^{3\text{ MHz}} &= 3\text{ dB/cm} = \frac{3}{8.7} = 0.345\text{ np/cm} \\ \mu_a^{6\text{ MHz}} &= \frac{6}{8.7}\text{ dB/cm} = 0.69\text{ np/cm} \end{aligned}$$

so the switchover range is:

$$\alpha z_{\text{switch}} = 30\text{dB} = 3\text{ dB/cm} \times 2z_{\text{switch}} = 5\text{ cm}$$

(e) Knowing z_{switch} we can solve for the ratio:

$$\begin{aligned} A_0^{3\text{ MHz}} e^{-\mu_a^{3\text{ MHz}} z_{\text{switch}}} &= A_0^{6\text{ MHz}} e^{-\mu_a^{6\text{ MHz}} z_{\text{switch}}} \\ A_0^{3\text{ MHz}} e^{-0.345\text{ (np/cm)5cm}} &= e^{0.69\text{ (np/cm)5cm}} \\ \frac{A_0^{3\text{ MHz}}}{A_0^{6\text{ MHz}}} &= e^{-0.69\text{ (np/cm)5cm}-(-0.345\text{ (np/cm)5cm})} \\ &= 0.178\,. \end{aligned}$$

HARMONIC IMAGING

Solution 11.17

(a) $A_1 = A_0 e^{-\mu_a d} = A_0 e^{-f_0/8.7d}$.

(b) Use linearity: $G(t) = A_1 \frac{2}{\pi} \sum_{n=1}^{\infty} (-1)^n \frac{1}{n} \frac{1}{2i} (\delta(f - nf_0) - \delta(f + nf_0))$.

(c) $A_2 = A_1 \frac{1}{\pi} = A_0 e^{-f_0/8.7d} \frac{1}{\pi}$. Then $A_3 = A_0 e^{-f_0/8.7d} \frac{1}{\pi} e^{-2f_0/8.7d} = A_0 e^{-3f_0/8.7d} \frac{1}{\pi}$.

(d) We observe that $-20 \log \frac{A_3}{A_0} = L$. So

$$\begin{aligned} L &= -20 \log e^{-3f_0/8.7d} \frac{1}{\pi} \\ &= -20 \ln e^{-3f_0/8.7d} \frac{1}{\pi} / \ln(10) \\ &= 20 \cdot 3f_0/8.7d/\ln(10) + 20 \ln \pi / \ln(10)\,, \\ 80 &= 3f_0 d + 9.94\,, \\ d &= 23.35/f_0 \\ &= 23.35/2.5 \\ &= 9.34\text{ cm}\,. \end{aligned}$$

(e) We can use the simple formula $d_p = \frac{L}{2\alpha} = \frac{L}{2 \cdot 8.7 \mu_a} = \frac{L}{2f_1} = \frac{80}{10} = 8$ cm. This is a 16% increase in depth of penetration.

(f) In the Fourier domain we can write our filter as a difference of two rect functions.

$$\begin{aligned} H(f) &= \text{rect}(f/12\text{MHz}) - \text{rect}(f/8\text{MHz}) \\ &= \text{rect}(f/12 \times 10^6) - \text{rect}(f/8 \times 10^6)\,. \end{aligned}$$

The filter in the time domain is then

$$h(t) = 12 \times 10^6 \text{sinc}(12 \times 10^6 t) - 8 \times 10^6 \text{sinc}(8 \times 10^6 t)\,.$$

12

Physics of Magnetic Resonance

MAGNETIZATION

Solution 12.1

The magnetic field B at $z = 0$ and $z = 1$ cm is

$$B(0) = 1 \text{ Tesla} \quad \text{and} \quad B(1) = 1.5 \text{ Tesla}\,.$$

The Larmor frequencies at these positions are

$$f(0) = 42.58 \text{ MHz} \quad \text{and} \quad f(1) = 63.87 \text{ MHz}\,.$$

The next time when the magnetization vectors on two planes have same phase is when $|2\pi f(0)t - 2\pi f(1)t| = 2\pi$. Solve for t, we have

$$t = 0.047\,\mu\text{s}\,.$$

Solution 12.2

The static magnetic filed is oriented in z-direction, $\mathbf{B}(t) = B_0\hat{z}$. By substituting the equations (12.12) into (12.7), we have on the left hand side:

$$\begin{aligned}
\frac{dM_x(t)}{dt} &= 2\pi\nu_0 M_0 \sin\alpha \sin\left(-2\pi\nu_0 t + \phi\right), \\
\frac{dM_y(t)}{dt} &= -2\pi\nu_0 M_0 \sin\alpha \cos\left(-2\pi\nu_0 t + \phi\right), \\
\frac{dM_z(t)}{dt} &= 0\,.
\end{aligned}$$

On the right hand side:

$$\gamma\mathbf{M}(t) \times \mathbf{B}(t) = \gamma\mathbf{M}(t) \times B_0\hat{z} = \gamma B_0 M_0 \sin\alpha \sin\left(-2\pi\nu_0 t + \phi\right)\hat{x} - \gamma B_0 M_0 \sin\alpha \cos\left(-2\pi\nu_0 t + \phi\right)\hat{y}\,,$$

where $\hat{x}$, $\hat{y}$, and $\hat{z}$ are the unit vectors in x, y, and z directions. Since $\nu_0 = \gamma B_0$, we have $2\pi\nu_0 = \gamma B_0$. It is easy to see that equations (12.12) are solutions to (12.7).

Solution 12.3

The transverse magnetization is

$$M_{xy}(t) = \sum_{i=1}^{N} A_i e^{-t/T_{2_i}} e^{-j(2\pi\nu_i t - \phi_i)} .$$

The Fourier transform of this time domain signal yields the NMR spectrum of the sample. This multispectral character of the signal must be included as a constraint when designing appropriate imaging protocols when fat is present; this includes most tissues other than brain.

RF EXCITATION AND RELAXATION

Solution 12.4

(a) The tip angle is given by

$$\begin{aligned} \alpha &= \gamma \int_0^t B_1^e(\tau) d\tau \\ &= \gamma \int_0^t \frac{1}{10} \left(1 - \frac{|\tau - T|}{T}\right) d\tau . \end{aligned}$$

In the range $0 \le t \le T$, we have

$$\begin{aligned} \alpha &= \gamma \int_0^t \frac{1}{10} \left(1 - \frac{T - \tau}{T}\right) d\tau \\ &= \gamma \int_0^t \frac{1}{10} \left(\frac{\tau}{T}\right) d\tau \\ &= \gamma \frac{t^2}{20T} . \end{aligned}$$

In the range $T \le t \le 2T$, we have

$$\begin{aligned} \alpha &= \gamma \int_0^T \frac{1}{10} \left(\frac{\tau}{T}\right) d\tau + \gamma \int_T^t \frac{1}{10} \left(1 - \frac{\tau - T}{T}\right) d\tau \\ &= \frac{\gamma T}{20} + \frac{\gamma}{10} \int_T^t \left(2 - \frac{\tau}{T}\right) d\tau \\ &= \frac{\gamma t}{5} - \frac{\gamma t^2}{20T} - \frac{\gamma T}{10} . \end{aligned}$$

(b) At the end of the pulse, that is, at $t = 2T$, the angle is

$$\alpha = \frac{\gamma 2T}{5} - \frac{\gamma T}{5} - \frac{\gamma T}{10} = \frac{\gamma T}{10} .$$

To make $B_1(t)$ a $\pi/2$ pulse, we have

$$\pi/2 = \frac{\gamma T}{10} \quad \Rightarrow \quad T = \frac{5\pi}{\gamma}\,.$$

Solution 12.5

Both equations are first-order, ordinary differential equations and are therefore governed by a simple exponential growth or decay. The initial value of $M_z(t)$ is $M_z(0)$ and the final value $M_z(\infty)$ satisfies

$$0 = -\frac{M_z(\infty)}{T_1} + \frac{M_0}{T}\,,$$

so $M_z(\infty) = M_0$. The solution is therefore given by

$$\begin{aligned} M_z(t) &= (M_z(0) - M_0)e^{-t/T_1} + M_0 \\ &= M_0(1 - e^{-t/T_1}) + M_z(0)e^{-t/T_1}\,. \end{aligned}$$

The initial value of $M_{xy}(t)$ is $M_{xy}(0)$ and the final value is 0. Therefore,

$$M_{xy}(t) = M_{xy}(0)e^{-t/T_1}\,.$$

Solution 12.6

Use the equation

$$M_z(t) = M_0(1 - e^{-t/T_1}) + M_0 \cos\alpha e^{-t/T_1}.$$

The last term of the above equation denotes the initial magnetization after an α pulse. Let

$$M_z^n(t) = M_0(1 - e^{-t/T_1}) + M_z^{SS} \cos\alpha e^{-t/T_1}, \tag{S12.1}$$

where M_z^{SS} is the steady-state magnetization defined by

$$M_z^n(T_R) = M_z^{SS}. \tag{S12.2}$$

From (S12.1) and (S12.2), we have

$$M_z^{SS} = M_0 \frac{1 - e^{-T_R/T_1}}{1 - \cos\alpha e^{-T_R/T_1}}.$$

Solution 12.7

(a) It is given in the problem statement that the transverse magnetization is gone before the next imaging pulse occurs; therefore,

$$M_{xy}(0^-) = 0\,.$$

The longitudinal magnetization recovery follows [see Equation (12.40)]

$$M_z(t) = M_0(1 - e^{-t/T_1}) + M_z(0^+)e^{-t/T_1}\,.$$

So, in the steady state, just before the next imaging pulse (at time $t = T_R$) the z-magnetization is

$$M_z(0^-) = M_0(1 - e^{-T_R/T_1}) + M_z(0^+)e^{-T_R/T_1} .$$

But $M_z(0^-)$ and $M_z(0^+)$ are also related by the flip angle α as follows

$$M_z(0^+) = M_z(0^-)\cos\alpha .$$

Substitution yields

$$M_z(0^-) = M_0(1 - e^{-T_R/T_1}) + M_z(0^-)\cos\alpha e^{-T_R/T_1} .$$

which is solved as follows

$$M_z(0^-) = \frac{M_0(1 - e^{-T_R/T_1})}{1 - \cos\alpha e^{-T_R/T_1}} .$$

(b) $M_z(0^-)$ is the effective longitudinal magnetization just prior to an imaging pulse. With reference to (12.39), the transverse magnetization after the imaging pulse (ignoring the arbitrary phase and assuming demodulation at the Larmor frequency) is

$$\begin{aligned} M_{xy}(T_E) &= M_z(0^-)\sin\alpha e^{-T_E/T_2} \\ &= \frac{M_0(1 - e^{-T_R/T_1})}{1 - \cos\alpha e^{-T_R/T_1}}\sin\alpha e^{-T_E/T_2} . \end{aligned}$$

(c) Simplify the above expression as follows:

$$\begin{aligned} A &= M_{xy}(T_E) , \\ M &= M_0 , \\ R &= e^{-T_R/T_1} , \\ E &= e^{-T_E/T_1} . \end{aligned}$$

Then

$$A = \frac{EM(1 - R)\sin\alpha}{1 - R\cos\alpha} .$$

To maximize this with respect to α, take the derivative of A

$$\frac{dA}{d\alpha} = \frac{EM(1 - R)}{1 - R\cos\alpha}\cos\alpha + (-1)EM(1 - R)\sin\alpha(1 - R\cos\alpha)^{-2}R\sin\alpha ,$$

set it to zero, and solve for α, as follows

$$\begin{aligned} \frac{EM(1 - R)}{1 - R\cos\alpha}\left(\cos\alpha - \frac{R\sin^2\alpha}{1 - R\cos\alpha}\right) &= 0 \\ \cos\alpha &= \frac{R\sin^2\alpha}{1 - R\cos\alpha} \\ \cos\alpha - R\cos^2\alpha &= R\sin^2\alpha \\ \cos\alpha &= R(\cos^2\alpha + \sin^2\alpha) \\ &= R \end{aligned}$$

Therefore,

$$\alpha = \cos^{-1}\left(e^{-T_R/T_1}\right) ,$$

which is known as the *Ernst angle*.

Solution 12.8

(a) Assume the sample is in equilibrium with magnetizations of $M_x(0^-) = M_y(0^-) = 0$ and $M_z(0^-) = M_0$. After the π-pulse applied at $t = 0$, the magnetizations are

$$\begin{aligned} M_x(0^+) &= 0 , \\ M_y(0^+) &= 0 , \\ M_z(0^+) &= -M_0 . \end{aligned}$$

After a delay of τ, the magnetizations become

$$\begin{aligned} M_x(\tau^-) &= 0 , \\ M_y(\tau^-) &= 0 , \\ M_z(\tau^-) &= M_0\left(1 - 2e^{-\tau/T_1}\right) . \end{aligned}$$

In the time interval $(0, \tau)$, since there is no precession about the $\mathbf{B}_0$ field, there is no FID signal. After the $\pi/2$-pulse, the bulk magnetization is tilted into x-y plane. Assume the $\pi/2$-pulse is applied along the y-axis, we have:

$$\begin{aligned} M_x(\tau^+) &= M_0\left(1 - 2e^{-\tau/T_1}\right) , \\ M_y(\tau^+) &= 0 , \\ M_z(\tau^+) &= 0 . \end{aligned}$$

The bulk magnetization then precess around the $\mathbf{B}_0$ field to generate FID signal:

$$M_{xy}(t) = M_0\left(1 - 2e^{-\tau/T_1}\right) e^{-(t-\tau)/T_2} e^{-2\pi\nu_0(t-\tau)}, \quad t > \tau .$$

(b) From the above derivation, we can see that the strength of the FID signal depends on the delay τ. If we can take a measure right after the $\pi/2$-pulse, the signal strength is $M_0\left(1 - 2e^{-\tau/T_1}\right)$. Therefore we can use two different values for the delay $\tau = \tau_1$ and $\tau = \tau_2$. The signal strength measured right after the $\pi/2$-pulse are:

$$\begin{aligned} M_{xy}^{(1)}(\tau_1) &= M_0\left(1 - 2e^{-\tau_1/T_1}\right) , \\ M_{xy}^{(2)}(\tau_2) &= M_0\left(1 - 2e^{-\tau_2/T_1}\right) . \end{aligned}$$

Solve the above equations, we can determine T_1.

BLOCH EQUATIONS AND SPIN ECHOES

Solution 12.9

The Bloch equation is given as

$$\frac{dM}{dt} = \gamma M \times B - R[M - M_0]\,. \tag{S12.3}$$

$M \times B$ and $R[M - M_0]$ apply in any frame. Assume that the rotating frame rotates with angular frequency Ω with respect to the lab frame and that M' is the magnetization vector in the rotating frame (B' is B in the rotating frame). From classical mechanics, we have

$$\frac{dM}{dt} = \frac{dM'}{dt} + \Omega \times \frac{dM'}{dt}\,. \tag{S12.4}$$

Using Equations S12.3 and S12.4, we get

$$\frac{dM'}{dt} = \gamma M' \times B' - R[M' - M_0] - \Omega \times \frac{dM'}{dt}\,.$$

Solution 12.10

(a) Different isochromats in a sample precess in different frequencies around the $\mathbf{B}_0$ filed. The difference in precession frequency causes the progressive defocusing of the isochromats after their magnetization vectors are rotated to the x-y plane (see Figure 12.8). After the π-pulse applied at time $t = \tau$, the magnetization vectors are flipped in the transverse plane and the faster precessing vectors are lagging behind the slower ones. The time it takes to rephase (for the faster precessing vectors to catch the slower ones) equals τ. A phase coherence will be recreated at time $t = 2\tau$ to generate an echo. Therefore, the π-pulse should be applied at $t = T_E/2$ in order to generate an echo at $t = T_E$.

(b) Suppose the sample is in equilibrium with magnetization $M_z(0^-) = M_0$. The $\pi/2$-pulse is applied at $t = 0$. This pulse rotates the bulk magnetization vector into the x-y plane:

$$M_{xy}(0^+) = M_0\,.$$

The series of π-pulses will flip the magnetization in the transverse plane and form echoes at $t = (k+1/2)T_E$, $k = 1, 2, \cdots$. The magnitude of the transverse magnetization decays with constant T_2. So

$$M_{xy}(kT_E) = M_0 e^{-kT_E/T_2}\,.$$

Solution 12.11

$15^\circ \times \frac{2\pi}{360^\circ} = 2\pi \times 42.6 \times 10^6\ \text{Hz/T} \times A \times 10^{-5}s \Rightarrow A = 9.78 \times 10^{-5}T.$

Solution 12.12

(a) Just before applying the π pulse, the phase angle is given by

$$\phi(\mathbf{r}, \tau^-) = -\gamma(B_0 + \Delta B(\mathbf{r}))\tau\,.$$

The π pulse will cause the magnetization vectors to rotate about the y axis by 180-degrees. The vector on the $+x$ axis goes to the $-x$ axis (a phase difference of π) and vectors that were leading are now lagging (by the same amount). Therefore, the phases are given by

$$\phi(\mathbf{r}, \tau^+) = \pi + \gamma(B_0 + \Delta B(\mathbf{r}))\tau\,.$$

(b) Magnetization vectors that were leading at τ^- are lagging at τ^+, and since they will continue to precess faster they will be in phase after the second time interval of τ. Therefore, at time $T_E = 2\tau$, the phase will be π.

(c) An echo will form at T_E throughout the image plane, regardless of the presence of a spatially varying gradient.

CONTRAST MECHANISM

Solution 12.13

In P_D-weighted images, the image intensity should be proportional to the number of hydrogen nuclei in the sample. We start with the sample in equilibrium, apply an excitation RF pulse, and image quickly, before the signal has a chance to decay from T_2 effects. Thus, a P_D-weighted contrast can be obtained by using a long T_R, which allows the tissues to be in equilibrium, and either no echo or a short T_E. The preferred tip angle is $\pi/2$, in order to get the maximum signal. Large T_E cannot be used because it will introduce large T_2 decay.

Solution 12.14

(a) The magnitude of the transverse magnetization is given as:

$$\begin{aligned} |M_{xy}(t)| &= |M_{SS} \sin\alpha e^{j\phi} e^{-t/T_2}| \\ &= M_0 \frac{1 - e^{-T_R/T_1}}{1 - \cos\alpha e^{-T_R/T_1}} \sin\alpha e^{-t/T_2}. \end{aligned}$$

Now, $\alpha = \pi/2$, also the signal is measured just after excitation, so $t = 0$. Hence,

$$|M_{xy}| = M_0 \left(1 - e^{-T_R/T_1}\right).$$

The local contrast between GM and CSF can be written as:

$$C = \frac{|M_{xy}|_{\mathrm{CSF}} - |M_{xy}|_{\mathrm{GM}}}{|M_{xy}|_{\mathrm{CSF}}} = \frac{e^{-T_R/T_1^{\mathrm{CSF}}} - e^{-T_R/T_1^{\mathrm{GM}}}}{1 - e^{-T_R/T_1^{\mathrm{CSF}}}}$$

This function is a monotonically decreasing function of T_R. Thus, lower the T_R, better the contrast. However, we cannot have an arbitrarily low T_R. It has to be approximately in the range of T_1, to allow a reasonable decay. A good contrast can be obtained by using $T_R = T_1^{\mathrm{GM}} = 760$ ms.

(b) The contrasts can be obtained by plugging in values in the above equation.

Solution 12.15

(a) This is not a T_2-weighted contrast. In order to obtain a T_2-weighted contrast we need to include spin echoes in the pulse sequence.

(b) We would need to use spin echoes as in Figure 12.9.

(c) Reasonable values for the parameters:

τ. The sampling should be done at twice the pulse period T_E, since at that time, the dephasing due to T_2^* is completely removed and the signal truly represents T_2.

T_R. In order to bring the tissue back to equilibrium, in between the pulses, T_R should be as long as possible. In practice, however, 6,000 ms is an unusually long repetition time and is impractical.

T_E. The echo time should be approximately equal to the T_2 values of the tissue being imaged.

α. The tip angle should be $\pi/2$ to obtain the maximum signal.

Flip angle: During the echo, the transverse vector should be shifted by a phase angle of π.

13

Magnetic Resonance Imaging

MR IMAGING INSTRUMENTATION

Solution 13.1

The magnetic field is still oriented in the z direction. But the strength of the field is not uniform. At points with same x-coordinates, the magnetic fields have the same strength. At points with different x-coordinates, the magnetic field have different strength. The difference depends on the difference in x-coordinates and the magnitude of the gradient.

Solution 13.2

The functions of RF coils are twofold. (1) During radio frequency excitation, a relatively large amount of current is generated in the coil using an RF amplifier (with a power requirement of approximately 2 kW for human imaging). Ideally, this coil then produces a relatively uniform B_1 field throughout the entire imaging volume in order that the same tip angle is generated in each isochromat in the volume. (2) On reception, an RF coil must pick up very low-amplitude magnetic fields, which produce very small currents in the coil. Transmission and receiver RF coils can be the same coil but are different when high SNR or fast imaging is required.

ENCODING SPATIAL POSITION AND MR IMAGING EQUATION

Solution 13.3

(a) We have

$$\Delta\nu = \gamma G_z \Delta z = 4.258 \text{ kHz} \times 1 \text{ G/mm} \times 10 \text{ mm} = 42.58 \text{ kHz}\,.$$

(b) We have

$$B_1(t) = A\Delta\nu \,\mathrm{sinc}(\Delta\nu t) e^{j2\pi\bar{\nu}t}\,,$$

where $\bar{\nu} = \bar{z}\gamma G_z + \gamma B_0 = 212.9 \text{ kHz} + \gamma B_0$. Therefore, we have:

$$B_1(t) = A \times 42.58 \,\mathrm{sinc}\, 42.58t e^{j2\pi 212.9t} e^{j2\pi\gamma B_0 t}\,.$$

In rotating frame,

$$B_1(t) = A \times 42.58 \,\mathrm{sinc}\, 42.58t e^{j2\pi 212.9t}\,,$$

where A depends on the tip angle.

Solution 13.4

(a) Start with the Fourier transform pair

$$\mathcal{F}\{e^{-\pi t^2}\} = e^{-\pi u^2}\,.$$

Then since

$$A_0 \exp\{-t^2/\sigma^2\} = A_0 \exp\left\{\pi\left(\frac{t}{\sqrt{\pi}\sigma}\right)^2\right\}\,,$$

we can use the Fourier scaling theorem to get

$$\mathcal{F}\left\{A_0 \exp\{-t^2/\sigma^2\}\right\} = A_0\sqrt{\pi}\sigma \exp\left\{-\pi^2\sigma^2u^2\right\}\,.$$

The FWHM is found as follows:

$$\begin{aligned}
1/2 &= \exp\left\{-\pi^2\sigma^2u^2\right\}\,,\\
\ln(1/2) &= -\pi^2\sigma^2u^2\,,\\
u^2 &= \frac{1}{\pi^2\sigma^2}\ln 2\,,\\
u &= \sqrt{\frac{1}{\pi^2\sigma^2}\ln 2} = 265 \text{ Hz}\,,\\
\text{FWHM} &= 2\times 265 \text{ Hz} = 530 \text{ Hz}\,.
\end{aligned}$$

This defines the frequency interval that is excited $\Delta\nu = 530$ Hz, and using Equation (13.12) gives

$$\Delta z = \frac{530 \text{ Hz}}{42.58\times 10^6 \text{ Hz/T}10^{-4} \text{ T}} \text{ cm} = 1.2 \text{ mm}\,.$$

(b) The new gradient strength is $G_z' = 0.5G_z$. So, the new slice thickness is

$$\begin{aligned}
\Delta z &= \frac{\Delta\nu}{\gamma G_z'}\\
&= \frac{\Delta\nu}{\gamma 0.5 G_z}\\
&= 2\times\Delta z\,.
\end{aligned}$$

Halving the gradient strength doubles the slice thickness. Now suppose that $\sigma' = 0.5\sigma$. Starting from the original (without using G_z'), we have from previous work that

$$\begin{aligned}
u' &= \sqrt{\frac{1}{\pi^2\sigma'^2}\ln 2}\\
&= \frac{1}{\sigma'}\\
&= \frac{1}{0.5\sigma'}\sqrt{\frac{1}{\pi^2}\ln 2}\\
&= 2u\,.
\end{aligned}$$

Therefore, the new frequency range $\Delta\nu'$ is double what it was before, which doubles the slice thickness. If used in combination, the slice thickness would be four times thicker.

(c) In this case, only the RF pulse is changed, so the slice thickness is doubled: $\Delta z' = 2.4$ mm.

(d) Doubling the slice thickness improves the SNR by a factor of two. The overall imaging time is slightly smaller (although this will not affect SNR since the actual ADC time is unaffected). Image resolution will be degraded in the through-plane direction.

Solution 13.5

The RF signal is given by

$$s(t) = A\Delta\nu\,\mathrm{sinc}(\Delta\nu t)e^{j2\pi\bar{\nu}t}.$$

For isochromats whose Larmor frequency is ν, the excitation signal in the rotating coordinate system is

$$B_1^e(t) = s(t)e^{-j2\pi\nu t}\,.$$

The duration of the above signal is from $-\infty$ to ∞. So the tip angle is:

$$\begin{aligned}
\alpha(\nu) &= \gamma\int_{-\infty}^{\infty} B_1^e(t)dt \\
&= \gamma\int_{-\infty}^{\infty} A\Delta\nu\,\mathrm{sinc}(\Delta\nu t)e^{j2\pi\bar{\nu}t}e^{-j2\pi\nu t}dt \\
&= \gamma A\Delta\nu\int_{-\infty}^{\infty}\mathrm{sinc}(\Delta\nu t)e^{-j2\pi(\nu-\bar{\nu})t}dt \\
&= \gamma A\int_{-\infty}^{\infty}\mathrm{sinc}(\tau)e^{-j2\pi\frac{\nu-\bar{\nu}}{\Delta\nu}\tau}d\tau, \quad \text{let } \tau = \Delta\nu t \\
&= \gamma A\,\mathrm{rect}\left(\frac{\nu-\bar{\nu}}{\Delta\nu}\right).
\end{aligned}$$

The slice location z and the Larmor frequency ν are related by the following equation:

$$z = \frac{\nu - \gamma B_0}{\gamma G_z}\,.$$

Therefore,

$$\begin{aligned}
\bar{z} &= \frac{\bar{\nu} - \gamma B_0}{\gamma G_z}\,, \\
\Delta z &= \frac{\Delta\nu - \gamma B_0}{\gamma G_z}\,,
\end{aligned}$$

which lead us to

$$\mathrm{rect}\left(\frac{\nu-\bar{\nu}}{\Delta\nu}\right) = \mathrm{rect}\left(\frac{z-\bar{z}}{\Delta z}\right).$$

So, the tip angle is

$$\alpha(z) = \gamma A\,\mathrm{rect}\left(\frac{z-\bar{z}}{\Delta z}\right).$$

Solution 13.6

Slice selection uses a narrowband RF excitation during a constant gradient (taken to be in the z direction without loss of generality). Spins on the high-frequency side of the slice accumulate transverse phase faster than spins on the low-frequency side. When the slice selection pulse ends, all spins rotate at the Larmor frequency, but are out of phase across the slice, and may add destructively during imaging. From Section 13.2.2, we know that the ideal slice selection excitation signal is (Equation 13.14)

$$s(t) = A\Delta\nu \operatorname{sinc}(\Delta\nu t) e^{j2\pi\bar{\nu}t} .$$

In addition to required truncation, which we ignore in this derivation, this pulse must be shifted to a positive time, $\tau_p/2$, where τ_p is the duration of the slice selection gradient. This shift in time implies a phase shift of its frequency content, that is,

$$S(\nu) = A \operatorname{rect}\left(\frac{\nu - \bar{\nu}}{\Delta\nu}\right) e^{j2\pi(\nu-\bar{\nu})\tau_p/2} .$$

This frequency spectrum forms the following spatial excitation

$$S(z) = A \operatorname{rect}\left(\frac{z - \bar{z}}{\Delta z}\right) e^{j2\pi\gamma G_z(z-\bar{z})\tau_p/2} .$$

Application of a z gradient with strength $-G_z$ for a duration $\tau_p/2$ will exactly cancel this phase accumulation.

Solution 13.7

The reconstruction process will presume the following frequencies

$$\begin{aligned} u &= \gamma G_x t , \\ v &= \gamma A_y . \end{aligned}$$

A Fourier transform function (a discrete matrix, in practice) will be formed as follows

$$\begin{aligned} F(u,v) &= s_0\left(\frac{u}{\gamma G_x}, \frac{v}{\gamma}\right) , \\ &= Ae^{-u/\gamma G_x T_2} \int_{-\infty}^{\infty}\int_{-\infty}^{\infty} M(x,y;0^+) e^{-j2\pi xu} e^{-j2\pi yv}\, dx\, dy . \end{aligned}$$

Thus, $F(u,v)$ is a *product* of the Fourier transform of $M(x,y;0^+)$ with another Fourier function. This implies that the inverse transform of $F(u,v)$ will be $M(x,y;0^+)$ convolved with a spatial kernel that depends only on x. At the very least, the magnetization will be blurred to some extent in the x direction because of this term.

To find a mathematical description of this impulse response function requires an understanding of the pulse sequence used. If the readout gradient is large, then the readout time T_s will be short, and the effect of the T_2 decay will be minimized. In this case, the Fourier resolution of the scan adequately describes the effect of this term. If the readout is long, however, then T_2 could have a significant effect.

Given the pulse sequence shown in Figure 13.10, we can assume that frequencies in the range $0 \le u \le \gamma G_x T_s$ are acquired for all v. The complete Fourier transform is reassembled by conjugate symmetry. In this case, the function actually multiplying the Fourier transform of $M(x,y;0^+)$ is given by

$$H(u,v) = \exp\left\{-|u|/\gamma G_x T_2\right\} ,$$

which is separable as follows:

$$\begin{aligned} H_1(u) &= \exp\{-|u|/\gamma G_x T_2\}\,, \\ H_2(v) &= 1\,. \end{aligned}$$

From tables or direct calculation, we have the Fourier transform pair

$$\mathcal{F}\left\{e^{-|x|}\right\} = \frac{2}{1+(2\pi u)^2}\,.$$

Therefore, we have

$$\begin{aligned} h_1(x) &= \frac{2\gamma G_x T_2}{1+(2\pi\gamma G_x T_2 x)^2}\,, \\ h_2(y) &= \delta(y)\,. \end{aligned}$$

Ignoring all constant amplitude terms, the reconstructed image is

$$f(x,y) = M(x,y;0^+) * \frac{1}{1+(2\pi\gamma G_x T_2 x)^2}\delta(y)\,,$$

$h_1(x)$ is a "Gaussian-like" function that gets wider as the product $G_x T_2$ gets smaller. Thus, this demonstrates that slower readouts or faster T_2's will cause blurring in the readout direction because of transverse relaxation.

It is worth noting that if the pulse sequence scans across the v axis, acquiring both positive and negative u frequencies, then conjugate symmetry will not hold because of this term. In this case, the reconstruction will be both blurred, and will be a complex-valued image.

Solution 13.8

(a) The phase that is accumulated during a time-varying x gradient pulse is

$$\phi(t) = \gamma \int_0^t G_x(\tau) x(\tau)\, d\tau\,.$$

Therefore, the phase accumulation for the given gradient waveform and x trajectory is

$$\begin{aligned} \phi(T) &= \gamma \int_0^T G(\tau)(x_0 + v\tau)\, d\tau \\ &= \gamma \int_0^T G(\tau) x_0\, d\tau + \gamma \int_0^T G(\tau) v\tau\, d\tau \\ &= 0 + \gamma \int_0^{T/2} (-G) v\tau\, d\tau + \gamma \int_{T/2}^T (G) v\tau\, d\tau \\ &= -G\gamma\, \frac{v\tau^2}{2}\bigg|_0^{T/2} + G\gamma\, \frac{v\tau^2}{2}\bigg|_{T/2}^T \\ &= G\gamma \frac{vT^2}{4}\,. \end{aligned}$$

(b) Intuitively, we see that the final phase should be zero. This is because (1) the pulse has zero area, so the term

related to x_0 will cancel out and (2) starting at $t = T$, the pulse is symmetric in comparison to the first half, starting at $t = 0$, so the accumulated phase due to velocity in the second half should be the negative of that of the first half. We now go through the calculations:

$$\begin{aligned}
\frac{\phi(2T)}{\gamma} &= \int_0^{2T} G(\tau)(x_0 + v\tau)\, d\tau \\
&= \int_0^{T/2} (-G)(x_0 + v\tau) d\tau + \int_{T/2}^{3T/2} G(x_0 + v\tau) d\tau + \int_{3T/2}^{2T} (-G)(x_0 + v\tau) d\tau \\
&= \int_0^{T/2} (-G)x_0 d\tau + \int_0^{T/2} (-G)v\tau d\tau + \int_{T/2}^{3T/2} Gx_0 d\tau + \int_{T/2}^{3T/2} Gv\tau d\tau \\
&\quad + \int_{3T/2}^{2T} (-G)x_0 d\tau + \int_{3T/2}^{2T} (-G)v\tau d\tau \\
&= -Gx_0 \frac{T}{2} + \frac{-Gv\tau^2}{2}\bigg|_0^{T/2} + Gx_0 T + \frac{Gv\tau^2}{2}\bigg|_{T/2}^{3T/2} + (-G)x_0 \frac{T}{2} + \frac{-Gv\tau^2}{2}\bigg|_{3T/2}^{2T} \\
&= \frac{-Gv(T/2)^2}{2} + \frac{Gv(3T/2)^2}{2} - \frac{Gv(T/2)^2}{2} + \frac{-Gv(2T)^2}{2} - \frac{-Gv(3T/2)^2}{2} \\
&= \frac{-GvT^2}{8} + \frac{9GvT^2}{8} - \frac{GvT^2}{8} + \frac{-4GvT^2}{2} - \frac{9(-G)vT^2}{8} \\
&= (-1 + 9 - 1 - 16 + 9)\frac{GvT^2}{8} \\
&= 0\,.
\end{aligned}$$

(c) Integrals are linear operators, so we can use the results of previous parts. (In fact, we should have done this in part (b), but it was a good check to do it out anyway.) Using past results we can find the phase for the first waveform as follows:

$$\begin{aligned}
\frac{\phi_1(T)}{\gamma} &= 0 + \frac{GvT^2}{4} + \int_0^{T/2} (-G)\frac{1}{2}a\tau^2 d\tau + \int_{T/2}^{T} G\frac{1}{2}a\tau^2\, d\tau \\
&= \frac{GvT^2}{4} + \frac{-Ga}{2}\frac{\tau^3}{3}\bigg|_0^{T/2} + \frac{Ga}{2}\frac{\tau^3}{3}\bigg|_{T/2}^{T} \\
&= \frac{GvT^2}{4} + \frac{-Ga}{2}\frac{(T/2)^3}{3} + \frac{Ga}{2}\frac{T^3}{3} - \frac{Ga}{2}\frac{(T/2)^3}{3} \\
&= \frac{GvT^2}{4} + \frac{GaT^3}{6}\,.
\end{aligned}$$

For the second waveform, we get

$$\begin{aligned}
\frac{\phi_2(2T)}{\gamma} &= 0+0+\int_0^{T/2}(-G)\frac{1}{2}a\tau^2 d\tau+\int_{T/2}^{3T/2}G\frac{1}{2}a\tau^2\,d\tau+\int_{3T/2}^{2T}(-G)\frac{1}{2}a\tau^2\,d\tau \\
&= \frac{-GaT^3}{48}+\frac{Ga}{2}\tau^3 3\Big|_{T/2}^{3T/2}+\frac{-Ga}{2}\tau^3 3\Big|_{3T/2}^{2T} \\
&= \frac{-GaT^3}{48}+\frac{Ga(3T/2)^3}{6}-\frac{Ga(T/2)^3}{6}+\frac{-Ga(2T)^3}{6}-\frac{-Ga(3T/2)^3}{6} \\
&= \frac{-GaT^3}{48}+\frac{27GaT^3}{48}-\frac{GaT^3}{48}-\frac{64GaT^3}{48}+\frac{27GaT^3}{48} \\
&= (-1+27-1-64+27)\frac{GaT^3}{48} \\
&= \frac{-GaT^3}{4}\,.
\end{aligned}$$

We see that the first gradient waveform has phase effects from both velocity and acceleration, while the second only has phase effects from acceleration.

(d) We use the same "trick" that took us from part (a) to part (b). We invert the pulse sequence in part (b) and replay it, as shown in Figure S13.1. The static position term and the velocity is still nulled because the integrals evaluated in the second phase are still zero. The acceleration term is now nulled as well, since the integral will be negated.

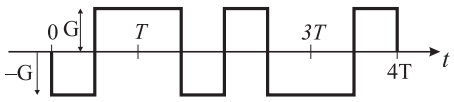

Figure S13.1 See Problem 13.8.

(e) It is possible. Now we need to show it. Consider the general gradient pulse of height A and duration T starting at t_0. Suppose a particle has the position $r(t) = x + vt + at^2/2$. What is the phase accumulation after this pulse? We have gone through this exercise above, but in not quite this general way. Here we do it again.

$$\begin{aligned}
\frac{\phi}{\gamma A} &= \int_t^{t_0+T}(x+v\tau+\frac{a\tau^2}{2})d\tau \\
&= xT+\frac{v}{2}(T^2+2t_0T)+\frac{a}{6}(3t_0^2T+2T^2t_0+T^3)\,,
\end{aligned}$$

where the second equation follows after some algebra. Now consider a sequence of three pulses starting at $t = 0$, with heights A, B, and C, and each of duration T. What is the phase accumulation after this

sequence? We apply the previous result three times and add the result.

$$\begin{aligned}\frac{\phi}{\gamma} &= xAT + \frac{Av}{2}(T^2) + \frac{Aa}{6}(T^3) \\ &\quad + BxT + \frac{Bv}{2}(3T^2) + \frac{Ba}{6}(7T^3) \\ &\quad + CxT + \frac{Cv}{2}(5T^2) + \frac{Ca}{6}(19T^3)\,,\end{aligned}$$

where the second equation follows after some algebra. Now the sequence should be independent of position, which implies

$$A + B + C = 0\,.$$

And the phase should be dependent on velocity, so the sum of the coefficients multiplying v should not be zero, for convenience, we make that sum equal to $T^2/2$, which implies

$$A + 3B + 5C = 1\,.$$

And finally, there should be no dependence on acceleration, which implies

$$A + 7B + 19C = 0\,.$$

Solving these equations for A, B, and C yields

$$\begin{aligned}A &= -1\,, \\ B &= 1.5\,, \\ C &= -0.5\,.\end{aligned}$$

The implied pulse sequence is shown in Figure S13.2.

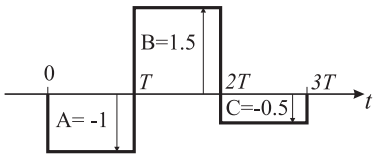

Figure S13.2 See Problem 13.8.

Solution 13.9

(a) The sampling interval is

$$T = \frac{10\text{ ms}}{256} = 39.1\,\mu\text{s}$$

The FOV in the x-direction is

$$\text{FOV}_x = \frac{1}{42.58\text{ MHz/T} \times 1\text{ G/cm} \times 39.1\,\mu\text{s}} = 6\text{ cm}$$

(b) The (nominal) pixel size is

$$\Delta x = \frac{\text{FOV}_x}{256} = 0.234 \text{ mm}$$

The spatial extent of the cube is 5 cm, so the number of pixels across the object is $50 \text{ mm}/0.234 \text{ mm} = 213.3$.

(c) Halving the gradient, doubles the FOV. Doubling the readout time, while keeping the number of samples the same doubles T, which in turn halves the FOV. Thus, there is no net effect on the FOV by making these collective changes.

(d) This pulse sequence will require reassembling Fourier space by conjugate symmetry. It will scan higher spatial frequencies than the previous pulse sequence. Nevertheless, the answers to (a) to (c) are the same.

Solution 13.10

(a) Use the following algebraic manipulation:

$$\begin{aligned}
f &= AM_0 \sin\alpha e^{-T_E/T_2} \frac{1 - e^{-T_R/T_1}}{1 - \cos\alpha e^{-T_R/T_1}} \\
f(1 - \cos\alpha e^{-T_R/T_1}) &= AM_0 \sin\alpha e^{-T_E/T_2}(1 - e^{-T_R/T_1}) \\
\frac{f - f\cos\alpha e^{-T_R/T_1}}{\sin\alpha} &= AM_0 e^{-T_E/T_2}(1 - e^{-T_R/T_1}) \\
\frac{f}{\sin\alpha} &= e^{-T_R/T_1}\frac{f}{\tan\alpha} + AM_0 e^{-T_E/T_2}(1 - e^{-T_R/T_1})
\end{aligned}$$

(b) Let

$$\begin{aligned}
x &= \frac{f}{\tan\alpha}\,, \\
y &= \frac{f}{\sin\alpha}\,.
\end{aligned}$$

Then the equation proven in part (a) becomes

$$y = e^{-T_R/T_1}x + AM_0 e^{-T_E/T_2}(1 - e^{-T_R/T_1})\,,$$

which is the equation of a line with slope

$$m = e^{-T_R/T_1}$$

and y-intercept

$$b = AM_0 e^{-T_E/T_2}(1 - e^{-T_R/T_1})\,.$$

Since only x and y will vary when we change α, the computed points from the three acquisitions will form different points on the same line.

(c) The slope of a line is found as follows:

$$\begin{aligned} m &= \frac{y_2 - y_1}{x_2 - x_1} \\ &= \frac{f_2/\sin\alpha_2 - f_1/\sin\alpha_1}{f_2/\tan\alpha_2 - f_1/\tan\alpha_1}\,. \end{aligned}$$

Since $m = e^{-T_R/T_1}$, we have

$$\begin{aligned} \hat{T_1} &= \frac{-T_R}{\ln m} \\ &= \frac{-T_R}{\ln\left(\frac{f_2/\sin\alpha_2 - f_1/\sin\alpha_1}{f_2/\tan\alpha_2 - f_1/\tan\alpha_1}\right)} \\ &= \frac{T_R}{\ln(f_2/\tan\alpha_2 - f_1/\tan\alpha_1) - \ln(f_2/\sin\alpha_2 - f_1/\sin\alpha_1)}\,. \end{aligned}$$

SAMPLING THE FREQUENCY SPACE

Solution 13.11

The basic relationship between the pulse sequence parameters and the Fourier frequencies is

$$\begin{aligned} u &= \gamma G_x t\,, \\ v &= \gamma A_y\,. \end{aligned}$$

There are four regions to consider.

(1) $0 \le t \le 1$ ms: The u component is given by

$$\begin{aligned} u &= \gamma G_x t \\ &= 4,258 \text{ Hz/G} \times 10 \text{ G/cm}\, t \\ &= 4,258 \text{ mm}^{-1}\,\text{s}^{-1}\, t\,. \end{aligned}$$

The v component requires a determination of the area of the y gradient as a function of time. Since

$$\begin{aligned} G_y(t) &= \frac{10 \text{ G/cm}}{1 \text{ ms}}\, t \\ &= 1 \times 10^3 \frac{\text{G}}{\text{mm}}\,\text{s}^{-1}\, t\,. \end{aligned}$$

the area is

$$\begin{aligned} A_y(t) &= \int_0^t G_y(\tau)\, d\tau \\ &= 1 \times 10^3 \frac{\text{G}}{\text{mm}}\,\text{s}^{-1}\, \frac{t^2}{2}\,. \end{aligned}$$

Therefore,

$$\begin{aligned} v &= \gamma A_y(t) \\ &= 4,258 \text{ Hz/G} \times 1 \times 10^3 \frac{\text{G}}{\text{mm}} \text{ sec}^{-1} \frac{t^2}{2} \\ &= 2.129 \times 10^6 \text{ mm}^{-1} \text{ sec}^{-2}\, t^2 \,. \end{aligned}$$

Writing v in terms of u yields:

$$v = 0.117u^2 \,,$$

both in units of mm^{-1}. Thus, the first segment of the Fourier trajectory is a parabola, starting at $u = v = 0$ and ending at $(u, v) = (4.258, 2.129)$ mm^{-1}.

(2) 1 ms $\leq t \leq$ 2 ms: In this interval, u is the same as in the previous interval. However, although v continues to increase, its rate of increase is decreasing. We have

$$\begin{aligned} G_y(t) &= 20 \text{ G/cm} - \frac{10 \text{ G/cm}}{1 \text{ ms}}\, t \\ &= 2\frac{\text{G}}{\text{mm}} - 1 \times 10^3 \frac{\text{G}}{\text{mm}} \text{ s}^{-1}\, t \,. \\ A_y(t) &= \int_{1 \text{ ms}}^{t} G_y(\tau)\, d\tau \\ &= 2\tau - 1 \times 10^3 \frac{\tau^2}{2}\bigg|_{0.001 \text{ s}}^{t} \\ &= -500t^2 + 2t - 0.001 \,. \end{aligned}$$

The vertical spatial frequency is then

$$\begin{aligned} v &= \gamma A_y(t) \\ &= 4,258(-500t^2 + 2t - 0.001) \\ &= -2.129 \times 10^6\, t^2 + 8,516t - 4.258 \,. \end{aligned}$$

This is a quadratic function that peaks at $t = 2$ ms. The final value (at 2 ms) is $v = 4.258$ mm^{-1}.

(3) 2 ms $\leq t \leq$ 3 ms: This range can be worked out in a fashion similar to the work in intervals (1) and (2). However, it is not necessary to do this since there is symmetry in the gradient pulses. Since both gradients are negative in this range, their Fourier trajectories will be decreasing. Since G_x is constant, u will decrease with uniform speed. Since G_y is a linear function with negative slope, it will cause the v component of the trajectory to behave parabolically, as in intervals (1) and (2). For a given increment in time (and equivalently a decrement in u), the drop in area in this time interval starts off small and gets larger over time. Therefore, by appealing to symmetry, we see that the trajectory will trace over that of interval (2).

(4) 3 ms $\leq t \leq$ 4 ms: Using a similar argument to that in interval (3), we see that this trajectory is identical to that in interval (1), only traveling toward the origin.

A sketch of the resulting Fourier trajectory is shown in Figure S13.3. Since the net area of the two gradients is zero, this pulse sequence ends exactly where it starts—at the origin.

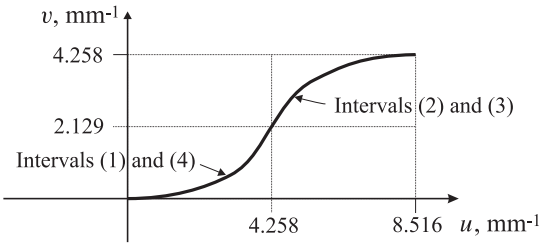

Figure S13.3 [Problem 13.11]

Solution 13.12

(a) In this interval, the Fourier trajectory goes from the origin to the point $(-0.25, -0.5)$ mm^{-1}. Using the relations:

$$\begin{aligned} u &= \gamma G_x t\,, \\ v &= \gamma G_y t\,, \end{aligned}$$

leads to

$$\begin{aligned} G_x &= \frac{u}{\gamma t} = \frac{-0.25 \text{ mm}^{-1}}{4,258 \text{ Hz/G}\, 0.0001 \text{ s}} = -0.587 \text{ G/mm}\,. \\ G_y &= \frac{v}{\gamma t} = \frac{-0.5 \text{ mm}^{-1}}{4,258 \text{ Hz/G}\, 0.0001 \text{ s}} = -1.174 \text{ G/mm}\,. \end{aligned}$$

(b) A similar argument as in (a) leads to

$$\begin{aligned} G_x &= \frac{\Delta u}{\gamma T_s} = \frac{0.5 \text{ mm}^{-1}}{4,258 \text{ Hz/G}\, 0.01 \text{ s}} = 11.7 \text{ mG/mm}\,, \\ G_y &= \frac{\Delta v}{\gamma T_s} = \frac{1.0 \text{ mm}^{-1}}{4,258 \text{ Hz/G}\, 0.01 \text{ s}} = 23.5 \text{ mG/mm}\,. \end{aligned}$$

The sampling rate is

$$f_s = \frac{128}{10 \text{ ms}} = 12.8 \text{ kHz}\,.$$

Solution 13.13

The required timing diagram is shown in Figure S13.4. The timings and the amplitudes of the gradients:

$$k_x = \gamma \int G_x\, dt, \quad k_y = \gamma \int G_y dt$$

are determined by

$$-1 \text{ mm}^{-1} = -1,000 \text{ m}^{-1} = 42.6 \times 10^6 \times (-G_1) \times t_1 \quad \Rightarrow \quad G_1 \times t_1 = 23.5 \times 10^{-6} \left(\frac{\text{T} \cdot \text{ s}}{\text{m}} \right)$$

$$0.5 \text{ mm}^{-1} = 500 \text{ m}^{-1} = 42.6 \times 10^6 \times G_2 \times t_1 \quad \Rightarrow \quad G_2 \times t_1 = 11.7 \times 10^{-6} \left(\frac{\text{T} \cdot \text{ s}}{\text{m}} \right)$$

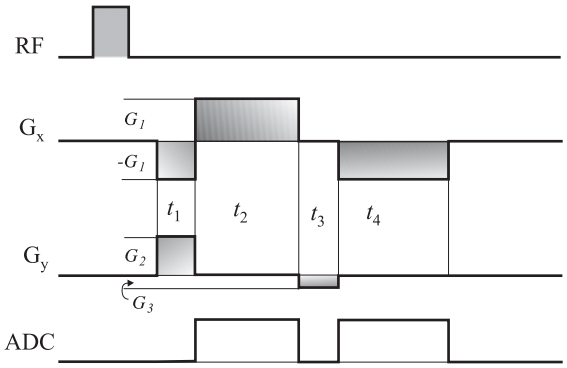

Figure S13.4 See Problem 13.13.

$$2\ \text{mm}^{-1} = 2000\ \text{m}^{-1} = 42.6 \times 10^6 \times G_1 \times t_2 \quad \Rightarrow \quad G_1 \times t_2 = 47 \times 10^{-6} \left(\frac{\text{T} \cdot \text{ s}}{\text{m}} \right)$$

$$0.1\ \text{mm}^{-1} = 100\ \text{m}^{-1} = 42.6 \times 10^6 \times G_3 \times t_3 \quad \Rightarrow \quad G_3 \times t_3 = 2.3 \times 10^{-6} \left(\frac{\text{T} \cdot \text{ sec}}{\text{m}} \right)$$

$$-2\ \text{mm}^{-1} = -2,000\ \text{m}^{-1} = 42.6 \times 10^6 \times (-G_1) \times t_4 \quad \Rightarrow \quad G_1 \times t_4 = 47 \times 10^{-6} \left(\frac{\text{T} \cdot \text{ s}}{\text{m}} \right)$$

Now, let $G_1 = 10$ mT/m, $G_2 = 5$ mT/m, and $G_3 = 1$ mT/m. Then, $t_1 = 2.3$ ms, $t_2 = 4.7$ ms, $t_3 = 2.3$ ms, and $t_4 = 4.7$ ms.

Solution 13.14

Suppose the objects are at positions y_o and y_1. Also, let's suppose that the amplitude of the signal from the point samples is A_0 and A_1 respectively. If we acquire data from a pulse sequence, such as that shown in Figure 13.15, with $\text{G}_y = \text{G}_y^0$, we can apply a Fourier transform to the signal to yield a profile $S^o(x)$. Because the two point objects are at the same x coordinate, we are only interested in the value of the profile at $S^o(x_o)$. We can write the equation for the amplitude and phase of this value as

$$S^0(x_o) = A_0 e^{-i\gamma(G_y^0 t_y y_o)} + A_1 e^{-i\gamma(G_y^0 t_y y_1)}\,. \tag{S13.1}$$

In a separate acquisition, if we acquire data with $\text{G}_y = \text{G}_y^1$, the amplitude and phase of this point in the profile becomes

$$S^1(x_o) = A_0 e^{-i\gamma(G_y^1 t_y y_o)} + A_1 e^{-i\gamma(G_y^1 t_y y_1)}\,. \tag{S13.2}$$

Because the $S^i(x_o)$ are complex, the above equations represent four equations in four unknowns (A_o, A_1, y_o, y_1); therefore, if A_o, A_1 are real numbers, we can determine the y coordinates of the objects exactly.

Solution 13.15

All three pulses are concerned with the phase of the precessing transverse magnetization. The refocusing lobe is correcting the linear phase that is produced by the slice selection pulse. This is done by applying a negative gradient to that of the slice selection for a duration half of that of the slice selection gradient. The phase-encoding gradient

is deliberately applying a linear phase in the phase encode (y) direction, so that Fourier space position is encoded. The gradient echo formation lobe can be called a prefocusing lobe, since it essentially corrects the phase prior to the readout gradient so that the spins are in phase at the center of the readout gradient.

Since all these phase corrections are accomplished by either increasing or decreasing the Larmor frequency in a spatially encoded fashion, they can all be combined. The net effect will be that the overall phase of each point will arrive at its correct final value faster than if each of these corrections had been done sequentially.

MR IMAGE RECONSTRUCTION

Solution 13.16

(a) The baseband signal is given by

$$\begin{aligned} s_0(t) &= \int_{-\infty}^{\infty}\int_{-\infty}^{\infty} f(x,y)e^{-j2\pi\gamma G_x xt}e^{-j2\pi\gamma G_y yt}\,dx\,dy \\ &= \int_{-\infty}^{\infty}\int_{-\infty}^{\infty} f(x,y)e^{-j2\pi\gamma G\cos\theta\, xt}e^{-j2\pi\gamma G\sin\theta\, yt}\,dx\,dy \\ &= \int_{-\infty}^{\infty}\int_{-\infty}^{\infty} f(x,y)e^{-j2\pi\gamma Gt(x\cos\theta+y\sin\theta)}\,dx\,dy\,. \end{aligned}$$

(b) The Fourier transform of $f(x,y)$ is

$$F(u,v) = Ae^{-j2\pi u} + Be^{+j2\pi v}\,.$$

The baseband signal is sampling the Fourier transform according to the following formulas

$$\begin{aligned} u &= \gamma Gt\cos\theta\,, \\ v &= \gamma Gt\sin\theta\,. \end{aligned}$$

When $\theta = 0$, we have

$$\begin{aligned} u &= \gamma Gt\,, \\ v &= 0\,, \end{aligned}$$

and therefore

$$s_0(t)|_{\theta=0^\circ} = F(\gamma Gt, 0) = Ae^{-j2\pi\gamma Gt} + B\,.$$

This is a complex signal having two components, as shown in Figure S13.5(a). Similar reasoning yields the following baseband signal for $\theta = 90^\circ$

$$s_0(t)|_{\theta=90^\circ} = F(0, \gamma Gt) = A + Be^{+j2\pi\gamma Gt}\,,$$

which is shown in Figure S13.5(b).

(c) This is a polar scanning technique. In order to image the cross section (rather than just a projection of the cross section), one needs to apply this basic pulse sequence for different values of θ ranging over 180 degrees, say $0 \le \theta < \pi$. This will cover half of Fourier space. The remainder is filled in using conjugate

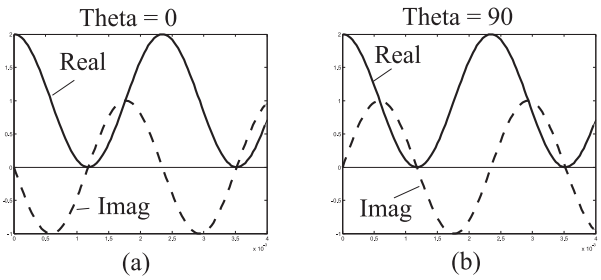

Figure S13.5 Baseband signals. See Problem 13.16.

symmetry:

$$F(u,v) = F^*(-u,-v)\,.$$

Since data are acquired along rays passing through the origin (and conjugate symmetry assures us that the data are defined in both directions), we can use convolution backprojection to do the reconstruction.

Solution 13.17

First, it is useful to see what happens during standard rectilinear scanning. All aspects of imaging are linear. So, the object can be decomposed and analyzed separately:

$$f(x,y) = f_1(x,y) + f_2(x,y)\,,$$

where $f_2(x,y)$ corresponds to the point object in the perturbed field. By linearity, the resultant baseband signal is the sum

$$s_0(t) = s_1(x,y) + s_2(x,y)\,.$$

During phase encoding, a phase equal to $2\pi\gamma\Delta BT_p$, where T_p is the duration of the phase encode pulse, is added to the signal arising from $f_2(x,y)$. During readout, a phase equal to $-2\pi\gamma\Delta Bt$ accumulates. Putting both terms together yields the baseband signal equation for $f_2(x,y)$

$$s_2(t) = \int_{-\infty}^{\infty}\int_{-\infty}^{\infty} f_2(x,y) e^{j2\pi\gamma\Delta BT_p} e^{-j2\pi\gamma\Delta Bt} e^{-j2\pi\gamma G_x x t} e^{-j2\pi\gamma G_y T_p y}\,dx\,dy\,.$$

Using the usual equivalences

$$\begin{aligned} u &= \gamma G_x t\,, \\ v &= \gamma G_y T_p\,, \end{aligned}$$

yields

$$\hat{F}(u,v) = e^{j2\pi\gamma\Delta BT_p} e^{-j2\pi(\Delta B/G_x)u} \int_{-\infty}^{\infty}\int_{-\infty}^{\infty} f_2(x,y) e^{-j2\pi(ux+vy)}\,dx\,dy\,.$$

The inverse Fourier transform of $\hat{F}(u,v)$ is

$$\hat{f}(x,y) = e^{j2\pi\gamma\Delta BT_p} f(x-(\Delta B/G_x),y)\,.$$

The leading phase term is irrelevant, since the complex modulus is typically displayed. The second phase term, since it was a linear phase term in the x-direction causes a shift of f_2 in the x-direction by $\Delta B/G_x$. Thus, the

relative positions of $f_1(x,y)$ (which will be reconstructed correctly) and $f_2(x,y)$ will be altered in the x-direction, but otherwise, the two point functions will be reconstructed correctly as point functions.

Reconstruction using the 2-D projection (polar scanning) method leads to a different—less desirable—result, primarily because the readout direction is different with each excitation pulse. With no phase encoding in this pulse sequence, there is no leading phase constant. However, both x and y gradients are on at the same time, in general. This gives the baseband signal for $f_2(x,y)$ as follows

$$s_2(t) = \int_{-\infty}^{\infty}\int_{-\infty}^{\infty} f_2(x,y) e^{-j2\pi\gamma\Delta B t} e^{-j2\pi\gamma(G_x x + G_y y)t}\, dx\, dy\,.$$

Let the gradients be given by

$$\begin{aligned} G_x &= \bar{G}\cos\theta\,, \\ G_y &= \bar{G}\sin\theta\,, \end{aligned}$$

and make the spatial frequency associations

$$\begin{aligned} u &= \gamma G_x t\,, \\ v &= \gamma G_y t\,. \end{aligned}$$

Then it follows that

$$\varrho = \sqrt{u^2+v^2} = \gamma t \bar{G}\,,$$

and the observed signal becomes

$$\begin{aligned} \hat{G}(\varrho,\theta) &= s_0\left(\frac{\varrho}{\gamma\bar{G}}\right) \\ &= \int_{-\infty}^{\infty}\int_{-\infty}^{\infty} f_2(x,y) e^{-j2\pi(\Delta B/\bar{G})\varrho} e^{-j2\pi(x\varrho\cos\theta/\bar{G} + y\varrho\sin\theta/\bar{G})}\, dx\, dy \\ &= e^{-j2\pi(\Delta B/\bar{G})\varrho}\int_{-\infty}^{\infty}\int_{-\infty}^{\infty} f_2(x,y) e^{-j2\pi(x\varrho\cos\theta/\bar{G} + y\varrho\sin\theta/\bar{G})}\, dx\, dy \\ &= e^{-j2\pi(\Delta B/\bar{G})\varrho} F_2(\varrho\cos\theta/\bar{G}, \varrho\sin\theta/\bar{G})\,. \end{aligned}$$

The inverse Fourier transform of this gives a projection of $f_2(x,y)$ shifted by $\Delta B/\bar{G}$. Each projection is shifted by the same amount on the ℓ axis. For example, if $f_2(x,y) = \delta(x,y)$, whose Radon transform is $g(\ell,\theta) = \delta(\ell)$, the observed "projection" would be $\hat{g} = \delta(\ell - \Delta B/\bar{G})$.

Unfortunately, $\hat{g}$ is not a Radon transform, which can be proven by showing that there is no object whose center of mass agrees with the centers of mass of the collection of projections. This makes it difficult to determine the precise effect that this term will have on the resulting reconstruction. It should be apparent, however, that shifting each projection of an impulse function by $\Delta B/\bar{G}$ creates a disk with radius $\Delta B/\bar{G}$ in the object domain. Thus, although the precise details are not developed here, we can conclude that rather than being shifted, as in the case of rectilinear scanning, 2-D projection imaging will blur objects when the Larmor frequency varies across the FOV.

Solution 13.18

We have

$$\begin{aligned} s_0(t) &= \int_{-\infty}^{\infty}\int_{-\infty}^{\infty} f(x,y)e^{-j2\pi\gamma G_x x t}\,dx\,dy \\ &= \int_{-\infty}^{\infty}\int_{-\infty}^{\infty} AM_{xy}(x,y;0^+)e^{-t/T_2}e^{-j2\pi\gamma G_x x t}\,dx\,dy \\ &= e^{-t/T_2}\int_{-\infty}^{\infty}\int_{-\infty}^{\infty} AM_{xy}(x,y;0^+)e^{-j2\pi\gamma G_x x t}\,dx\,dy\,. \end{aligned}$$

The inverse Fourier transform of $s_0(t)$ is

$$\begin{aligned} S_0(\nu) &= \mathcal{F}^{-1}\{s_0(t)\} \\ &= \mathcal{F}^{-1}\{e^{-t/T_2}\} * \mathcal{F}^{-1}\left\{\int_{-\infty}^{\infty}\int_{-\infty}^{\infty} AM_{xy}(x,y;0^+)e^{-j2\pi\gamma G_x x t}\,dx\,dy\right\} \\ &= \mathcal{F}^{-1}\{e^{-t/T_2}\} * \int_{-\infty}^{\infty}\int_{-\infty}^{\infty}\int_{-\infty}^{\infty} M_{xy}(x,y)e^{-i\gamma G_x x t}e^{+j2\pi\nu t}\,dt\,dx\,dy \\ &= \mathcal{F}^{-1}\{e^{-t/T_2}\} * \int_{-\infty}^{\infty}\int_{-\infty}^{\infty} M_{xy}(x,y)\delta(2\pi(\nu-\gamma G_x x))\,dx\,dy\,. \end{aligned}$$

Therefore, the amplitude of the function $S_0(\nu)$ at a specific frequency ν_0 will be proportional to the line integral of $M_{xy}(x,y;0^+)$ along the y direction at the x position $x_0 = \nu_o/\gamma G_x$; hence, $S(\nu)$ is a projection of the object $M_{xy}(x,y;0^+)$ onto the x axis. This data, however, will be convolved with $\mathcal{F}^{-1}\{e^{-t/T2}\}$, which is called a *Lorentzian function*. If the data are acquired fast enough, this convolution can be ignored.

MR IMAGE QUALITY

Solution 13.19

(a) With reference to Figure 13.6, we see that the through-plane direction coincides with the x axis, which is therefore the slice selection gradient direction as well. There is no choice in this matter.

In a standard (axial) image, it is customary to make the $+y$ direction be the phase encode direction. Although this is arbitrary, provided that the direction is within the y-z plane, it makes sense to retain the $+y$ direction as the phase encode direction [see part (b)].

The standard (axial) image uses the $+x$ direction as the frequency encode direction. The frequency encode direction should be orthogonal to the phase encode direction, so it could be either the $-z$ or $+z$ direction. For simplicity, we choose the $+z$ direction to be the readout direction.

(b) Aliasing in the phase encode direction is prevented by making sure that the object being imaged is confined to the FOV in the phase encode direction,

$$\text{FOV}_y = \frac{1}{\Delta v}\,,$$

where Δv are the phase encode increments in the frequency domain.

With reference to Figure 13.6, it becomes a bit more clear, why the phase encode direction should be in the y direction. In this figure, the extent of the patient in the y direction is given by distance from the back to the chest, whereas the extent in the z direction is the entire height of the patient. It is usually the case that the thinnest section of the patient is chosen as the phase-encode direction in an arbitrary scan.

Aliasing is prevented in the frequency encode direction by using an anti-aliasing filter prior to sampling, as usual.

Solution 13.20

(a) The spatial extent is defined by the field-of-view in the y (phase encode) direction, which is given by

$$\text{FOV}_y = \frac{1}{\gamma \Delta A_y} .$$

Since γ is fixed, it is the change in the area of the phase encode gradient, ΔA_y, between imaging pulses that determines the spatial extent in the y direction. This parameter is independent of the number of phase encodes—that is, 256 in the problem statement—that are acquired.

(b) The spatial extent in the readout direction is defined by the field-of-view in the x (readout) direction, which is given by

$$\text{FOV}_x = \frac{f_s}{\gamma G_x} .$$

Thus, the sampling rate f_s and the readout gradient strength G_x determine the spatial extent in the readout direction. If that is the case, it must be assumed that the readout gradient is left on for a duration that is long enough to collect 256 samples. It is also possible to view the duration of the readout interval T_s as a parameter. In this case, the sampling rate is determined by the number of samples acquired over the interval, $f_s = 256/T_s$. Then the spatial extent can be written as

$$\text{FOV}_x = \frac{256}{\gamma T_s G_x} .$$

(c) Spatial resolution is not determined by the pixel size but rather by the amount of Fourier space that is acquired. From Section 13.4.2, we have

$$\text{FWHM}_y = \frac{1}{N_y \gamma \Delta A_y} .$$

Here, $N_y = 256$, so the only parameter actually affecting resolution is ΔA_y. Increasing ΔA_y reduces FWHM_y, improving the resolution. But given the result in part (a), we see that this can only be done provided that the spatial extent covers the object (otherwise wraparound will occur).

(d) In the readout direction, we have

$$\text{FWHM}_x = \frac{1}{\gamma N_x T G_x} .$$

Here, $N_x = 256$, so we can change either T or G_x in order to change the spatial resolution in the readout direction. Since the readout time is $T_s = N_x T$, it is more fundamental to write

$$\text{FWHM}_x = \frac{1}{\gamma T_s G_x} .$$

Now we see that the readout resolution is actually inversely proportional to the product $T_s G_x$ and increasing either T_s or G_x will improve this resolution.

Solution 13.21

(a) The spatial extent in the diagonal direction is

$$D = \sqrt{2} \times 25.6 \text{ cm} = 36.2 \text{ cm}\,.$$

There are 256 samples.

(b) The sampling rate in the x and y directions are

$$\begin{aligned} f_u = 1/\Delta v &= \text{FOV}_y = 25.6 \text{ cm}\,, \\ f_v = 1/\Delta u &= \text{FOV}_x = 25.6 \text{ cm}\,, \end{aligned}$$

But the sampling rate in the diagonal direction is lower, equal to

$$f_d = \frac{25.6 \text{ cm}}{\sqrt{2}} = 18.1 \text{ cm}\,.$$

Solution 13.22

(a) The average power dissipated in the object is:

$$P_{\text{ave}} = \frac{1}{T}\int_0^T I^2(t) R dt\,,$$

where T is the period of the current and R is the effective electrical resistance. Substitute $I(t) = \cos(2\pi\nu_0 t)$ into the above equation, we have

$$\begin{aligned} P_{\text{ave}} &= \frac{1}{T}\int_0^T \cos^2(2\pi\nu_0 t) R dt \\ &= \frac{R}{2\pi}\int_0^{2\pi} \cos^2(u) du, \quad \text{let } u = 2\pi\nu_0 t \\ &= \frac{R}{2}\,. \end{aligned}$$

Since the current in the coil is $I(t) = \cos(2\pi\nu_0 t)$, the magnetic flux density is $B_1(t) = \mu_0 N I(t)$. And the induced voltage in a cylindrical shell of radius r is given by

$$V(t, r) = \frac{d\phi}{dt} = \frac{d(AB_1)}{dt} = 2\pi^2 \nu_0 r^2 \mu_0 N \sin(2\pi\nu_0 t),$$

where ϕ is the magnetic flux and $A = \pi r^2$ is the area subtended by the cylindrical shell.

(b) Given the differential conductance in a thin shell of radius r, the average power dissipated in the shell is:

$$dP_{\text{ave}} = \frac{1}{T}\int_0^T V^2(t, r) dG dt = \frac{1}{2}\frac{(2\pi^2\nu_0 r^2 \mu_0 N)^2 L}{2\pi r \rho} dr.$$

The average power dissipated in the object can also be expressed using the voltage as:

$$P_{\text{ave}} = \int_0^{r_0} dP_{\text{ave}} = \frac{R}{2}.$$

Therefore, the effective electrical resistance is:

$$\begin{aligned} R &= 2P_{\text{ave}} \\ &= \int_0^{r_0} \frac{(2\pi^2\nu_0 r^2 \mu_0 N)^2 L}{2\pi r \rho} dr \\ &= \frac{2\pi^3 \nu_0^2 \mu_0^2 N^2 L}{\rho} \int_0^{r_0} r^3 dr \\ &= \frac{\pi^3 \nu_0^2 \mu_0^2 N^2 L r_0^4}{2\rho}, \end{aligned}$$

which is Equation (13.79).

Solution 13.23

Start with the imaging equation

$$f(x,y) = AM_0 \sin\alpha e^{-T_E/T_2(x,y)} \frac{1 - e^{-T_R/T_1}}{1 - \cos\alpha e^{-T_R/T_1}},$$

Using $T_E = 0$ and $\alpha = \pi/2$, and setting the overall gain to unity, gives

$$f(x,y) = 1 - e^{-T_R/T_1}.$$

The two tissues have values

$$f_a = 1 - e^{-T_R/T_1^a}, \quad \text{and} f_b = 1 - e^{-T_R/T_1^b},$$

so the image difference between these two tissues is

$$\begin{aligned} \Delta &= f_a - f_b \\ &= (1 - e^{-T_R/T_1^a}) - (1 - e^{-T_R/T_1^b}) \\ &= e^{-T_R/T_1^b} - e^{-T_R/T_1^a}. \end{aligned}$$

Taking the derivative of this expression with respect to T_R yields

$$\begin{aligned} \frac{d\Delta}{dT_R} &= \frac{d}{dT_R}(e^{-T_R/T_1^b} - e^{-T_R/T_1^a}) \\ &= \frac{-1}{T_1^b} e^{-T_R/T_1^b} - \frac{-1}{T_1^a} e^{-T_R/T_1^a}. \end{aligned}$$

Now set this equal to zero and solve for $\hat{T}_R$:

$$\begin{aligned}
\frac{-1}{T_1^b}e^{-T_R/T_1^b} - \frac{-1}{T_1^a}e^{-T_R/T_1^a} &= 0 \\
T_1^b e^{-\hat{T}_R/T_1^a} &= T_1^a e^{-\hat{T}_R/T_1^b} \\
\ln T_1^b - \frac{\hat{T}_R}{T_1^a} &= \ln T_1^a - \frac{\hat{T}_R}{T_1^b} \\
\hat{T}_R\left(\frac{1}{T_1^b} - \frac{1}{T_1^a}\right) &= \ln T_1^a - \ln T_1^b \\
\hat{T}_R &= \frac{\ln T_1^a - \ln T_1^b}{\frac{1}{T_1^b} - \frac{1}{T_1^a}}\,.
\end{aligned}$$

Whether this expression should yield a maximum or minimum depends on the relationship between T_1^a and T_1^b, and hence the sign of Δ. Suppose $T_1^a < T_1^b$; then $\Delta > 0$ and our goal is to maximize Δ. Otherwise, our goal is to minimize Δ (making the difference more negative). It is readily verified by plotting Δ as a function of T_R that these conditions are satisfied by the expression we have derived for $\hat{T}_R$.

Solution 13.24

The conventional magnet strength of whole-body scanners today is 1.5 T. Therefore, Larmor frequency is

$$\begin{aligned}
f &= \gamma B_0 \\
&= 42.58 \text{ MHz/T} \times 1.5 \text{ T} \\
&= 63.84 \text{ MHz}\,.
\end{aligned}$$

In air, the wavelength of radio frequency waves at this frequency is

$$\begin{aligned}
\lambda &= \frac{3 \times 10^8 \text{ m/s}}{63.84 \times 10^6 \text{ Hz}} \\
&= 4.7 \text{ m}.
\end{aligned}$$

The Rayleigh limit is $\lambda/2 = 2.35$ meters. Clearly, MRI does not work according to conventional optical imaging principles.

Solution 13.25

From Chapter 12, we know that the Larmor frequency of fat is

$$\nu_0(\text{fat}) = \nu_0(\text{water})(1 - \varsigma)\,.$$

where $\varsigma = 3.35 \times 10^{-6}$. The frequency difference is

$$\Delta\nu_0 = -\varsigma\gamma B_0\,,$$

which at 1.5 T is -214 Hz. But the above analysis is in a static field. When a readout gradient is turned on, the

Larmor frequencies of water and fat will be

$$\begin{aligned} \nu_0(\text{water}) &= \gamma(B_0 + G_x x)\,, \\ \nu_0(\text{fat}) &= \gamma(B_0 + G_x x) - \varsigma\gamma(B_0 + G_x x)\,. \end{aligned}$$

After demodulation to baseband (assuming that the Larmor frequency of water is used for demodulation), the following frequencies are encoded during the readout interval

$$\begin{aligned} \nu(\text{water}) &= \gamma G_x x\,, \\ \nu(\text{fat}) &= \gamma G_x x - \varsigma\gamma(B_0 + G_x x)\,. \end{aligned}$$

Therefore, during frequency encoding (the readout interval), the fat signal will be slightly mispositioned in the readout direction relative to that of water.

To suppress the fat signal, we can apply a 180-degree (so-called inversion) pulse and then wait for both components of longitudinal magnetization to recover. Since the fat T_1 is so much shorter than the water T_1, it will recover faster, passing the $M_z = 0$ point at a predictable time. At that time, one can begin imaging with the application of a standard $\pi/2$ RF pulse. Because the fat signal has $M_z = 0$ at that time, it will not contribute to the transverse signal, and only water will be imaged. This type of sequence, called *inversion recovery* sequence, can be tuned to suppress the water signal as well by waiting for the longitudinal magnetization recovery of water to cross zero.

Solution 13.26

(a) When $G_x \to 0.5G_x$, the FOV doubles, that is, $\text{FOV}_x \to 2\text{FOV}_x$. Since image size remains unchanged, the pixel size must double as well, that is, $V_s \to 2V_s$. Therefore, the SNR also doubles, that is,

$$\text{SNR} \to 2\text{SNR}\,.$$

(b) $N_y \to 2N_y$ means to double the number of phase encodes. If everything else is to remain unchanged, this implies that these phase encodes either repeat the first set of phase encodes or add on to those already acquired but at a different v locations in Fourier space. In either case, the net effect is to double the scan time; therefore, the SNR will improve, but only by a $\sqrt{2}$ factor. In other words,

$$\text{SNR} \to \sqrt{2}\text{SNR}\,.$$

(c) Since $f_s \to 2f_s$ the sample period is halved, $T \to 0.5T$. Since T_s remains constant and $N_x \to 2N_x$, the total time has remained constant, that is, $T_A \to T_A$. The only possible remaining factor affecting SNR is voxel size. If the image size is assumed to follow $J = N_x$, then the image size has doubled, $J \to 2J$. But since FOV_x is inversely proportional to T, we also have that $\text{FOV}_x \to 2\text{FOV}_x$. Under this assumption, voxel size is constant and SNR is constant

$$\text{SNR} \to \text{SNR}\,, \quad \text{assuming } J = N_x\,.$$

(d) It is reasonable to make the assumption from the problem statement that the image size should not change, that is, $J \to J$. In this case, since the FOV_x has doubled, the voxel size would also double, $V_s \to 2V_s$ and

$$\text{SNR} \to 2\text{SNR}\,, \quad \text{assuming } J \to J\,.$$

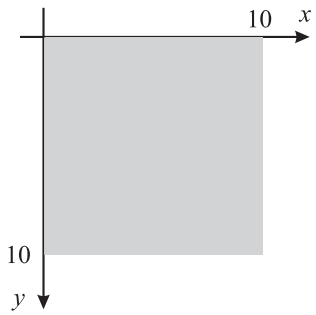

Figure S13.6 See Problem 13.27(a).

APPLICATIONS, EXTENSIONS, AND ADVANCED TOPICS

Solution 13.27

(a) The 2D function $f(x,y)$ is

$$f(x,y) = \text{rect}\left(\frac{x-5}{10}, \frac{y-5}{10}\right).$$

It is sketched in Figure S13.6. The Fourier transform of $f(x,y)$ is

$$F(u,v) = 10\,\text{sinc}(10u) \times 10\,\text{sinc}(10v)e^{-j2\pi(5u)}e^{-j2\pi(5v)},$$

and

$$|F(u,0)| = 100\,\text{sinc}(10u)\,.$$

(b) We have

$$\gamma G_x t = 42.58 \text{ kHz/G} \cdot 0.5 \text{ G/mm} \cdot t = 0.4 \text{ cm}^{-1}\,,$$

and after solving yields

$$t = 18.788\,\mu\text{s}\,.$$

(c) The gradient echo will occur after $18.788\ \mu$ s, because that is when the phases will be realigned.

(d) Perfect $g(\ell, 0^\circ)$ needs perfect $G(u,0)$. We collect only partial information of $G(u,0)$, since we do not collect data outside of $-0.4\ \text{cm}^{-1} \le u \le 0.4\ \text{cm}^{-1}$. Therefore, we cannot get a perfect reconstruction of $g(\ell, 0^\circ)$.

Solution 13.28

(a) We have

$$\begin{aligned}\omega_0 &= \gamma B_0 = 2\pi \times 4,258 \text{ (rad/s)/G} \times 1.5 \text{ T} \times 10^4 \text{ G/T} = 4.01 \times 10^8 \text{ rad/s}\,,\\ f_0 &= 6.39 \times 10^7 \text{ Hz}\,.\end{aligned}$$

The tip angle can be computed as

$$\alpha = \gamma \int_{-1\times10^{-3}}^{1\times10^{-3}} B_1^e(t)dt = 2\pi \times 4,258 \int_{-1\times10^{-3}}^{1\times10^{-3}} 2 \times 4.258 \times 10^4\,\text{sinc}(4.258 \times 10^4 t)dt\,.$$

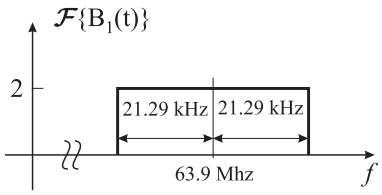

Figure S13.7 See Problem 13.28(b).

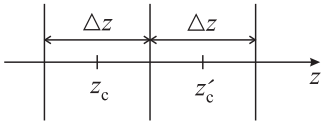

Figure S13.8 See Problem 13.28(d).

(b) Carry out the following manipulations

$$\begin{aligned} B_1(t) &= A\Delta f\,\mathrm{sinc}(\Delta f t)e^{j\omega_0 t}\,, \\ \mathcal{F}\{B_1(t)\} &= A\,\mathrm{rect}\left(\frac{f-f_0}{\Delta f}\right)\,, \\ &= 2\,\mathrm{rect}\left(\frac{f-6.39\times 10^7}{4.258\times 10^4}\right)\,, \\ \Delta\omega &= 2\pi\Delta f = 267,538 \text{ rad/s}\,. \end{aligned}$$

(c) Carry out the following

$$\omega_c = \gamma(B_0 + G_z\cdot z_c) = \omega_0 \Rightarrow z_c = 0$$

$$\Delta\omega = \gamma G_z\cdot\Delta z \Rightarrow \Delta z = \frac{\Delta\omega}{\gamma G_z} = \frac{267,538}{1\pi\cdot 4,258\cdot 2} = 5 \text{ cm}$$

(d) We have

$$z_c' = z_c + \Delta z = 5 \text{ cm}\,,$$

$$\omega_c' = \gamma(B_0 + G_z\cdot z_c') = \omega_0 + \gamma G_z\cdot z_c' = \omega_0 + 2\pi\cdot 4,258\cdot 2\cdot 5 = \omega_0 + 2.68\times 10^5 \text{ rad/s}\,.$$

So in order to select the adjacent slice, we need

$$B_1'(t) = A\Delta f\,\mathrm{sinc}(\Delta f t)e^{j(\omega_0+\omega_c')t}\,.$$

(e) Carry out these steps:

$$\begin{aligned} \omega_1 &= \gamma(B_0 + G_z z_1)\,, \\ \omega_2 &= \gamma(B_0 + G_z z_2)\,, \\ \Delta\omega &= \gamma G_z\Delta z\,, \\ \Delta\phi &= \Delta\omega\cdot\frac{\tau_p}{2} = \gamma G_z\Delta z\frac{\tau_p}{2} = 2\pi\cdot 4,258\cdot 2\cdot 5\cdot 1\times 10^{-3} = 267.5 \text{ rad}\,. \end{aligned}$$

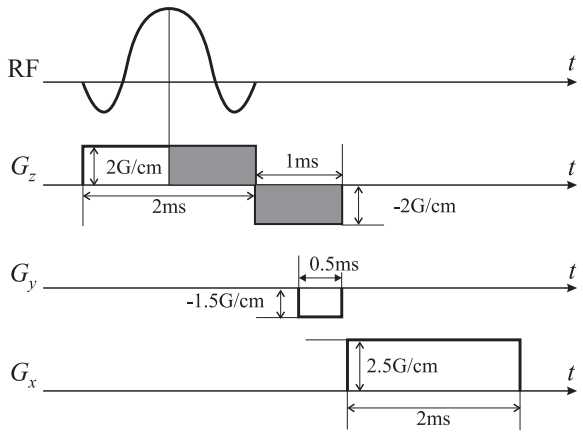

Figure S13.9 See Problem 13.28(f).

In order to rephase the spins, we need to use a refocussing lobe on G_z.

(f) We have

$$\begin{aligned} k_x &= \frac{\gamma}{2\pi}\int_0^{t_1} G_x(\tau)d\tau = \frac{\gamma}{2\pi}G_x \cdot t_1 \\ k_y &= \frac{\gamma}{2\pi}\int_0^{t_2} G_y(\tau)d\tau = \frac{\gamma}{2\pi}G_y \cdot t_2 \\ t_1 &= \frac{k_x}{\frac{\gamma}{2\pi}G_x} = 2 \text{ ms} \\ t_2 &= \frac{k_y}{\frac{\gamma}{2\pi}G_y} = 0.5 \text{ ms} \end{aligned}$$

The pulse sequence is shown in Figure S13.9.

(g) We have

$$\text{FOV}_x = \frac{2\pi}{\Delta k_x} = \frac{2\pi}{\gamma G_x T} = \frac{2\pi f_s}{\gamma \cdot G_x}$$

$$f_s = \frac{\text{FOV}_x \cdot \gamma \cdot G_x}{2\pi} = \frac{50 \text{ cm} \cdot 4,258 \cdot 2\pi \cdot 2.5}{2\pi} = 5.32 \times 10^5 \text{ Hz}\,.$$

Solution 13.29

(a) We will use phase encoding in both the y and z directions. The pulse sequence shown in Figure S13.10, a modification of Figure 13.16, shows the general idea (though this is not a realistic pulse sequence).

(b) The following baseband signal is the same as the standard 2D gradient echo pulse sequence, except that there is a new term that depends on the z phase encoding:

$$s_0(t) = \int_{-\infty}^{\infty}\int_{-\infty}^{\infty} f(x,y)e^{-j2\pi\gamma G_x x t}e^{-j2\pi\gamma G_y T_p y}e^{-j2\pi\gamma G_z T_p z}\,dx\,dy\,.$$

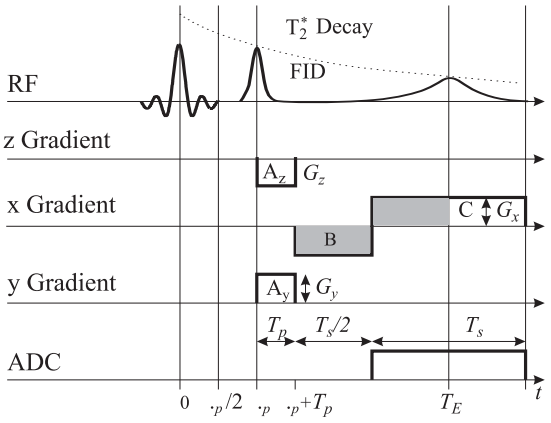

Figure S13.10 See Problem 13.29.

(c) The image would be reconstructed using an inverse three-dimensional Fourier transform. Comparing the above expression to the 3-D Fourier transform yields the following identifications:

$$\begin{aligned} u &= \gamma G_x t\,, \\ v &= \gamma G_y T_p\,, \\ w &= \gamma G_z T_p\,. \end{aligned}$$

Therefore, the 3D Fourier transform $F(u,v,w)$ of $f(x,y,z)$ is built up by successive imaging pulses as follows

$$F(u, \gamma G_y T_p, \gamma G_z T_p) = s_0\left(\frac{u}{\gamma G_x}\right) \quad 0 \le u \le \gamma G_x T_s\,.$$

where G_y and G_z must take on a series of different values in order to cover 3D Fourier space.

Solution 13.30

In general, if we have N points, we can write the set of signal equations as

$$S^m(x_o) = \sum_{j=0}^{j=N} A_j e^{-i\gamma(G_y^m t_y y_j)}\,, \tag{S13.3}$$

which is 2N equations with 2N unknowns. Figure S13.11 shows one possible scheme for changing the value of the phase-encoding gradient amplitudes. For each acquisition, we have $G_y^m = m\Delta G_y$.

It is important to note that while the data acquisition is similar to that used in *spin-warp imaging*, the procedure described here for *reconstructing* the MR image is *not* what is usually done. Usually, the positions of the objects are assumed to be known; that is, we reconstruct the signal amplitudes (and phases) of a set of decaying oscillators that are sitting on a fixed coordinate grid by using the Fast Fourier Transform (FFT). This coordinate grid is the pixel array in the image. If the assumption is not true (which in most cases it is not), image artifacts from Gibbs ringing occur.

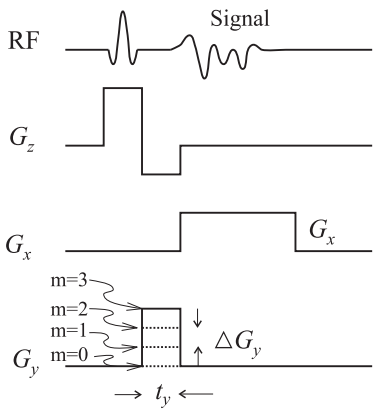

Figure S13.11 Pulse sequence for phase encoding. See Problem 13.30.